Structure and Function Studies of K2P Channels

Submitted in partial fulfilment of the
requirements for the degree of
Doctor of Philosophy



Chetan Sharma

Linacre College, University of Oxford
Michaelmas 2012

Declaration of Authorship

The work described in this thesis was carried out in the laboratory of Dr. Stephen Tucker, in the Department of Physics and the Department of Physiology, Anatomy and Genetics, University of Oxford, between October 2009 and December 2012. All work within this thesis is entirely my own, unless otherwise stated and has not been previously submitted to this University or any other for the award of a degree.

Chetan Sharma

December 2012

Abstract

Members of the two-pore potassium-selective (K2P) ion channel superfamily control cell excitability by contributing to the resting membrane potential. Through this, K2P channels are involved in a variety of physiological processes and dysfunction of these channels has been linked to diseases such as epilepsy, depression and migraine. The aim of this study was to develop a greater understanding of how K2P channels, in particular TREK-1, are gated.

In the initial stage of this study we hoped to identify mutations which alter the function of the TREK-1 channel by screening a random mutant library using a K^+-auxotrophic strain of *S. cerevisiae*, SGY1528. From the assay we identified a number of gain-of-function (GoF) mutations, primarily distributed through the pore-lining transmembrane (TM) helices TM2 and TM4. The clustering of mutations in these regions suggested a major role for these helices in channel gating.

Subsequent electrophysiological characterisation of these mutations revealed an increase in basal channel activity and altered sensitivity to modulation by extracellular pH, as well as by activators DEPC and BL-1249.

The publication of two K2P channel crystal structures, TWIK-1 (pdb code: 3UKM) and TRAAK (3UM7), enabled us to build an accurate homology model of TREK-1 and more accurately interpret these functional studies. This approach revealed a number of interesting points, the most important being an interaction between TM4 and pore-helix 1 (PH1). Further mutagenesis studies of this region confirmed that this interaction is essential for normal channel function. Another interaction was identified involving a number of residues within the interface between TM helices TM2, TM3 and TM4 emphasised the importance of helical movements for gating TREK-1 channels.

Based on our findings we therefore present a model for gating of the TREK-1 channel, which suggests that the movement of TM4 in particular, is transduced to the selectivity filter gate via PH1.

Acknowledgements

I would like to take this opportunity to thank everyone who supported and contributed to the completion of this work; particularly to Dr. Stephen Tucker, for the resources, priceless knowledge and continued encouragement he offered throughout this project. I am also grateful to members of Prof. Thomas Baukrowitz' and Prof. Mark Sansom's laboratory for their collaboration on this project.

As is the way with such things, I am grateful to so many people in Oxford for making my time here so memorable, so I won't name names, but a special thank you to my fellow Tuckerites, Kapanidians and, erm, Amadeus for making this such a special place to work. The 5AM international phone calls, Jaffa Ball, Mexican nights etc. will never be forgotten! Also, to my friends from Linacre college and the various sports teams I've been fortunate enough to be involved with during my time here, thank you for everything.

I will be forever indebted to you Mum, Dad, Raj and all my family, by blood or otherwise; you made me the man I am today (so its time to take some bloody responsibility!). I hope I can repay your kind support in the future.

As with all scientific work, serendipity had a huge part to play in the progression of this study. Logical thought and procedure will only take you so far! And so to take any credit as a scientist is opportunistic at the best of times. But if I am to take anything away from this thesis, it's that after three (long) years, I finally feel as though I've contributed my grain of sand to the Sahara.

Chetan Sharma

(Lifelong member of 4CR)

Dedicated to my Daadhi;

All the letters after my name and I still strive

for a degree of your wisdom.

Contents

Declaration of authorship I

Abstract II

Acknowledgements III

1 Introduction 1

1.1 Potassium channels 1

1.2 K2P channels and cellular excitability 4

1.2.1 The physiology of K2P channels 5

1.3 K2P channel subfamilies 6

1.3.1 TWIK channels 7

1.3.2 TASK channels 8

1.3.3 TALK channels 9

1.3.4 THIK channels 10

1.3.5 TRESK channels 11

1.3.6 TREK channels 12

1.4 K2P structure 14

1.5 K^+ selectivity in K2P channels 16

1.6 K2P gating 17

1.6.1 The lower-gate 18

1.6.2 The upper-gate 20

1.7 TREK-1 as a model of K2P channel function 20

1.7.1 TREK-1 regulation by the C-terminal regulatory domain 21

1.7.2 TREK-1 regulation by extracellular pH 24

1.8 Overview of thesis 26

2 Methods and Materials 28

2.1 Molecular biology materials 28

2.1.1 Original genes, constructs and vectors 28

2.1.2 Enzymes 29

2.1.3 Kits for purification, mutagenesis and *in vitro* transcription 29

2.1.4 Oligonucleotides 29

2.2 Molecular biology methods 30

2.2.1 Random mutant library construction 30

2.2.2 Gel electrophoresis 30

2.2.3 Gel extraction 31

2.2.4 Ligation 31

2.2.5 Site-directed mutagenesis 31

2.2.6 Extension overlap PCR 32

2.2.7 mRNA transcription 32

2.3 Microbiology – *Escherichia coli* 33

2.3.1 Materials 33

2.3.2 Propagation of plasmid DNA using *E.coli* 34

2.3.3 Sequencing 35

2.4 Microbiology – *Saccharomyces cerevisiae* 35

2.4.1 Yeast strains and vectors 35

2.4.2 Growth media 36

2.4.3 Making competent yeast cells 38

2.5 Genetic complementation assay 39

2.5.1 Screening mutant libraries 39

2.5.2 *S. cerevisiae* transformation 41

2.5.3 Yeast drop tests 41

2.5.4 Growth curves 43

2.6 Electrophysiology 43

2.6.1 The two-electrode voltage clamp method 44

2.6.2 TEVC materials 44

2.6.3 Drug stock solutions 46

2.6.4 Antibiotics 47

2.6.5 Preparation of *Xenopus laevis* oocytes for mRNA injection 48

2.6.6 mRNA injection 49

2.6.7 Data acquisition 49

2.6.8 Data analysis 50

3 The use of a genetic complementation assay to identify activatory mutations 52

3.1 Introduction 52

3.1.1 The genetic complementation assay 53

3.1.2 Searching for K2P gating mutants using SGY1528 54

3.2 The identification of GoF mutations in TREK-1 55

3.2.1 Complementation of growth in liquid media 58

3.3 Limitations of the genetic complementation assay 59

3.3.1 Screening drugs using the complementation assay 60

3.4 Location of GoF mutation in TREK-1 61

3.4.1 Activatory mutations identified near the pore helices 63

3.4.2 GoF mutations in the lower TM helices 65

3.4.3 Limitations of using homology models based on prokaryotic K^+ channels 66

3.4.4 Validation of the homology models 67

3.5 External corroboration of the genetic complementation assay 68

4 Alteration of TREK-1 pH sensitivity by activatory mutations 69

4.1 Investigation of activatory mutations identified using the genetic complementation assay 69

4.1.1 Why do GoF mutations complement yeast growth 70

4.2 The effects of GoF mutations to intracellular pH sensitivity 71

4.2.1 Poor expression of TREK-1 GoF mutant channels in *Xenopus* oocytes 72

4.2.2 The effects of intracellular pH on GoF mutant channels 72

4.3 The effect of mutations on whole cell currents 74

4.4 The effects of extracellular pH on GoF mutant channels 77

4.4.1 The S164P mutant 78

4.4.2 TM2 mutants 79

4.4.3 Upper-TM4 mutants 79

4.4.4 Lower-TM4 mutants 80

4.4.5 The I230N mutant 81

4.4.6 C-terminus mutants 82

4.5 The correlation between external pH sensitivity and complementation of growth 83

4.5.1 Alternative substitutions to residue S164 85

4.6 Conclusions 85

5 The use of activators to probe the TREK-1 gating mechanism 87

5.1 Activation of TREK-1 by DEPC 90

5.1.1 The role of H141 in proton sensitivity 92

5.2 Activation of TREK-1 by BL-1249 93

5.3 The effect of high extracellular [K^+] on TREK-1 channels 94

5.4 Response of GoF mutations to DEPC, BL-1249 and extracellular [K^+] 95

5.4.1 C-terminus mutants 95

5.4.2 TM2 mutants 96

5.4.3 Upper-TM4 mutants 99

5.4.4 Mutants within an interhelical interface 100
5.5 Conclusions 103

6 The roles of TM4 and the selectivity filter in channel gating 104
6.1 Activatory mutations in the upper-TM4 helix 104
6.1.1 Aromatic residues at the interface between TM4 and PH1 106
6.1.2 The effect of PH1 phenylalanine substitutions on channel function 108
6.1.3 The effect of G152 on C-type gating 109
6.2 The effects of mutations to L282 at the top of TM4 110
6.3 Probing the interface between TM2, TM3 and TM4 112
6.3.1 I230 in TM3 112
6.3.2 Functional characterisation of residue Y299 115
6.3.3 Functional characterisation of alternative mutations to A301 and A302 117
6.4 The unique properties of S164 mutations 118
6.4.1 Alternative mutations to residue S164 119
6.4.2 The structural consequences of S164 mutation 120
6.4.3 The effect of I163 and P165 mutations on TREK-1 function 121
6.4.4 The role of S164 and the external vestibule in extracellular pH sensitivity 121
6.5 Reintroduction of DEPC sensitivity to H141C mutant channels 125
6.6 Is gating of TREK-1 asymmetric? 126

7 Conclusions and suggested future studies 129
7.1 Summary 129
7.2 Our TREK-1 gating model 130
7.3 Suggested further investigation of K2P gating 135

Appendices 137

Bibliography 162

Chapter 1

Introduction

1.1 Potassium channels

For more than 200 years, physiologists have known that electrical currents play a role in cellular function (Galvani 1791). The most fundamental physiological processes are based on the ability of cells to receive, process and transmit electrical signals in the form of ion flow across the membrane. Central to this process are transmembrane proteins known as ion channels. Expressed throughout the various kingdoms of life, ion channels act as macromolecular pores embedded within cell membranes, opening and closing to regulate the flow of ions with a remarkable level of precision (Hille 2001).

In order to achieve the accurate ionic balance required for cells to thrive, there can be as many as 300 types of ion channels present at the membrane of a single cell (Gabashvili *et al.* 2007). Morever, there are several hundred genes encoding ion channels in man alone, suggesting an extremely high level of fine tuning for specific, specialised function. While there are some channels which non-selectively

conduct either cation or anions, ion channel families are generally categorised according to the ion they conduct most preferentially.

Potassium (K^+) channels, selectively control the flow of K^+ ions across the cell membrane. Involved in a plethora of functions from cell volume regulation to neuronal firing, K^+ channels are essential for cellular life in both prokaryotes and eukaryotes alike (Hille 2001). In all, thousands of K^+-selective channel genes have been identified, though the large majority share an particularly well-conserved ion conduction pathway. Two α-helical transmembrane (TM) domains are connected via an extracellular pore domain, containing a K^+-specific T-*X*-G-F/Y-G motif selectivity filter (Zylbergold *et al.* 2009).

In 1952, Hodgkin, Huxley and Katz first described a K^+ current, in the Squid giant axon (Hodgkin *et al.* 1952), though it wasn't until 1987 that the first K^+ channel was successfully cloned, from *Drosophilia melanogaster* (Papazian *et al*. 1987), and the '*Shaker*' channel is now one of the most well-characterised K^+ channels. Following the identification of the *Shaker* channel, K^+ channel genes have been isolated from sources as diverse as fungi and viruses to bacteria and man. The human genome alone encodes at least eighty different K^+ channels (Heitzmann and Warth *et al.* 2007).

Along with the identification of novel channels, the field of ion channel research continues to grow with greater understanding of the functional characteristics of K^+ channels. However, the mechanisms of gating and selectivity were not particularly well-understood until the first structure of a K^+ channel was resolved using x-ray crystallography (Doyle *et al.* 1998). Due to the well conserved ion conduction pathway and selectivity filter, the KcsA channel (from *Sacchromyces lividans)* structure provided a platform on which other K^+ channels can be modelled. More recently, the structures now available for different K^+ selective channels, such as KvAP and MthK, provide the scientific community with an insight into the structural aspects of gating, inactivation, selectivity and ligand binding.

K^+ channels are most commonly divided into separate families by their structural and functional characteristics into separate families, which includes the voltage-gated (K_V), calcium-gated (K_{Ca}), inwardly rectifying (K_{ir}) and twin-pore (K2P) K^+ channel subfamiles. While the number of TM helices

varies in an individual subunit from 2 to 8 (as in the case of the *S. cerevisiae* Tok1 channel), the general archetecture of a tetrameric pore remains highly conserved (Plant *et al.* 2005).

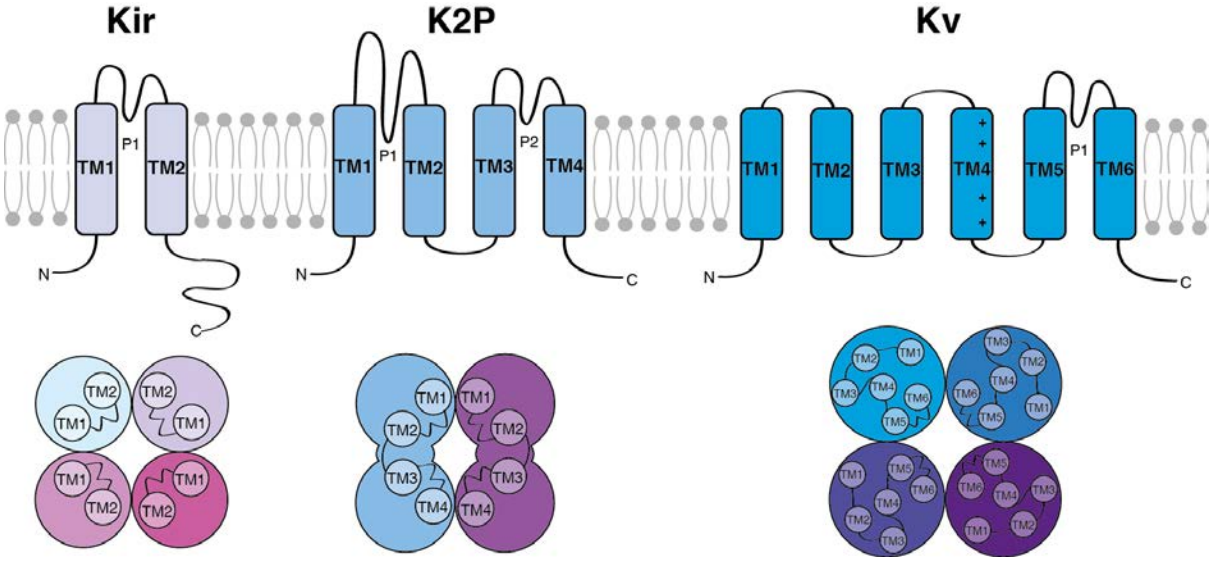


Figure 1.1: *Three of the known major structural subfamilies of K^+ channels; K^+-selective inwardly rectifying (K_{ir}), twin-pore (K2P) and voltage-gated channels (K_v) are shown from left to right. Shown underneath each topology model is the tetrameric arrangement for each channel subfamily, with a central cavity for ion conduction in each case.*

Mammalian K2P channels have a number of characteristics which distinguish them from other K^+ channels. Key among these is that they contain two-pore domains per subunit, resulting in a unique two-pore / four-TM arrangement (Figure 1.1). Given that the vast majority of identified K^+-selective channels contain a single pore domain per subunit and fold as tetramers, with either conventional four-fold or pseudo four-fold symmetry around the ion conduction pathway, it is noteworthy that K2P channels are arranged as a 'dimer of dimers'. This unique assembly means that, while the central ion conduction pathway is believed to maintain four-fold symmetry, the channel appears to possess an asymmetric structure (Brohawn *et al.* 2012), possibly providing a region for specific modulation (Enyedi and Czirjak 2010).

1.2 K2P channels and cellular excitability

The resting membrane potential (RMP) is determined by the differnt ionic composition of the intra- and extracellular milieu, which results in a voltage gradient across the plasma membrane. Under normal physiological conditions, the RMP is highly electronegative (approximately -70mV). This is determined primarily by the relative concentrations of sodium (Na^+) and K^+, but also by the calcium (Ca^{2+}) and chloride (Cl^-) concentrations, on either side of the membrane (Kandel *et al.* 2001). The equilibrium potential can be quantified for each type of ion using the Nernst equation, provided the intra- and extracellular concentrations of the specific ion are known.

$$E_K = \frac{RT}{ZF} \ln \frac{[K^+]_o}{[K^+]_i}$$

Equation 1: *The Nernst equation applied to K^+ ions. Where 'E_K' is the value of membrane potential at which K^+ is in equilibrium, 'R' the gas or Boltzmann constant, 'T' the temperature in degrees Kelvin, 'Z' the valence of K^+, 'F' the Faraday constant, and '$[K^+]_O$' and '$[K^+]_i$' the concentrations of K^+ on the outside and inside of the cell, respectively.*

Furthermore, using the Nernst equation, the membrane potential can be calculated using the Goldman-Hodgkin-Huxley (GHK) equation:

$$V_m = \frac{RT}{F} \ln \frac{P_K[K^+]_o + P_{Na}[Na^+]_o + P_{Cl}[Cl^-]_i}{P_K[K^+]_i + P_{Na}[Na^+]_i + P_{Cl}[Cl^-]_o}$$

Equation 2: *The GHK equation, which is used to calculate the membrane potential (V_m). Where 'P' is the relative membrane permeability for a given ion (e.g. P_K is the relative membrane permeability for K^+ ions).*

When an excitable cell is stimulated, Na^+ enters the cell through voltage-gated sodium channels (Na_V) channels, causing the membrane potential to reach approximately +40mV. Na_V channels are responsible for the rapid flow of Na^+ ions from the extracellular to intracellular space; likewise, K_V channels are responsible for a release of intracellular K^+ ions to the extracellular milieu to repolarise the cell membrane, back to a negative potential. This process, known as the action potential, underlies the activity of the millions of neuronal networks responsible for processing sensory information. The excitability of a cell, i.e. the ability to fire an action potential, is therefore highly dependent upon the RMP.

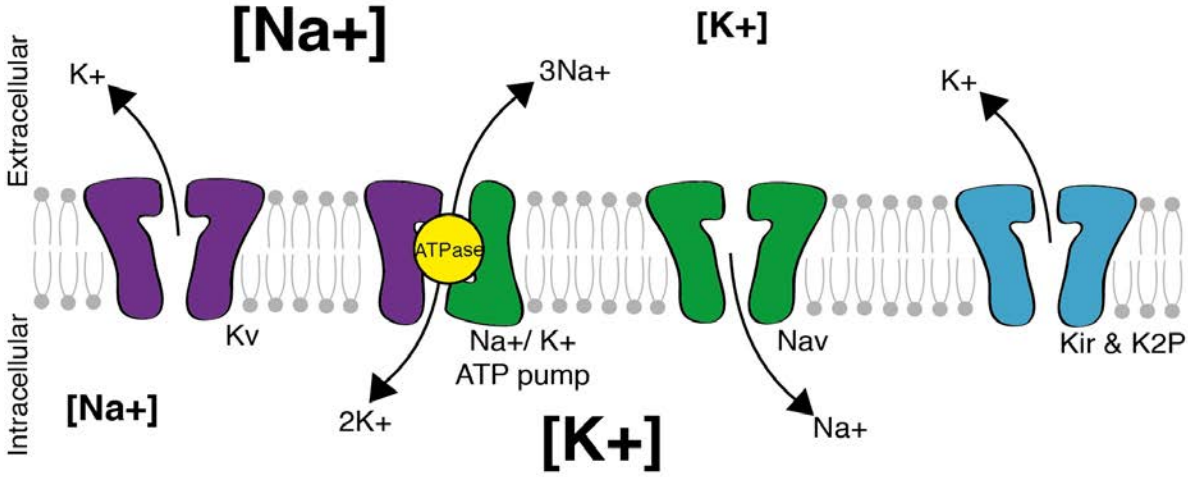


Figure 1.2: *Membrane embedded systems involved in determining the RMP and action potential. The Na^+/K^+ ATP pump (purple and green), Kir and K2P channels (blue) are major contributors to the maintenance*

While the ATP-driven Na^+/ K^+ pump is involved in establishing the K^+ concentration ($[K^+]$) gradient across the cell membrane, K2P and K_{ir} channels dissipate this gradient via efflux of K^+ out of the cell (Figure 1.2). In doing so K2Ps are involved in the control of the RMP, and thus the regulation of cellular excitability. The mechanism by which this is achieved is often refered to as 'background leak'; currents produced by channels that are constituitively open, simply facilitating the transition of K^+ ions out of the cell down their concentration gradient. Indeed, the characteristic near-linear current-voltage (I-V) relationship of some K2P channels under symmetrical extra- and intracellular $[K^+]$ is indicative of this behaviour

1.2.1 The physiology of K2P channels

However, because of their important role in determining the RMP of cells it is not surprising that all K2Ps exhibit polymodal regulation, suggesting that the channels are not simply constituitively open, but are instead strictly controlled. The range of K2P modulators is varied and includes intra- and extracellular pH, polyunsaturated fatty acids, volatile anaesthetics, temperature and membrane stretch as well as GPCR-mediated regulation. This wide range of regulatory inputs partly explains why K2P channels are thought to be involved in diverse processes such as taste and odour, through to immune response and apoptosis (Goldstein 2011).

As K2P channels are involved in a range of physiological processes, they may be of great importance as potential therapeutic targets (Mathie *et al.* 2007). Channelopathies and directed knock-out studies have shown K2Ps to be involved in conditions of both neuronal hyper- and hypoexcitability, ranging from migraine (Lafreniere *et al.* 2010) to a loss of thermosensation (Noël *et al*. 2009). Therefore, it is apparent that these channels must be both functionally expressed and carefully governed to maintain regular cell function. And so it follows that, as dysfunction of the channel leads to dysfunction of the cell, the K2P channel superfamily is a suitable therapeutic target, which makes the study of K2P channels of particular importance (Es-Salah-Lamoureux *et al.* 2010).

1.3 K2P channel subfamilies

Cloning and functional expression of K2Ps began with an atypical two-pore potassium channel (Tok1) isolated from budding yeast *S. cerevisiae* in 1995 (Ketchum *et al*. 1995). Tok1 was different from other K^+ channels known at the time in that it produced a novel, non-voltage-gated outward current. In addition, Tok1 also differed from other K^+ channels in structure as it was predicted to have a two-pore / eight-TM helix arrangement, where the pore helices lie between the TM5-TM6 and TM7-TM8 interfaces.

Exploration into mammalian K2P channels began with the identification of TWIK-1 (**T**andem of pore domains in a **W**eak **I**nward rectifying **K^+** channel) (Lesage *et al.* 1996). This is a K^+ selective channel which exhibits the attributes of a voltage-independent membrane imbedded pore showing Goldman-Hodgkin-Katz (GHK) rectification (Goldstein *et al.* 2005, Figure 1.3). The following decade saw a rapid rise in the number of known K2P channels, with an additional 14 mammalian K2P genes discovered. These have been divided into seven functional subfamilies (TWIK, TREK, TRESK, TRAAK, THIK, TALK and TASK) with an additional uncharacterised, silent channel encoded by the KCNK7 gene (Figure 1.4).

Nomenclature and categorisation of K2P channels has proven to be difficult. Misunderstanding has arisen by the asignment of multiple names for a single channel; TASK-1, for example, is also known

as TBAK1, OAT1 and *KCNK3.* In addition, many channels are classed together, though only because they initially seemed to share functional attributes which were later shown to be inconsequential or inaccurately assessed (e.g. TASK-2 channels as alkaline sensitive channels). Moreover, channels with similar functional attributes from nonhomologous genes makes the nomenclature of K2P channels extremely complicated; TASK-1 is encoded by *KCNK3* gene, while TASK-2 and -3 are encoded by *KCNK5* and *KCNK9*, respectively. For simplicity, K2P channels are herein described using the conservative name from the majority of published scientific literature (i.e. names beginning with 'T'), with gene names (*KCNK*) and more contemporary names (e.g. K2P1.1) given within parentheses.

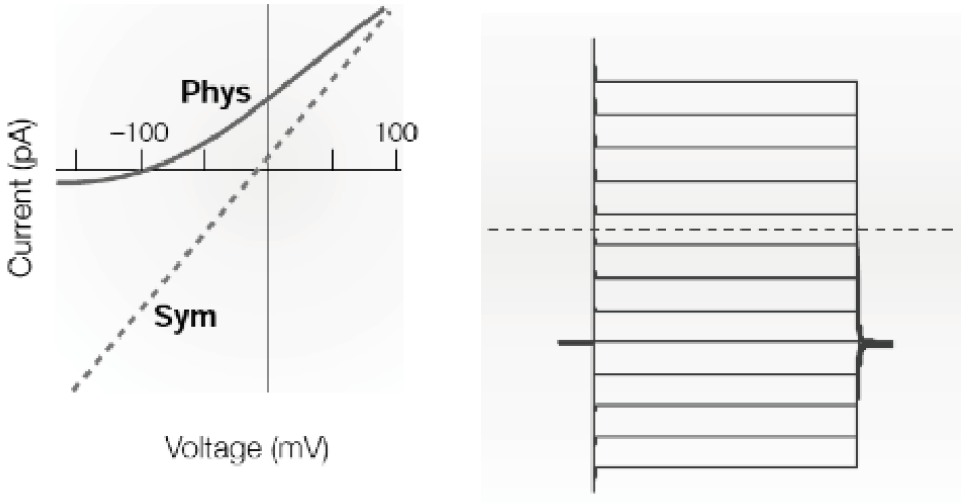


Figure 1.3: *Two representations of an ideal K2P channel current-voltage relationship. (Left) The current-voltage curve under physiological (phys, solid line) and symmetrical (sym, dashed line) [K^+] conditions. (Right) Symmetrical [K^+] conditions, with an absence of inhibitory or blocking agents (e.g. divalent cations) produces a near-linear open rectification in K2P channels (adapted from Goldstein et al. 2001).*

1.3.1 TWIK channels

TWIK-1 (also known as KCNK1, K2P1.1, hOHO) is a weak open rectifier have a single-channel conductance of approximately 32pS. These channels are proposed to be regulated primarily by the small ubiquitin-related modifier protein (SUMO-1); removal of the SUMOlation site lysine 274 by mutation has been reported to increase currents significantly, which is imporatant for electrophysiological study of these channels given the small conductance of the wild type channel

(Rajan *et al.* 2005). However, the effects of TWIK-1 SUMOlation is highly controversial, as some studies report no biochemical evidence of this process (Feliciangeli *et al.* 2010).

TWIK-1 is also mildy sensitive to inhibition by extracellular protons (< pH 6.7), thought to be due to a titratable histidine residue in the first pore loop (Rajan *et al.* 2005). In addition, these channels are also inhibited by intracellular acidification and protein kinase C, though possibly due to an off-target effect rather than direct modification of the TWIK-1 channel (Lesage *et al.* 1996).

TWIK-2 channels are considerably less well-understood due to their near-absent functional expression in conventional electrophysiological expression systems. Interestingly, both members of the TWIK subfamily are widely distributed; TWIK channels have been found in the brain, heart, lung, kidney, liver and placenta (Goldstein *et al.* 2005).

KCNK7 (K2P7.1) is also thought to encode a TWIK-like K2P channel, though the product of this gene has not yet been shown to form a functional channel (Salinas *et al.* 1999). Five splice variants have been identified in the human brain and retinal tissue, as well as being found in rats and mice, though a discernable function for these channels is yet to be established (Goldstein *et al.* 2005).

1.3.2 TASK channels

The TASK channel subfamily is the largest K2P subfamily with five members. TASK (**T**WIK-related **a**cid-**s**ensitive $\mathbf{K}^+$) channels show exteme sensitivity to variations of extracellular, but not intracellular, pH within the physiological range (Bittner *et al.* 2010). TASK-1 (*KCNK3*, K2P3) is inhibited most potently by changes in extracellular pH (pK = 7.1) in comparison with its most structurally and functionally close relative TASK-3 (pK = 6.7). The two channels also differ in that TASK-1 exhibits an instantaneously activating and non-inactivating K^+ current, close to the predicted form of an ideal GHK leak channel, while TASK-3 (*KCNK9*, K2P9.1) current are both non-instantaneous and time-dependent (Bittner *et al.* 2010).

These two channels also differ in their single channel conductance – considerably larger in TASK-3 (27pS) than TASK-1 (10pS) – and tissue distribution; TASK-1 channels are widely expressed in the brain, heart, lung, kidney, intestines, pancreas, prostate, uterus and placenta, while TASK-3 channels are rarely found outside the CNS (Goldstein *et al* 2005, Enyedi and Czirjak 2010). The widespread central distribution of both these channels makes gene knockout studies problematic and, while TASK-3 has been implicated in epilepsy and tumour growth, the role(s) of these channels in both healthy and diseased tissue has not yet been fully resolved (Pei *et al.* 2003, Holter *et al.* 2005).

Where TASK-1 and -3 channels are similar, beyond the 55-60% conserved sequence, is in modulation by the 14-3-3 protein, which is essential for forward trafficking of both proteins (Talley *et al*. 2000). Given their varied function and distribution, it is curious that TASK-1 and 3 are able to form the only reported successful K2P heterodimer in native tissue (La *et al.* 2006).

TASK-5 (*KCNK15*, K2P15.1) is the most recently discovered mammalian K2P gene in the TASK family. However, the classification of TASK-5, along with TASK-2 and TASK-4, as TASK channels is controversial as acid-sensitivity doesn't appear to be the most prominent feature of these channels. The function of TASK-5 channels remains a mystery as currents have not yet been observed in either mammalian cell lines nor *Xenopus laevis* oocytes, despite being present at the membrane (Ashmole *et al*. 2001).

1.3.3 TALK channels

Re-examination of the functional proerties of TASK-2 channels resulted in its redefinition as a member of a novel K2P channel subfamily 'TALK' (**T**wik-related **al**kaline pH-activated $\mathbf{K}^+$ channel) subfamily. Unlike TASK channels, TALK channels are near-inactive at physiological pH and are opened by external alkalinisation (Niemeyer *et al.* 2010). TASK-2 (*KCNK5,* K2P5.1) is expressed in the kidney, pancreas and liver, and in small quantities in the nervous system (Talley *et al.* 2001), though TALK channels are thought to be mainly involved in cellular function outside the nervous system. These

processes include bicarbonate reabsorption in the kidney, pancreatitis and pulmonary arterial smooth muscle activity (Duprat *et al.* 2005, Niemeyer *et al.* 2010).

Lke TALK-1 (*KCNK16*, K2P16.1), TASK-2 has been found to be sensitive to inhibition by extracellular pH within the range pH 7.5 and 10 (Enyedi and Czirjak 2010). The threshold for TALK-2 (TASK-4, *KCNK17*, K2P17.1) pH sensitivity is notably more alkaline, meaning it differs from other channels within the TALK subfamily. However, TALK-2 channels do observe an important TALK family characteristic; external pH alters the opening frequency of TALK channels, rather than current amplitude (Decher *et al.* 2001, Kang *et al.* 2004). In addition, all TALK channels conduct currents which exhibit near-linear rectification in symmetrical [K^+] (Morton *et al.* 2005).

1.3.4 THIK channels

THIK (**T**andem pore domain **h**alothane-**i**nhibited $\mathbf{K}^+$ channel) channels are a small class of K2Ps which are heavily regulated by the volatile anaesthetic halothane and while other K2Ps show limited sensitivity to halothane, the THIK channels are inhibited, not activated, by the application of halothane (Rajan *et al.* 2001). However, despite their halothane-sensitivity, the clinical relavance of THIK-1 channels in halothane-mediated anaesthesia remains unclear. Interestingly, the THIK family members appear to lack of sensitivity to moderate intra- or extracellular pH, temperature and lysophospholipds, which are common modulators of most other K2P channels (Enyedi and Czirjak 2010).

THIK-1 (*KCNK13*, K2P13.1) and THIK-2 (*KCNK12*, K2P12.1) are believed to be widely distributed throughout the nervous system and major organs, though THIK channels are relatively uncharacterised in native tissue, owing to a lack of significant expression or current amplitude for electrophysiological examination (Rajan *et al*. 2001). Nonetheless, THIK-1 has been found in Purkinje cells and regions of the cochlear nucleus following deafness (Bushell *et al*. 2002, Holt *et al.* 2006).

1.3.5 TRESK channels

The TRESK (**T**wik-**r**elated **s**pinal cord $\mathbf{K}^+$ channel) subfamily contains a single member channel. TRESK (*KCNK18*, K2P18.1) channels were originally thought to be acutely distributed in only the spinal cord neurons in humans (Sano *et al.* 2003), though subsequent studies have identified TRESK mRNA in the human brain (Liu *et al.* 2004) and T cells (Pottosin and Bonales-Alatore 2008). Moreover, the murine variant has been found in tissues as diverse as the testis and cerebellum (Enyedi *et al.* 2012). Curiously, the human and murine channels share such limited sequence homology (65%) that they were initially named TRESK-1 and TRESK-2, before being identified to be genuine orthologs of one another (Kang *et al.* 2004, Enyedi *et al.* 2012).

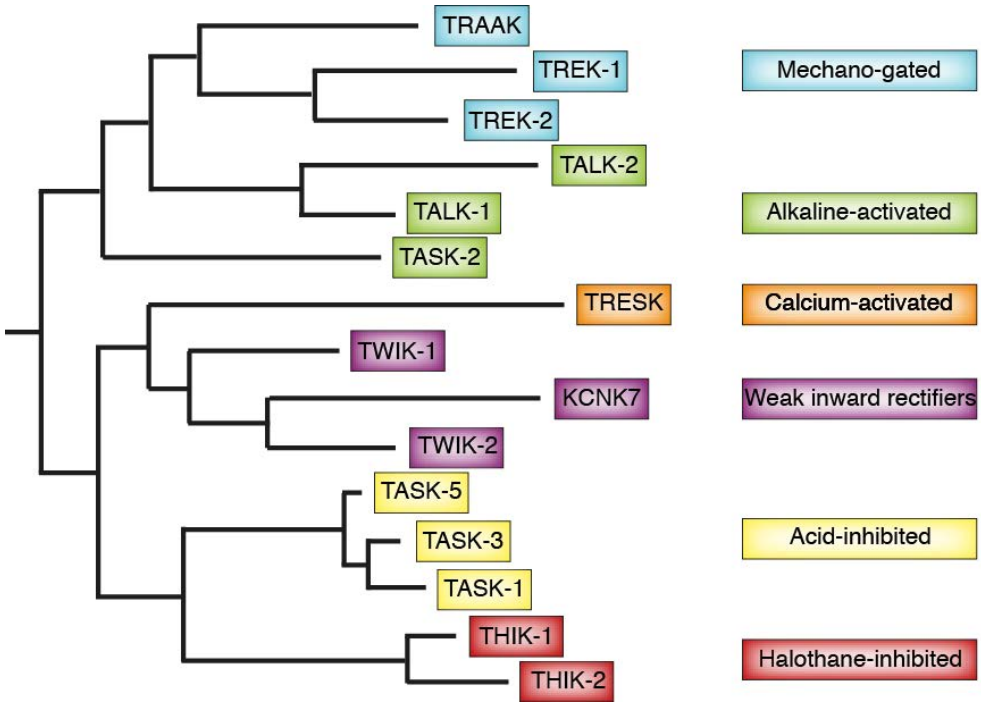


Figure 1.4: *The phylogenetic tree of human K2P channels. While there are argubly eight sperate K2P channel subfamilies, they can be grouped into 6 functional families, as indicated in the figure. In some cases, there is crossover, e.g. TREK-1 is alkaline-activated, though channel subtypes are grouped here by their most dominant and/or unique characteristic. Adapted from Honoré 2007*

The most striking feature that distinguishes TRESK from other K2Ps is its unique single channel activity; the channel exhibits a peculiar asymmetrical gating behaviour producing square, wave-like openings at depolarised membrane potentials, but bursts of short openings at hyperpolarised membrane potentials (Sano *et al.* 2003). Stimulated by calcineurin following Gqα-receptor activation,

TRESK channels appear to be involved in calcineurin inhibitor-induced pain syndrome (Mathie 2007). Futhermore, a recently identified dominant-negative frame shift mutation in TRESK has been associated with migraine with aura. This mutation produces a truncated channel which coassembles with normal TRESK subunits to downregulate channel activity (Lafrenière *et al.* 2011). However, the association with migraine is complex and recently other dominant-negative TRESK variants have been identified which show no association with migraine with aura (Andres-Enguix *et al.* 2012).

1.3.6 TREK channels

Discovered in 1996, The TREK family (**T**WIK-**re**lated $\mathbf{K}^+$ channel) exhibits one of the most versatile patterns of regulation known for any class of ion channel. Indeed, TREK-1 (*KCNK2*, K2P2.1) and TREK-2 (*KCNK10*, K2P10.1) are gated by intra- and extracellular pH, temperature, mechanical stress, polyunsaturated fatty acids (e.g. arachidonic acid), volatile anaesthetics and a variety of other chemicals (Honoré 2007). Moreoever, the role of selective serotonin reuptake inhibitors (SSRIs), such as fluoxetine and norfluoxetine, in regulating channel function appear to be important as TREK channel modulation occurs at clinically relevant concentrations (Eckert *et al.* 2011, Moha ou Maati *et al.* 2011). Given the abundant distribution of these channels in regions of the brain linked to cognitive and emotional dysfunction symptomatic of clinical depression, the study of fluoxetine as a TREK-1 modulator is of particular interest (Kennard *et al.* 2005, Heurteaux *et al.* 2006, Eckert *et al.* 2011).

TREK-1 channels conduct a large outward-rectifying, instantaneous and inactivating current (Fink *et al.* 1996) and exhibit a high single channel conductance (>90pS) (Goldstein 2005). Two independent mechanisms are believed to be responsible for the deviation from of TREK-1 currents from the ideal leak conductance as predicted by the GHK equation. Extracellular divalent cations (such as Mg^{2+}) are believed to block inward currents at progressively more negative membrane potentials (Maingret *et al.* 2002). The mechanism of binding or modulation by extracellular Mg^{2+} is, as yet, unresolved. However, it has been suggested that extracellular Mg^{2+} regulates inward TREK K^+ currents by the same method through which intracellular Mg^{2+} regulates outward currents in K_{ir} channels (Enyedi and Czirjak 2010).

In addition, TREK-1 has a unique property among K2P channels in that it is highly voltage-dependent. In single channel recordings, regular bursts of TREK-1 activity at positive membrane potentials, the rate of which is significantly reduced to become more sporadic at negative potentials, limiting inward current (Bockenhauer *et al.* 2001).

TREK-1 is acutely distibuted, predominantly in the heart and brain, though deletion or silencing of the *KCNK2* gene has profound effects on healthy cellular function. Most notably, *KCNK2* deletion in mice results in a loss of sensitivity to general anaesthetics and a depression-resistant phenotype (Heurteaux *et al.* 2004, Heurteaux *et al.* 2006). In addition, TREK-1 may also have a role in neuroprotection following ischemic injury (Buckler and Honoré 2005).

By contrast, the physiological role of TREK-2 is relatively unknown despite its widespread distribution in the kidney, pancreas, prostate, thymus, liver and heart (Gu *et al.* 2002). TREK-2-like channels are found in cerebellar granuar neurons and magnocellular neurosecretory cells in the rodent thalamus, as well as insulin-secreting MIN6 cells in mice (Han *et al.* 2002, Kang *et al.* 2004). While this suggests that TREK-2 may be specifically involved in regulating cellular excitability of secretory / glandular tissue, current evidence is inconclusive.

A third member of the TREK family, TRAAK (**T**WIK-**r**elated **a**rachidonic **a**cid activated $\mathbf{K}^+$ channel, *KCNK4*, K2P4.1), is arachadonic acid and mechano-sensitive (Fink *et al.* 1998). Furthermore, TRAAK and TREK channels share other modulatory inputs such as extracellular pH sensitivity. This is most likely due to a relatively high amino acid sequence conservation; human TREK-1 / TRAAK, TREK-2 / TRAAK and TREK-1 / TREK-2 sequence conservation is approximately 39%, 40% and 57%, respectively. This shared homology is highly uncommon for K2P channels, as conservation across members of the same subfamily can be as low as 35% (Fink *et al.* 1998). However, all members of the TREK family are able to achieve tissue-specific functional divergence either through splice variants and / or alternative translation initiation sites, which suggests a fine tuning of TREK / TRAAK channels for specific cellular functions (Thomas *et al.* 2008).

1.4 K2P structure

Mammalian K2P channels are immediately recognisable by their unique structure in contrast to other K^+ channels; K2P channels comprise two subunits combined around a central K^+-conduction pathway, as a 'dimer of dimers' (see figure 1.1). In other classes of K^+ channel, such as voltage-gated K^+ channels, four homologous subunits each contribute a single pore forming α-helix (e.g. Taglialatela *et al.* 1994, Schulteis *et al.* 1996, Raab-Graham and Vandenberg 1998). A single K2P subunit consists of an intracellular amino (N) terminus, four TM-helices (TM1-4) a carboxyl (C) terminus and two pore forming helices, within each pore-forming loop (PH1 and PH2) (Figure 1.5).

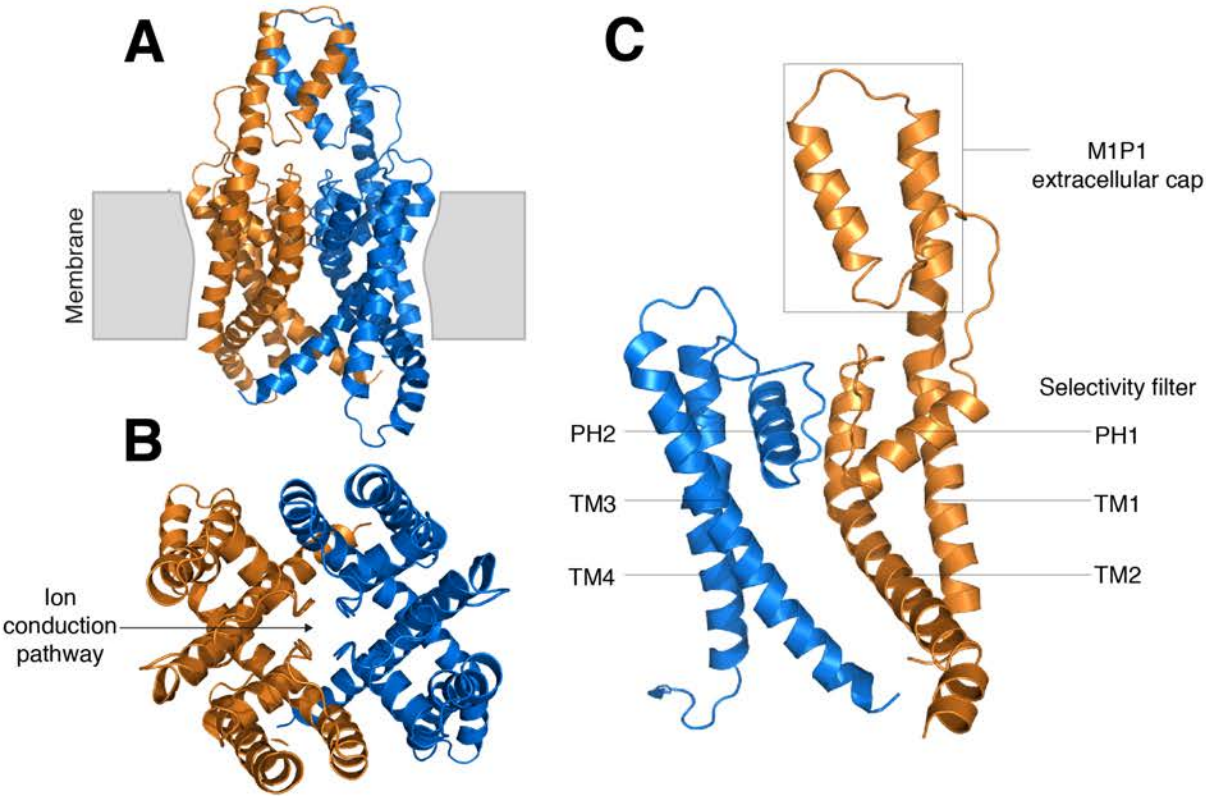


Figure 1.5: *K2P channel structure illustrated using a TREK-1 homology model based on TWIK-1 (3UKM) and TRAAK (3U7M) structures. In all figures, monomers are shown in separate colours (subunit 1, orange; subunit 2, blue). (**A**) Side profile of the K2P channel within predicted membrane position (grey) and relative orientation. (**B**) A top-down view of the model, with extracellular cap removed for greater visibility of the ion conduction pathway. (**C**) TM1-2 from subunit 1 and TM3-4 from subunit 2 form half of the functional channel. Key features of the two subunits are labelled. Model courtesy of Mr. M. R. Schmidt, SBCB, Oxford.*

When the initial experiments for this thesis were conducted, in 2009, there were no crystal structures available for K2P channels. As a result, our understanding of K2P structure was initially founded upon

homology models based on prokaryotic K^+ channel crystal structures of KcsA (pdb code: 1BL8, Doyle *et al.* 1998) and KvAP (1ORS, Jiang *et al.* 2003). However, in early 2012, two K2P channel crystal structures, TWIK-1 (3UKM, Miller and Long 2012) and TRAAK (3UM7, Brohawn *et al.* 2012, Figure 1.5), were solved and so were used for our later studies, reported in chapter five and onwards.

Argubly the most striking characteristic of the K2P crystal structures is the presence of a unique α-helical-cap, above the selectivity filter. This cap was previously predicted for TASK channels (Yuill *et al.* 2007) and extends as a helix from TM1, enters an unordered region at its peak, before refoming an α-helix leading down to PH1. It is believed that the M1P1 extracellular cap, seen clearly in figures 1.5 and 1.6, is given structural stability due to highly conserved cysteine disulphide-bonding at the top of the cap (Brohawn *et al.* 2012).

However, the extracellular cap clearly presents a logistical problem to the flow of ions through the channel and it is proposed that ions are able to permeate the extracellular vestibule through a small fenestration close to the extracellular interface of the channel, as shown in figure 1.6 (Miller and Long 2012).

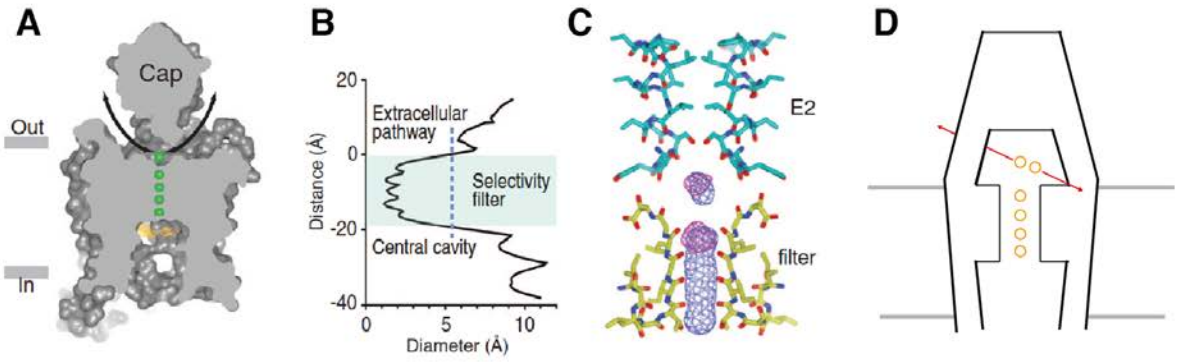


Figure 1.6: *Extracellular ion pathway. (**A**) cutaway view of the molecular surface of TWIK-1 (gray). K^+ ions shown as green spheres. Orange mesh depicts electron density assigned to alkyl chains. (**B**) Diameter of the pore (separation between van der Waals surfaces) as a function of distance along the ion conduction pathway. A dashed line indicates the diameter of a K^+-H_2O complex. (**C**) Ion binding in the extracellular pathway. Amino acids of the selectivity filter (yellow) and extracellular cap (cyan). (**D**) Cartoon depiction of the bifurcated ion pathway created by the K2P helical cap. Figure A – C and accompanying text adapted from Miller and Long 2012. Image D and text adapted from Brohawn et al. 2012.*

A significant 90˚ kink in the fourth transmembrane helix was also identified in the TWIK-1 structure, causing the helix to run parallel to the cell membrane (Miller and Long 2012). By contrast, the TRAAK crystal structures do not conserve such a sharp kink of the helices; TRAAK channels posess a gradual bend of the helix conferring significant flexibility of the TM4 helix (Brohawn *et al.* 2012). It is possible that the difference in the helical kink / bend in the two structures is due to a crystallisation artefact of the TWIK-1 structure. However, it may be that both structures are valid representations of the two distinct K2P channels, given the low homology between these two K2P subtypes.

1.5 K^+ selectivity in K2P channels

Conventionally, the T-*X*-G-Y/F-G selectivity filter is thought to confer K^+ selectivity in other K^+ channels. Selectivity for K^+ ions has previously been explained by the prevailing 'Goldilocks hypothesis'; the dimensions of the conduction pathway are too small to facilitate the passage of larger ions, too large to coordinate smaller Na^+ ions, but are able to mimmick the structural chemistry of the K^+-ion inner hydration shell and satisfy the energetic cost of its dehydration (Morais-Cabral *et al.* 2001, Goldstein 2011). The Goldilocks hypothesis for selectivity is based upon the assumption that proteins are at a constant, fixed position and does not account for the likely thermal fluctuation of the filter. However, molecular dynamics simulations show that the selectivity filter is able to undergo conformational changes dramatic enough to permit Na^+-ion permeation (Bernèche and Roux 2005). Therefore, it appears that K^+ channels employ a flexible selectivity filter that dynamically selects K^+ ions for permeation.

In all other forms of K^+ channel the filter is four-fold symmetrical. However, K2P channels encode a complex, asymmetric signature sequence (P1, T-I/T/V-G-Y/F-G; P2, T-I/V-G-F/L-G) and it has been proposed that mechanisms for selectivity and gating may be slightly altered (Goldstein 2011). Indeed, the side chain variation may affect the conserved backbone carbonyl oxygen atoms, which make up the K^+ binding sites in the selectivity filter (Figure 1.7). Interestingly, it has been suggested that alternative translation in some K2P channels contribute to ion selectivity (Thomas *et al.* 2008).

The permeability ratio for Na^+ over K^+ (P_{Na}/P_K) is <0.03 for TREK-1 channels compared to ~0.001 in other K^+-selective channels (Hille 2001, Honoré 2007, Ma *et al.* 2011). Nevertheless, while this represents a more than 10 fold increase in Na^+ permeability, given the K^+ gradient across the membrane, and the distinct favourability for K2Ps to conduct K^+ over Na^+, the significance of marginally increased Na^+ permeability in native tissues is questionable. Indeed, a recent study suggests that only in cases of extreme pathological hypokalemia can Na^+ leak currents permeate K2P channels (Ma *et al.* 2011)

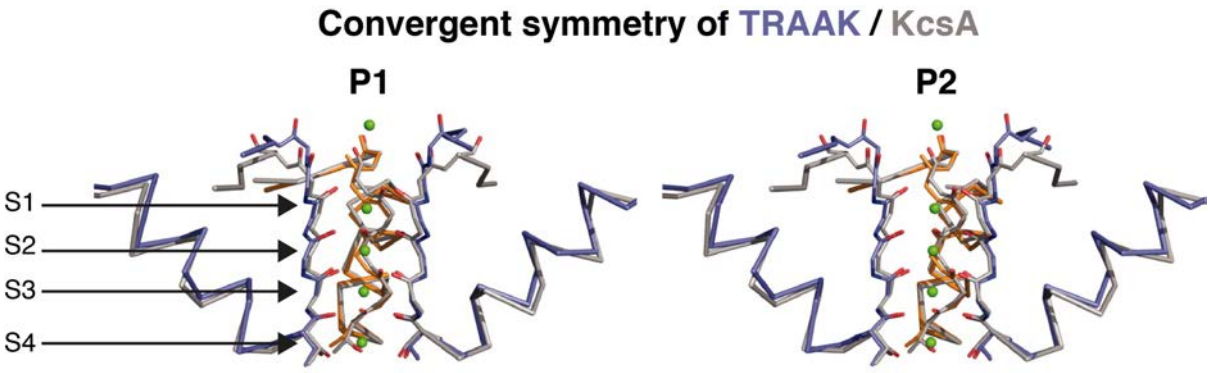


Figure 1.7: *Convergent symmetry of TRAAK / KcsA PHs and selectivity filters. Pore helices are shown as wires and selectivity filters as backbone sticks. TRAAK pore domain 1 is blue, TRAAK pore domain 2 is orange, and KcsA is gray, with backbone carbonyl and threonine hydroxyl oxygen atoms from selectivity filter residues shown in red. K^+ ion (green spheres) binding sites S1-S4 are indicated. Figure and text adapted from Brohawn et al. 2012.*

1.6 K2P gating

In order for ion channels to control the flow of ions through the conduction pathway, channels must open and close in response to a host of biological or chemical signals; whether due to a change in membrane potential, enzymatic modification or interaction with regulatory agents. The opening and closing of a channel involves a change of conformational state and is described as gating. The mechanism by which a channel is gated usually requires small movements, as little as a few angstrom, increasing the accessibility of ions to the conduction pathway.

In general, K^+ channels are believed to contain three possible sites for gating and control of channel function. One gating mechanism seen in larger K^+ channels is the 'ball and chain' or N-type gating (Yellen *et al.* 2002). This involves an auto-inhibitory peptide sequence, known as the N-terminal (or associated β subunit) inactivation domain, which blocks the channel shortly after activation (Hoshi *et*

al. 1990). Fast acting and self-regulatory, N-type inactivation is an effective and efficient method of channel gating. However, this mechanism is not possible for K2P channel gating as it requires the N-terminal peptide domain, which is not present in K2P channels (Bockenhauer *et al.* 2001). Instead K2P channels must gate at one, or both, of the other two reported gating mechanisms in other K^+ channels; the lower- and upper-gates (Figure 1.8).

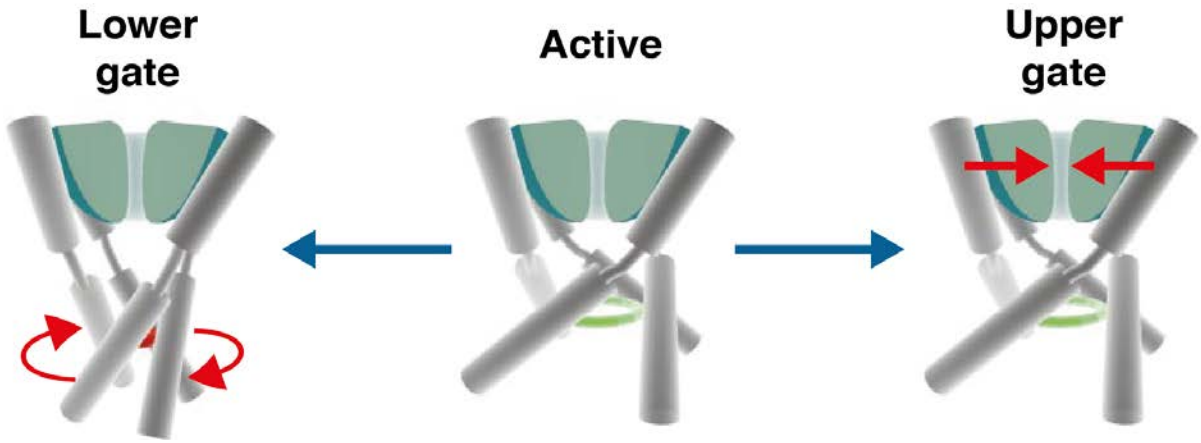


Figure 1.8: *The proposed gating mechanisms for K2P channels on the basis of the MthK structure. The selectivity filter (green) is shown with a cutaway to reveal the narrow pore. In the active state these are splayed apart. Movement of the lower pore lining helices (i.e. below the glycine hinge) shown in red, results in inactivation of the channel. Similarly, a pinching shut of the selectivity filter (teal) is responsible for upper-gating of K^+ channels. Figure adapted from Yellen 2002.*

1.6.1 The lower-gate

The lower- or helix-bundle crossing (HBC) gate is commonly seen in a number of ion channel subtypes, including K_{ir} channels (e.g. Xiao *et al.* 2003). Following the modelling of the motion between the closed-state KcsA and open-state MthK structures, it has been proposed that gating by the TM helices involves a change in conformation from a straight formation (in which the conduction pathway is constricted) to a bent form, via an aperture-like motion near the intracellular interface, causing the helices to splay open to a diameter of about 12Å (Jiang *et al.* 2002).

It has been previously shown that a degree of flexibility provided by a conserved glycine residue in the pore lining helices (G83 in MthK, G99 in KcsA, G166 in K_{ir}1.1), which confers a bend in the helix

serving the aperture-like gating motion of these helices (Figure 1.9) (Jiang *et al.* 2002, Sackin *et al.* 2006, Rapedius *et al.* 2007).

K2P channels also contain conserved glycine residues in pore-lining TM helices TM2 and TM4 (G142 and G248, resepectively, in TWIK-1), in theory providing the required flexibility for HBC-like gate in K2P channels (Appendix IV) (Kollewe *et al.* 2009). Interestingly, alanine substitution of homologous glycine residues in TASK-3 channels results in a significant alteration to wild-type channel function, suggesting that these residues are important to channel gating (Ashmole *et al.* 2009). In addition, a *Drosophila* K2P channel (KCNK0) chimera was able to gate via a lower-gating mechanism, which showed that K2P channel activity can be regulated in this region (Ben-Abu *et al.* 2009). However, in this case only a single pore domain from KCNK0 was fused to the voltage sensor domain of the *Shaker* channel.

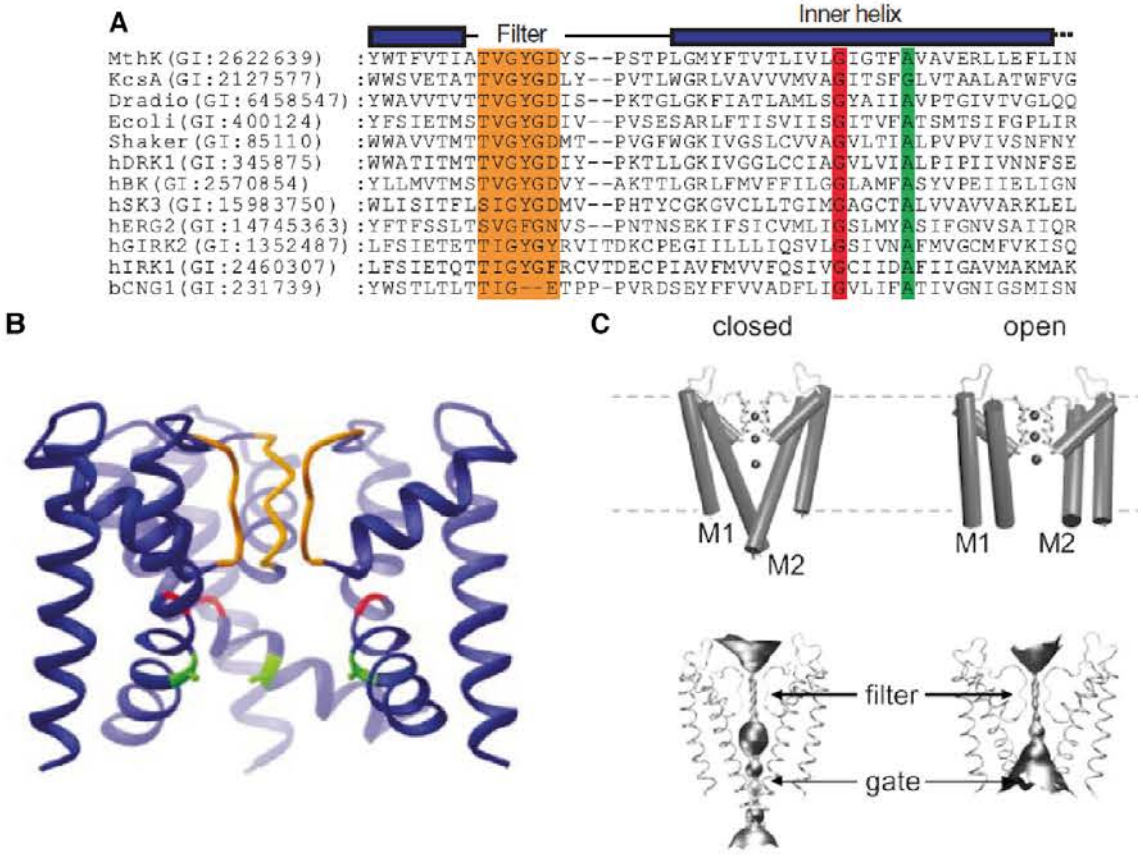


Figure 1.9: *Structure-based sequence analysis suggests conserved gating conformations. (**A**) Sequences from the inner helices of various K^+ channels and a CNG channel. The selectivity filter is coloured orange, the gating hinge glycine red, and the amino acid at the narrowest point of the MthK intracellular pore entryway, green. Protein ID numbers are indicated in parentheses. (**A**), Three subunits of the MthK pore with colours corresponding to '**A**'. (**D**) Comparison of the closed- and open-*

state in KcsA. Cyndrical representation (top) and Cα trace plus the pore lining surface (bottom) of the closed-state KcsA structure (left) and open-state KcsA model (right).
Figures A - B and text adapted from Jiang et al. 2002, Figure C and text adapted from Holyoake et al 2004.

Therefore, the extent to which a lower-gate operates in native, mammailian K2Ps is still unclear and recent studies would suggest that this gate is constituitvely open (Piechotta *et al.* 2011), which is supported by observations made based on the currently available K2P channel crystal structures. In particular, the 90˚ kink shown in TM4 of the TWIK-1 crystal structure means that movement of this TM helix may be severly restricted, which may mean that the channel is unable to gate lower down the helices. However, as the structures for TWIK-1 and TRAAK are both in the open conformation, and the movement of the helix may be lateral, the presense of a HBC-like lower gate in mammalian K2Ps cannot be ruled out.

1.6.2 The upper-gate

The third and final gating mechanism previously described for K^+-selective ion channels is the upper-gate which operates by C-type inactivation at the selectivity filter. C-type inactivation involves subtle movements at the selectivity filter narrowing the ion permeation pathway at one (or more) of the K^+ contact sites (S1-4, figure 1.7), locking K^+ ions at the selectivity filter and halting any intra- or extracellular ionic movement (Cuello *et al.* 2010). The flexibility of the selectivity filter is key to this kind of gating, though because of the miniscule scale of movement, changes of conformation would not be resolved in crystal structures which do not have a high enough resolution. Nonetheless, experimental evidence points towards the presence of C-type gating in mammailian K2P channels (Zilberberg *et al.* 2001, Morton *et al.* 2005, Niemeyer *et al.* 2006, Cohen *et al.* 2008).

1.7 TREK-1 as a model of K2P channel function

K2P channels appear to be unique among ion channels in that the same regulator can have completely opposite effects on different K2Ps; volatile anaesthetics, for example, can open TASK-1 but potently inhibit THIK-1. Curiously, even within K2P subfamilies, different channels can respond to

the same modulatory input in completely different ways; e.g. TREK-1 and TREK-2 currents are inhibited or activated, respectively, by extracellular protons via a shared histidine residue (Sandoz *et al.* 2009). Despite this peculiar phenomenon, the structural similarity between two functionally diverse channels in TWIK-1 and TRAAK suggests that the movements required for gating may well be conserved. Indeed, a recent study has shown that gating apparatus is conserved across some K2P channel subfamilies (Bagriantsev *et al.* 2011).

TREK-1 is the most extensively studied K2P channel and, as much of the knowledge of how K2Ps gate is based on empirical evidence obtained by studying the TREK-1 channel, it is often refered to as the prototypical K2P channel. Furthermore, given the proposed role of TREK-1 in a range of disease states, highlighting it as channel that should be at the forefront of medical research. For these reasons, TREK-1 was chosen as the primary candidate for the focus of this study.

1.7.1 TREK-1 regulation by the C-terminal regulatory domain

A large number of regulatory inputs have been identified to modify TREK-1 channel activity including mechanical stress (Maingret *et al.* 1999), heat (Maingret *et al.* 2000), volatile anaesthetics and lysophospholipids (Patel *et al.* 1999), intracellular (Honoré *et al.* 2002) and extracellular acidosis (Cohen *et al.* 2008) and several drugs, including riluzole (Duprat *et al.* 2000), fluoxetine (Kennard *et al.* 2005) and spadin (Mazella *et al.* 2010). Moreover, while K2P channels generally show limited voltage sensitivity, TREK-1 conductance is highly voltage-dependent following phosphorylation of a serine residue in the C-terminus (Bockenhauer *et al.* 2001).

Indeed, the C-terminus appears to play a key role in regulating TREK-1 function. In particular, a small regulatory domain of several residues is responsible for sensitivity to a several forms of modulation. The proposed mechanism of gating at the C-teriminus involves interaction of the generally positively charged regulatory domain with the negatively charged phosphate headgroups of the inner leaflet lipid bilayer (Figure 1.10).

It is believed that the few negatively charged residues in and around the regulatory domain inteferes with any electrostatic interaction between the C-terminus and membrane bilayer. Neutralisation of these residues by protonation is thought to be responsible for activation of TREK-1 channels in response to decreased intracellular pH (Maingret *et al.* 2000). It is highly interesting that neutralisation of even a single glutamate residue within this domain, E321, via protonation or site-directed mutagenesis, leads to a channel with a constituitively active phenotype (Honoré *et al.* 2002). Movement of the cytosolic regulatory domain as a result of bilayer interaction may cause the protein as a whole to move, resulting in a change in conformation at one or both of the proposed lower- and / or upper-gates, activating the channel.

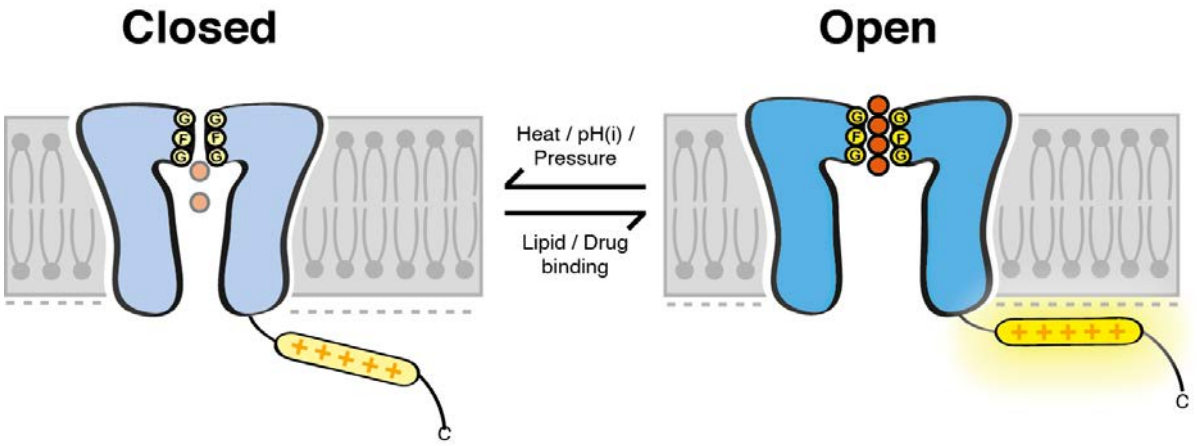


Figure 1.10: *Cartoon model of TREK-1 activation by intracellular modulation. Heat, mechanosensitivity and chemical regulation of these channels is believed to occur via modification of a C-terminal regulatory domain. Several regulatory agents are believed to alter this interaction between this positively charged domain and the negatively charged inner leaflet of the plasma membrane including temperature, internal proton concentration, stretch and agonist binding.*

Intracellular pH regulation of TREK-1 by E321

TREK-1 channels are activated by low pH to become constitutively active, leak channels (Honoré *et al.* 2002). Removal of the putative protonation site at residue E321 has a profound effect on channel function as a whole, particularly intracellular pH sensitivity (Honoré *et al.* 2002). While the surrounding charge cluster is critical for the channel's polymodal regulation by membrane stretch, for example, mutation of E321 to amino acids not carrying a negative charge can almost completely abolish pH sensitivity, even with an otherwise intact C-terminus (Honoré *et al.* 2002).

Lipid regulation of TREK-1

Both polyunstaurated fatty acids (PUFAs) and lysophospholipids are able to stimulate TREK and TRAAK channels, via the proximal C-terminus (Patel *et al.* 1998, Kim *et al.* 2001a, Kim *et al.* 2001b). Curiously, this region does not appear as important for channel regulation in TRAAK channel regulation, as it can be substituted by a homologous region of TASK-3 without a loss of fatty acid sensitivity (Kim *et al.* 2001b). Application of the archetypical PUFA in K2P activation, arachidonic acid, causes a delayed opening of members of the TREK-subfaimly. By contrast, lysophospholipids, such as lysophosphatidylcholine, act rapidly to induce stimulation of channel currents, though only when cells are kept intact; indeed, application of lysophospholipids to TREK-1 and TRAAK channels in the excised patch configuration is ineffective in altering channel function (Lesage *et al.* 2000, Maingret *et al.* 2000). Phosphatidylinositol-4,5-biphosphate (PIP_2) has also been shown to activate TREK-1 via the C-terminus (Rohács *et al.* 1999, Lopes *et al.* 2005).

TREK-1 activation by volatile anaesthetics

The importance of the TREK-1 C-terminal regulatory domain to gating and normal channel function is underlined by its importance in TREK-1 sensitivity to several drugs. Volatile anaesthetics, for example, activate several different K2Ps leading to decreased cellular excitability, though TREK-1 and -2 are unique in their modulation by a wide variety of different anaesthetics. Chloroform, diethyl ether, halothane and isoflurane, among others, have all been found to activate TREK channels (Patel *et al.* 1999). Moreover, because of the localisation of TREK-1 channels on GABAergic neurons, the role of these ion channels in responding to anaesthetics may well be clinically relevant. This is further emphasised by the role of volatile anaesthetics on affecting synaptic transmission and the subsequent identification of presynaptic TREK-1 channels co-localised with synapsin (Lauritzen *et al.* 2000). Indeed, the observation that additional anaesthetics including xenon, N_2O and cyclopropane, which are unable to affect $GABA_A$ receptor function, can be used to regulate cellular activity via TREK-1 channels and may prove highly valuable in a clinical setting (Gruss *et al.* 2004).

Phosphorylation of TREK-1

It has been proposed that the electrostatic repulsion caused by phosphorylation of key residues within the C-terminus is responsible for closing the channel. S348 is thought to be a key phosphorylation site for protein kinase A (PKA) and it is believed that following phosphorylation of this residue, channels are inactivated due to reduced interaction between the distal C-terminus and the membrane (Fink *et al.* 1996). Accordingly, S348D mutants, which mimick the phosphorylated state at the PKA consensus site, exhibited a notable reduction in activity (Bockenhauer *et al.* 2001), while S348A mutations lose sensitivity to changes in cyclic adenosine monophosphate (cAMP) concentration, required for PKA function and PKA-independent regulation of the channel (Liu *et al.* 2008).

S315, adjacent to the regulatory domain in TREK-1 channels is believed to be an alternative site for phosphorylation, by protein kinase C (PKC). The effect of PKC-mediated phosphorylation was lost following S315A mutants and mimicked by S315D mutation, though these effects were only seen following removal of the PKA phosphorylation site, S348. Furthermore, S315A / S348D mutations resulted in enhanced current density, while S315D / S348A mutations strongly diminished channel currents. Together, these findings validate a sequential phosphorylation model in which kinase activation drives modification at S348, enabling subsequent phosphorylation of S315 to inhibit channel activity (Mubartian *et al.* 2005).

While it appears that the cytosolic regulatory domain is well characterised, the mystery behind C-terminal regulation of the channel as a whole nonetheless remains, as the mechanism for transduction of cytosolic signals to the gate(s) and ion-conduction pathway is poorly understood. It is unclear if the movement caused by the C-terminus / bilayer interaction causes an aperture-like opening of the lower-gate or whether the lower gate remains open and signals are transduced to the upper-gate. Alternatively, the channel may gate by a combination of the two mechanisms, via a long range allosteric communcation between the two gates.

1.7.2 TREK-1 regulation by extracellular pH

Although modulation by the C-terminal regulatory domain has been extensively studied, less is known about the conformational changes during channel gating that occur close to the selectivity filter. The most examined regulatory input that appears to change channel function via the selectivity filter is extracellular pH. Other significantly proton-sensitive K2Ps are gated by a number proposed mechanisms. TASK-1 channels are closed upon protonation due to a histidine residue in the first pore domain, next to the selectivity filter (i.e. GYGH) (Lopes *et al.* 2001). By contrast, TASK-2 channels contain five charged residues in the M1P1 loop that are needed for pH sensitivity and neutralisation of these residues removed channel sensitivity to alkalinisation, stabilising the open-state conformation of the channel (Morton *et al.* 2005). A third mechanism, which superseded that mechanism, involves a highly-conserved positively charged residue near the pore sensing changes in pH. At neutral or acidic pHs, this residue (R244 in TASK-2, K242 in TALK-2) is thought to block the channel through an electrostatic effect on the pore. This effect is proposed to be alleviated by alkalinisation, resulting in opening of the channel (Niemyer *et al.* 2006).

Experimental evidence suggests that the TREK family has a conserved proton-sensing histidine residue – H141 and 152 in TREK-1 and 2, respectively – in the extracellular loop preceding PH1 (Sandoz *et al.* 2009). It is common for histidine to fulfil the role of proton sensor in a number of proteins (e.g. Adranga and Lauf 1998, Clarke *et al.* 2000, Thompson *et al.* 2008). Indeed, as histidine residues are uniquely titratable within the physiological range, this means that subtle changes in environmental pH can result in the side chains changing from being neutral to charged and vice versa (Betts and Russell 2003).

Curiously, the conserved histidine residue is responsible for activation of TREK-2 in cases of extracelullar acidification, while inhibiting TREK-1 channels under the same conditions (Sandoz *et al.* 2009). Structural modelling of this residue in two separate studies using KcsA-based TREK models suggested a role for the residue in controlling channel function via two mechanisms. The first suggests a similar molecular mechanism of pH sensing in KcsA channels (Thompson *et al.* 2008)

which involves a complex network of intrasubunit salt bridges and hydrogen bonds focused around the extracellular region of PH1, along with an additional histidine residue (H87) not conserved in TREK-2 channels (Cohen *et al.* 2008).

Alternatively, a more recent study suggested a different structure for the area surrounding residue H141 residue, changing the orientation of the residue. This means that protonated H141 residues instead interact with the PH2 / TM4 interdomain of TREK-1 channels (Sandoz *et al.* 2009). Nonetheless, both studies predict C-type inactivation due to a collapse of the external vestibule around the pore helices.

1.8 Overview of Thesis

The aim of this project as a whole was to address the question of how TREK-1 channels are gated. Our initial hypothesis was that these K2P channels is gated at both a lower, HBC-like gate and an upper-gate in, or close to, the selectivity filter. However, as more literature around the subject of TREK-1 gating became available our thinking was inevitably affected, meaning that our experiments in the later stages of this project were tailored towards confirming the presence and nature of a selectivity filter gate, while better understanding how this predominant gate is affected by movements of the lower-helix regions. The materials and methods we employed to do so are described in the following chapter. In addition, during the progression of our experimental work, several additional areas of interest were examined and reported in the appropriate chapter.

In chapter three, the generation of a library of mutations and the subsequent establishment of a genetic complementation assay for the identification of gain of function (GoF) mutants is described. These mutants were then dissected to isolate individual activatory mutations, which were mapped onto the homology models available at the time. Following this, the effects of these individual mutations on basal activity on pH sensitivity was studied. This is because we hypothesised that mutations which were able to complement would have an effect on both basal activty and either

external or internal pH sensitivity of the channel. The rational behind our thinking as well as the results is explained in more detail in chapter four.

The focus of chapter five is the characterisation of GoF mutants using the TREK-1 activators, diethylpyrocarbonate and BL-1249, as well as high extracellular K^+ concentration, in order to understand how these different GoF mutations affect channel activity. Here we hypothesise and determine the location of the diethylpyrocarbonate sensor of TREK-1.

In chapter six, the different regions proposed to be involved in channel gating are further dissected by making a range of additional mutations and testing their effects on channel function. In addition to this, we test and report some of our theories surrounding the dynamic nature of the selectivity filter gate, as well as the role of the TM helices in gating. Following this, in chapter seven, we present our gating model as well as proposing further experiments which may be instructive to support our hypotheses regarding TREK-1 channel gating.

Chapter 2

Methods and Materials

2.1 Molecular biology materials

2.1.1 Original genes, constructs and vectors.

Wild type TREK-1 clones from *Homo sapiens* and *Rattus norvegicus* were used directly or as templates to make new clones. New clones were made by either subcloning, random mutagenesis, site-directed mutagenesis and overlap-extension PCR (or a combination of these techniques).

Vectors employed were limited to the methionine regulated yeast-bacterial shuttle vectors pYES2m and p416met25, as well as *Xenopus laevis* oocyte expression vectors pGEM-3Z and pBF.

2.1.2 Enzymes

Restriction and DNA polymerase enzymes were purchased from Promega, New England Biolabs or Fermentas, unless otherwise stated. Enzymes were used in accordance with the manufacturer's instructions with their supplied with x 10 reaction buffer.

2.1.3 Kits for purification, mutagenesis and *in vitro* transcription

Kits purchased from Qiagen:

- QIAprep Spin kit – for rapid isolation of plasmid DNA.
- QIAquick PCR purification kit – for cleaning DNA following enzymatic reactions.
- QIAquick Gel Extraction kit – for gel purification of restriction digests.
- QIAEXII Gel Extraction System – for high yield gel purification of restriction digests.
- RNAeasy Mini kit – for purification of mRNA.

Kits purchased from other suppliers:

- GeneMorph II Random mutagenesis kit (Stratagene) – for unbiased random mutagenesis.
- mMessage mMachine T7 kit (Ambion) – for *in vitro* transcription of mRNA from linear DNA with a T7 promoter sequence.
- mMessage mMachine SP6 kit (Ambion) and AmpliCap SP6 message maker kit (Cambio)- for *in vitro* transcription of mRNA from linear DNA with an SP6 promoter sequence.

All protocols involving these kits were derived from their respective manuals and are shown in Appendix I.

2.1.4 Oligonucleotides

All oligonucleotides were purchased in dry form (Sigma-Aldrich) and were resuspended to 100μM using molecular biology grade H_2O (Lonza).

2.2 Molecular biology methods

2.2.1 Random mutant library construction

The 'GeneMorph II Random Mutagenesis' protocol was used to perform random mutagenesis of the wild-type *KCNK2* gene, in order to create random mutant libraries. Primers were designed to amplify the gene to be mutated from each direction, also adding a restriction site to either end of the gene. 100ng of template DNA was found to yield a high number of mutants in the final screen, each containing 1-3 mutations per gene.

PCR products were then cloned into either pYES2m or p416met25 using HindIII and XhoI.

2.2.2 Gel electrophoresis

DNA, whether isolated following propogation in *E.coli*, restriction digest or PCR was loaded into the wells of a 1% (w/v) agarose gel. Gels were made using analytical grade agarose (Promega) in tris-acetate-EDTA (TAE) gel buffer (Fisher Scientific). 0.5 μg/ml ethidium bromide (Promega) was added for visualisation of DNA.

DNA was loaded into gels after mixing with 10x loading buffer (Qiagen). The loading buffer contained glycerol, TAE, deionised H_2O, bromophenol blue and xylene cyanol, and was supplied by Promega.

Agarose gels were placed in electrophoresis tanks (BioRad) and ran for approximately 30 minutes, at 110 mV and 100 mA. Following electrophoresis, the agarose gel was visualised over an ultra violet light (BioDoc-it, UVP).

2.2.3 Gel extraction

In most cases, the 'QIAquick gel extraction kit' was used to purify the excised gel segment. However, for experiments where a particularly high yield of DNA was needed, the 'QIAEXII gel extraction system' was implemented. The final product was eluted in molecular biology grade H_2O.

2.2.4 Ligation

T4 DNA ligase (Promega / New England Biolabs) was used to join DNA fragments together following restriction digests. Typically, ligation reactions were performed for a minimum of three hours at 18˚C.

In vivo ligation using modified yeast cells was also utilised for this study, for ligating random mutant libraries into the yeast expression vectors, p416met25 and pYES2m. This method involves transformation of DNA fragments into yeast cells at an optimised concentration and ratio, allowing DNA repair mechanisms in yeast to recombine the DNA, without added ligase (Prado and Aguilera 1994).

2.2.5 Site-directed mutagenesis

Site directed mutagenesis involves annealing two synthetic oligonucleotides encoding the desired mutation to a DNA template (typically human or rat TREK-1), followed by amplification of DNA by thermocycling. Dpn1 enzyme was added to the PCR solution following amplification, to digest any methylated or hemimethylated DNA (a marker of cell division which is only found on template DNA). The mutated plasmids were then purified (DNA purification, appendix I) and transformed into *E. coli* for propagation (section 2.3.2).

2.2.6 Extension overlap PCR

Extension overlap PCR was used for inserting or deleting fragments of DNA from a plasmid or gene. Briefly, this method requires the creation of two short fragments of the mutated gene, by PCR, which are then rejoined by an additional PCR (figure 2.1). This longer fraction can then be digested and subcloned as previously described.

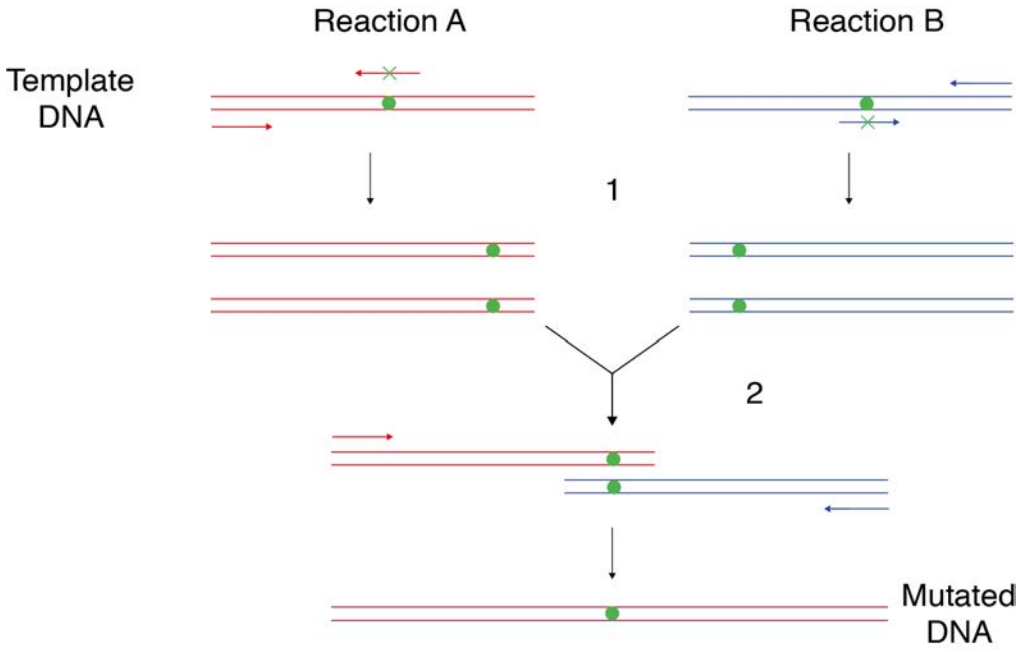


Figure 2.1: *A schematic diagram of the extension overlap PCR technique for site directed mutagenesis. Two different fragments of the same gene were amplified in separate PCRs, reactions A and B. The primers, signified by small red and blue horizontal arrows, encoded the mutation (green cross) and template start (reaction A) or stop (reaction B) codon. Step 1 results in the amplification of gene fragments. Step 2 combines the two products using a further PCR. The complementary strands were allowed to anneal during this stage resulting in a longer fragment (purple), which could be cloned into the expression vector of choice.*

2.2.7 mRNA transcription

In vitro transcription was used to produce messenger RNA (mRNA) for expression in *Xenopus oocytes* and subsequent electrophysiological study. mRNA transcription begins with the subcloning or mutagenesis of TREK-1 genes in a *Xenopus laevis* oocyte expresion vector (pGEM-3Z or pBF), followed by propogation and purification of plasmid DNA (see section 2.3). 2.5μg plasmid DNA was then linearised with a specific restriction enzyme; Nhe1 and Mlu1 were used to linearise the pGEM-3Z

and pBF vectors, respectively. Linearisation was followed by a purification step using the modified QIAquick PCR purification spin protocol (appendix I); linearised DNA was eluted in 30μl RNA-free H_2O (Stratagene).

In vitro transcription was carried out using the mMESSAGE mMACHINE manufacturers protocol. Transcription of pGEM-3Z and pBF plasmid DNA was conducted using the T7 and SP6 transcription kits, respectively. Transcription reactions were incubated for 2-3 hours at the recommended temperature before 1μl DNAase was added. The DNA digestion mixture was then incubated for 15 minutes at 37˚C.

mRNA solutions were subsequently purified using the RNAeasy kit, using the manufacturer's standard protocol. mRNA concentrations were tested using a Nanodrop 2000 Spectrophotometer (Thermo Scientific) and adjusted to 35 ng / μl. mRNA stock solutions were stored at -80˚C for long term storage; aliquots of dilute mRNA were stored at -20˚C if due to be used within three months of production.

2.3 Microbiology - *Escherichia coli*

2.3.1 Materials

Competent bacteria strains were purchased from Invitrogen. Subcloning efficiency DH5α cells were utilised for routine propogation of DNA, while Maximum or efficiency DH5α cells were employed when greater transformation efficiency was needed.

Luria broth, LB, was purchased in powder form from Sigma, and made as follows:

LB:

25g dry LB (Sigma)

1 litre distilled H_2O (d.H_2O, Millipore)

Solid LB media was made by adding *12.5g Agar* (Sigma) per litre of LB media.

LB solution was sterilised[1] immediately after mixing and stored for a maximum of 6 months.

2.3.2 Propagation of plasmid DNA using *E. coli*

DNA transformation in *E. coli*

Chemically competent DH5α cells were mixed with DNA samples and stored on ice for approximately 30 minutes. This was followed by a 45 second heat-shock period at 42°C, before being returned to ice for five minutes. The transformed bacteria solutions were then spread thinly over LB-agar petri dishes containing 100μg/ml carbenicillin disodium and grown in a 37°C incubator for 18 hours. All vectors utilised for this study contained a gene which confers resistance to ampicillin; a key component for the selection of only bacteria which have been successfully transformed with the DNA plasmid.

Rapid isolation of plasmid DNA

Rapid isolation of plasmid DNA was carried out following propogation in *E. coli*. Colonies grown on solid LB-agar petri dishes were individually selected and innoculated into a small volume of liquid LB and grown overnight in an incubator / shaker at 37°C, 220RPM. Plasmid DNA was then isolated from bacterial cultures, as described in the QIAprep Spin miniprep protocol (appendix I). This method

[1] All media was sterilised by autoclave, unless stated otherwise.

allows for a yield of between 15,000 and 40,000 ng of DNA which was sufficient for the functional experiments described in this study. DNA samples were diluted to 100ng/μl using molecular biology grade H_2O and stored at -20˚C.

2.3.3 Sequencing

DNA sequencing was performed using the service offered by the Oxford branch of Source Bioscience's gene service. Sequencing results were evaluated using DNA analysis software EnzymeX and 4Peaks (Mekentosj) and / or ClustalW (European Bionformatics Institute).

2.4 Microbiology – *Saccharomyces cerevisiae*

2.4.1 Yeast strains and vectors

A *Saccharomyces cerevisiae* strain, SGY1528, with a disruption of native K^+ transporters *trk1* and *trk2*, was used for functional experiments (Figure 2.2). Loss of functioning K^+ uptake transporters means that this strain unable to grow media with low levels of K^+, unless an alternate route for K^+ entry into the cell is introduced (Tang *et al.* 1995). In addition, due to a mutation to the uracil synthesis enzyme orotidine-5'phosphate decarboxylase renders SGY1528 unable to grow on uracil dropout medium unless transformed with a URA3+ plasmid. More details about this strain are given in chapter three.

SGY1528 (geneotype: *MATa ade2-1 can1-100 his3011,15 leu2-3,112 trp1-1 trk::HIS3 trk2::TRP1*) was kindly donated by Dr. D. L. Minor Jr. (UCSF, USA).

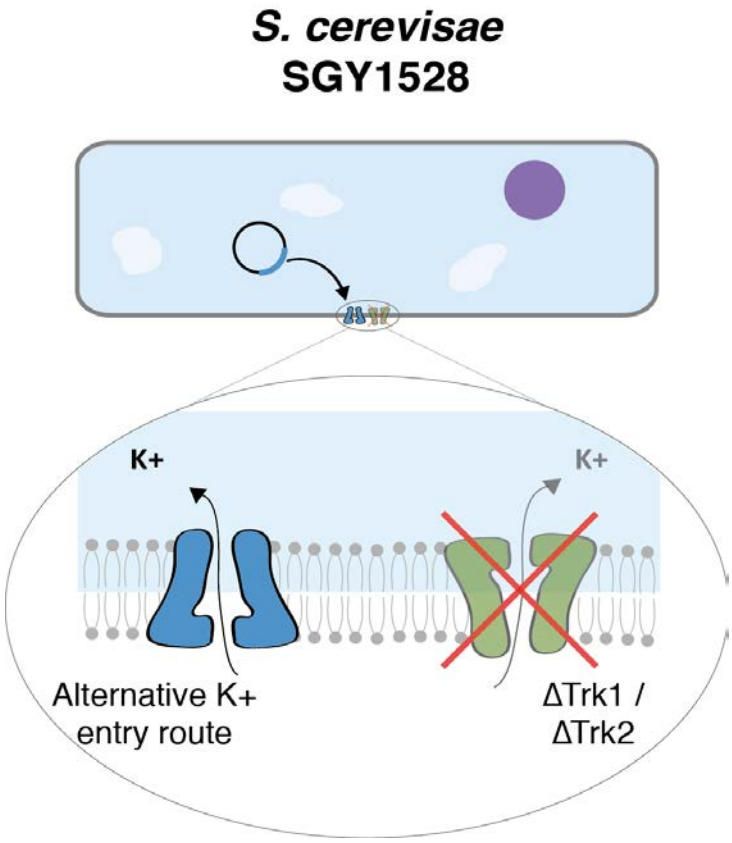


Figure 2.2: *A schematic representation of modified S. cerevisiae strain SGY1528. This strain has a disruption to native K^+ uptake transporters (trk1 and trk2) and is unable to survive in low [K^+] media, unless an alternative route for K^+ entry is provided.*

2.4.2 Growth media

d.H2O was used to make all growth media. Recipes for one litre volumes are given in this section, unless otherwise stated, and all growth media was sterilised immediately after mixing. The desired [K^+] was reached by subsequent addition of sterilised 2.5M KCl.

YPDA medium (100mM [K^+])

Yeast extract peptone destrose (YPD) medium with added adenine hemisulphate (YPDA) is a non-selective yeast medium utilised in making competent yeast cells.

50g YPD medium (Clontech)

0.3g adenine hemisulphate

Sterilised 2.5M KCl was added to supplement the medium to final [K^+] to 100mM.

APKO media using CSM synthetic base

Synthetic amino acid drop-out media were used to control expression of the plasmid. The two bases utilised in this study were CSM-uracil (CSM-u) and CSM-methionine-uracil (CSM-m-u) (BIO101 systems). Both drop out bases contained no uracil so only allowed for proliferation of yeast cells successfully transformed with a URA3+ plasmid (p416met25 or pYES2m). As transcription from both vectors was methionine regulated, the CSM-methionine-uracil base was used to control both cell survival and plasmid expression. Furthermore, both dropout-bases used in the study contained very little potassium (<0.01mM [K^+]) and so were ideal for producing low-[K^+] media.

Yeast dropout media

0.554ml 85% ortho-phosphoric acid (Fluka)

2.1g L-arginine base (non-animal)

1ml 1M $MgSO_4$

1ml 1M $CaCl_2$

For APKO-uracil (APKO-m-u) media: *0.77g CSM-u*

For APKO-methionine-uracil (APKO-m-u) media: *0.73g CSM-m-u*.

For solid media, 12.5g molecular biology grade, low-[K^+] agaose (Eurogentec) was added per litre, prior to sterilisation.

APKO-u and APKO-m-u media were supplemented immediately before use. The minerals and vitamins used are broken down by high temperatures and so could not be heated and so were filter sterilised and added to media prior to use. In full, the following supplements were added:

- *Sterilised 2M Glucose solution* (to a final concentration of 50mM)

- *1000x Trace minerals solution* (to final concentrations: H_3BO_3 8.1μM, $MnSO_4.H_2O$ 2.6μM, $FeSO_4.7H_2O$ 1.8μM, $ZnSO_4.7H_2O$ 1.4μM, NH_4molybdate.$4H_2O$ 0.73μM, $CuSO_4.5H_2O$ 0.16μM)
- *1000x Vitamin solution* (to final concentrations of: inositol 10μM, nicotinic acid 3.2μM, pyridoxine HCl 1.9μM, D-panthothenic acid 1.7μM, thiamine 1.2μM and biotin 8.2nM)
- *Sterilised 2.5M KCl solution* (to a final concentration of 100mM [K^+] in APKO-u, and to varied concentrations of 0.5, 1, 2 or 100mM [K^+] in APKO-m-u)

(More details about these solutions can be found in Appendix II)

2.4.3 Making competent Yeast cells

While chemically competent *E. coli* could be purchased, competent SGY1528 cells were not available commercially. Lithium acetate (LiAc) treatment of *S. cerevisiae* cells is belived to increase both the permeability and DNA binding capacity of the cell wall, allowing for highly efficient transformaion (Gietz *et al.* 1995). Therefore yeast cells were treated with LiAc prior to and during transformation. This process was based on a previously described method (Gietz & Schiestl 2007).

Yeast cells in liquid culture were always grown at 30˚C. YPDA solutions were always supplemented to 100mM [K^+] to allow growth of SGY1528.

1. SGY1528 yeast cells stored in 5% glycerol at -80˚C were spread onto a YPDA-agar (100mM [K^+]) petri dish and incubated for 48-60 hours at 30˚C.
2. Subsequently, competent cells were prepared by incubating a selection of yeast cells in liquid YPDA media for approximately 16 hours.
3. 1ml of the culture was then innoculated into 50ml YPDA media and was incubated until an optimal cell concentration was reached, as measured by the optical density of the cell culture at 600nm wavelength (OD_{600}) using a spectrophotometer (Genequant 1300, GE healthcare).

4. Cells were washed of any remaining YPDA and K^+ by centrifugation (2,500 RPM, 10 minutes). The resulting supernatant was discarded and cells were resuspended in sterilised 10ml d.H_2O.
5. Step 3 was repeated twice more to ensure removal of all impurities. Cells were resuspended in 10ml LiAc transformation solution (below) instead of sterilised d.H_2O solution following the third centrifugation step.
6. Cells were next centrifuged and supernatent discarded. Finally, cells were resuspended in 250*µ*l LiAc transformation solution.

N.B. If cells were to be frozen for long term storage 5-10% sterile glycerol was added to the LiAc transformation solution. Cell samples were aliquoted into individual 1.5ml tubes and wrapped in an insulant to slow cell freezing at -80°C. Competent cell solutions were stored at -80°C for no longer than three months, as transformation efficiency was significantly reduced after this period.

LiAc solution for competent cells:

500µl Tris/EDTA (TE) buffer

500µl 1M LiAc solution

4ml 50% Poly(ethylene glycol) (PEG) solution

2.5 Genetic complementation assay.

2.5.1 Screening mutant libraries

For each library the following procedure was carried out:

1. The transformation solution containing yeast cells and the digested vector and mutant library , was innoculated into 25ml APKO-u liquid media (100mM [K^+]) and incubated for one hour at 30˚C, 220RPM

2. The growth culture was centrifuged for five minutes at 2,500 RPM. The supernatant was discarded and cells were resuspended in 25ml APKO-met-ura (1mM [K^+]).
3. Cells were centrifuged for five minutes at 2,500RPM. Again, the supernatant was discarded and the cell pellet resuspended with 1ml APKO-m-u (1mM [K^+]). This step ensured removal of excess [K^+] from the initial growth culture.
4. As a positive control, 50μl of the concentrated cell solution was pipetted and spread onto APKO-u (100mM [K^+]) agar plates.
5. The remaining solution was pipetted evenly between five large APKO-m-u (1mM or 2mM [K^+]) petri dishes. This equated to approximately 250μl per petri dish.
6. Plates were incubated for 72-86 hours at 30˚C. High [K^+] plates were used to confirm successful transformation of the target DNA. The the number of colonies observed were used to estimate the number of mutations in the library.
7. Colonies grown on the APKO-m-u screening plates were inocculated into 4ml APKO-u (100mM [K^+]) and grown overnight at 30˚C and 220RPM.
8. Overnight cultures were centrifuged at 3,500RPM and supernatant discarded before DNA was extracted with a modified plasmid DNA isolation method, utilising the Qiagen miniprep kit (see Rapid isolation of plasmid DNA from *S. cerevisiae* - Appendix I).

Plasmid DNA extracted from yeast cells was typically at low concentrations and so in order to increase the concentration of plasmid DNA, 5μl of DNA purified from yeast would be transformed into subcloning efficiency *E. coli* for DNA propogation (section 2.3.2). DNA could then be isolated from these cells at a higher concentration, followed by transformation back into SGY1528 to confirm that the complementary phenotype. False positives were discarded, while GoF mutants were sequenced; individual mutations were identified and then created using site-directed mutagenesis. This process is outlined in figure 3.1.

2.5.2 *S. cerevisiae* transformation

The yeast transformation process involves mixing a small amount of competent yeast cells with the target DNA plasmid, PEG solution and denatured carrier DNA solution. For each plasmid, these were mixed in individual 15ml polypropelene tubes as follows:

8µl (20µg) denatured carrier DNA solution

1µg target DNA plasmid

300µl 50% PEG solution

50µl competent yeast cells (in LiAc solution)

(See Appendix II for solutions)

Transformation mixtures were incubated for 30 minutes (30˚C, 220RPM), before heat shock for 15 minutes at 42˚C. This extended period of heat shock has been shown to improve the transformant yield more than 8-fold (Gietz *et al.* 1995). During the heat shock process, the transformation solution was shaken at approximately three minute intervals to resuspend the cells. Following heat shock, 150µl of the transformation mixture was pippeted onto APKO-ura (100mM KCl) petri dishes at 30°C for 72 hours. Subsequently, plates containing yeast cells could be stored at 4˚C for a maximum of 10 days following transformation.

2.5.3 Yeast drop tests

Prior to starting a drop test, SGY1528 cells were transformed with the GoF mutants / single mutations of interest. In addition, for each drop test yeast cells transformed with the wild type TREK-1 gene to provide a basal / backgound growth reference, as well as the empty yeast expression vector (most commonly p416met25) and $K_{ir}2.1$ plasmid DNA. The empty vector and $K_{ir}2.1$ were used as negative and positive controls, respectively. All cells were transformed onto non-selective growth media. (APKO-u (100mM $[K^+]$)).

APKO-u (100mM [K^+]) plates containing transformed yeast cells were incubated for 36 hours in a 30˚C incubator. Also in preparation for the drop tests, APKO-m-u plates were poured containing various K^+ concentrations (0.5, 1, 2 and 100mM [K^+]) and stored at 4˚C for 24 hours. Regularly, both yeast and bacterial media were pre-warmed prior to plating, in order to aid absorption of cells into the media. However, for drop tests it was more favourable to use the plates as cold as possible; slightly drying and chilling APKO-m-u plates limits the spread of cells on the media surface, resulting in more evenly sized drops.

Drop test were conducted as follows:

1. A short streak of yeast cells from each transformation plate were selected and innoculated into 4ml APKO-u liquid media (100mM [K^+]). Samples were then incubated overnight at 30˚C, 220RPM.
2. Overnight growth cultures were centrifuged for 10 minutes at 2,500 RPM. The supernatant was discarded before cells were resuspended in 4ml APKO-m-u. The [K^+] of the resuspension media was the same as the lowest [K^+] used on drop test plates (typically 0.5mM [K^+]).
3. Resuspended cells were incubated for 30 minutes at 30˚C, 220RPM.
4. Step two was repeated twice. In combination with the 30 minute incubation (step 3) this ensures cells are washed to ensure removal of excess K^+ ions that may have remained from the overnight incubation in non-selective APKO-u (100mM [K^+]).
5. The cleansed cell solutions were seperated into three 1.5ml tubes (eppendorf) to dilutions of 1/1, 1/10 and 1/1000[2].
6. 3-4μl drops of each cell solution (including wild type TREK-1 and the positive / negative controls), and each dilution, were pipetted onto the APKO-m-u plates of various [K^+]. Once the droplets had dried, the petri dishes were closed and left to incubate for 72 hours at 30˚C.
7. Following the incubation period, drop tests plates were photographed and analysed for our records.

[2] The solution used to dilute cells was APKO-m-u (0.5mM [K^+]). Cell solutions were still viable after being stored at 4˚C for up to 24 hours. However, most commonly, the cell solutions were drop tested within an hour.

2.5.4 Growth curves

To assess growth in liquid media, cells were added to 50ml APKO-m-u media (2mM [K^+]) to reach a final concentration of an optical density (OD_{600}) of 0.05. Cultures were then grown at 30˚C, 220RPM with OD_{600} measured every hour for 20 hours and repeated in triplicate.

2.6 Electrophysiology

Xenopus laevis oocytes were typically delivered in 2-(*N*-morpholino)ethanesulfonic acid (MES)-buffered Barth's solution (Appendix III) on ice, as intact ovaries from the European Xenopus Resource Centre (EXRC, University of Portsmouth). Oocytes were also occassionally obtained from frogs stored at the animal facilities at the University.

In general, the eletrophysiological studies secribed in this thesis were the result of measuring macroscopic currents, where intact whole cells were examined, typically expressing at least a few hundred channels. All data from single-channel and microscopic current studies reported here were collected in collaboration with Prof. T. Baukrowitz' laboratory in the Christian-Albrechts-Universität zu Kiel (Kiel, Germany). The technique used for excised patch recordings is shown below in figure 2.3.

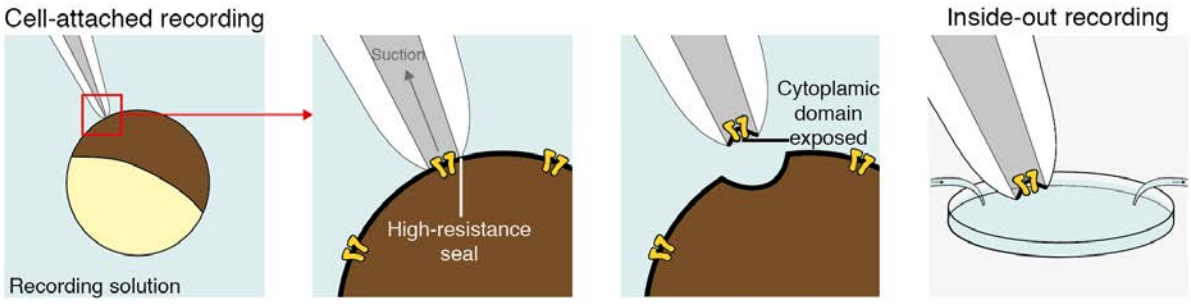


Figure 2.3: *A schematic representing the inside-out excised patch recording method. In the cell-attached mode, the pipette is retracted and the patch separated from the rest of the membrane. The cytosolic surface of the membrane is exposed to an external application system for rapid exchange of solutions, shown here as petri dish. Adapted from the Leica Microsystems.*

2.6.1 The two-electrode voltage clamp method

The two-electrode voltage clamp (TEVC) technique involves inserting two micropuncture electrodes into an oocyte; one electrode to clamp the membrane potential at a desired voltage, the other to measure the whole cell current. TEVC was employed to investigate GoF mutant channel function in response to several modulatory inputs including extracellular pH and activatory agents DEPC and BL-1249 (section 2.6.3).

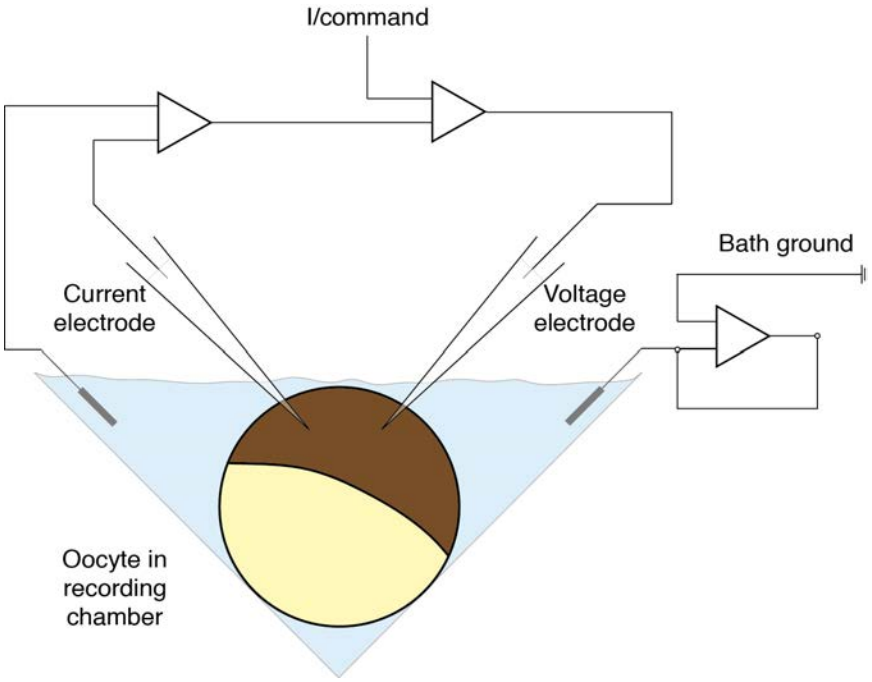


Figure 2.4: *A schematic representation of a typical TEVC recording arrangement. The oocyte is placed in the middle of an experimental chamber filled with a recording solution. Using a peristaltic pump to slowly perfuse the chamber prevents excessive movement of oocytes. One electrode feeds into the amplifier, while the other is used to ground the electrical signal. Two glass micropipettes are shown to impale the oocytes. A small section of AgCl wire (the electrode) is in contact with the conductive pipette solution (3M KCl). One electrode measures changes in current, while the other is the voltage clamp electrode. Both electrodes, or rather their holders/ headstages, are connected to the amplifier. The voltage measured by this device is fed into one of the inputs of the amplifier to form the negative feedback loop. Observed voltages are compared with the voltage command (Vcommand), typically set by a computer. The connections to the computer and additional equipment including a digital decoder are not shown here. Figure adapted from Dascal 2001*

2.6.2 TEVC materials

An example of a TEVC system assembled with Mr. M. F. Abd Wahab is shown in figure 2.5 (overleaf).

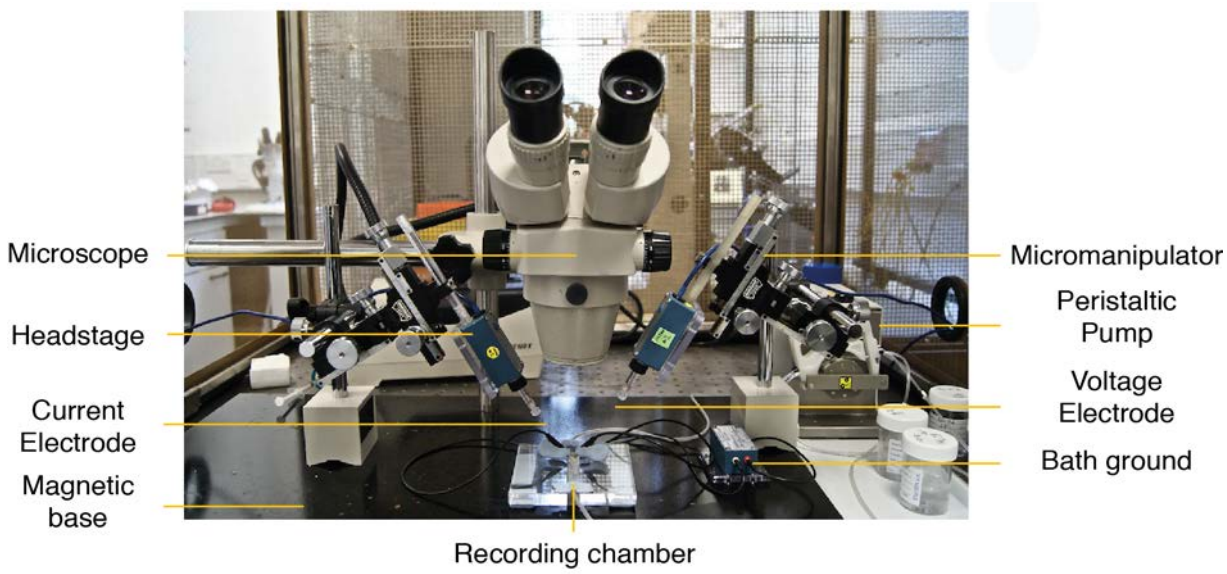


Figure 2.5: *A functional TEVC recording setup. A central recording chamber is filled with recording solution, using the peristaltic pump far right. The oocyte is placed inside the recording chamber, as are the two reference / ground electrodes (connected to the amplifier via the bath ground headstage).*

In table 2.1 a comprehensive list of items shown in figure 2.5 is given. Where known, the brand / model and supplier are detailed.

Component	**Brand / Model**	**Supplier**
Micromanipulator	Narishige	Narishige, Japan
Magnetic stands	Narishige	Narishige, Japan
Light source	Leica CLS50X	
Peristaltic pump	Ismatec ISM829	Michael Smith Engineers Ltd., U.K.
Pump tubing	Tygon R3607	Michael Smith Engineers Ltd., U.K.
Data acquisition system	Digidata 1322A, Axon inst.	Molecular Devices, Germany
Amplifier	Geneclamp 500, Axon inst.	Molecular Devices, Germany
Voltage-clamp electrode headstage	HS2A x1LU	Molecular Devices, Germany
Component	**Brand / Model**	**Supplier**
Current electrode headstage	HS2A x10MGU	Molecular Devices, Germany
Current electrode headstage	HS2A x10MGU	Molecular Devices, Germany
Bath ground headstage	VG-2A x100 bath clamp	Molecular Devices, Germany
Microscope	World Precision Instuments	World Precision Instuments, U.S.
Perspex recording chamber	Designed personally	Physics department research workshop, University of Oxford
Vibration-reducing magnetic base	Designed personally	Physics department research workshop, University of Oxford

Table 2.1: A list of components, their respective brands / Model numbers and suppliers used in constructing the TEVC recording set up shown in figure 2.5.

Further materials, not shown in figure 2.5, are the glass micropipettes used for impaling the oocytes during recordings, as well as those used for microinjection of mRNA into oocytes:

Component	Composition / Model	Supplier
Injection pipettes	10*µ*l borosilicate glass capillaries	Drummond Scientific, U.S.
Recording pipettes	1.5mm (OD) x 1.17 (ID) borosilicate glass capillaries	Harvard Apparatus, U.S.
Micropipette puller	Narishige PC-10	Narishige, Japan
Microprocesser-controlled injector	Nanoliter 2000	World Precision Instuments, U.S.

Table 2.2: Pipettes for injection and recordings, as well as the vertical micropipette puller used to pull the fine tips required for impaling *Xenopus* oocytes. Details of the microinjection set up are also outlined.

For convenience, details of solutions used for oocyte storage and electrophysiology are provided in the appendices (Appendix III). All solutions were filter sterilised, stored at 4˚C and discarded within a month of sterilisation. Unless otherwise stated, all solutions were buffered to pH 7.4 using NaOH (*sodium hydroxide*) or HCl (*hydrochloric acid*). pH was measured using the pH meter 3320 (Jenway, Bibby Scientific, UK)

2.6.3. Drug stock solutions

TREK-1 channel activity in response to pharmacological agents diethylpyrocarbonate (DEPC) and BL-1249 were examined in this study. More information about their respective functions and unique properties is given in chapter five. In all cases, drugs were stored as 1000x stock solutions and diluted into ND96 on the day of experiments. The diluted (1x) solutions were stored at room temperature for less than 18 hours. Drug solutions were disposed of accordance with the manufacturer's / University's guidelines.

DEPC (Sigma) was delivered as a liquid at ≥97% purity, and was diluted to 0.1% for experiments. However, because DEPC is highly sensitive to hydrolysis when exposed to traces of moisture, the solution bottle was stored in a sealed plastic bag with a desiccant, at 4˚C. It is also suggested that

MOPS-buffered solution should be used for DEPC storage in the medium and long term, to reduce the rate of hydrolysis. However, as solutions were routinely made on the day of an experiment, regular ND96 (appendix III) buffered with HEPES was used for DEPC application to oocytes.

BL-1249 ([(5, 6, 7, 8-tetrahydro-naphthalen-1-yl)-[2(1*H*-tetrazol-5-yl)-phenyl]-amine]) (Sigma) was dissolved in dimethylsulfoxide (DMSO) and d.H_2O, in a 2:1 ratio. 10mM BL-1249 stock solutions were stored at -20˚C. These stock solutions were diluted in ND96 to a concentration of 10μM for experiments.

2.6.4 Antibiotics

When beginning this study, oocytes were routinely stored in Barth's solution with 100 U/ml penicillin and 100 μg/ml streptomycin, to prevent bacterial growth. However, oocytes would routinely develop very soft, non-viable membranes. Furthermore, as shown in figure 2.6, the uninjected oocytes developed dark foci, similar to scar tissue formed by impalement of oocytes with a microelectrode. Cellular death two days after oocyte excision was also common and highly problematic.

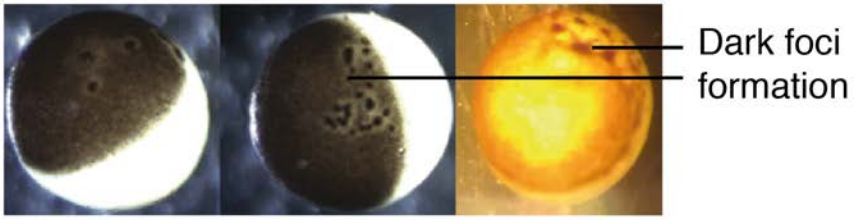


Figure 2.6: *Xenopus laevis oocytes infected with multi-drug resistant bacteria. Two oocytes (left) imaged with a bright field micrograph, and one using a taken personally using a VGA camera (right) showing the characteristic dark spots and unpigmented halo. Image adapted from O'Connell et al. 2011.*

Therefore, Barth's solution was always supplemented with a previously described antibiotic cocktail containing ciprofloxacin (100μg/ml), amikacin (100μg/ml) and tetracycline (10mg/ml) (O'Connell *et al.* 2011). Barth's solution was also supplemented with 2mM sodium pyruvate. Barth's solution and antibiotic is, herein, referred to as modified Barth's solution (MBS).

Antibiotic stock solutions (x1000) were made up in a 1:1 (v/v) mix of pure ethanol and dH_2O, and stored at -20˚C.

2.6.5 Preparation of *Xenopus laevis* oocytes for mRNA injection.

Ovarian lobes were were delivered, in a MES-buffered Barth's solution with antibiotic (see section 2.5.3.1 and appendix III for details), stored in 50ml tubes (Falcon) on ice.

In order to be used for electrophysiological study, the connective tissue surrounding the oocytes was digested, to allow isolation and defolliculation of individual cells. This was achieved as follows:

1. Ovarian lobes were cut into small clusters (roughly <5mm) using sterilised surgical and a scalpel. Tools were sterilised prior to every operation to minimise contamination.
2. The ovarian tissue was washed 4-5 times in Ca^{2+}-free oocyte ringer's-2 (OR-2) solution (appendix III) to remove any cell debris or blood produced when cutting cells.
3. Clusters underwent a primary digestion phase with 2mg/ml collagenase A from *Clostridium histolycum* (Roche diagnostics) in OR-2 solution. To aid detachment of cells, the clusters were gently rocked on a rotating platform.
4. Cells were examined under a stereomicroscope in order to determine wether or not a further, secondary digestion was required[3]. Mature (stage V or VI) oocytes with a healthy appearance, i.e. cells with clear, well-separated poles with no scarring or de-pigmentation, were selected. Unhealthy or immature oocytes were then discarded.
5. If cells then required a second round of digestion, step 3 was repeated, though for a shorter period of time (15-45 minutes) determined by the characteristics of individual samples.
6. Where necessary, cells were manually defolliculated.

[3] Many factors effect the rate at which single cells would associate from a cell cluster in oocytes, including the health of the animal at the time of excision, the age of the animal and how fresh the tissue was prior to digestion.

7. Oocytes were washed in Barth's solution, until the liquid ran clear, before being stored in MBS. This ensured removal of any remaining collagenase as well as any potentially toxic cell debris.

2.6.6 mRNA injection

Injection of mRNA was conducted on defolliculated mature oocytes, using 10μl Drummond capillary-pipettes. Microinjection pipettes were prepared using a vertical PC-10 Narishige micropipette puller; the tips were broken to approximately 10μm manually before use. Pipettes were back filled with pure mineral oil (0.84g/ml, Promega). Filled pipettes were cleared of any trapped air and loaded onto the injection needle of the microprocessor-controlled mRNA injection set up.

2μl of target mRNA was pipetted onto the lid of a sterile petri dish, before being filled into the microinjection pipette by mechanical suction. Oocytes were then individually injected with the target mRNA. Swelling of the oocyte observed while injecting mRNA was taken to show successful injection. The amount of mRNA injected varied between 0.05 and 7ng per oocyte (dependent on expression) and was controlled by diluting a stock solution rather than varying the volume of mRNA injected (held consistently at 50.6nl). For expression and basal current measurements, 3ng mRNA was injected into oocytes.

Xenopus oocytes were stored at 18˚C in MBS for 1-2 days following injection. Due to the robust expression of TREK-1 channels in oocytes, recordings were usually made within 24 hours of injection to avoid overexpression.

2.6.7 Data acquisition

Oocytes were placed into a small recording chamber (3ml) and perfused with fresh modified-ND96 recording solution (appendix III). The glass microelectrodes were prepared using the Narishige PC-10 vertical puller to form tips of 0.3-1.5MΩ resistance, and half-back filled with 3M KCl. Microelectrodes

were firmly tapped to remove any air bubbles before being mounted on to the headstages. Importantly, at this stage it was ensured that the 3M KCl solution inside the microelectrode was in contact with bleached AgCl (*silver chloride*) electrodes.

Following the impalement of oocytes with the microelectrodes, the membrane potential was clamped at a holding potential of -80mV. Test recordings (not shown) were then made using a variety of protocols. However, measurements reported in this thesis were made by evoking currents from -125 to +100 mV. A voltage step protocol from -125mV up to +100mV in 25mV increments, using consecutive 500ms step changes was used for all of the TEVC measurements presented in this thesis. There was no interval between steps, though a 250ms return to holding potential (-80mV) followed each sweep. Recordings were taken over five sweeps.

The membrane potential was clamped using a TEVC amplifier (Geneclamp 500, Molecular Devices analytical technologies) which was controlled by the pClamp 9.0 software (Molecular Devices). Pulsed data was filtered and digitised at 1kHz using a digital data acquisition system (Digidata 1332A, Molecular Devices analytical technologies) and written to hard disc.

2.6.8 Data analysis

Data was analysed using AxoGraph X software (Axograph). The data exclusion criteria was set to exclude data where the standard error of the mean (SEM) between sweeps was >2%; if data failed the exclusion test, the recording was invalidated and not included in subsequent analysis.

A combination of Microsoft Excel (Microsoft) and Origin professional 8.0 (Origin Lab) were used for producing graphs. Dose-response curves (e.g. figure 4.2) were fitted with the following equation:

$$I = I_{\min} + \frac{I_{\max} - I_{\min}}{1 + ([H^+]_o / K_{1/2})^p}$$

Equation 3: *where I_{max} and I_{min} are the maximal and minimal current values, respectively, $K_{1/2}$ is a half-maximal effective concentration of extracellular protons ($[H^+]o$) and p is the hill coefficient.*

Data are presented as ± SEM; where error bars cannot be distinguished in figures, the error bars are smaller than the plot point. Significance of errors was evaluated by the student's t-test and a *P*-value of <0.05 were taken as statistically significant differences.

Testing oocytes from different tissue samples was an important control due to the high variability in oocyte quality and so experiments were conducted on a minimum of 2 separate batches of oocytes ($N \geq 2$), while at least six individual oocytes were used for averaging data ($n \geq 6$).

Chapter 3

The use of a genetic complementation assay to identify activatory mutations

3.1 Introduction

A traditional approach to determining the residues and regions important for protein function is to systematically mutate individual residues to a different amino acid and then re-examine the functional properties of the protein. Commonly residues are mutated to small, non-polar amino acids such as alanine or valine as they are generally tolerated in areas of little importance to protein function. When studying ion channels, this approach can be useful for determining regions that are involved in channel gating.

When beginning the experiments for this thesis, a systematic cysteine scan had already been initiated in the Tucker laboratory, where the inner pore regions (TM2, TM4 and parts of PH1 and PH2) had been mutated to identify the quaternary amine blocker-binding site in TREK-1 (Piechotta *et al.* 2011). The results of that project provided the rational to continue examining the effect of a cysteine-

mutagenesis scan in the 'outer-helices' TM1 and TM3. However, as this project is still on going, many of the mutants are yet to be functionally characterised.

Concurrently, a more innovative method to identify regions potentially important to channel gating was employed. Random mutagenesis of a gene using error-prone PCR can rapidly produce a vast number of mutations. This is not only more cost effective than systematically mutating single residues, but also considerably less time consuming and therefore can be more efficient than the traditional approach. However, this approach also requires a high throughput method for screening the large number of mutations produced. Therefore, a previously described genetic complementation assay (Minor *et al.* 1999, Paynter *et al.* 2008, Paynter *et al.* 2010) was employed.

3.1.1 The genetic complementation assay

The genetic complementation assay is a high throughput screening method that can be used to identify mutant channels which rescue growth of K^+-auxotrophic cells in conditions of low extracellular [K^+]. The yeast strain used for this assay is SGY1528, which a modified strain of *S. cerevisiae,* with disruptions to the K^+-transporters *Trk1* and *Trk2*. Encoded for by the TRK1 and TRK2 loci, these transporters are responsible for mediating K^+ flux into the cell and, as such, disruption of these means that the levels of intracellular [K^+] required for cellular proliferation are not reached. Cells are therefore unable to grow, unless an alternative route for K^+ entry is provided or the growth medium is supplemented with high levels of K^+ (>50mM).

Expression of TREK-1 in SGY1528 was hoped to form an alternative route for K^+ entry into the cell, as these channels would be activated by the acidic intracellular environment of *S. cerevisiae*, which can reach as low as pH 5.5 at some stages of the cell cycle (Madrid *et al.* 1998). Therefore, we expressed TREK-1 in SGY1528.

We found that, while SGY1528 was able to survive on media supplemented with >50mM [K^+], by expressing wild type TREK-1, cells grew in media supplemented with >10mM [K^+]. Therefore, in order

to identify activatory mutations of TREK-1, the selective growth media were supplemented with a maximum of 2mM [K^+]. Importantly, even though 2mM external [K^+] is low in comparison to the intracellular [K^+], there is still a favourable gradient for the entry of K^+ due to the extremely hyperpolarised RMP of yeast cells (Madrid *et al.* 1998). Therefore, if we activate TREK-1 channels either by the use of drugs or by introducing a GoF mutation, the channels should complement growth.

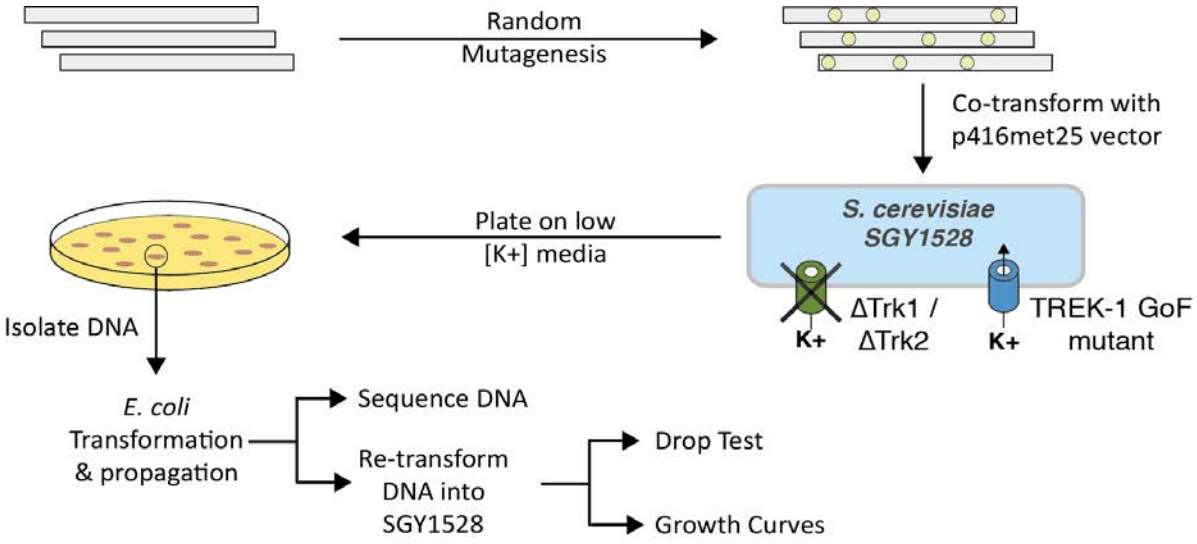


Figure 3.1: *Schematic diagram of the SGY1528 yeast complementation assay. Represented above is the creation of a random mutant library, screening in SGY1528 auxotrophic S. cerevisiae, isolation of mutant GoF plasmids, DNA sequencing and subsequent further functional experimentation.*

3.1.2 Searching for K2P gating mutants using SGY1528

Two random mutant libraries were constructed for the TREK-1 gene (*KCNK2*) from *Rattus norvegicus*. The first mutant library was originally constructed by Dr J. Paynter, who was largely responsible for refining the original SGY1528-based genetic complementation assay for K^+ channels in the Tucker laboratory. From this first library, a small number of activatory mutants were idenfitied. However, subsequent sequencing of these genes revealed that GoF mutant channels typically contained between four to five individual mutations per gene.

I therefore created a second library hoping to reduce the number of mutations per gene; this would ensure that dissecting the mutants and identifying single activatory mutations was less time and

resource consuming. Construction of this library was optimised so that each mutant clone typically contained two to three mutations per gene. In order to isolate single, activatory mutations, GoF mutant clones from all of the mutant libraries were dissected using site-directed mutagenesis. GoF single mutations were then verified by using the yeast drop test experiments described in chapter two (section 2.5.3).

3.2 The identification of GoF mutations in TREK-1

From the combined random mutant libraries approximately 180 mutant clones were isolated, of which nearly 120 were unique; defined as containing a combination of mutations not seen in any of the other mutant clones. After isolation, mutant DNA was propagated in *E. coli* before being retransformed into SGY1528 cells for confirmation of an activatory phenotype and sequencing. The final 14 activatory single mutations that were isolated are shown, in figure 3.2. A more comprehensive list of the mutant clones identified from the random mutant libraries are shown in Appendix V.

Amongst the mutations identified to be activatory using the genetic complementation assay included a previously described mutation to the C-terminal pH sensor, E321A (Honoré *et al.* 2002). Many different mutations at position E321 were found and this was one of the most commonly identified sites for mutation (Appendix V).

Mutation of a nearby residue, G323, was also found to complement growth. Both E321 and G323 are within the small cluster of charged residues (K316 to E324, figure 3.3) reported to be critical for chemical and mechanical activation of TREK-1 channels (Patel *et al.* 1998). In particular, truncations of the C-terminal regulatory domain are able to reduce pressure-activation of the channel making the mutant channels resistant to stretch (Maingret *et al.* 1999), while replacing the regulatory domain of TREK-1 with a homologous region in TASK-1 produces a constitutively active channel with no observable arachadonic acid or halothane sensitivity (Maingret *et al.* 2000).

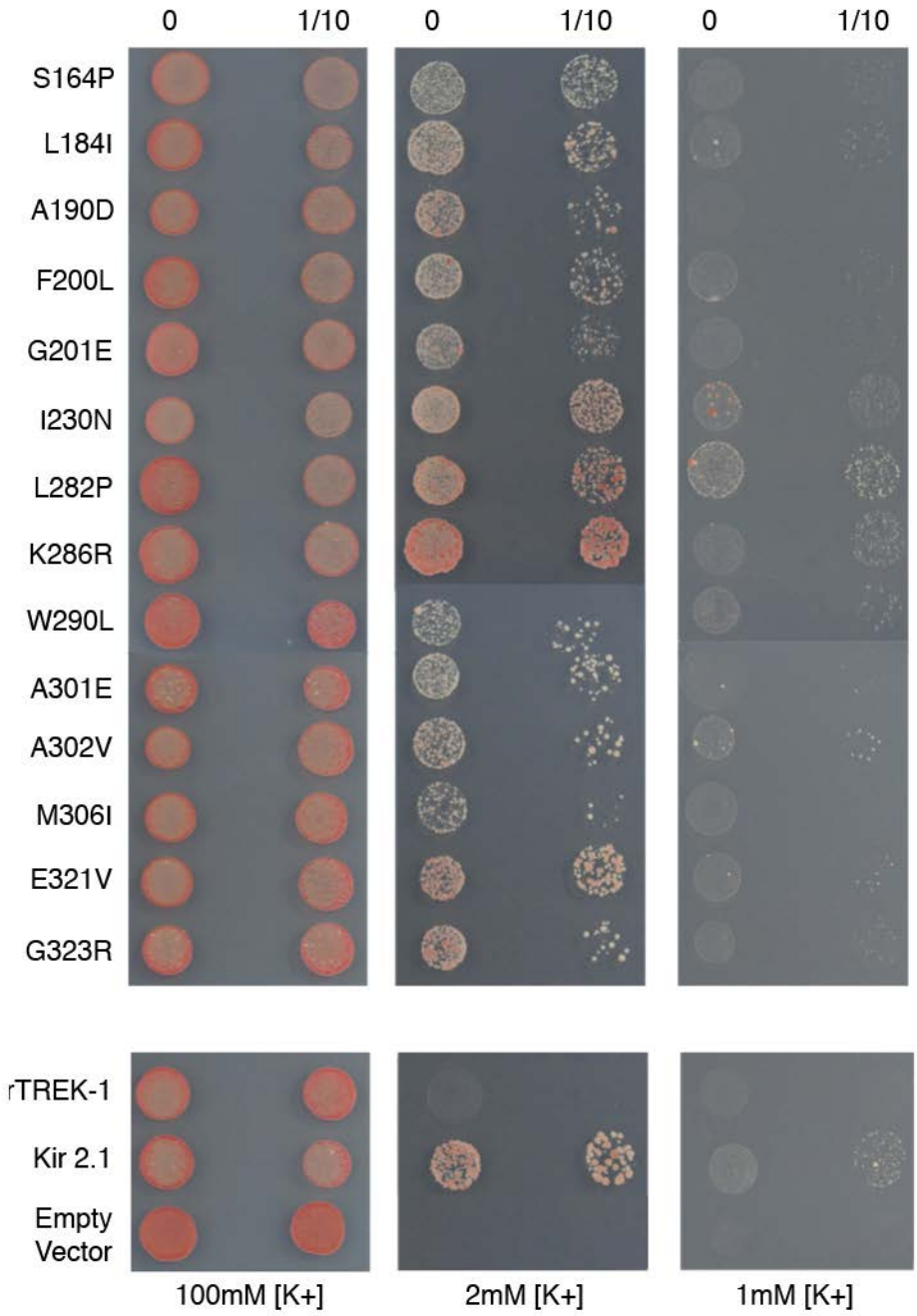


Figure 3.2: *rTREK-1 wild type and confirmed GoF mutants drop tested on 100mM, 2mM and 1mM [K^+] APKO-m-u dropout media, expressed in SGY1528 Yeast. $K_{ir}2.1$ and the empty p416met25 vector were used as positive and negative controls, respectively. Cells were drop tested at 1 and 1/10 dilutions.*

Mutant Name	Strength of complementation
S164P	+
L184I	++
A190D	+
F200L	+
G201E	+
I230N	++
L282P	++
K286R	+++
W290L	+
A301E	++
A302C	++
M306I	+
E321V	+++
G323R	+

Table 3.1: *A list of mutations identified collected from the genetic complementation assay and the relative strength of complementation and putative locations. Strength of complementation in drop test is indicated by + (weak), ++ (medium) and +++ (strong).*

It was highly promising that mutations of the proximal C-terminal regulatory domain were identified using this approach, as mutations such as E321A have been previously reported to be constituently active (Honoré 2002). Therefore, mutations to residues G323 and, in particular, E321 validated this genetic complementation approach as a useful tool to identify activatory mutations, and justified progressing further with the functional characterisation of the GoF mutants, described in chapters four to six.

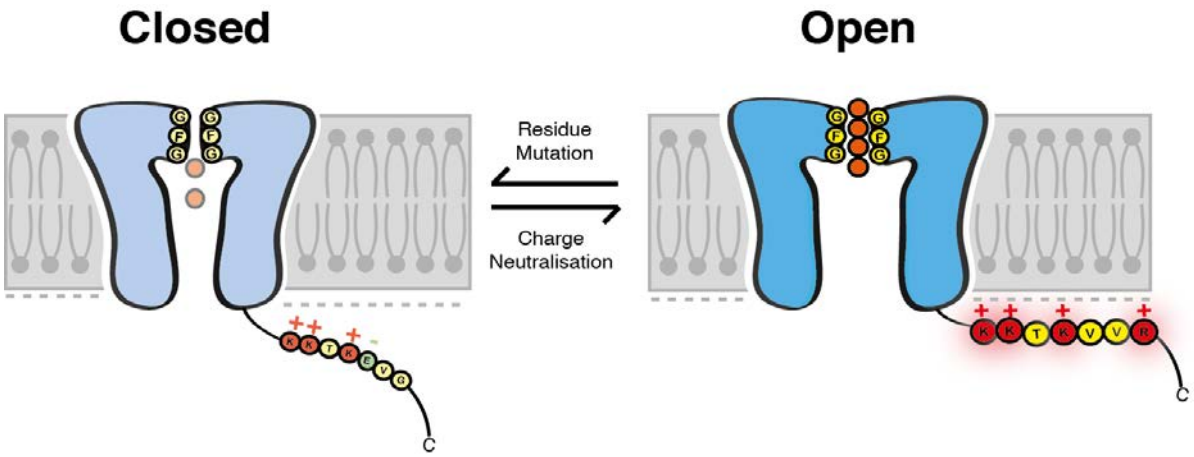


Figure 3.3: *Cartoon model of TREK-1 activation by mutagenesis of the cytosolic regulatory domain. Strong electrostatic interaction between the C-terminus and the inner leaflet of the membrane is thought to be important to channel activation by several stimulatory agents. This effect is believed to be responsible for transducing the effect of heat, membrane stretch, lipid and anaesthetic binding, but can also be achieved via by negative charge neutralization via protonation or amino acid substitution. Red, yellow and green residues represent positive-, neutral or negatively charged amino acid side chains, respectively.*

3.2.1 Complementation of growth in liquid media

As there was little apparent difference in growth of these mutants on 1 and 2mM [K^+] plates, it was hoped that an alternative measure of the strength of complementation could be determined by measuring their rate of growth in liquid media. This method involved making hourly measurements of the optical density of liquid growth cultures over a period of 20 hours (see section 2.5.4 for further details).

There was no observable growth in yeast cells expressing wild type TREK-1 (figure 3.4) and, as expected, cells expressing the positive control $K_{ir}2.1$ grew successfully in media supplemented with 1mM [K^+] (not shown). However, examination of a selection of GoF mutations using liquid growth cultures, also revealed no appreciable difference in growth patterns for the various activatory mutations identified (figure 3.4) and so this approach was not pursued further.

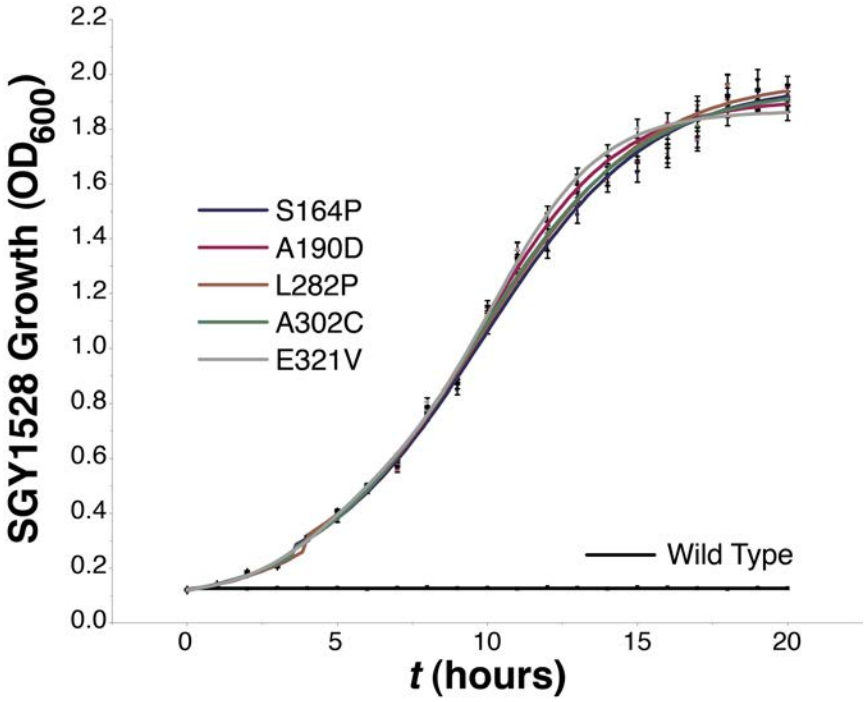


Figure 3.4: *Growth of SGY1528 cells when transformed with the indicated rTREK-1 channels. There is no discernable difference between the tested GoF mutations, though all were able to successfully rescue growth of yeast unlike wild type TREK-1 channels.*

3.3 Limitations of the genetic complementation assay

Genetic complementation assays have proven to be powerful tools for the identification of mutant channels exhibiting an activatory phenotype (Minor *et al.* 1999, Paynter *et al.* 2010, Bagriantsev *et al.* 2011). However, the complementation assays have several limitations, For example, the lack of quantifiable functional data that can be obtained about GoF mutant channels using this method, aside from their increased activity in comparison to wild type channels, means that subsequent functional analysis would be required.

Another problem comes in the form of determining the optimal [K^+] included in the growth media in order to fully exploit random mutant libraries. Use of a very low [K^+] growth media means that weakly activatory mutations would not be able to complement growth and therefore would not be identified in the screen. Conversely, if [K^+] is too high then exceptionally active channels may not complement growth as excess K^+ can enter the cell, having toxic effects. This means that, in theory, the complementation assay has a theoretical sensitivity range set by the minimum [K^+] required for

cellular proliferation and maximum [K^+] current before GoF mutations become toxic or wild type background-complementation becomes too high.

However, rather than choosing a single [K^+] for growth media, we screened the mutant libraries using several different concentrations of K^+. In doing so, the probability of identifying GoF mutations was maximised. Interestingly, even under control conditions (100mM [K^+]) none of the mutations were found to be completely toxic to yeast cells; the activatory mutations did result in a reduction of cellular growth in high [K^+] conditions, though not enough to result in complete loss of growth. Indeed, consitituitively active mutant channels (e.g. E321A) were identified using this method, suggesting that highly active mutants can be found in the screening process.

3.3.1 Screening drugs using the complementation assay

It was hoped that the complementation assay could be adapted and applied as a high-throughput screening method for identifying small molecule activators of TREK-1, which would have the same effect as activatory mutations by stimulating channel activity to complement yeast growth. Moreover, the relative simplicity of setting up the assay makes it an ideal candidate for screening large numbers of compounds across a range of concentrations. BL-1249, had been previously reported to activate TREK-1 channels (Tertyshnikova *et al.* 2005) and was therefore used to develop the screening method. An additional TREK-1 activator, flufenamic acid (Takihira *et al.* 2005), was also used to modify the complementation assay for drug screening.

However, when grown on solid media containing different concentrations of the drugs there was no difference in yeast growth density in the presence of the activators, at any of the tested drug concentrations (not shown). It is possible that the drug delivery or distribution was poor in the solid media used for growth assays and therefore both drugs were also tested in liquid media, but were unable to rescue SGY1528 growth at low [K^+] (not shown).

Following failure to succesfully screen drugs using a number of methods to improve distibution, it became evident that this may not have been the primary reason behind a lack of success in developing the drug screen. For example, the complex and robust extracellular membrane of yeast cells may have influenced the ability of the drugs to reach their channel target(s).

Thus, despite several attempts to modify the methodology, this assay was not pursued further to examine the effect of TREK-1 activators. Nonetheless, it is still possible that the complementation assay described here has great potential as a high throughput method for drug discovery, though the technique clearly requires development before it can be succesfully utilised.

3.4 Location of GoF mutations in TREK-1

In order to understand the role of the identified activatory mutations (table 3.1) in channel gating, it is important to understand where these residues are located within the channel. From their position in the linear sequence it is apparent in figure 3.5, there is a distinct grouping of mutations in TM-helices TM2 and TM4 (figure 3.5). A small number of mutations lie outside these key areas of interest, including the C-terminal regulatory domain (Patel *et al.* 1998) as well as residue S164, a residue thought to be involved in C-type gating (Cohen *et al.* 2008).

As these experiments were conducted at a time when there were no available three-dimensional structures of K2P channels, structural homology models were required in order to achieve a greater appreciation of where the residues of interest are located within the channel. Fortunately, homology models based on prokaryotic K^+ channels were made available to us by our collaborators in the structural bioinformatics and computational biochemistry (SBCB) unit (Oxford, UK). Homology models based on the proton-activated K^+ channel from *Streptomyces lividans* (KcsA) (PDB code: 1BL8, Doyle *et al.* 1998) and voltage-gated K^+ channel from *Aeropyrum pernix* (KvAP) (1ORS, Jiang *et al.* 2003) crystal structures were used to map out GoF mutations on to the structure of TREK-1. Sequence alignments used to generate these models are shown in Appendix IV.

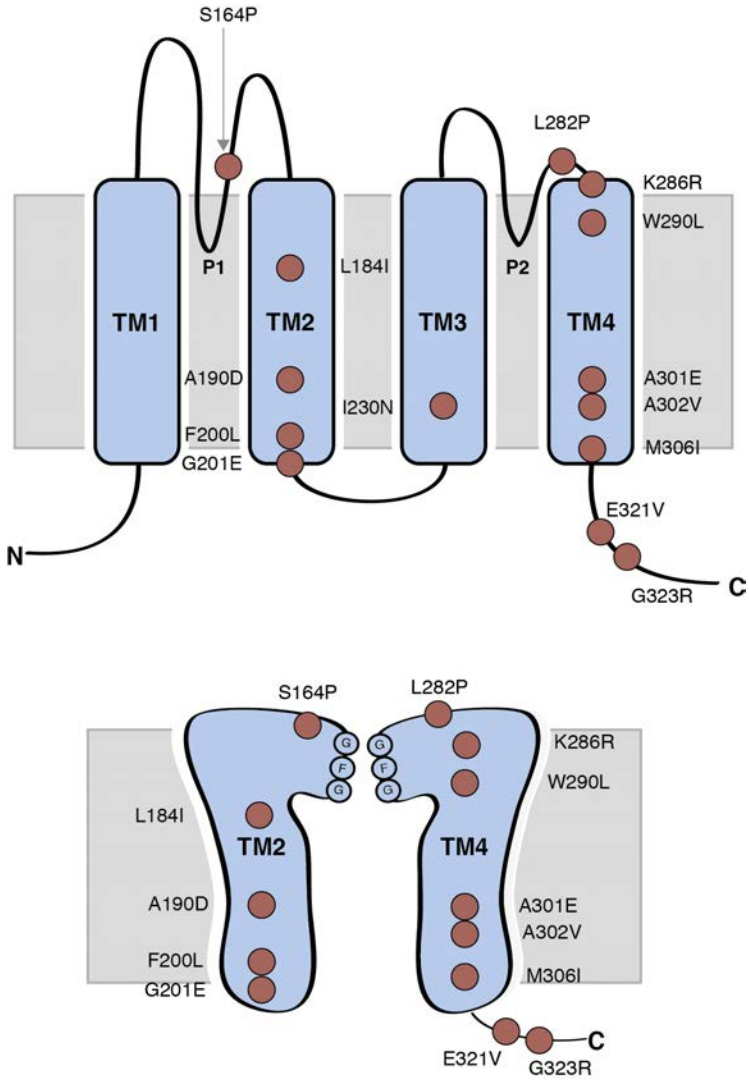


Figure 3.5: *TREK-1 subunit two-dimensional topology models showing the location of GoF mutations on cartoon models of (top) the four TM helices and (bottom) pore lining helices TM2 and TM4.*

Examination of the location within these structures revealed that GoF mutations clustered in two distinct regions, either in close proximity of PH1 or further down the TM helices, towards a proposed lower-gate (figure 3.5 and 3.6). In addition, mutations in the outer helices were notable in their absence; the one exception is I230N, which may result in an activatory phenotype via interaction with TM2 and TM4, close to a putative lower gate (figure 3.9).

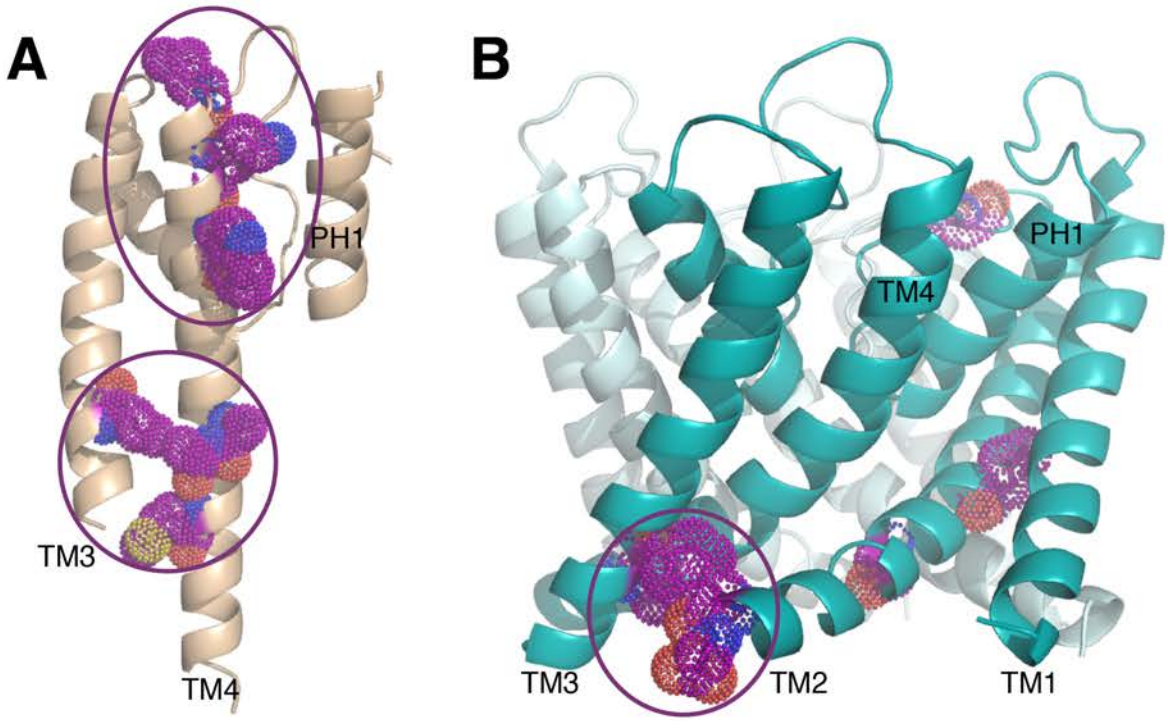


Figure 3.6: *Residues identified as important to gating using the genetic complementation assay. When mutated, these residues were able to complement the growth of K^+-auxotrophic yeast. Residues – shown as purple mesh – are mapped onto (**A**) a fragment of a closed-state KcsA-based TREK-1 model (gold) and (**B**) A complete KvAP-based TREK-1 model (subunit 1 teal, subunit 2 pale cyan). For clarity, TM4 mutations are not shown on the KvAP-based model; though residue S164 is shown close to PH1 and the selectivity filter. Clusters of activatory mutations are shown circled in purple.*

3.4.1 Activatory mutations identified near the pore helices

GoF mutations found towards the extracellular interface of the channel include TM4 mutations L282P, K286R and W290L as well as the L184I mutation in TM2. Interestingly, PH1 lining mutations in the upper-TM4 region were pointing to the pore helix, suggesting a possible direct interaction between these two regions (figure 3.7). However, L184 appears to be facing away from the pore, meaning that interaction between this residue and PH1 is unlikely (figure 3.7). Although L184I is a highly conservative mutation, in is possible that it may be involved in a reorientation or movement of the helix resulting in disruption of important interactions at either end of TM2. Importantly, L184I is also in close proximity to the highly conserved upper glycine hinge (G181) proposed to be involved in lower-gating in other K^+ channels (see section 1.6.1), as well as a proline residue (P183) which is conserved

in all K2P channels. However, how such a conservative L184I mutation would affect the channel is unclear.

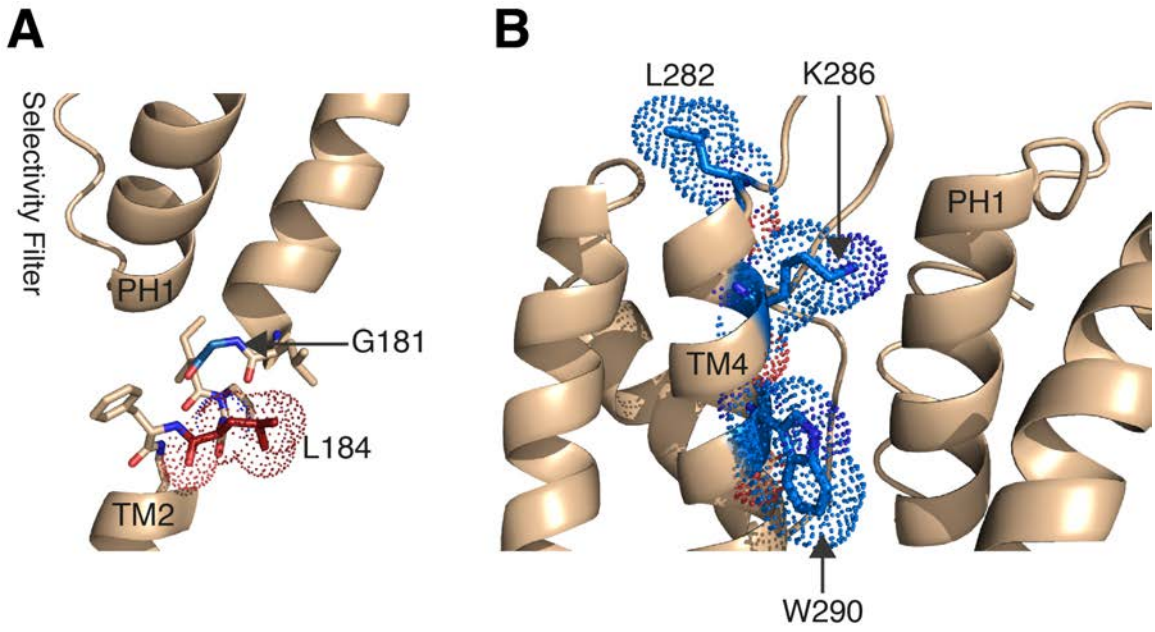


Figure 3.7: *Residues identified as activatory when mutated, towards the extracellular region of TREK-1, when mapped onto a KcsA based homology model. (**A**) L184 (red) to isoleucine substitutions were found to complement growth of K^+-auxotrophic yeast. The orientation of this residue awat from any potential interaction, it is possible that L184I mutations activate TREK-1 channels due to disruption of the position of highly conserved G181 residue (light blue). (**B**) Upper-TM4 mutations are close to the first pore helix (PH1) shown as dots (blue).*

The L282P mutation may increase rigidity in the extracellular linker-domain between TM helices TM3 and TM4, potentially causing significant alteration to channel architecture. This mutation would likely change the orientation of the proceeding TM4 helix affecting residues further downstream, including K286 and W290, mutations of which were also found to activate TREK-1 channels. A K286R mutation would potentially introduce a longer, bulkier side chain into the highly ordered and tightly packed region between TM4 and PH1, possibly disrupting this region (figure 3.7).

W290L substitutions may also cause a similar disruption of interactions between PH1 and TM4 in the closed state model (figure 3.7). Examination of these structures suggest that, given the apparent locations of K286 and W290 in close proximity to the pore, the upper-TM4 mutations could possibly elicit conformational changes in the selectivity filter via their interaction with PH1.

3.4.2 GoF mutations in the lower TM helices

GoF mutations located further down the TM helices included A190D and A301E where small, non-polar alanine residues were replaced with larger, charged amino acids in roughly the same position in the two pore-lining TM helices (TM2 and TM4). Subsequent sequence alignment showed these alanine residues to be conserved across many K2P channels (Appendix IV), suggesting an important role for these residues in maintaining normal channel function. The position of A190 and A301 appears to be in the most constricted region of the ion conduction pathway and, based upon their position in the KcsA closed-state structure, introduction of a negative charge at these positions might affect packing of the TM helices in this region (figure 3.8).

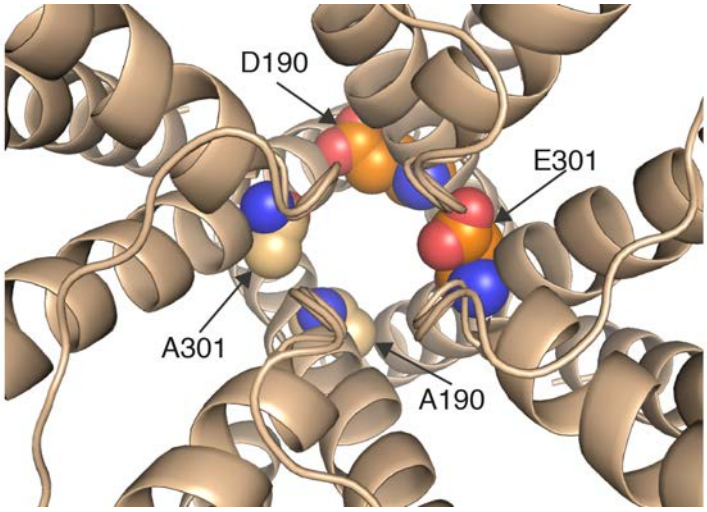


Figure 3.8: *Residues of interest mapped onto a KcsA-based TREK-1 structural model, shown from a bottom up view. Mutations A190D and A301E are shown as predicted by in silico substitution. Mutated residues (orange) reduce the space within the ion conduction pathway constriction, close to the proposed lower gate.*

Interestingly, the nearby substitution M306I, was also identified to have an activatory phenotype in the genetic complementation assay (figure 3.9). Together, these results indicate that the lower region of TM4 might be important for channel gating, as is seen in other K^+-selective channels (Paynter *et al.* 2010).

An activatory mutation, I230N, was identified in the non-pore-lining helix TM3 and indicates that the outer helices may also play a part in channel gating. This mutation could result in disruption of interactions between I230 and residues F200 and M306 (figure 3.9). Interestingly, both of these

residues were also identified as GoF mutations (F200L and M306I). Alternatively, I230N could activate TREK-1 simply because of the introduction of a hydrophilic residue, within the lipid phase of the membrane, resulting in restructuring of TM3. Consistent with this, no other substitutions were identified in this position (Appendix V).

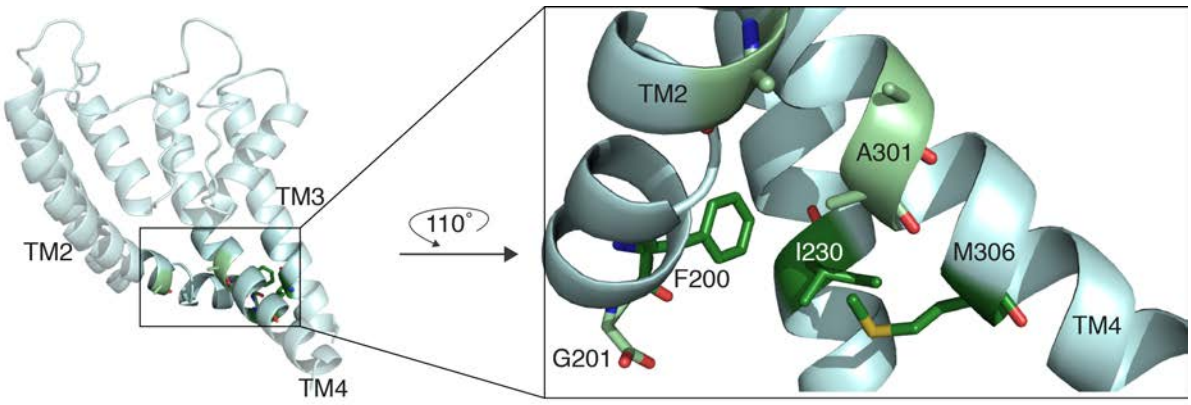


Figure 3.9: *Residues of interest mapped onto a KvAP-based TREK-1 homology models. Residues proposed to be involved in a putative TM2-TM3-TM4 connection (F200, I230, M306) are shown in Dark green. Other residues which, when mutated, complement growth of K^+-auxotrophic yeast are shown in light green.*

3.4.3 Limitations of using homology models based on prokaryotic K^+ channels

Using models based on prokaryotic K^+ channel structures inevitably has its pitfalls; key among these is that it is difficult to determine any intra-protein interactions with a great deal of accuracy, as there is a fairly large margin of error embedded in the modelling process. Of course, the high homology of the inner pore and ion conduction pathway means the models may be reasonably accurate within this region, though predicting possible interactions involving the outer helices is more difficult. Moreover, the use of a four-fold symmetrical template to model a channel which assembles as an asymmetric 'dimer of dimers' will inevitably produce some inaccuracies.

However, using the KvAP- and KcsA-based models as a guide to the structure of the pore has proven to be constructive in both computational and experimental studies (Cohen *et al.* 2008, Sandoz *et al.* 2008, Bagriantsev *et al.* 2011, Piechotta *et al.* 2011).

3.4.4 Validation of the homology models

In a parallel study of the TREK-1 structure pore also being carried out within the Tucker laboratory, structural models were made based on 18 different templates – including KcsA, NaK, MthK and $K_v1.2$ – and then examined with *in silico* docking of a quaternary ammonium pore blocker, tetrapentylammonium (TPenA). The results of the TPenA docking studies were then compared with data acquired by *in vitro* experiments and, from this, it was determined that the open-state KvAP-based structure was found to be the most accurate fit to experimental data, and hence this model was used during the early phase of this project (figure 3.10) (Piechotta *et al.* 2011). As the publication of these results followed the completion of this phase of our study, the KcsA closed-state model was also used to draw some of our preliminary conclusions, above.

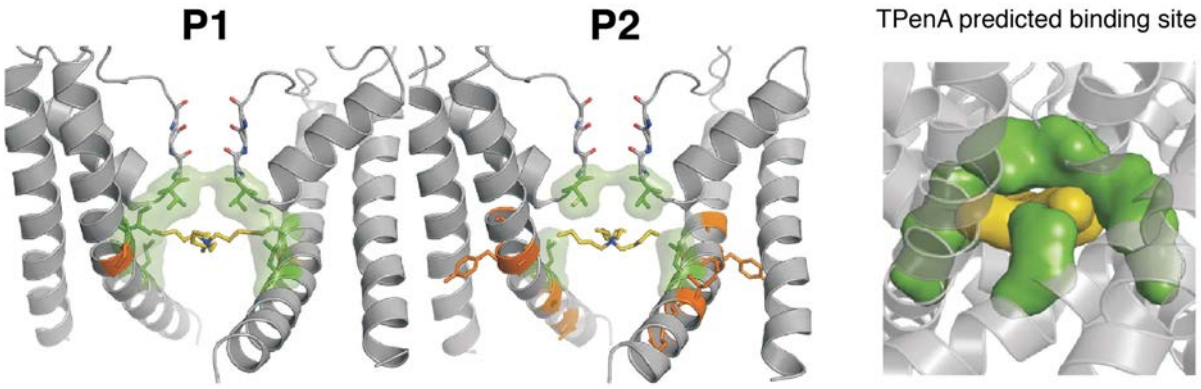


Figure 3.10: *The tetrapentylammonium (TPenA) binding site in TREK-1. TPenA is shown docked into the KvAP-based homology model of TREK-1. Two different side-view images are shown each with one pore-forming unit removed for clarity. Residues predicted to directly interact with TPenA are show in green while those which do not appear to contribute directly to the binding site are shown in orange. The right hand panel shows a side view of how TPenA (yellow) docks well into the predicted binding site. Figure and text adapted from Piechotta et al. 2011*

Interestingly, the same study suggested that the channel is primarily gated at the C-type 'upper-gate', because the binding site for TPenA is just below the selectivity filter remain accessible, irrespective of whether the channel is open or closed. Nevertheless, even in the absence of a HBC-like gate, the identification of a large number of mutations located towards the intracellular membrane-interface of the TREK-1 channel suggests that the lower TM helices can influence channel gating, without necessarily opening and closing by an aperture like movement.

In later chapters as new, closely related K2P crystal structures and further experimental evidence became available the mutations and their possible methods of activation are discussed in more detail. However, the results of the genetic complementation assay can be used to conclude that, from the putative locations of the GoF mutations, TM helices TM2 and TM4 appear to be key elements of TREK-1 gating apparatus.

3.5 External corroboration of the genetic complementation assay

A study published shortly after the completion of our genetic complementation assay used a similar approach for identifying mutations involved in TREK-1 gating (Bagriantsev *et al.* 2011). Mutations to a number of residues found in the N-terminal region if TM4 (L282, W290 and F291) as well as close to the selectivity filter-adjacent S164 mutation (I163) were identified. That some of the mutations identified by us were also identified by Bagriantsev *et al.* validates the approach adopted thus far. However, further characterisation of the GoF mutations was still required.

The following chapter describes initial electrophysiological experiments conducted to determine how activatory mutant channels are able to complement the growth of K^+-auxotrophic yeast.

Chapter 4

Alteration of TREK-1 pH sensitivity by activatory mutations

4.1 Investigation of activatory mutations identified using the genetic complementation assay

The genetic complementation assay has been a valuable approach for identifying residues and regions important for gating in other K^+ channels (Minor, *et al.* 1999, Paynter *et al.* 2010). As described in the previous chapter, application of this assay identified 14 residues potentially involved in the control of TREK-1 activity. GoF mutations were primarily focussed around three regions: the selectivity filter, proximal C-terminal regulatory domain and two pore-lining TM helices. Moreover, within the pore lining helices mutations were clustered in two distinct regions towards the PH1-lining region and the cytosol / membrane interface.

Unfortunately, while the complementation assay was useful for indentifying residues of possible interest, it provides little information about the mechanisms by which they modulate the activity of TREK-1.

4.1.1 Why do GoF mutations complement yeast growth?

The genetic complementation assay involved expression of TREK-1 channels in the cellular membrane of K^+-uptake deficient yeast. TREK-1 channels are able to then provide an alternative route of entry for K^+ ions into the cell, resulting in cellular proliferation. There are three parameters that are able to affect the amount of K^+-current which flows through these channels, most commonly represented in the equation $I = NP_oi$ (where I = whole cell current, N = number of channels expressed, P_o = open probability and i = single channel current) (Hille 2001).

The overall number of channels (N) would, of course, play a part in determining the whole cell current. A mutation that increases the rate or duration of TREK-1 expression would increase the likelihood of complementation. Although TREK-1 channels have been extensively studied, mechanisms and regions of the channel responsible for the regulation of functional expression *in vivo* are still poorly understood. However, the wide distribution of the mutations across the channel suggests that mutations that were all believed to affect one (or both) of the other parameters responsible for an increased K^+ current. Given the large single channel conductance of TREK-1 channels, it is likely that the open probability (P_o) of the activatory channels is increased, leading to complementation of yeast growth.

Promisingly, a similar study conducted previously showed that expression of GoF mutant channels identified using the SGY1528 genetic complementation assay all had increased P_o in comparison to wild type TREK-1. Moreover, GoF mutants and wild type TREK-1 channels were expressed at similar levels (figure 4.1) (Bagriantsev *et al.* 2011). Note the labelling from this particular study is of the short form of TREK-1, 15 N-terminal residues shorter than the TREK-1 clone we used. The two forms of TREK-1 do not differ functionally.

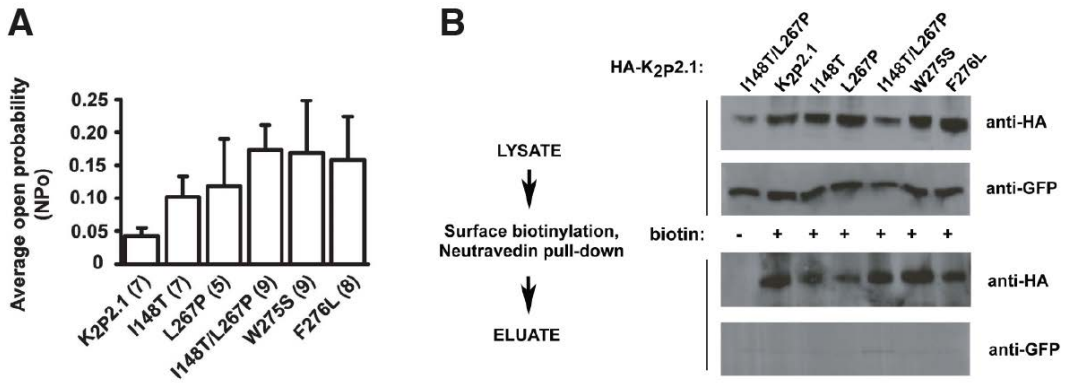


Figure 4.1: *Properties of GoF mutations in mammalian TREK-1 channels (short form). (**A**) Open channel probabilities from single channel analyses calculated on recordings of ~30 s duration. K2P2.1 (TREK-1) (n = 7), I148T (n = 7), L267P (n = 5), I148T/L267P (n = 9), W275S (n = 9), F276L (n = 8). Data represent mean ± s.e. (**B**) Immunoblot analysis of total COS7 cell surface expression of TREK-1 ($K_{2P}2.1$) bearing an N-terminal HA tag, for the indicated wild type / mutant channels. Cells were labelled with membrane-impermeable biotinylation reagent followed by cell lysis and capture of the labelled proteins on neutravidin beads. The intracellular GFP was expressed from the same vector. Figure and text adapted from Bagriantsev et al. 2011.*

4.2 The effects of GoF mutations to intracellular pH sensitivity

It has been previously established that the intracellular environment of SGY1528 is highly acidic (Madrid *et al.* 1998) and the yeast cells are grown in acidic media (pH 6.5). The link between complementation of growth in yeast and a change of pH sensitivity has been documented before. $K_{ir}2.1$, used initially as a positive control for some of the complementation assays here, is known to not complement growth at low $[K^+]$ when a region important for intracellular pH sensitivity was mutated (Minor *et al.* 1999, Chatelain *et al.* 2005). For example, when a threonine residue is introduced in place of methionine at position 84, the channel is unable to complement growth, though it is unclear if complementation is due solely to a change in intracellular pH sensitivity.

Nonetheless, it is interesting to note the tentative link between intracellular pH sensitivity and complementation of SGY1528 by K^+ channels, particularly as TREK-1 channels are robustly modulated by changes to intracellular pH. Indeed, the identification of E321A – a mutation previously reported to cause a complete loss of TREK-1 intracellular pH sensitivity (Honoré *et al.* 2002) – using the genetic complementation assay, suggested that a loss of intracellular pH sensitivity may be

involved in complementation of growth[1]. Therefore, we began functional analysis of the GoF mutants, by examining their effects on intracellular pH sensitivity of TREK-1.

4.2.1 Poor expression of TREK-1 GoF mutant channels in *Xenopus* oocytes

The effect of intracellular pH modulation was investigated with giant patch recordings in the laboratory of Prof. T. Baukrowitz. However, when many of the GoF mutants were expressed in oocytes,very little current could be observed. The TREK-1 wild type clone from *Rattus norvegicus* was routinely used for heterologous expression in *Xenopus* oocytes in the Tucker and Baukrowitz laboratories and produced robust currents prior to examination of these GoF mutations. Indeed, a large number of mutations were made and functionally expressed using the same rat TREK-1 (rTREK-1) gene for a systematic scan of the channel (Piechotta *et al.* 2011). Nonetheless, of the 14 GoF mutations identified here, only five novel mutant channels consistently produced currents which could be measured (figure 4.2).

4.2.2 The effects of intracellular pH on GoF mutant channels

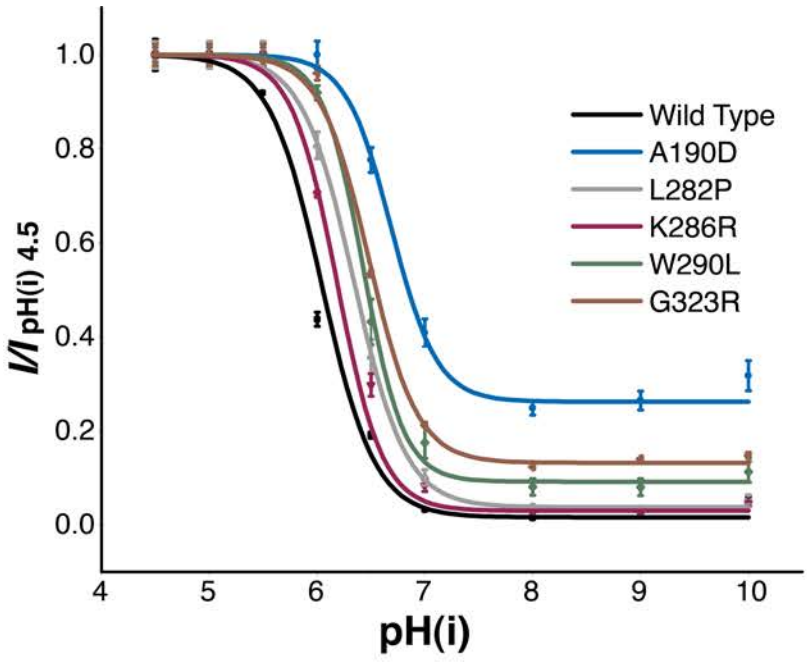


Figure 4.2: *TREK-1 GoF mutations affect channel response to intracellular acidosis. Normalized intracellular pH (pH(i)) responses for the functionally expressed channels. (Experiments were conducted by members of Prof Thomas Baukrowitz' laboratory)*

[1] see section 1.7.1 for more details about TREK-1 intracellular pH sensitivity

The dose-response relationships shown above reveal that all of the GoF mutations tested result in reduced intracellular pH sensitivity, though to differing extents; an example of this is shown in figure 4.3. The slope of the fitted curves for each mutant appear very similar to wild-type channels, but all show an increased level of activity in conditions of extreme intracellular alkinisation. This suggests that the slight blunting of channel responses by the majority of GoF mutations to cytosolic protonation could simply be because of the anticipated increase in basal activity, rather than a direct interference with proton sensing. Indeed it is highly interesting that mutations of residues 282, 286 and 290 close to the pore all produce similar changes to pH sensitivity; as these mutations are not exposed to the cytoplasm and are therefore highly unlikely to be involved in directly sensing changes in intracellular [H^+]. However, it is possible that mutations in the upper-TM4 helix may be involved in somehow transducing intracellular signals the putative upper gate.

Mutation G323R supports previous evidence regarding the C-terminal regulatory domain as it was shown to significantly reduce intracellular pH sensitivity (figure 4.2). However, the effects of G323R did not appear to reduce intracellular pH sensitivity to the same extent as mutations of E321. One possible explanation for the marked but incomplete loss of proton sensitivity may be because G323 plays an important role in the movement involved in interactions between the C-terminus and the phosopholipid bilayer. An arginine subsititution would likely increase the electrostatic binding of the regulatory domain to the phospholipid headgroups of the membrane. However, the loss of flexibility which would result from glycine removal, may counteract these activatory effects, particularly as the adjacent negatively charged residue (E324) may disrupt the stability of interactions between the C-terminus and bilayer, preventing G323R from being a constitutively active mutant channel.

Given its location within the C-terminal regulatory domain it is interesting that G323R mutant channels retain more pH sensitivity that the A190D GoF mutation in TM2. Changes within this regulatory domain would be expected to have more marked effects on sensitivity to proton-mediated effects than a substitution close to the ion conduction pathway.

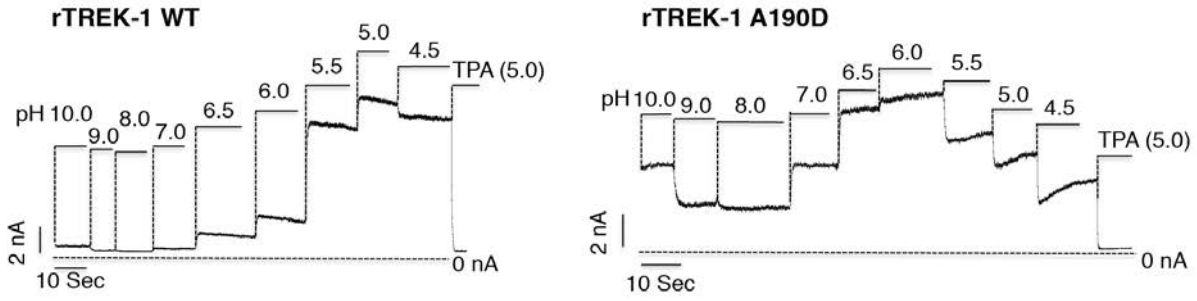


Figure 4.3: *Exemplar electrophysiological recordings of the indicated channels. The measurements, taken at -80mV, show the effect of intracellular protonation on currents produced by wild type (WT) and mutant (A190D) channels.*

From the investigation into the response of GoF mutants to intracellular pH, it is difficult to draw firm conclusions regarding the link between complementation of yeast growth and intracellular pH sensitivity. However, it is apparent that the mutant channels which were tested, generally caused a reduction of intracellular pH sensitivity. Nonetheless, there is clearly no correlation between changes internal pH sensitivity and the strength of complementation in yeast. For example, while K286R mutants greatly increased growth density in yeast more than the pH-insensitive E321A mutant channels (figure 3.2), the effects of K286R mutation to intracellular pH sensitivity were modest (figure 4.3). Consequently, the effects of GoF mutations to TREK-1 internal pH sensitivity were not followed up.

4.3 The effect of mutations on whole cell currents

To bypass the problems with expression of GoF mutations of rTREK-1, the mutations were also made in the highly homologous human TREK-1 (hTREK-1) channel. hTREK-1 GoF mutations were retested using the complementation assay to confirm that complementation of SGY1528 growth was preserved. This confirmed that hTREK-1 mutant channels behaved the same as rTREK-1 (not shown). The mutations in hTREK-1 were therefore expressed in *Xenopus* oocytes, initially to examine the effect of mutations to whole cell currents.

GoF mutations generally resulted in larger whole-cell currents than wild type channels; the only exception was S164P, which exhibited basal activity similar to wild type channels (figure 4.4). The

increased basal currents shown by other GoF mutations supported the hypothesis that mutations complement growth due to increased activity in comparison to wild type channels. It is worth noting that the inward current produced in conditions of extreme hyperpolarisation – as would be present in SGY1528 cells – is also larger for all of the GoF mutations (examples shown in figure 4.5). It is also worth noting that, while S164P mutants did not increase basal outward current, this mutant shows in increase in inward current at hyperpolarised potentials (i.e. in similar conditions to the SGY1528 cellular environment). This phenomenon may explain why this mutant is able to complement yeast growth, without notably increasing basal / outward current in *Xenopus* oocytes (figures 4.6 and 4.7).

The considerable increase in basal activity by the I230N mutant was particularly significant (figure 4.4). Indeed, as the only mutation identified on a non-pore lining TM helix (figure 3.9), the effect of I230N to basal current is all the more remarkable. Furthermore, there were dramatic changes to the I-V profile of I230N mutants in comparison to other GoF mutants and wild type TREK-1; I230N currents appear to reverse at a more negative potential than the other mutants (figure 4.5). The reason for this is not clear though may involve changes in selectivity by I230N mutation.

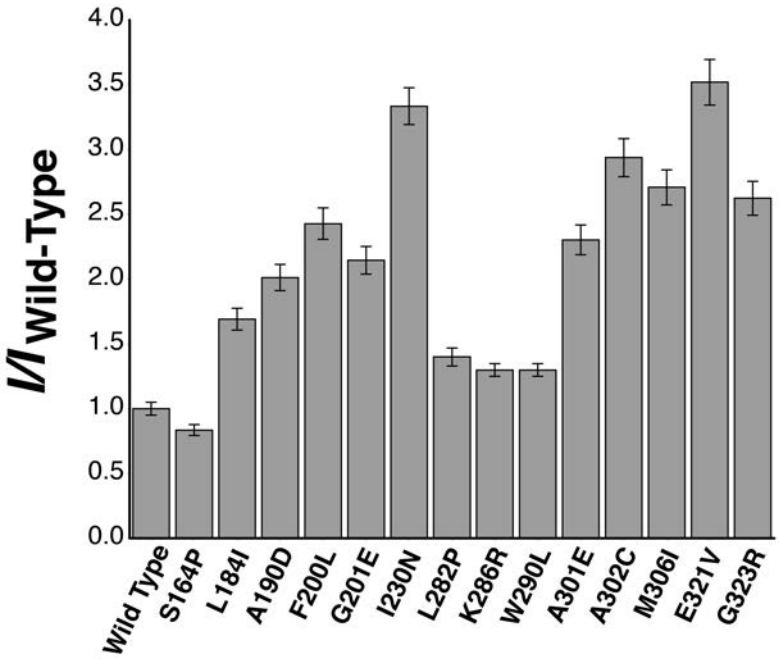


Figure 4.4: *Quantification of normalized current amplitudes at 100mV, when measured in ND96 solution, at pH 7.4. Oocytes were injected with 0.2ng of mRNA and recorded following 18 hours of incubation. (Wild type currents were measured as 5.05 ± 0.05 μA, n=9).*

The three mutations in TM4 identified in a cluster close to the PH1 in TM4 all activated TREK-1 channels to the same extent (figure 4.4). Taking into account the unique size of basal current increases and the well-conserved blunting of intracellular pH sensitivity by these mutant channels, it is likely that the mechanism by which alterations to channel function are made by the mutations clustered in the upper-TM4 region (L282P, K286R and W290L) may be similar.

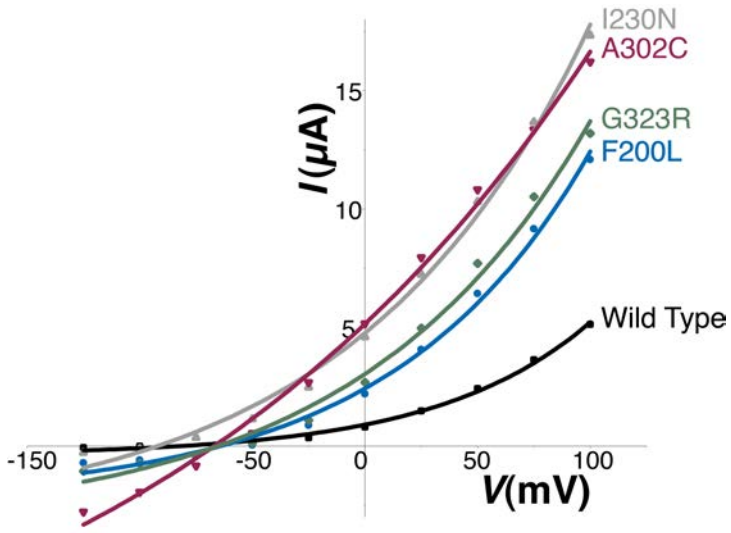


Figure 4.5: *Exemplar current-voltage (I-V) traces from whole-cell recordings the indicated channels at pH 7.4. Xenopus oocytes were injected with 0.2ng of mRNA and recorded following 18 hours of incubation.*

Mutations identified close to the C-terminal regulatory domain all had high levels of outward current (figure 4.4). The most active mutation here was the A302C mutation. This is interesting, as the negative charge introduced to the neighbouring residue in mutations A301E appear to have more dramatic effects in disrupting the architecture of this region than the smaller cysteine substitution to the adjacent residue (A302C), when mapped onto a KcsA-based homology model (figure 3.8).

The activatory phenotype exhibited by E321V mutants in yeast, was clearly reflected in a near 3.5-fold increase of whole cell current in oocytes. Moreover, the mutation G323R within the C-terminal regulatory domain also had high basal currents. It was noteworthy that G323R mutations produced currents twice as large as mutation K286R, though complemented growth of yeast cells particularly weakly by comparison (figure 3.2), highlighting the lack of correlation between electrophysiological activity and apparent strength of complementation. Interestingly, only for the I230N and E321V

mutations was the relative strength of complementation (figure 3.2) reflected in the levels of basal activity (figure 4.4).

4.4 The effects of extracellular pH on GoF mutant channels

A mutation found in the extracellular vestibule of the channel (S164P) is of a residue which has been previously implicated in extracellular pH sensitivity (Cohen *et al.* 2008) and uniquely results in minor changes to basal channel activity. Moreover, as the yeast were grown in acidic media (pH 6.5) it is possible that the loss of pH inhibition in acidic conditions could be the reason why this GoF mutant was able to complement yeast. Therefore, the effect of extracellular pH on all of the GoF mutations was examined. However, the wild type TREK-1 response was first studied.

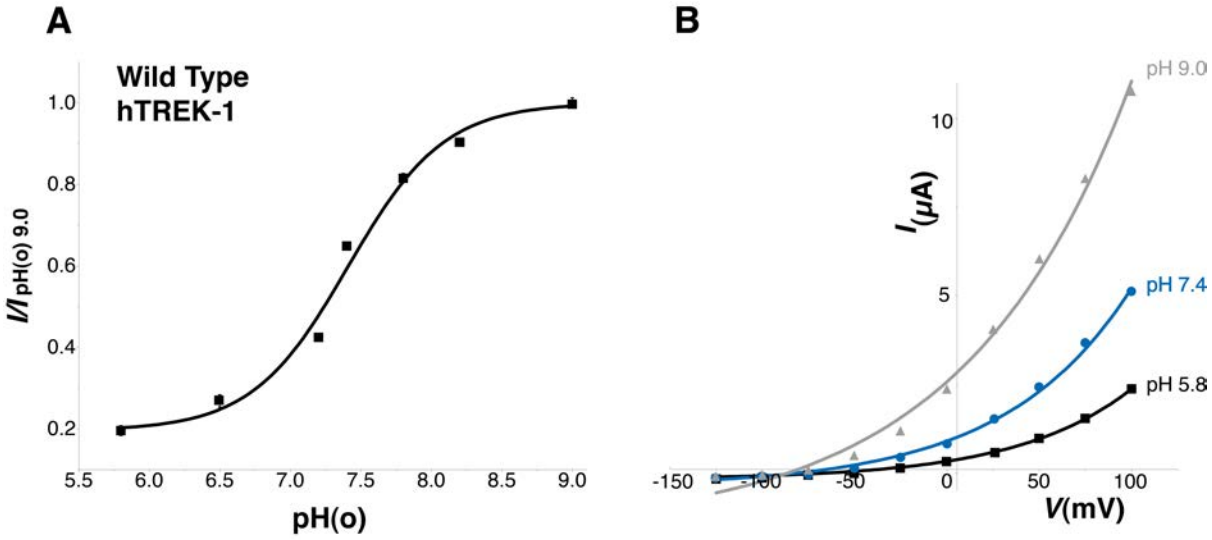


Figure 4.6: *Extracellular pH sensitivity of wild type hTREK-1 channels. (**A**) The dose-response relationship of wild type channels normalised against current at pH 9. (**B**) Exemplar I-V responses of wild type channels vary greatly when currents are stimulated in acidic (pH 5.8) neutral (pH 7.4) and alkaline (pH 9.0) extracellular environments.*

Unlike other TREK family members, TREK-1 has the unique property of displaying opposing responses to extra- and intracellular pH sensitivity. This means that while they are activated by intracellular acidification, by contrast they are activated by external alkalinisation. Notably, pH-mediated effects on the channel are particularly pronounced within physiological proton concentrations; the activity of TREK-1 wild type are doubled between pH 7.2 and 7.8 (figure 4.6).

4.4.1 The S164P mutants

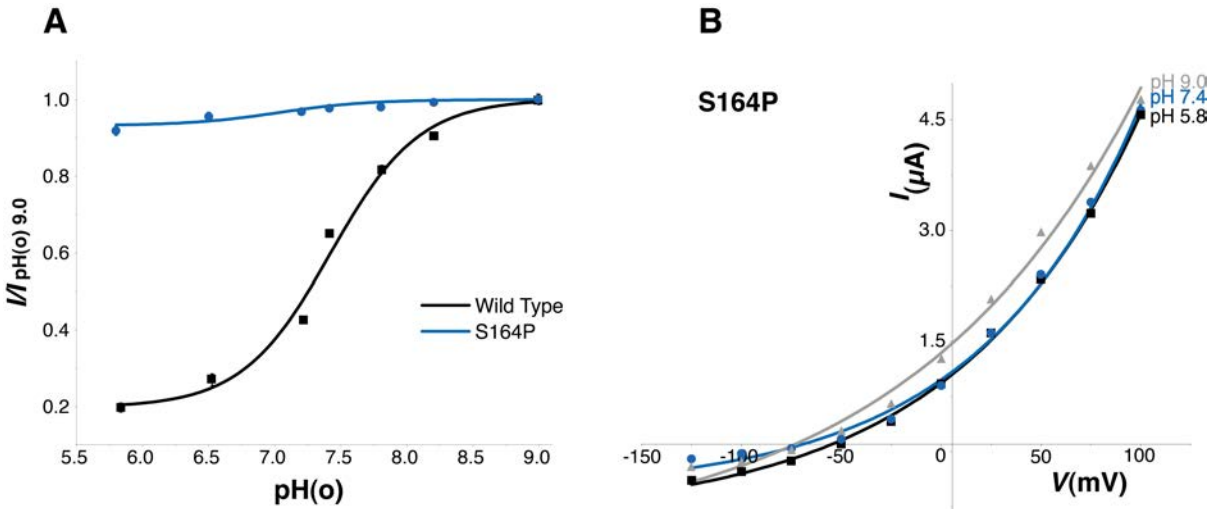


Figure 4.7: *External proton sensitivity of an activatory mutation identified in the external vestibule, S164P. (**A**) A normalised dose-response curve comparing S164P to wild type channels. (**B**) An exemplar I-V relationship of I230N mutant channels.*

In figure 4.7, it is clearly shown that S164P mutations caused a significant loss of inhibition by protons across the different external pH conditions used. Maximal activation of the wild type channel occurs at pH 9, though S164P channels are nearly fully active the lower end of normal physiological external proton concentration. In addition, the channel is 96 ± 1.5% active at pH 5.8 in comparison to wild type channels, which are only 20 ± 1.2% conductive under the same conditions.

Residue S164 is located only a few residues downstream of the selectivity filter and a mutation to this residue (S164Y) was previously reported to increase sensitivity to extracellular protonation and accelerate C-type gating at the selectivity filter (Cohen *et al.* 2008). Tyrosine mutations to the equivalent residue in other K^+ channels have also been reported to increase extracellular pH sensitivity (López-Barneo *et al.* 1993, Zilderberg *et al.* 2001)[2].

These results justified further examination of the relationship between sensitivity to extracellular protonation and complementation of K^+-auxotrophic yeast growth and so the the effects of the other GoF mutants on external pH sensitivity were examined.

[2] More details about these studies are given in section 4.5.

4.4.2 TM2 mutants

Mutations within the pore lining TM2 were examined for their effects on extracellular pH sensitivity. In figure 4.8, it can be seen that the largest effect on external pH sensitivity produced by a TM2 GoF mutation was by the A190D mutation. However, while the basal current produced by A190D is significantly higher than wild type TREK-1, the F200L mutation produced the greatest increase in current (figure 4.4). Interestingly, F200L channels exhibit only slight blunting of external pH sensitivity, particularly within the critical physiological range and above (pH 7.2-7.8).

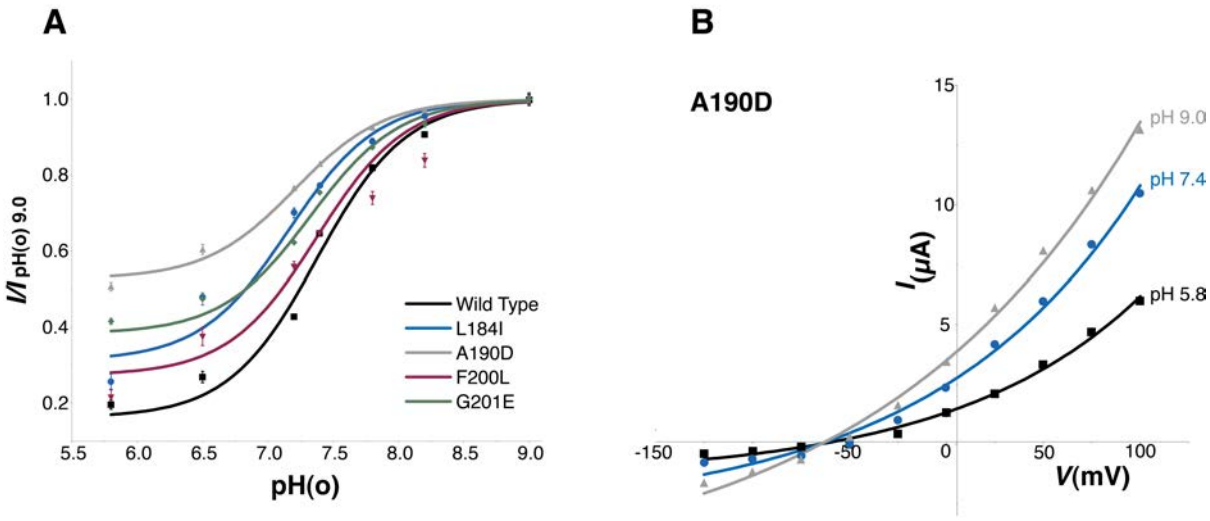


Figure 4.8: *External proton sensitivity of the indicated channels in the TM2 helix. (**A**) Normalised extracellular pHo responses at 100mV for the indicated channels. (**B**) Exemplar I-V responses for A190D mutant channels, when currents are stimulated in acidic (pH 5.8) neutral (pH 7.4) and alkaline (pH 9.0) extracellular environments.*

4.4.3 Upper-TM4 mutants

The three activatory mutations near the extracellular interface of TM4 were found to have varied effects on extracellular pH sensitivity (figure 4.9). The L282P mutation results in a major reduction in pH sensitivity as channels are essentially fully activated between pH 7.4 and pH 9. This is in stark contrast to W290L, which exhibits similar sensitivity to changes in external pH as wild type channels. By contrast, W290L produced the greatest reduction of intracellular pH sensitivity, compared to the other GoF mutations in the upper-TM4 region (figure 4.2). K286R mutant channels appear less

sensitive to external pH than W290L mutants, though still exhibited wild type-like sensitivity to pH above pH 7.8 (figure 4.9).

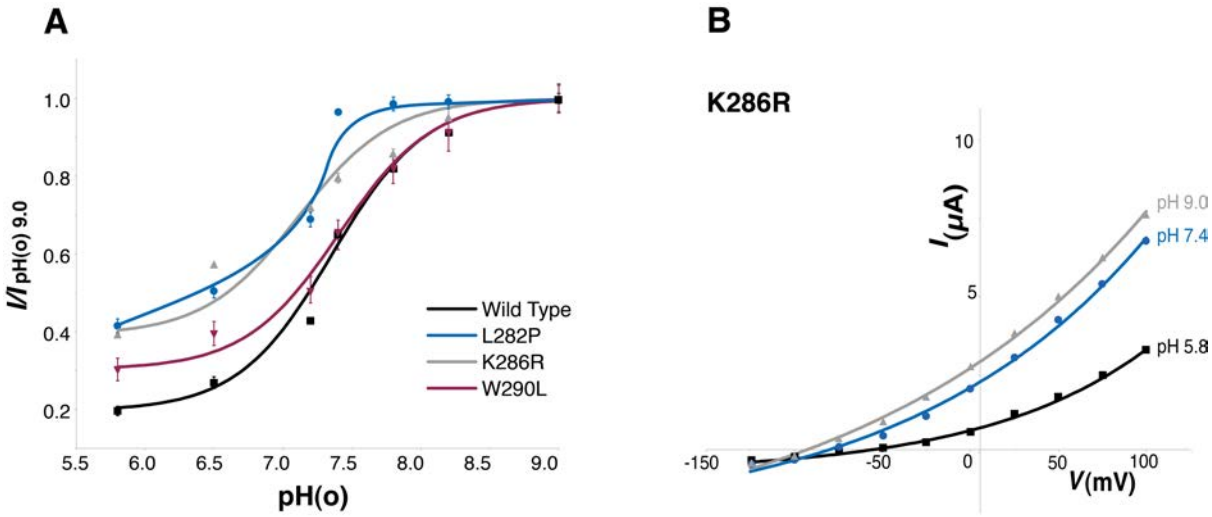


Figure 4.9: *External proton sensitivity of the indicated channels in the upper-TM4 region. (**A**) Normalised extracellular pHo responses at 100mV for the indicated channels. (**B**) Exemplar I-V responses for K286R mutant channels, when currents are stimulated in acidic (pH 5.8) neutral (pH 7.4) and alkaline (pH 9.0) extracellular environments.*

It is interesting to note that, while the effects of increasing basal currents (figure 4.4) and reducing intracellular pH sensitivity (figure 4.2) were similar for the upper-TM4 mutations, L282P, K286R, W290L, their effect on extracellular pH sensitivity were highly varied (figure 4.9), suggesting that this region may be involved in external proton sensing, particularly residue L282.

4.4.4 Lower-TM4 mutants

In contrast to the upper-TM4 mutations, all of the GoF mutations identified lower down in TM4 had a major effect on external proton sensitivty (figure 4.10). Where mutations in other regions of interest resulted in highly varied responses across different proton concentations, all lower-TM4 mutatons displayed a notable loss of sensitivity across the tested pH range. This is particularly interesting as these residues are located far away from any extracellular region of the channel, and therefore the H^+ sensor, as well as the upper-gate which is thought to be within the filter.

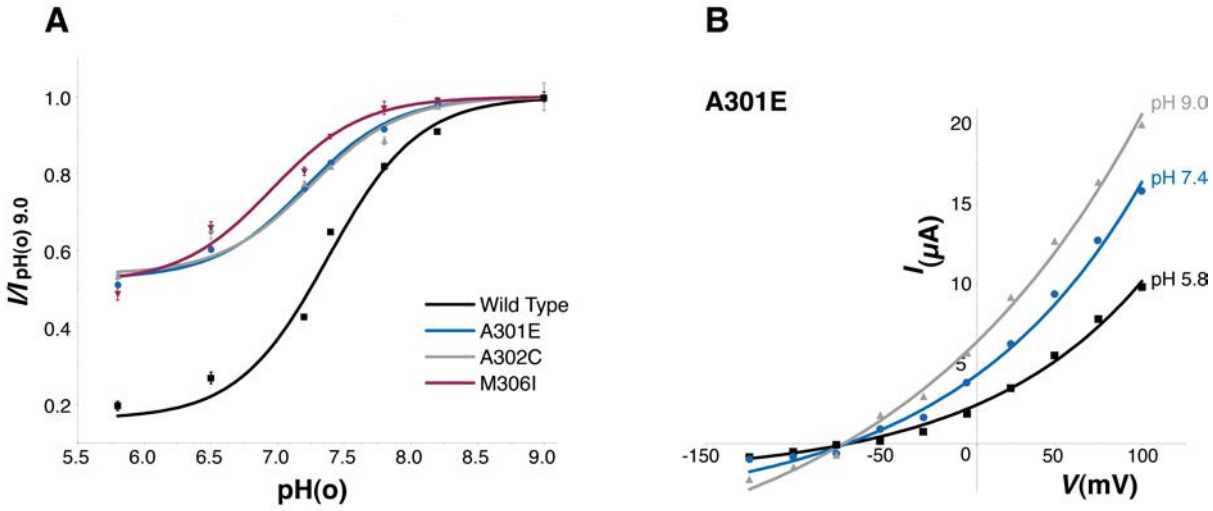


Figure 4.10: *External proton sensitivity of the indicated channels in the lower-TM4 region. (**A**) Normalised extracellular pHo responses at 100mV for the indicated channels. (**B**) Exemplar I-V responses for A301E mutant channels, when currents are stimulated in acidic (pH 5.8) neutral (pH 7.4) and alkaline (pH 9.0) extracellular environments.*

4.4.5 The I230N mutant

The remaining mutation in the TM helices was examined. The I230N mutation was found to exhibit a similar phenotype to the lower-TM4 mutants; this mutation also resulted in a large increase in basal activity (figure 4.4), complementation of growth in K^+-auxotrophic yeast (figure 3.2) and, interestingly, a dramatic loss of sensitivity to external proton modulation (figure 4.11).

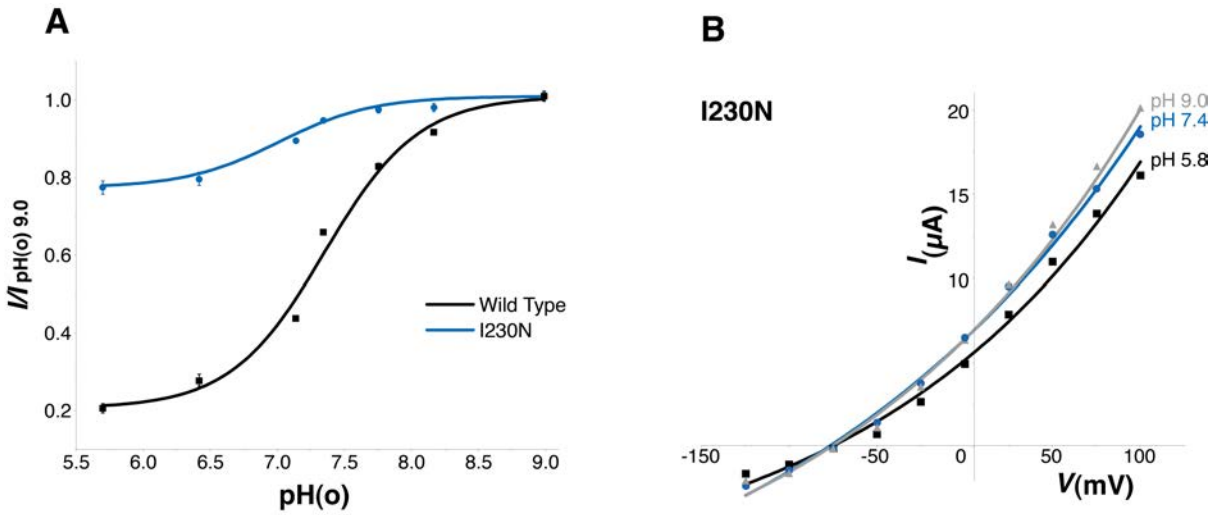


Figure 4.11: *External proton sensitivity of a TM3 helix mutant, I230N. (**A**) A normalised dose-response curve comparing I230N to wild type channels. (**B**) Exemplar I-V responses for I230N mutant channels, when currents are stimulated in acidic (pH 5.8) neutral (pH 7.4) and alkaline (pH 9.0) extracellular environments.*

As the only GoF mutation found in a novel region outside of the two pore-lining helices, I230N and the method by which it activates the channel is of great interest. The notable loss of pH sensitivity exhibited by this mutant in suggest that the asparagine substitution here results in a change of conformation of the upper gating apparatus, even though it is located within a lower, non-pore-lining TM helix. It is possible that I230N mutation activates the channel by influencing the position of nearby residues in the pore lining helices; residue 230 is located at the interface between TM2, TM3 and TM4 (figure 3.9).

4.4.6 C-terminus mutants

The activatory mutations identified in the proximal C-terminus exhibited highly increased whole-cell currents when expressed in oocytes (figure 4.4). In addition, it was found that E321V and G323R mutants were also both able to reduce pH significantly reduce external proton sensitivity (figure 4.12).

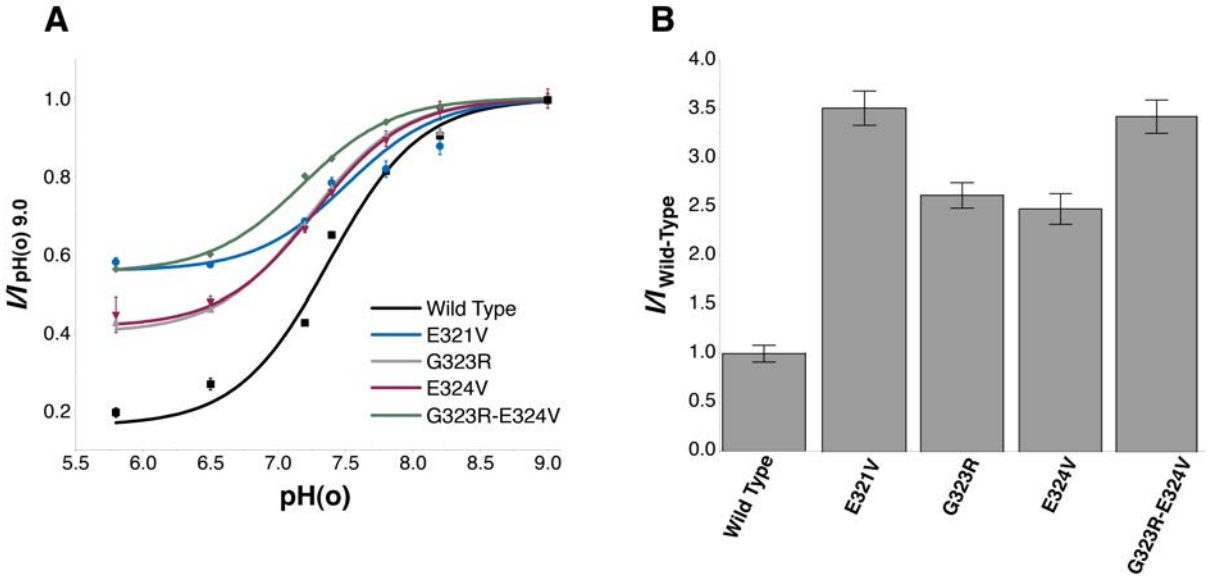


Figure 4.12: *Extracellular pH senstivity of C-terminal GoF mutations, as represented by (**A**) normalised extracellular pHo responses at 100mV and (**B**) changes to basal current, normalised against wild type, for the indicated channels.*

It was proposed in section 4.2.1 that the flexibility provided by a glycine at position 323 might prevent an adjacent negatively charged glutamate (E324) from disrupting the interaction between the C-terminal regulatory domain and the phospholipid head groups of the bilayer. To examine this theory, the E324V mutation were made and then tested. Neutralisation of this residue produces a channel

with a near-identical phenotype to G323R (figure 4.12). Moreover, double mutants containing G323R and E324V had an additive effect, producing currents of a similar magnitude to E321V channels. The double mutant channels were also able to reduce extracellular pH sensitivity to the same extent as E321V mutants (figure 4.12). These observations supported the idea that constitutive activation of G323R mutants may be inhibited by the adjacent negatively charged residue, E324.

4.5 The correlation between external pH sensitivity and complementation of growth

Generally, GoF mutations identified using the genetic complementation assay resulted in an increase in basal activity. However, the effects of some mutations on external pH sensitivity of TREK-1 channels are highly interesting. The near-complete insensitivity to changes in external pH of the S164P mutant channels is noteworthy, particularly as this was the only mutation which did not significantly alter basal current amplitude. Yeast are grown in acidic media at pH 6.5, in which wild type TREK-1 channels would presumable be inhibited (figure 4.6), Therefore the tentative link between complementation of K^+-auxotrophic yeast and extracellular pH sensitivity was explored. In order to do so, mutations known to affect TREK-1 external pH sensitivity were examined.

In the introductory chapter (section 1.7.2), the proposed roles of histidine residues 87 and 141 in pH sensing were outlined. Protonation of these M1P1 residues results in the opening of the channel via subtle allosteric movements, thought to produce a change in conformation of the pore (Cohen *et al.* 2008). This study also identified two other residues which can influence TREK-1 extracellular pH sensitivity, E84 and S164.

E84 is homologous to E418 in KcsA and E28 in KCNK0 and is believed to stabilse the upper-gate in the open conformation by forming hydrogen bonds with residues adjacent to the selectivity filter (R166). The negatively charged glutamate side chain is also thought to draw protonated H87 and H141 residues away from the selectivity filter causing a collapse of the pore region. Therefore

mutations of this residue (E84A) are proposed to result in disruption of these interactions and dramatically alter extracellular pH sensitivity (Cohen *et al.* 2008).

In the same study, S164 was mutated due to homology of this residue to T449 in the *Shaker* channels, which are thought to have a role in C-type gating (López-Barneo *et al.* 1993). Indeed, as it was shown that T449Y mutations in *Shaker* channels result in an acceleration of C-type inactivation, tyrosine substitutions were made in TREK-1 channels. Accordingly, S164Y was found to dramatically increase channel sensitivity to extracellular pH and accelerate C-type gating (Cohen *et al*. 2008).

Therefore, we re-created the S164Y and E84A mutants, and tested their ability to complement growth. Both mutants were examined using the genetic complementation assay as the two had completely different effects on external pH sensitivity of TREK-1. In addition, we also tested several mutations of residues H87 and H141, using the SGY1528 complementation assay.

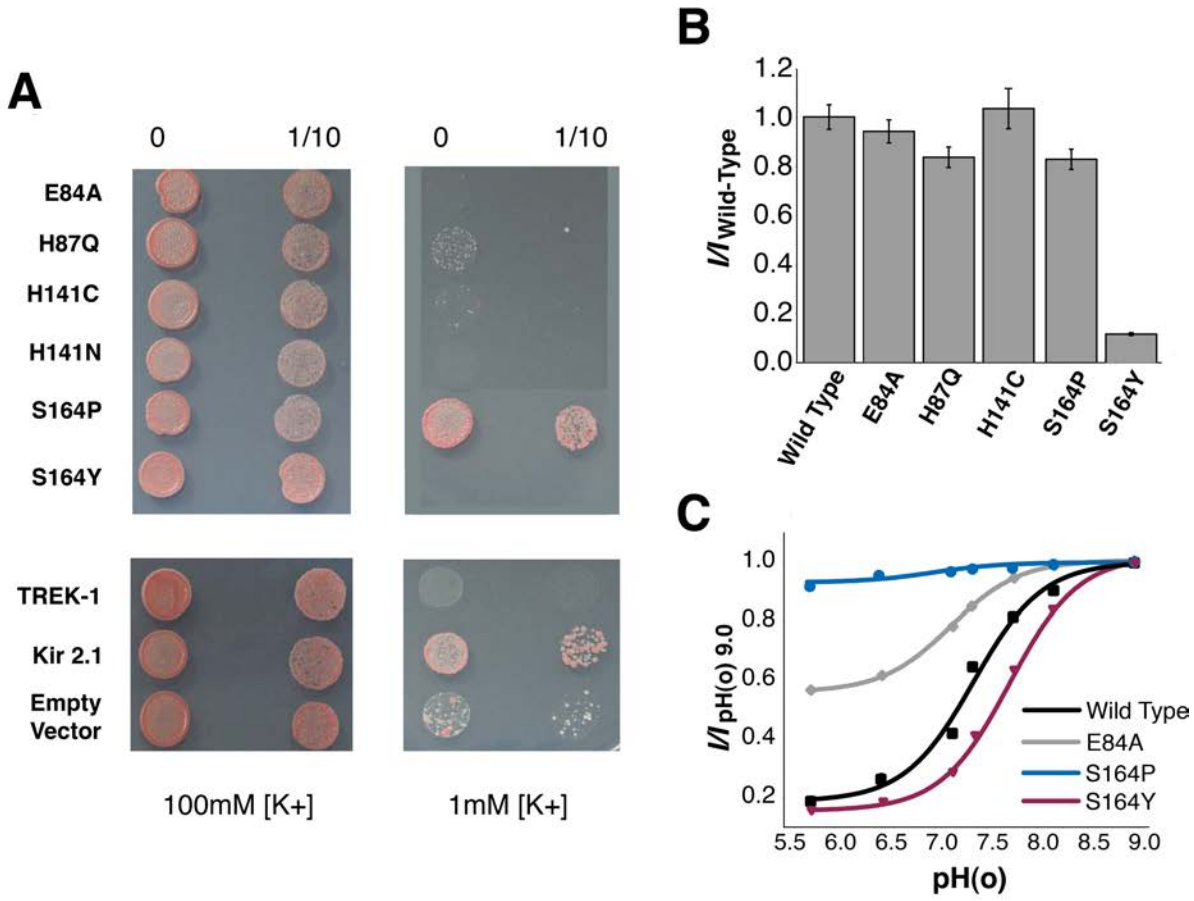


Figure 4.13: *Mutations known to alter TREK-1 pH sensitivity. (**A**) SGY1528 drop tests for the indicated mutations. (**B**) Changes in basal current and (**C**) extracellular pH (pH(o)) sensitivity by the indicated mutations.*

Following the complementation assay, it was clear that none of the mutations previously reported to alter extracellular pH sensitivity of the channel were able to complement growth in yeast (figure 4.13). In addition, of the tested mutations only the S164Y mutation significantly changed basal current levels when expressed in oocytes (figure 4.13). This reduced activity was expected for the S164Y mutant, because the increased pH sensitivity means that the channel is less active at neutral pH (figure 4.13). Importantly S164Y and wild type conducted currents of the same magnitude at high pH (not shown).

4.5.1 Alternative substitutions to residue S164

S164P mutations would significantly change the architecture of the extracellular cavity apparently resulting in a release of inhibition to external protons across the tested range (figure 4.13). It is possible that S164P mutations were the only mutations found in position 164 which were able to reduce external pH sensitivity sufficiently to complement growth in yeast without changing basal activity.

To examine the possibly unique role of proline in this position rather than mutate S164 residues to individual amino acids we constructed an S164*X* random mutant library, as described in section 2.2. The library of S164 random mutations was created, transformed into K+-auxotrophic yeast cells and treated as before (see section 2.5). Assuming that every possible combination was created during mutagenesis, only proline substitutions at position 164 were able to rescue yeast growth in low [K^+] (not shown).

4.6 Conclusions

In general, the GoF mutations identified markedly increased basal current amplitude, while many mutants were also able to affect TREK-1 sensitivity to both intra- and extracellular pH.

It is interesting to note that there appears to be little correlation between increased activity and a loss of sensitivity to external protonation for a selection of mutations, including L184I, F200L and G201E.

These three TM2 mutations result in large increases of basal current (figure 4.4), though only modest effects to pH sensitivity (figure 4.8). Furthermore, GoF mutants identified in the upper-TM4 region follow this trend; L282P, K286R and W290L all have similar effects in increasing basal activity, though these mutations result in channels with differential external proton sensitivity.

Only mutations found close to the cytosolic-interface in the third and fourth TM helices, I230N, A301E and A302C, are highly active (figure 4.4) and consistently exhibit a significant reduction in external pH sensitivity (figures 4.10 and 4.11) possibly because of the loss of a proposed connection between TM helices TM3 and TM4 (figure 3.9). Nonetheless, the experiments described in section 4.5 conclusively rule out the idea that mutant channels can complement growth because extracellular pH sensitivity is altered (figure 4.13).

The lack of experimental data regarding the effect of GoF mutations to intracellular pH sensitivity of the channels means it is difficult to determine the significance of shifts in sensitivity to cystosolic proton concentration seen in the tested GoF mutant channels. However, the effects of A190D substitutions in reducing TREK-1 sensitivity to intracellular pH sensitivity are particularly noteworthy. As A190 is unlikely to be involved in directly sensing protons on either side of the membrane, it is likely that the effects of A190D mutation are due to alteration of the channel structure, or a loss of of helical movement responsible for channel gating.

It appears that all of the mutants identified using genetic complementation assay exhibit some interesting and varied characteristics. Therefore, In order to understand these mutant channels better, in the following chapter the examination of GoF mutant channel responses to activatory agents and external [K^+] are reported.

Chapter 5

The use of activators to probe the TREK-1 gating mechanism

One of the benefits of studying TREK-1 as the archetypal K2P channel is the availability of a wide range of activatory ligands, which can be used to probe channel structure and function. In the following studies, several of these activators were used in an attempt to dissect the TREK-1 gating mechanism and to understand how some of the activatory mutations identified in chapter three influence channel function.

While conducting this study, the structures of the first K2P channels were determined using X-ray crystallography. These new structures revealed the presence of a previously predicted extracellular cap (Yuill *et al.* 2007). One of the consequences of this extracellular cap is change in the direction of ion flow; K^+ ions are believed to flow through the selectivity filter, as with other K^+ channels, though exits the channel through an extracellular fenestration, as the ion conduction pathway is bifurcated (figure 1.6, section 1.4). More details about the mechanisms for ion conduction and other differences

between the K2P structures and other K^+ channel structures, are provided in the introductory chapter (section 1.4).

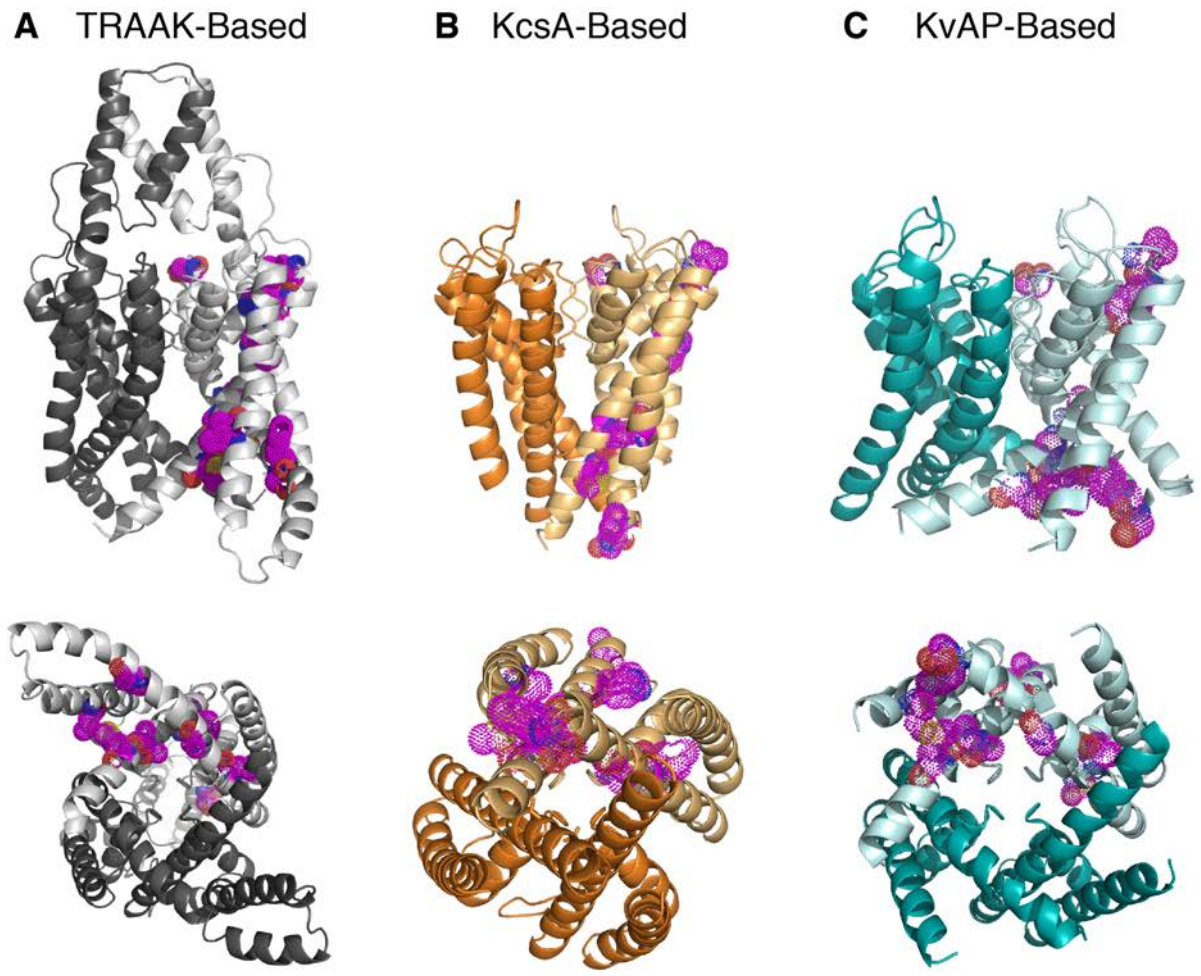


Figure 5.1: *Three TREK-1 models based on (**A**) TRAAK (**B**) KcsA and (**C**) KvAP crystal structures. Models are shown side-on and bottom-up views. GoF mutants are shown on the homology models (magenta).*

These new structures, in particular the structure of the closely related TRAAK channel, meant that a more accurate TREK-1 homology model could be built, which proved highly instructive towards understanding potential interactions involved in producing the activatory phenotype exhibited by GoF mutants. The predominantly TRAAK (3UM7) based homology model[1] (constructed by Mr M. R. Schmidt. SBCB, Oxford) was central to the conclusions drawn from this point.

[1] Where the resolution of the TRAAK structure was poor, the homology model was based on the TWIK-1 crystal structure (pdb: 3UKM)

Validation of the model using quaternary ammonium blockers was carried out, as had been conducted for the KvAP-based TREK-1 homology model (see section 3.4.4). *In silico* docking of TPenA showed the new K2P-based model to be more accurate at predicting residues important for pore-block than the previous KvAP-based model (figure 5.2) (Rapedius *et al.* 2012, Appendix VI). The result was perhaps not surprising given the high degree of homology between TREK-1 and TRAAK.

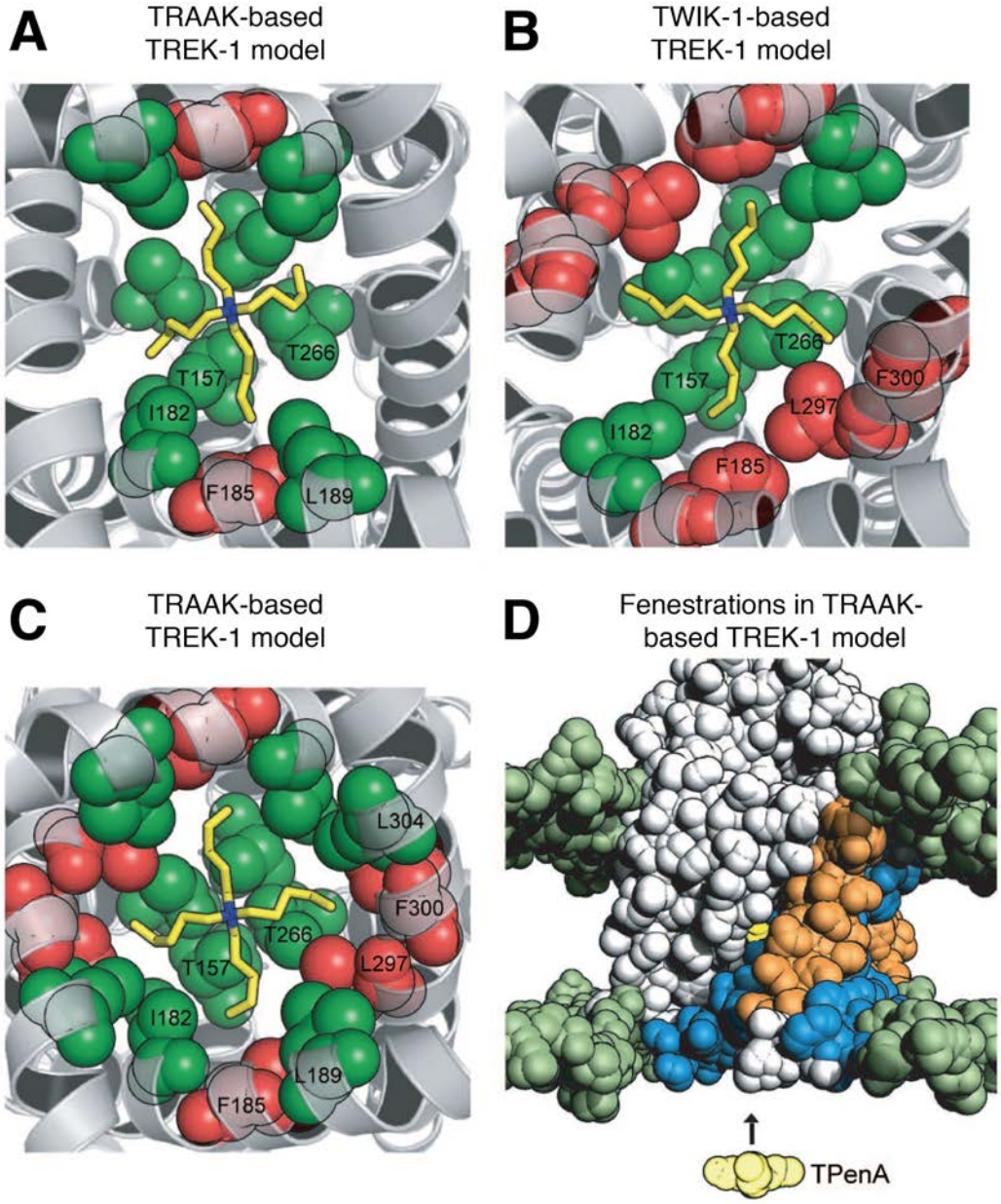


Figure 5.2: *Refined structural models of TREK-1 with TPenA bound. Bottom up view of the (**A**) TRAAK-based, (**B**) TWIK-1-based and (**C**) KvAP-based TREK-1 model pore with docked TPenA. Residues that interact with TPenA are shown as green spheres if they agree with our functional scanning mutagenesis study or red if a false positive. Only residues on one subunit are numbered (D) Solvent-accessible surface area (SASA) of a TREK-1 model, in which the side-fenestrations are still clearly visible. The SASA of the phospholipid head groups (green) whereas the TREK-1 model (gray). For one subunit, the outer (TM1 and TM3) and inner (TM2 and TM4) TM helices are highlighted in orange and blue, respectively. Figure and text adapted from Rapedius et al. 2012.*

The use of quaternary ammonium blockers to map the pore of TREK-1 has raised some controversy, as it has been suggested that the blocker can enter the conduction pathway via the external fenestration of the channel. However, we found that extracellular application of TPenA and THexA did not inhibit channel activity, as currents remained unchanged during the application of the blocker (up to 100μM) (Rapedius *et al.* 2012, Appendix VI).

5.1 Activation of TREK-1 by DEPC

Diethylpyrocarbonate (DEPC) is a commonly used laboratory reagent for producing ribonuclease free water (Denic *et al.* 1970). DEPC covalently modifies histidine residues to restructure the active site of ribonucleases, in a process that involves carbethoxylation of the N-omega-2 nitrogen of the imidazole ring (Safarian *et al.* 2003). It has also been used as a chemical probe for secondary structure in negatively supercoiled DNA (Herr *et al.* 1985, Kahl and Paule 2009) as well as in demonstrating the importance of histidine residues in the functioning of a variety of proteins (e.g. Burch *et al.* 1981, Mankelow and Henderson 2001, Pilarski *et al.* 2006, Karmakar and Das 2012). DEPC is of particular interest because it has been identified as an activator of mouse TREK-1, and this robust activation is thought to be due to a release of inhibition by external protons (Sandoz *et al.* 2009, Veale *et al.* 2010). For this reason, we decided to use DEPC to probe TREK-1 function.

Unlike mouse TREK-1, the extracellular domain of both human and rat TREK-1 contains an additional extracellular histidine residue (H87), meaning that three histidine residues are located in the M1P1 loop of human TREK-1; H87, H106 and H141. H87 is not thought to be involved in the in the DEPC sensitivity of the mouse TREK-1 (Sandoz *et al.* 2009), though does have a role in TREK-1 sensitivity to external protons (Cohen *et al.* 2008). However the role of the remaining two histidine residues (H106 and H141) in DEPC-modulation was unclear and so all three histidine residues in the M1P1 loop were mutated and their effects on DEPC activation was examined.

Assessment of the histidine residues in the extracellular M1P1 loop revealed that a single histidine residue (H141) is responsible for DEPC activation of TREK-1 channels (figure 5.3). This result is

consistent with the reduced extracellular pH sensitivity of the H141C mutation and suggests that DEPC activation is at least in part caused by a reduction in extracellular pH inhibition of channel activity, following chemical modification of H141.

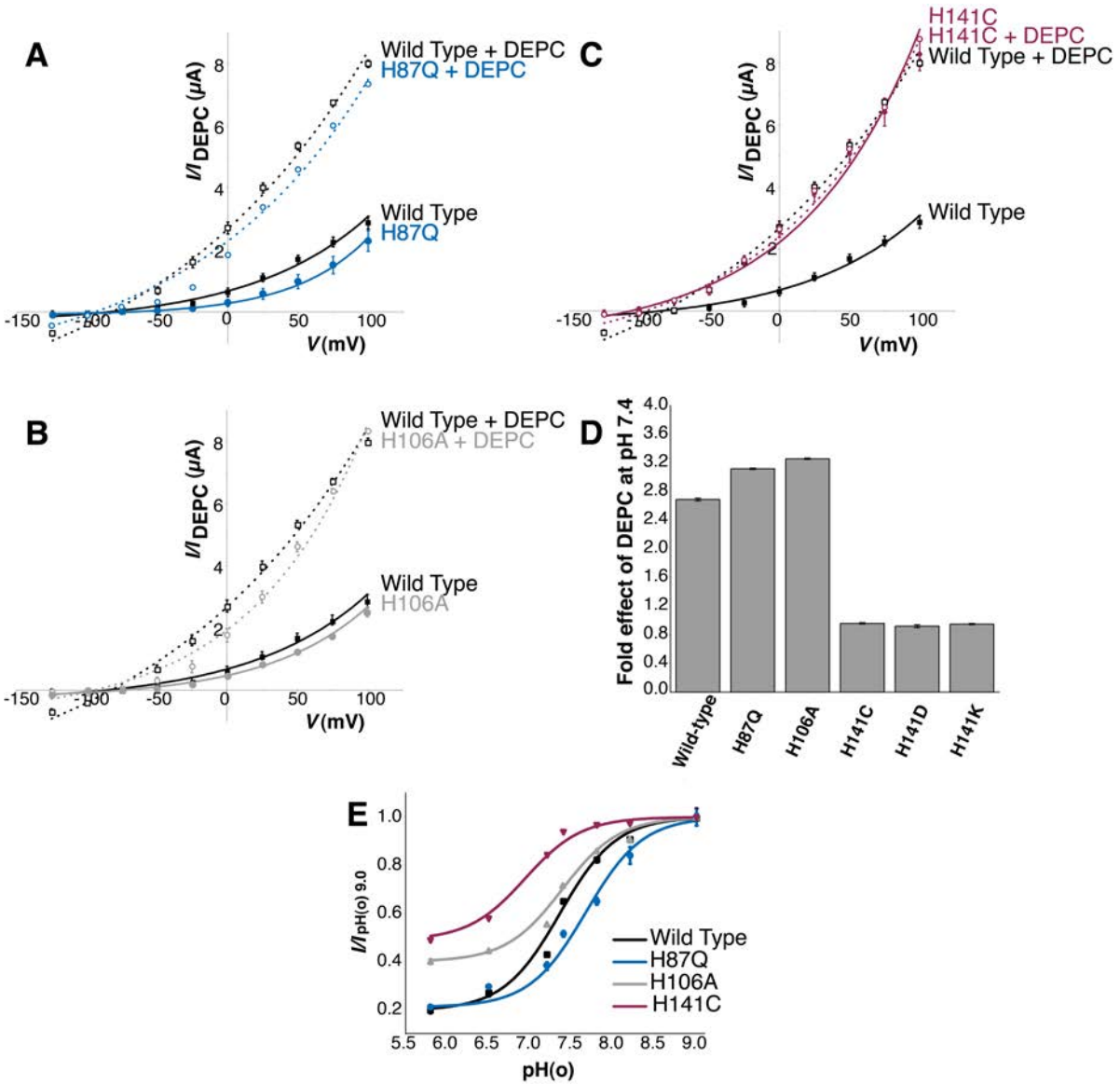


Figure 5.3: *Examination of the impact of amino acid substitutions to extracellular histidine residues. Averaged (± S.E.) I-V traces show that DEPC sensitivity remains intact despite histidine removal at sites (**A**) H87 and (**B**) H106. (**C**) DEPC modulation of TREK-1 is removed by mutation of residue H141. (**D**) Maximal current increase induced by DEPC-treatment of mutated histidine residues in comparison to wild type channels. (**E**) Normalised extracellular pH induced responses for the indicated channels*

5.1.1 The role of H141 in proton sensitivity

Examination of the new TRAAK-based homology model of TREK-1 revealed that the H141 residue is surrounded by four negatively charged residues (D143, D278, E280 and D283) which could clearly influence this histidine residue (figure 5.4). The closest aspartate (D283) is located at the top of PH1 and protonation of H141 could draw these residues closer, which would affect the position of the pore helix, thus modifying the orientation or structure of the selectivity filter. Indeed, such a movement would be consistent with the theory that extracellular pH sensitivity is a form of C-type gating and involves a collapse of the selectivity filter.

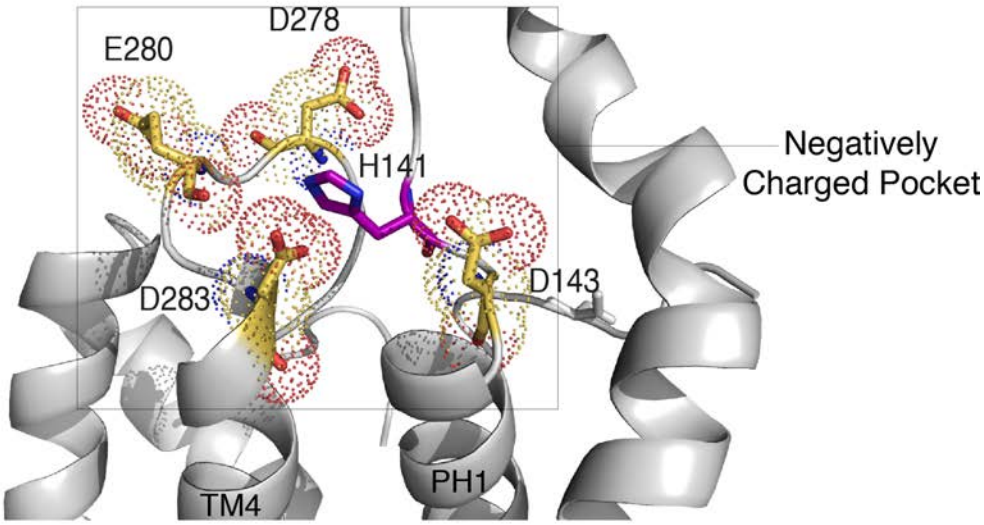


Figure 5.4: *Negatively charged residues (yellow) D143, D278, E280 and D283 envelope H141 (purple), forming a charged pocket in the extracellular vestibule of TREK-1 channels. These residues are mapped onto TREK-1 homology models based on a TRAAK and TWIK-1 crystal structures.*

Mutation of H141 to cysteine produced a significant loss of extracellular pH sensitivity (figure 5.3). In order to examine how the relative charge on the H141 residue was involved in TREK-1 proton sensitivity, the effects of the H141D and H141K mutations were also examined.

Replacing H141 with a negatively charged aspartate revealed a curious effect on external pH sensitivity of the channel (figure 5.5). H141D mutant channels exhibited a wild type-like response to extracellular pH, though they appeared entirely proton-insensitive within the range pH 7.2 – 7.8. By

contrast the H141K mutant channels exhibited a marked reduction in extracellular pH sensitivity, similar to H141C.

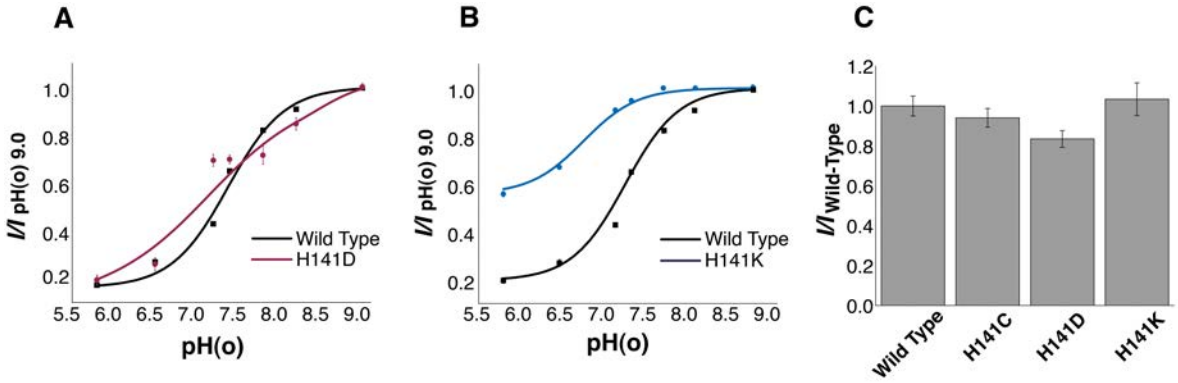


Figure 5.5: *The functional effects of mutations to residue H141. The effects of mutations (**A**) H141D and (**B**) H141K to TREK-1 extracellular pH sensitivity are shown. (**C**) The three tested H141 mutations cause little difference to TREK-1 basal activity.*

As both the H141K and H141C mutants had a similar effect on external pH sensitivity, it is difficult to draw conclusions about potential electrostatic interactions between H141 and the surrounding negatively charged residues. However, these experiments confirmed that all H141 mutations were able to abolish DEPC modulation of TREK-1 (figure 5.5) and that DEPC could be used as a tool to understand changes to the external vestibule caused by mutations elsewhere within the channel.

5.2 Activation of TREK-1 by BL-1249

Fenemates, such as BL-1249, are potent activators of TREK-1 channels. However, their binding site and mechanism of activation remain unknown. To date, there is only one published report of BL-1249 activation of TREK-1 channels (Tertyshnikova *et al.* 2005), though other fenamates have also been characterised to activate these channels (Takahira *et al.* 2005). Nonetheless, studies of BL-1249 activation of the K2P channel family are of great interest not only as tools for characterising K2P channels, but also due to their potential therapeutic application.

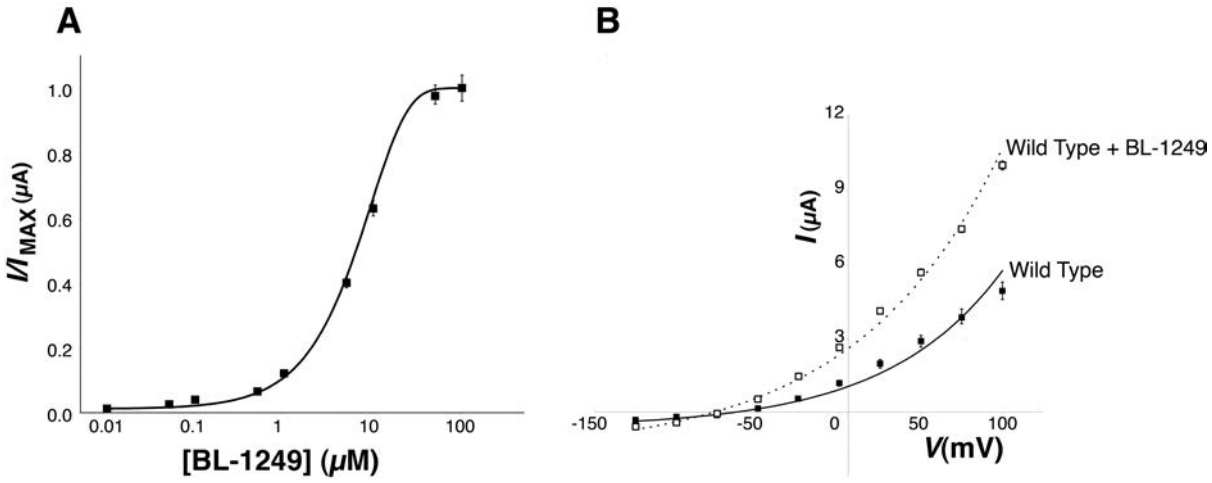


Figure 5.6: *The effect of BL-1249 on human TREK-1 channels. (**A**) The dose-response relationship reveals the concentration required to elicit a half maximal response (EC50) to be roughly 8μM. (**B**) An exemplary I-V relationship of TREK-1 channels pre- and post application of 10μM BL-1249.*

Figure 5.6 confirms that BL-1249 is a potent activator of TREK-1 channels, with approximately 8μM required to elicit the half maximal response (EC_{50}). Although little is known about the mechanisms involved in BL-1249 activation, 10μM of the drug was found to activate H141 mutants to a similar extent as wild type TREK-1 channels (not shown), suggesting that BL-1249 operates through a different mechanism to DEPC-modulation.

5.3 The effect of high extracellular [K^+] on TREK-1 channels

The effects of high extracellular [K^+] on TREK-1 channels are well documented (e.g. Cohen *et al.* 2008, Bagriantsev *et al.* 2011) and are known to slow C-type inactivation of other K^+ channels (Ogielska and Aldrich 1999). It was therefore hoped that examining the effect of varied extracellular [K^+] might also be useful in developing a better understanding of the effects of the GoF mutations on channel function. For example the constitutively active E321V mutation dramatically changes the response of TREK-1 channels to external [K^+] (figure 5.7) and given the location of this residue in the proximal C-terminal domain it would be interesting to indentify how a mutation in this intracellular region could influence gating within the selectivity filter.

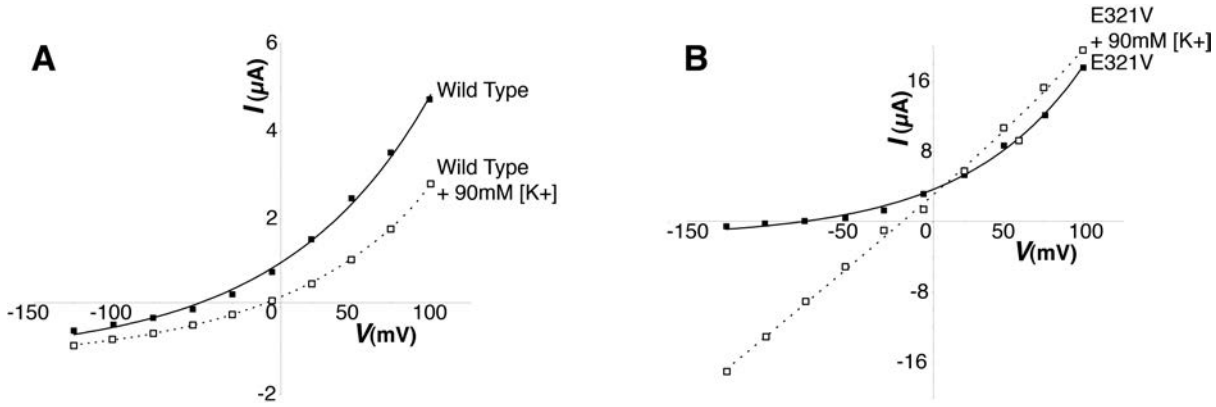


Figure 5.7: *I-V relationships of the indicated TREK-1 channels in differing external [K^+]. (**A**) Wild type and (**B**) E321V channel activity was measured in 2mM (filled line) and 90mM [K^+] (dotted line).*

5.4 Response of GoF mutations to DEPC, BL-1249 and extracellular [K^+]

The following section reports the response of the GoF mutations to the activatory agents and to high extracellular [K^+]. The responses of mutants in the C-terminus, TM2 and TM3 as well as the upper- and lower-TM4 region are presented under separate headings. Not discussed in here are the effects of DEPC and BL-1249 on the S164P mutant channel as these results are reported in detail in chapter six.

5.4.1 C-terminus mutants

Activatory mutations found within the C-terminal regulatory domain (E321V, G323R and E324V) were all found to not only result in increased inward current in the presence of high external [K^+], but also to be completely insensitive to activation by external agents DEPC and BL1249 (figures 5.7 and 5.8). These mutations also exhibit significantly increased basal currents (figure 4.4) and a reduced sensitivity to external pH (figure 4.13). Therefore, their inability to respond to activatory agents may be due to the fact that they are already maximally activated.

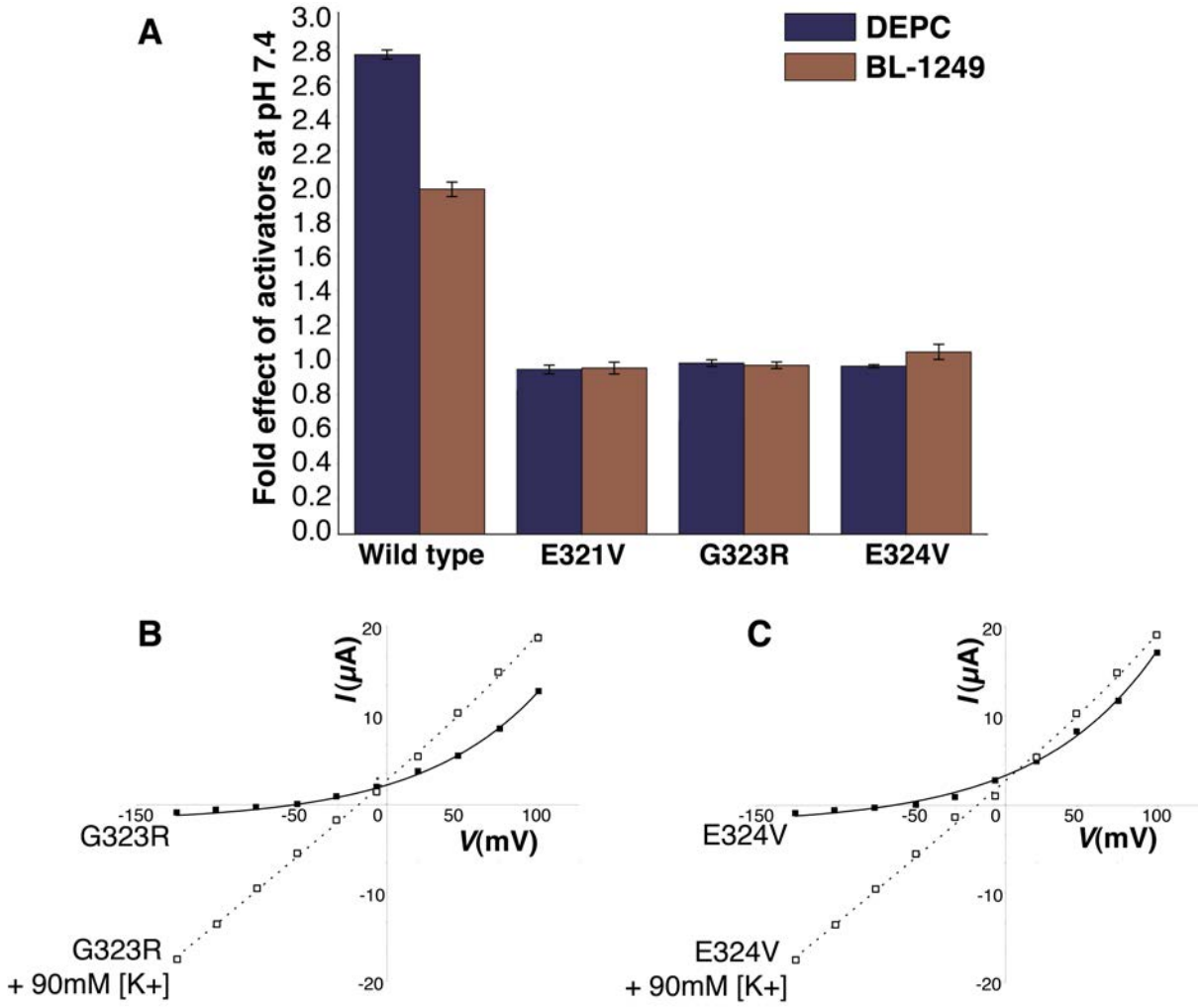


Figure 5.8*: The effects of TREK-1 activators and high external [K^+] on the indicated mutant channels. (**A**) Comparative fold-current activation by DEPC (purple) and BL-1249 (brown) for the upper-TM4 mutations and wild type TREK-1 channels. I-V relationships for (**B**) G323R and (**C**) E324V following application of 90mM extracellular [K^+].*

5.4.2 TM2 mutants

GoF mutations within the second TM helix had, with the exception of A190D, relatively weak effects on extracellular pH sensitivity in comparison to mutations within the other pore lining helix (TM4) (figures 4.8 – 4.10). However, the TM2 GoF mutants all had significantly larger basal currents than wild type TREK-1 channels (figure 4.4). Consistent with this, the mutations L184I, F200L and G201E all reduced the effects of DEPC, though none of these mutations completely abolished DEPC-mediated activation of the channel (figure 5.9). The effects of the TM2 GoF mutants on BL-1249 activation were less pronounced, particularly in the case of the A190D mutant, which was robustly activated by BL-1249 (figure 5.9). This was of particular interest as A190D exhibited relatively large

basal currents (figure 4.4) and a reduced sensitivity to both internal (figure 4.2) and external pH (figure 4.8).

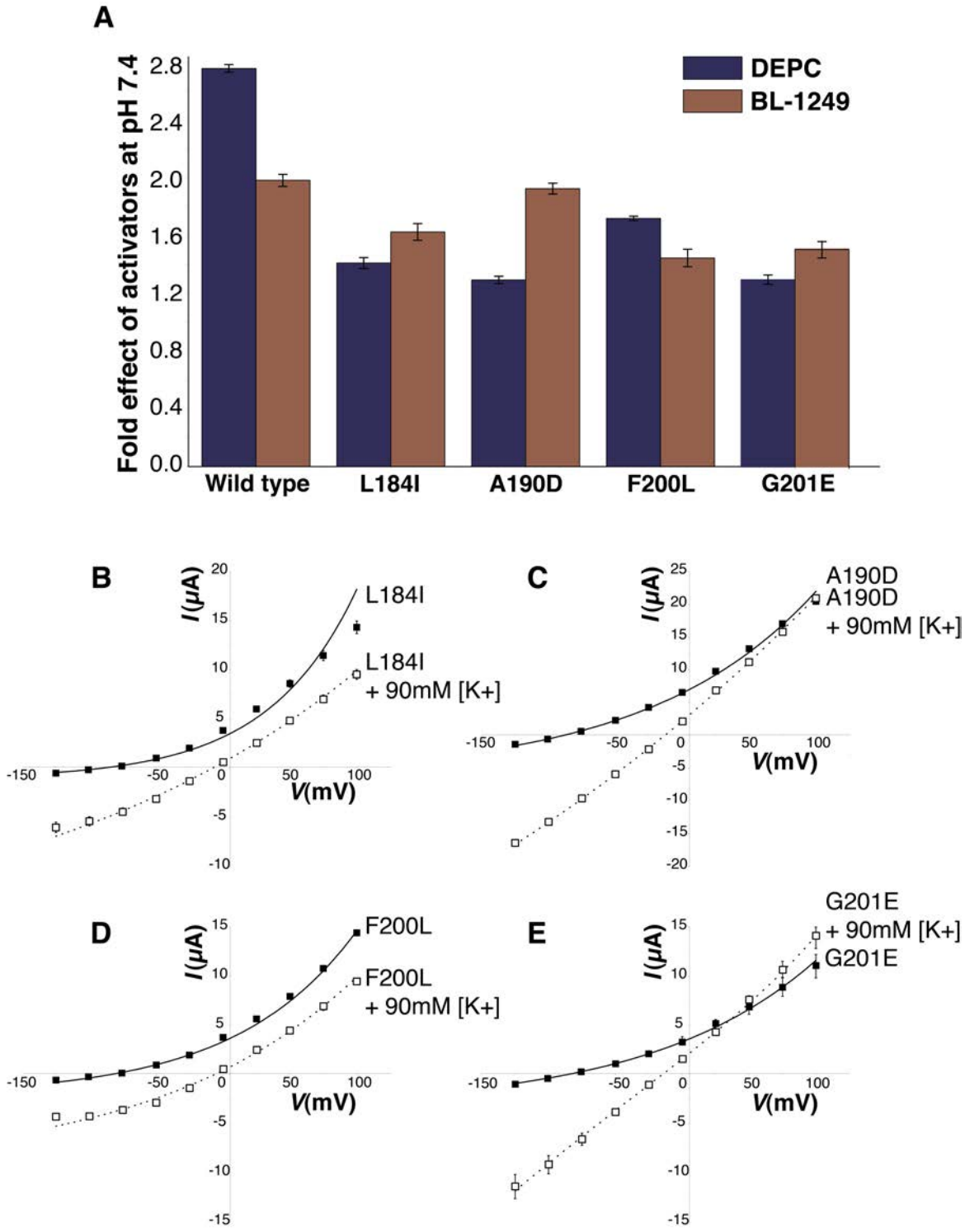


Figure 5.9: *The effects of TM2 mutations on TREK-1 sensitivity to external K^+ and activators DEPC and BL-1249. (**A**) Comparative fold-current activation by DEPC (purple) and BL-1249 (brown) for the TM2 mutations and wild type TREK-1 channels. The effects of high external [K^+] on TM2 helix GoF mutant channels. I-V relationships for (**B**) L184I, (**C**) A190D (**D**) F200L and (**E**) G201E are shown.*

Interestingly, despite their relatively minor effects on BL-1249 and DEPC sensitivity, all of the TM2 GoF mutants were able to conduct significantly larger inward K^+ currents than wild type TREK 1, in the presence of high extracellular [K^+] (figure 5.9). This was particularly pronounced for the A190D and G201E mutants, therefore it is interesting to speculate that this may be due to the introduction of negative charges in positions 190 and 201. The relative position of these mutations in the TREK-1 structure was therefore examined (figure 5.10).

Unfortunately, when mapped onto the new TREK-1 model it was not obvious what effect these mutations might have in altering conductance (figure 5.10). However, It is possible that the introduction of negatively charged residues close to the inner cavity of the channel could affect the permeation of K^+ ions through the channel and hence the larger inward current seen in figure 5.9. Alternatively, the A190D and G201E mutations may alter the orientation of the TM helices and indirectly affect the filter gate.

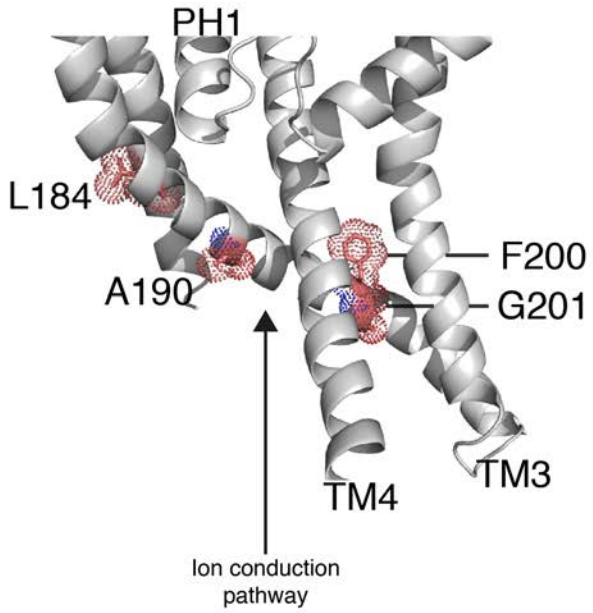


Figure 5.10: *Residues of interest in TM2 are mapped onto a TRAAK-based homology model. The position of GoF mutations (pink) are shown using a cross-section of the channel, seen from the inside of the ion conduction pathway.*

5.4.3 Upper-TM4 mutants

Mutations of residues L282, K286 and W290 within the upper-TM4 helix resulted in relatively modest changes to basal current, with all of the identified mutations increasing basal current by only 30% (figure 4.4). In addition, many of these mutations also had only a modest effect on external pH sensitivity of TREK-1. Consistent with this, many of the upper-TM4 GoF mutant channels largely retain wild type-like activation by DEPC and BL-1249 (figure 5.11). Conversely, the characteristic outward rectification of wild type TREK-1 channels in high external [K^+] solution was not retained by any of the upper-TM4 mutant channels (figure 5.11). In particular L282P exhibited a near-linear rectification profile in high [K^+]

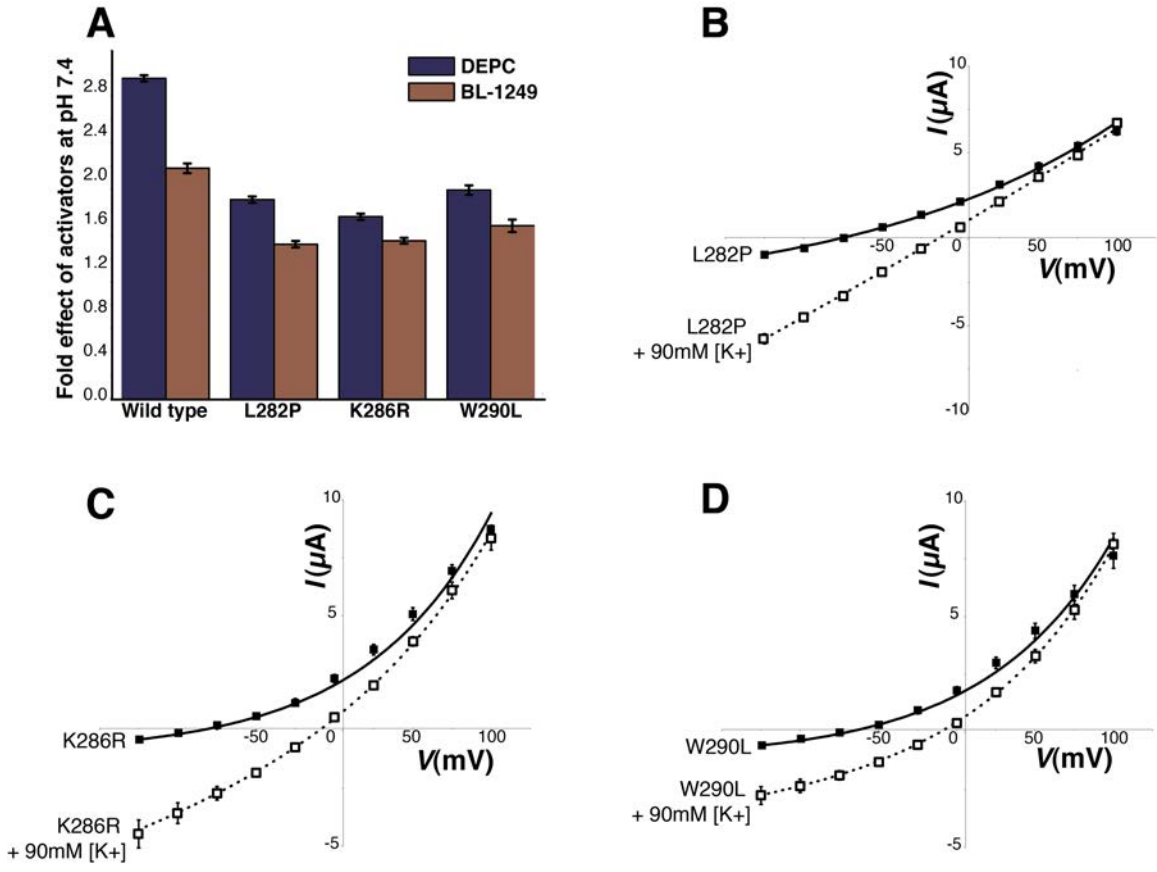


Figure 5.11: *The effects of TREK-1 activators and high external [K^+] on the indicated mutant channels. (**A**) Comparative fold-current activation by DEPC (purple) and BL-1249 (brown) for the upper-TM4 mutations and wild type TREK-1 channels. I-V relationships for (**B**) L282P, (**C**) K286R (**D**) and W290L following application of 90mM extracellular [K^+].*

The mutations to the upper-TM4 region appear to have curious effects on modulation of TREK-1 channels. Mutations within this cluster appear to affect sensitivity to both internal and external stimuli cell suggesting that this region may play an important role in the integration of these gating mechanisms. Moreover, it is noteworthy that several mutations were identified in this region, particularly as similar regions in other K^+ channels are intolerant to mutagenesis (Minor *et al*. 1999, Irizarry *et al.* 2002).

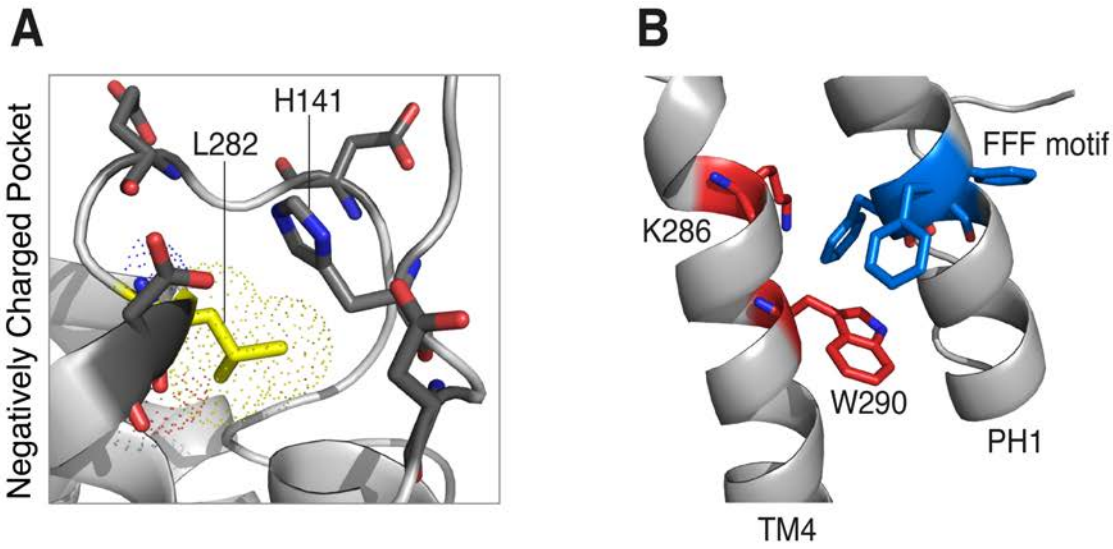


Figure 5.12: *Structural examination of the upper-TM4 region, using a TRAAK-based TREK-1 homology model. (**A**) The location of L282 inside the negatively charged pocket formed around the primary proton sensor, H141. (**B**) The close proximity of K286 and W290 to PH1 and the conserved aromatic FFF motif is shown.*

Structural examination of the locations of residues L282, K286 and W290 reveals a series of highly interesting potential interactions between PH1 and the upper-TM4 region. The close-packing between K286, W290 and a triple phenylalanine (FFF) motif on PH1 are highlighted in figure 5.12. Furthermore, L282 is positioned within the negatively charged pocket around the primary proton sensor, H141. The potential role of these residues is discussed in greater detail in chapter six.

5.4.4 Mutants within an interhelical interface

Our previous investigation into the lower-TM4 mutants (A301E, A302C and M306I) showed that they conduct large basal currents (figure 4.4) and a marked reduction to extracellular proton sensitivity

(figure 4.10). The response of these mutant channels to both DEPC and BL-1249 were interesting because mutations A301E, A302C and M306I appeared to be completely insensitive to activation by either activatory agent (figure 5.13). These mutant channels also exhibited large inward currents when measured high external [K^+], similar to constitutively active E321V mutants (figure 5.13), suggesting that they were highly active.

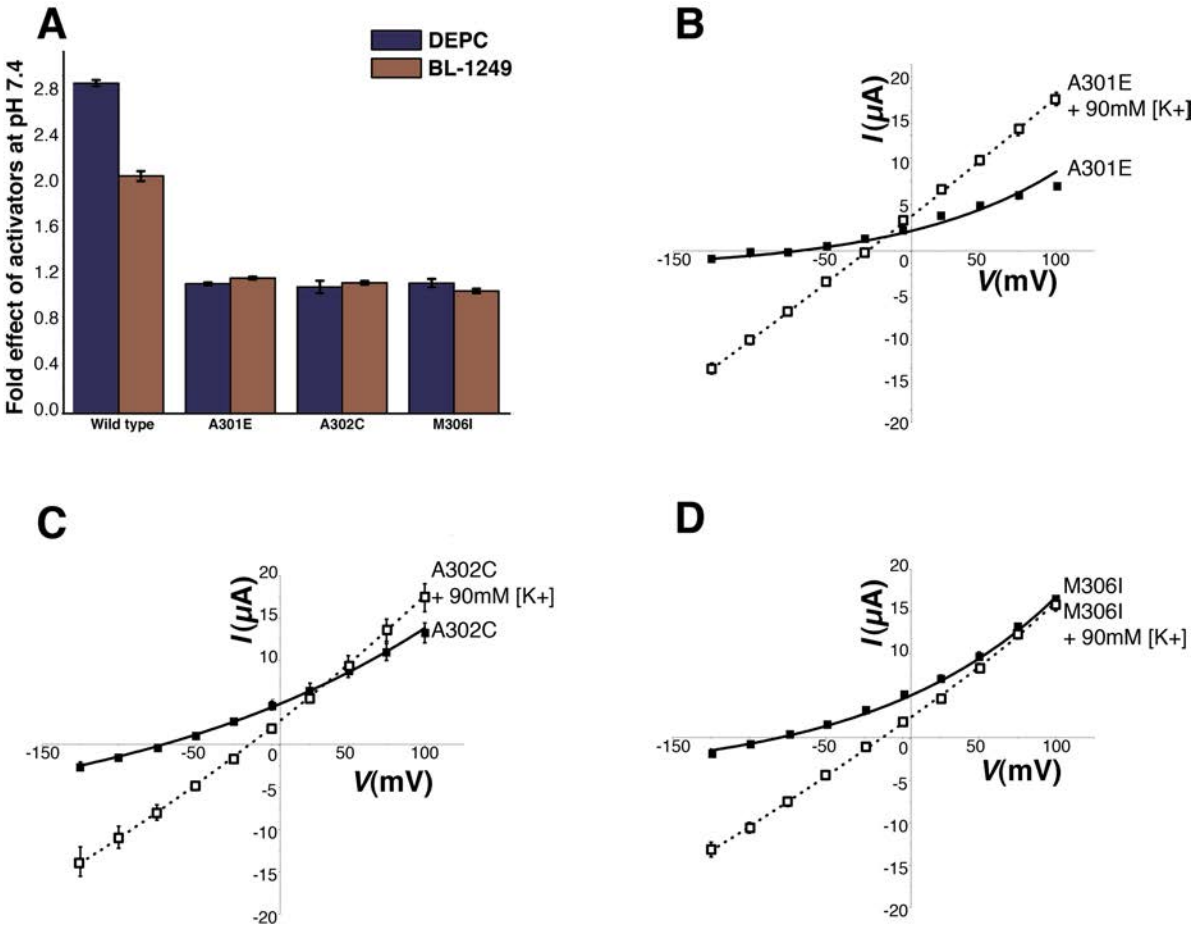


Figure 5.13: *The effects of TREK-1 activators and high external [K^+] on the indicated mutant channels. (**A**) Comparative fold-current activation by DEPC (purple) and BL-1249 (brown) for the upper-TM4 mutations and wild type TREK-1 channels. I-V relationships for (**B**) A301E, (**C**) A302C (**D**) and M306I following application of 90mM extracellular [K^+].*

Structural investigation of the homology model revealed an interesting interface between the lower-TM4 region and TM3. Intriguingly, the I230 residue is located at this interface TM3 and was identified as a highly active GoF mutation (I230N). In addition, F200 on TM2, identified as the activatory mutation F200L, is also located close to this TM helix interface and it is therefore tempting to speculate that this interface plays a critical role in TREK-1 gating and is consistent with the idea that

movement of the TM helices occurs during channel gating, even if there is not a HBC-like gate present in these channels.

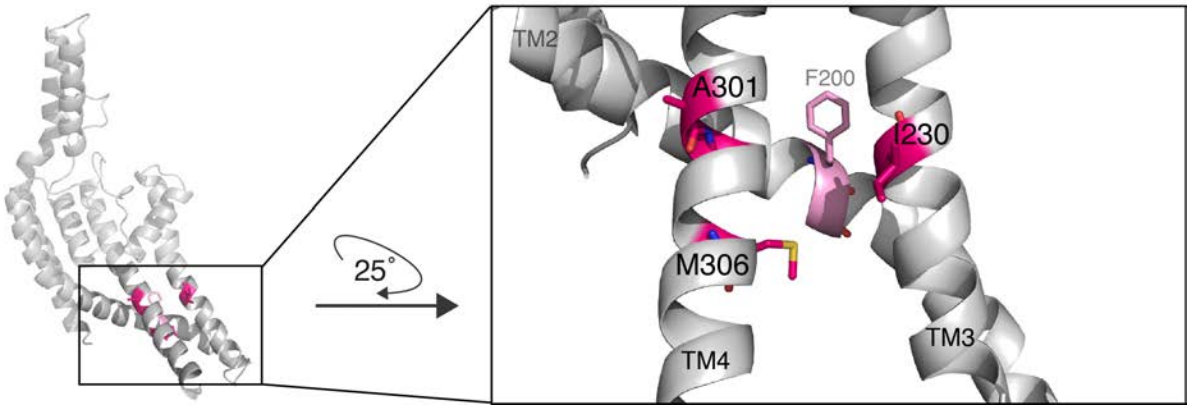


Figure 5.14: *The interface between TM2, TM3 and TM4. GoF mutations A301E, A302C, M306I in TM4 and I230N in TM3 (vivid pink) were identified using the genetic complementation assay. Also clustered nearby are TM2 GoF mutations F200L and G201E (light pink). The interhelical fenestration is clearly marked with a grey square.*

Interestingly, I230N mutant channels are not activated by DEPC or BL-1249, and produce increased inward currents in high [K^+] (figure 5.15). These findings are consistent with the increased basal current (figure 4.4) and reduced external pH sensitivity (figure 4.11) shown by I230N mutant channels. All of these characteristics were also exhibited by mutations in the adjacent TM4 helix (A301E, A302C and M306I) suggesting that the mutations around the TM3 / TM4 interface may modify channel function by the same mechanism.

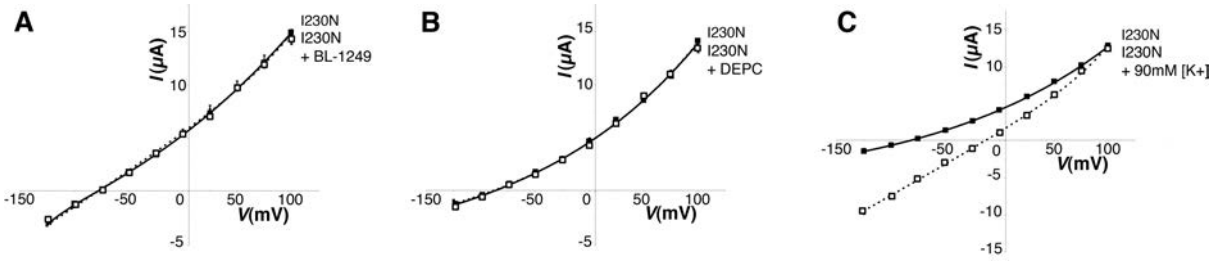


Figure 5.15: *The effects of BL-1249, DEPC and high [K^+] (90mM KCl) application to I230N mutant channels. I-V relationships for the indicated mutant channels upon application of (**A**) BL-1249, (**B**) DEPC and (**C**) 90mM extracellular [K^+] are shown.*

5.5 Conclusions

DEPC and BL-1249 are useful tools with which to characterise TREK-1 channels. In particular DEPC was particularly helpful in dissecting mutations which are able to modify external pH sensitivity. However, it is important to bear in mind that while DEPC modification causes activation of the channel somewhat similar to the alkalinisation of the extracellular vestibule, the gating responses are by no means identical. As such, the shift in DEPC sensitivity is not directly correlated with changes in external pH sensitivity for each mutant channel. Furthermore, because wild type channels retain some pH sensitivity following DEPC treatment, the two regulatory inputs may act via subtly different mechanisms. This apparent separation of DEPC and pH sensitivity may explain why some mutations are able to influence channel responses to one form of modulation and not the other.

Our results clearly demonstrate that the mutation of residues in and around the interhelical pocket is likely to lead to severe functional alteration of TREK-1 channels, as is exhibited by the mutations described above. However, the method of activation for these mutants remains ambiguous. While novel structural insights were gained from the mapping of these mutations onto TRAAK-based models, they pose some interesting questions, which are addressed in the following chapter. In order to do so the effect of other mutations in and around the pore-lining region of TM4, the interhelical fenestration between TM2, TM3 and TM4, as well as in the external vestibule around the selectivity filter were thoroughly examined.

Chapter 6

The roles of TM4 and the selectivity filter in channel gating

6.1 Activatory mutations in the upper-TM4 helix

The mutations identified in the upper-TM4 region have notable, though varied, effects on channel sensitivity to internal and external pH, as well as altering the rectification profile of TREK-1 following high extracellular [K^+] application. The GoF mutants L282P and W290L were also identified in a parallel study and have both been shown to significantly change channel function (Bagriantsev *et al.* 2011). Of the mutations reported in that study, W290S was thought to be the most interesting, because it was shown to increase TREK-1 basal current as well as reduce sensitivity to a variety of regulatory inputs. In particular the response of W290S mutant channels to heat, pressure and extracellular pH were all blunted in comparison to wild type.

Subsequently, tolerance of this residue to other mutations was examined, by Bagriantsev *et al.*, using a series of W290 substitutions, examining a diverse range of amino acids with varied biochemical

properties and their results are shown in figure 6.1. It is important to note that the short form of TREK-1 was employed in that study, though shows no known functional difference to the longer version of TREK-1. The short TREK-1 variant is 15 N-terminal amino acids shorter than the clone employed in our study, hence residue W290 is shown as W275 in figure 6.1.

It was found that mutation of W290 to residues with dissimilar structural characteristics (i.e. non aromatic amino acids) all resulted in increased channel activity. Consistent with this, conservative aromatic W290F and W290Y mutations produced channels that exhibited a wild type-like phenotype both in basal current and response to modulation by external pH. However, side chain volume was not necessarily the only reason for alteration of channel function. While mutations W290S, W290T and W290Q all produced channels with marked reduction in external pH sensitivity, the W290A mutant, for example, exhibited only slightly increased basal current and a modest reduction to external pH sensitivity. Importantly, these results were consistent with the effects we observed for the W290L mutant, as described in chapter 4.

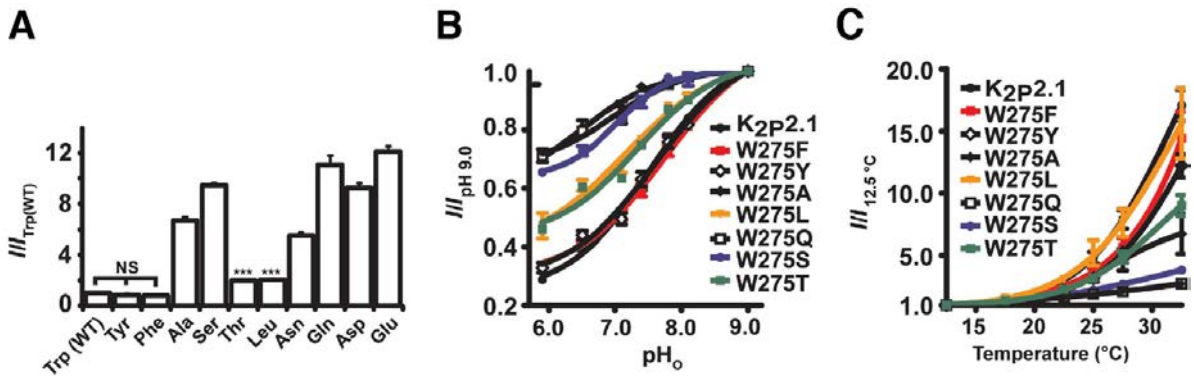


Figure 6.1: *Examination of the impact of amino-acid changes at W290. (**A**) Normalised whole cell current amplitude, as observed when channels are expressed in Xenopus oocytes at 0mV at pH 7.4. (**B**) Normalised external pH and (**C**) temperature induced responses for the indicated mutant channels. Figure adapted from Bagriantsev et al. 2011.*

Mutation of residue W290 is not only notable for changes to channel function in response to extracellular but also to intracellular stimuli. Temperature is a potent activator of TREK-1 channels, with ten-fold increases in current observed at 0mV between 12.5 and 32.5˚C (Figure 6.1) and temperature gating of TREK-1 is believed to occur via the proximal C-terminus. However, Bagriantsev *et al.* showed that mutation of residue W290 causes significant alteration to the temperature sensitivity

of TREK-1, despite the fact that it is not located in the C-terminus, but in the upper-TM4 region. Interestingly, our studies of the W290L mutations showed it to have the most robust effects in reducing intracellular proton sensitivity of the upper-TM4 mutants. However, because the internal pH sensitivity of W290 mutant channels was not tested with a variety of amino acid substitutions, the precise correlation between intracellular pH gating and temperature gating is difficult to understand.

Nonetheless, because the C-terminus is thought to be responsible for sensing changes in both intracellular proton concentration and temperature, it would appear that W290 plays a critical role in transducing channel responses to intracellular modulation to an upper-gating mechanism, located within the selectivity filter. This conclusion is supported by our identification of an additional residue (K286R) in the upper-TM4 helix, which suggests an important role for the region as a whole in TREK-1 gating.

Interestingly, aromatic residues appear to be highly conserved in place of W290 in other K2Ps and it was proposed that this upper-TM4 region may be the site of convergence for several gating stimuli. The conclusions drawn by Bagriantsev *et al.* clearly had a major influence on the interpretation of our results and this chapter begins by describing how we examined these ideas by making different amino acid substitutions in and around TM4

6.1.1 Aromatic residues at the interface between TM4 and PH1

Examination of our TRAAK-based homology model identified residues in this part of the channel which may provide insight into how TREK-1 activation is modulated by the upper-TM4 region (figure 6.2). In particular, the clustering of aromatic residues around W290 both within the TM4 helix and PH1 is of great interest.

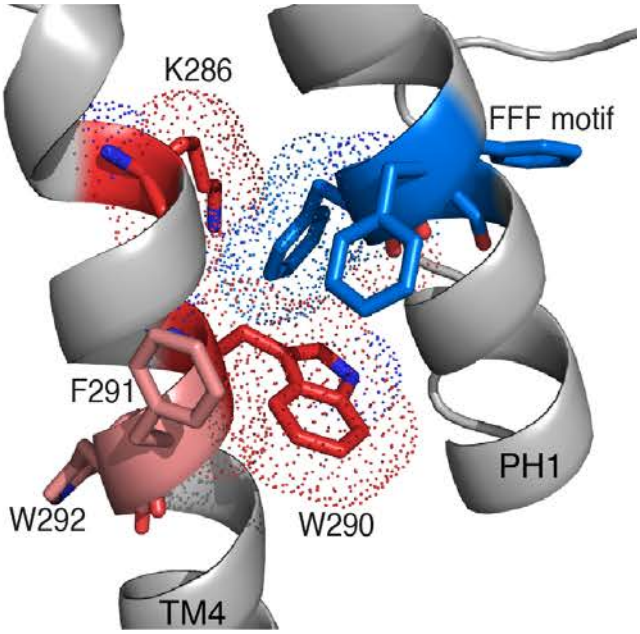


Figure 6.2 *Examination of the upper TM4-pore helix 1 interface. Residues that were identified as activatory when mutated – K286 and W290 (red dots) – are mapped onto a TRAAK-based TREK-1 homology model. These residues sandwich a well-conserved cluster of aromatic residues in PH1 (blue), in particular F149 (dots). An additional cluster of aromatic residues adjacent to residue W290 – F291 and W292 (pink) – was shown to cause less dramatic functional changes.*

In their study, Bagrianstev *et al.* identified W290 mutations to behave very differently from wild type TREK-1 channels in response to several stimuli, and in terms of basal activity. However, they also noted that an adjacent residue (F291) had little effect on basal activity and extracellular pH sensitivity (figure 6.3). We therefore examined the effect of F291L on DEPC and BL-1249 sensitivity.

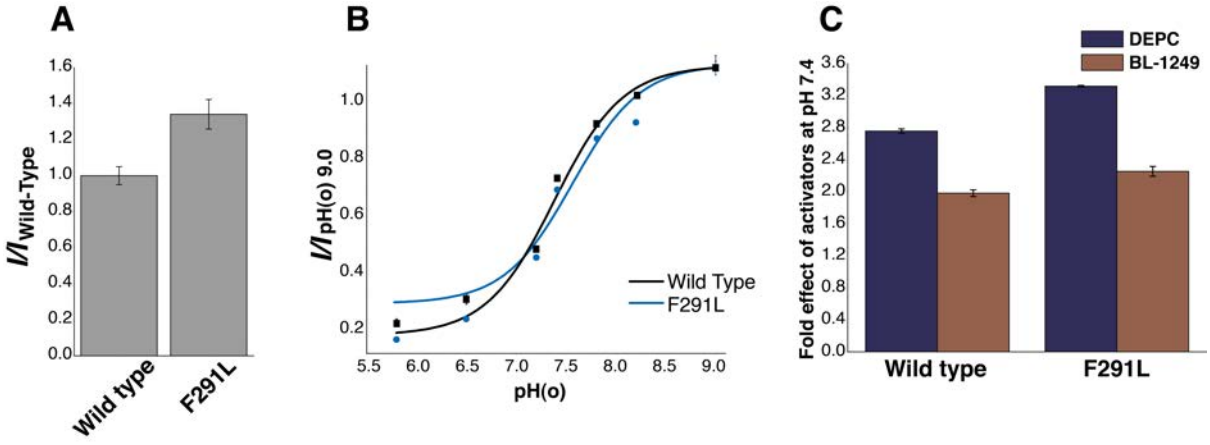


Figure 6.3: *Examination of the impact of F291L mutations. (**A**) Normalised whole cell current amplitude, as observed when channels are expressed in Xenopus oocytes at 0mV at pH 7.4. (**B**) Normalised external pH and (**C**) fold effect of activatory agents for F291L and wild type channels.*

Consistent with the lack of effect on external pH sensitivity, we found the F291L mutation had no effect on DEPC or Bl-1249 activation of TREK-1 channels (figure 6.3). However, while our structural model suggests that W290 does interact with PH1, it appears that F291L does not (figure 6.2). We therefore next examined the effect of mutating the triple phenylalanine (FFF) motif in PH1.

6.1.2 The effect of PH1 phenylalanine substitutions on channel function

The well-conserved FFF-motif appears to be in close proximity to both K286 and W290 (figure 6.2) and may be involved in stabilisation of the pore helix and / or transduction of gating signals from TM4 to the selectivity filter. Indeed, It is possible that the dramatic effects of W290S substitutions are brought about by changes at the interface between W290 and F149. Intriguingly, F149 in PH1 is equivalent to W67 in KcsA, which is thought to play an important role in coupling movement of TM2 to the selectivity filter gate (Cuello *et al.* 2010).

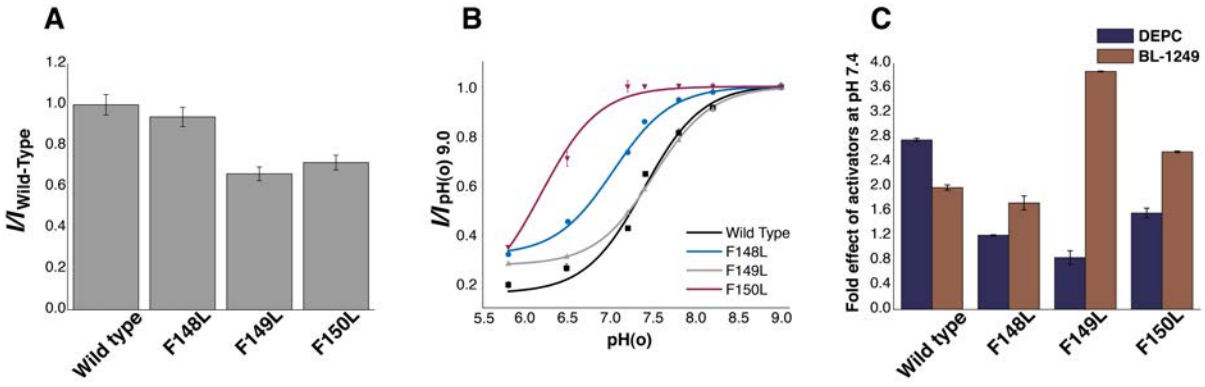


Figure 6.4: *Examination of the effects o FFF motif removal in PH1. (**A**) Normalised whole cell current amplitude, as observed when channels are expressed in Xenopus oocytes at 0mV at pH 7.4. (**B**) Normalised external pH and (**C**) fold effect of activatory agents for the indicated mutant channels.*

In order to examine the role of this aromatic cluster in TREK-1, a series of leucine point mutations were made to the PH1 FFF motif, and the functional consequences were measured (figure 6.4). Leucine substitutions were selected as these mutations result in a considerable loss of side chain volume, while conserving the hydrophobic nature of wild type phenylalanine residues in positions F148, F149 and F150.

Each of these mutations resulted in a lowered basal current, increased BL-1249 response and had varied effects on both external pH and DEPC mediated activation of TREK-1. The central F149L mutation, closest to K286 and W290, had a 33% reduction of basal current, in comparison to wild type (figure 6.4). However, BL-1249 application resulted in a dramatic increase in activity, though the level of 'activated' F149L current (i.e. the current produced by BL-1249 activation) was similar to the level of activated wild type current.

The F150L mutation also exhibited a 30% reduction in basal current and increased sensitivity to BL-1249 (figure 6.4). However, the effects of the F150L mutation on both external pH and DEPC sensitivity is perhaps themost interesting; F150L mutant channels have a markedly reduced external pH sensitivity, appearing to be maximally activated at pH 7.2, while also exhibiting reduced DEPC sensitivity.

Unlike F149L and F150L substitutions, F148L mutant channels exhibit wild type-like responses to BL1249, as well as unchanged basal current. However, F148L mutants do show blunted external pH and DEPC sensitivity. These results demonstrate that interaction between TM4 and the FFF motif in PH1 appears to be important for controlling TREK-1 channel gating.

6.1.3 The effect of G152 on C-type gating

In a follow up to their original study, Bagriantsev *et al.* recently identified a highly conserved glycine residue adjacent to the PH1 aromatic motif as critical for C-type gating in TREK-1 channels (Bagriantsev *et al.* 2012). It was suggested that the C-terminal regulatory domain transduces metabolic and thermal stimuli to an extracellular C-type gate through TM4 and PH1, with G152 playing a key role in this process.

G152I mutant channels were shown to be insensitive to internal modulation by membrane depolarisation as well as external pH inhibition (figure 6.12) (Bagriantsev *et al.* 2012). Furthermore,

the G152I mutation resulted in the absence of an apparent change in relative ion permeability from K^+ to Na^+ that is associated with closure of the C-type gate.

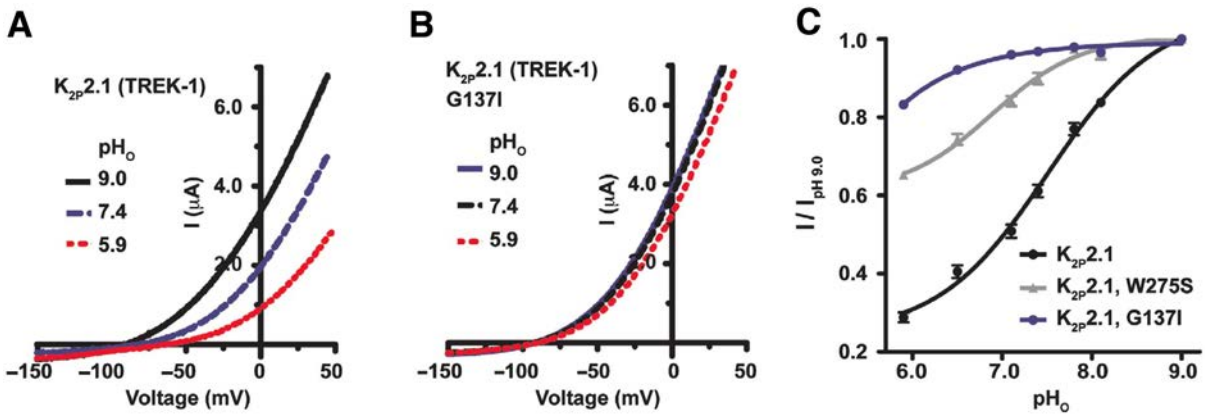


Figure 6.5: *PH1 is critical for K2P channels C-type gating. (**A**, **B**, **C**) Exemplar recordings of the response of the indicated TREK-1 channels to changes of external pH in 2mM extracellular [K^+] solution. Currents were elicited by a voltage ramp from -150 to +50mV, from a holding potential of -80mV. Figure adapted from Bagriantsev et al. 2012.*

The effects of the G152 mutant channels are entirely consitent with our hypothesis regarding the role of the upper TM4-PH1 interaction. Indeed, the observed changes to channel function following removal of large aromatic residues in position W290 and F148, F149 and F150 indicate an important role for this region in channel gating. The G152I mutation is likely to alter PH1 and possibly disrupt interaction between the upper-TM4 helix and PH1.

6.2 The effects of mutations to L282 at the top of TM4

The results shown in chapter five (section 5.1) indicate that H141 is the target for DEPC-mediated activation of TREK-1 channels as well as contributing to extracellular pH sensitivity (figure 5.3). It is possible that the mutations in the upper-TM4 helix and PH1 may affect pH and DEPC-modulation of the channel via restructuring the area adjacent to H141, which is located in the extracellular loop above PH1 (figure 6.6).

Mutation L282P exhibits similar functional characteristics to the upper-TM4 mutations K286R and W290L in terms of basal current and drug sensitivity. However, unlike the upper-TM4 mutants, L282P results in a major reduction in extracellular pH sensitivity within the normal physiological range (figure 4.9). When mapped onto the TREK-1 homology model, L282 is located in the extracellular loop above TM4 and therefore is unlikely to interact with the aromatic FFF motif in PH1. However, L282P mutations may alter external pH sensitivity of TREK-1 channels via modification of the negatively charged pocket surrounding H141 (figure 6.6).

The GoF mutation L282P lies adjacent to two of the negatively charged residues, E280 and D283, close to H141. A proline substitution at position L282 would result in a major change in the flexibility of the peptide backbone in this region. As already discussed, the movement of the pore helices appears to be central to gating at the selectivity filter (Yellen *et al.* 2002, Cohen *et al.* 2008, Sandoz *et al.* 2009) and so increased rigidity around PH1 could affect TREK-1 gating at the selectivity filter.

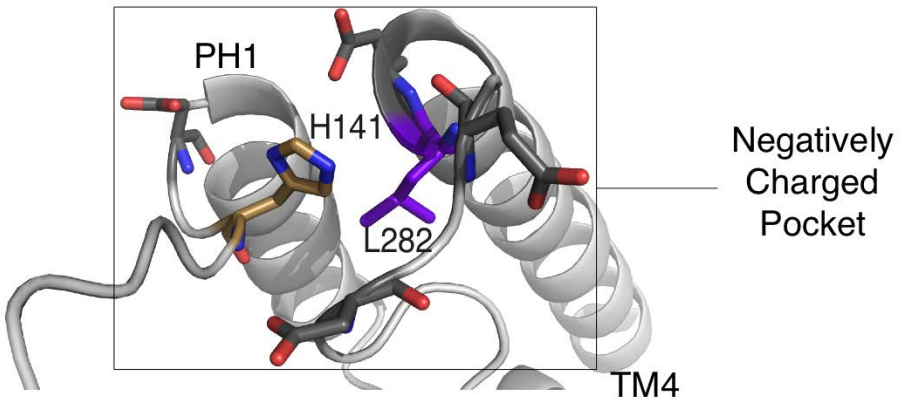


Figure 6.6: *The position of residue L282 shown on a TRAAK-based TREK-1 homology model. L282 (purple) is in close proximity to the primary proton sensor (gold) and four charged residues (dark grey), which make up the negatively charged pocket proposed to be responsible to channel responses to external pH.*

In order to determine if the change in backbone flexibility is responsible for the changes in activity of the L282P mutant, glycine mutations in this position (L282G) were made and functionally examined. Interestingly, the L282G mutant channels also exhibited a loss of extracellular pH sensitivity between pH 7.2 – 8.2. However, the L282G mutation caused a significant reduction in basal activity (figure 6.7). By contrast, the L282P mutation produced an increase in basal currents of approximately 30% (figure 6.7).

In addition, L282G mutant channels also exhibited a greater BL-1249 activation than both wild type and L282P mutants, though this is most likely due to their low initial basal activity (figure 6.7), which results in a higher 'fold' activation. In any case, these results demonstrate that the mechanism of activation for BL-1249 is still intact in these mutants.

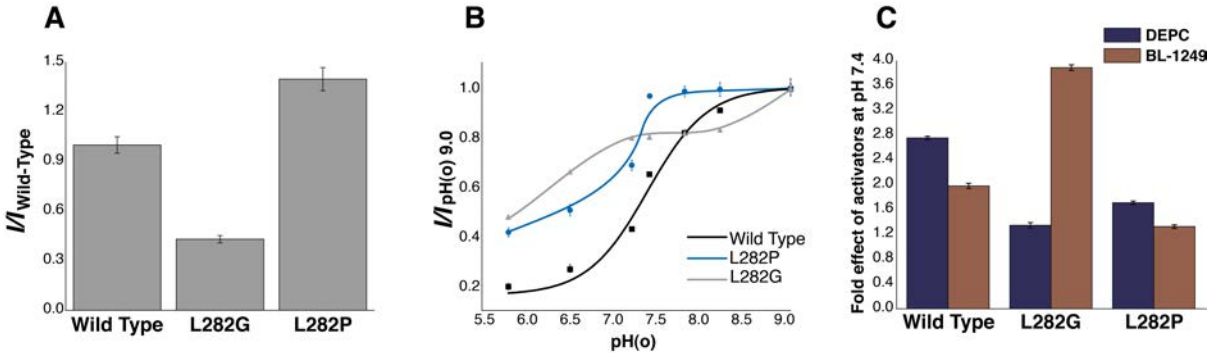


Figure 6.7: *Examination of the impact of amino-acid changes at L282. (**A**) Normalised whole cell current amplitude, as observed when channels are expressed in Xenopus oocytes at 0mV at pH 7.4. (**B**) Normalised external pH and (**C**) fold effect of activatory agents for the indicated mutant channels.*

6.3 Probing the interface between TM2, TM3 and TM4

As well as the cluster of mutations identified in the upper-TM4 region, another cluster of GoF mutations was identified at the interface between TM helices TM2, TM3 and TM4 (figure 5.14). The important role that TM4 plays in TREK-1 gating has already been illustrated the interactions between residues in the upper-TM4 region and PH1. It is possible that the GoF mutations identified lower down in TM4 (A301E, A302C and M306I) and in the nearby helices (F200L, G201E and I230N) could interact with each other at this interface and affect the movement of the helices, thereby influencing channel gating. In order examine these ideas, a series of mutations were made to residues at this interface.

6.3.1 I230 in TM3

The I230N GoF mutation was unique due to its presence on a non-pore-lining helix (TM3), as well as the dramatic reduction of external pH sensitivity (figure 4.11) and the very large basal currents conducted by this mutant (figure 4.4). Furthermore, I230N mutations completely abolished sensitivity

to BL-1249 and DEPC, as well as exhibiting no outward rectification in conditions of high external [K^+] (figure 5.15).

Hydrophobic residues are conserved in this position across the K2P channel family (see Appendix IV for protein sequence alignments). However, this is perhaps unsurprising given the location of I230 within the lipid membrane. Therefore, it was important to determine if these effects were the result of introducing a highly hydrophilic asparagine residue to position 230.

A series of alternative amino acid substitutions were therefore tested at position 230. A valine substitution would be predicted to conserve size, polarity and not disrupt the hydrophobic nature of the region. Consistent with this, we found that I230V mutant channels resulted in a wild type-like phenotype, with normal response to drug activation, as well as basal current (figure 6.8). A minor loss of extracellular pH sensitivity was the only observable difference between the function of I230V mutants and wild type channels.

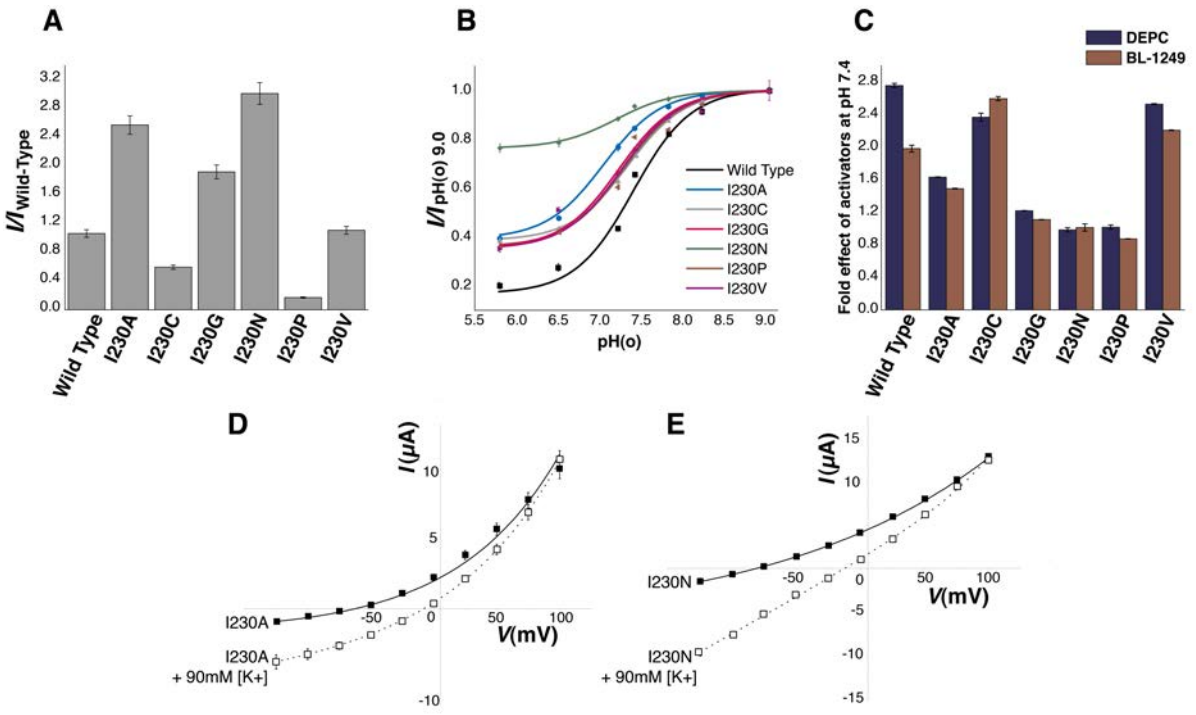


Figure 6.8: *Examination of the impact of amino-acid substitutions at residue I230. (**A**) Normalised whole cell current amplitude, as observed when channels are expressed in Xenopus oocytes at 0mV at pH 7.4. (**B**) Normalised external pH and (**C**) fold effect of activatory agents for the indicated mutant channels. The effect of high extracellular K^+ (90mM) on (**D**) I230A and (**E**) I230N mutant channels.*

Interestingly, the I230A mutation was highly activatory, similar to I230N, indicated by increased whole-cell current amplitude and relatively little effect of BL-1249 and DEPC (figure 6.8). However, unlike I230N there was a relatively insignificant inward current conductance in conditions of high external [K^+] (figure 6.8).

I230G mutant channels also exhibited increased basal activity, as well as a reduction in sensitivity to external activators, to a similar extent as I230A mutants (figure 6.8). Therefore, to examine whether changing the TM flexibility at position 230 was responsible for channel activation, a proline substitution was also made. I230P mutations had only a modest effect on external pH sensitivity of TREK-1 channels and were largely unresponsive to BL-1249 and DEPC. However, there was also a dramatic reduction in basal current by the I230P mutation (figure 6.8).

I230C mutant channels were also examined and responded to activatory agents DEPC and BL-1249 in a similar fashion to wild type channels. This was interesting because the I230C mutation also caused a significant loss external pH sensitivity and significantly reduced basal activity (figure 6.8).

Examination of residue I230 using the TRAAK-based TREK-1 homology model showed this residue to be close to the Y299 residue in TM4 (figure 6.9). Therefore, we decided to study the effect of mutations Y299A, Y299F and Y299L on TREK-1 channel function.

Continued overleaf.

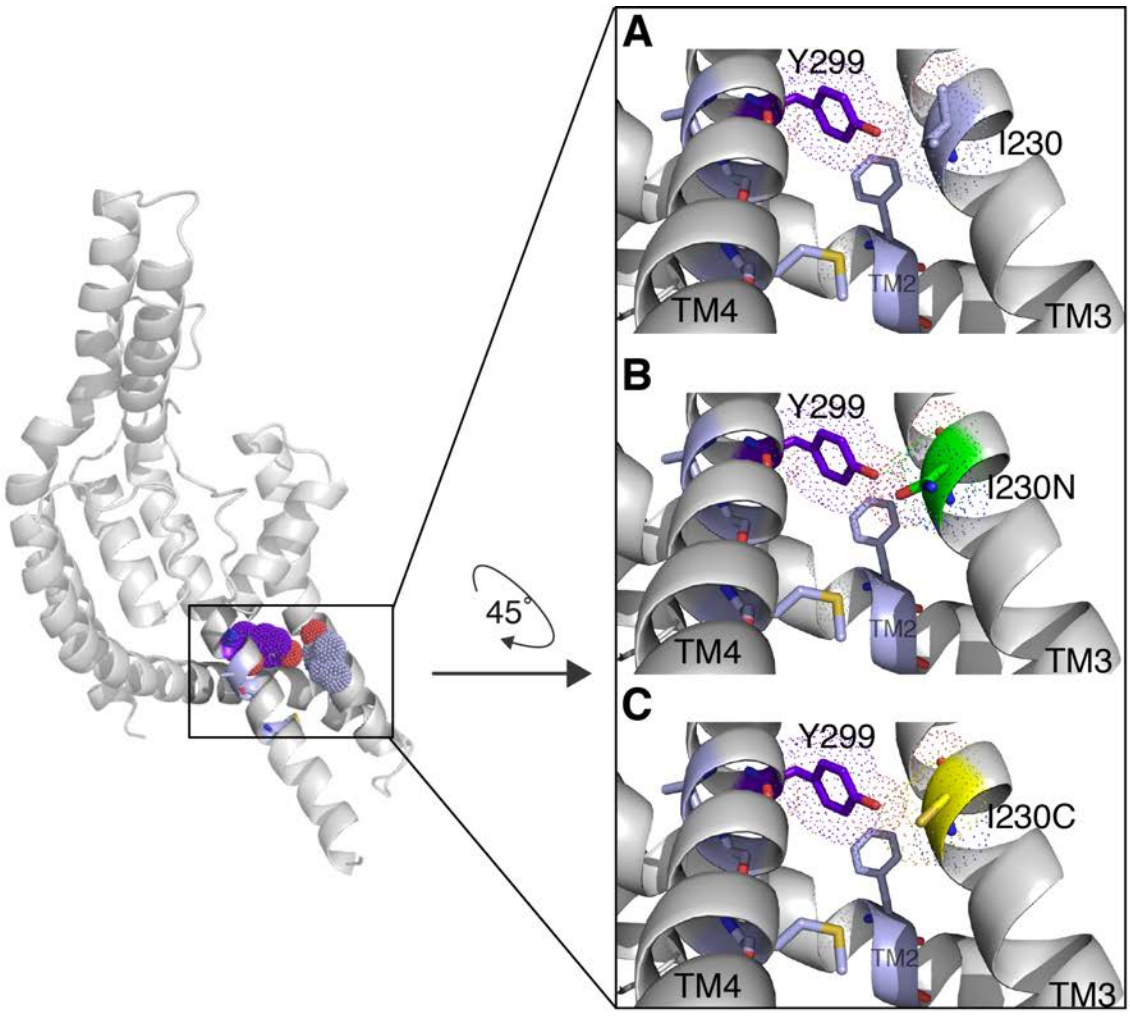


Figure 6.9: *A putative novel interaction between residue Y299 (purple) and I230N mutant residues within the interhelical pocket. (**A**) The distance between the hydroxyl group of Y299 is too far from I230 (light purple) to allow for interaction between these two residues in wild type channels. (**B**) I230N mutations (green) introduce an additional oxygen atom into the hydrophobic pocket increasing proximity hydroxyl group of Y299. (**C**) I230C mutations (yellow) introduce a reactive sulphur atom into the fenestration, within close proximity of the hydroxyl group of Y299. GoF mutations identified using the genetic complementation assay are also shown in all three figures (light purple).*

6.3.2 Functional characterisation of residue Y299

As shown in figure 6.10, Y299A mutations resulted in a dramatic increase in basal current levels, combined with a significant reduction in external pH sensitivity; at pH 5.8 Y299A mutant channels conduct nearly 70% of maximal current (i.e. the current at pH 9), similar to the highly active I230N mutation (figure 6.8). The reduction in sensitivity to BL-1249 and DEPC by the Y299A mutation was also consistent with the increase of basal currents for these mutant channels. Additionally, application of high external [K^+] produced the near-linear rectification profile exhibited by the constitutively active

TREK-1 channel, E321V (figure 6.10). These characteristics were shared with I230N mutant channels, supporting the idea that they are having similar functional effects.

Y299L mutations were made in order to introduce a hydrophobic side chain in place of the aromatic tyrosine residue, conserving the hydrophobic properties of this interface. Y299L mutant channels also exhibit increased basal activity, though to a lesser extent than alanine substitutions in the same position (figure 6.10). However, Y299L substitution resulted in a less dramatic reduction of external pH and BL-1249 sensitivity than Y299A. Moreover, the inward current produced by exposing Y299L mutant channels to high extracellular [K^+] is notably higher than currents conducted by wild type channels, though lower than the highly activatory Y299A mutant channels (figure 6.10).

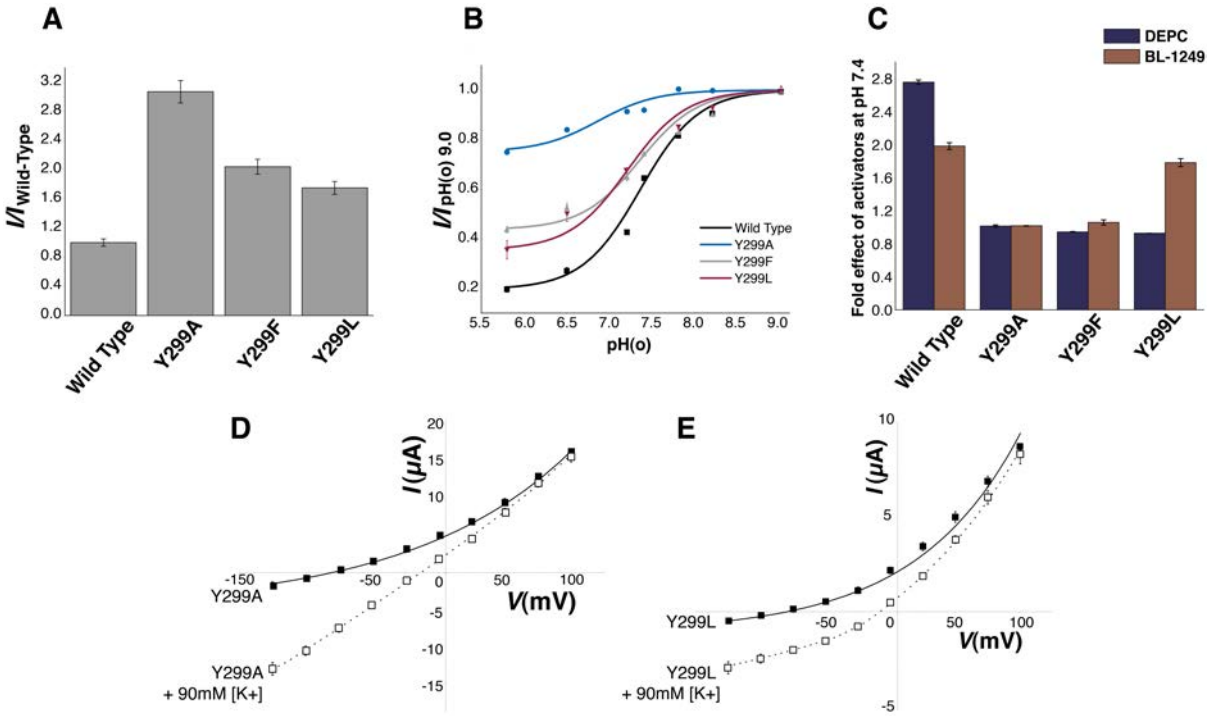


Figure 6.10: *Examination of the impact of amino-acid substitutions at residue Y299. (**A**) Normalised whole cell current amplitude, as observed when channels are expressed in Xenopus oocytes at 0mV at pH 7.4. (**B**) Normalised external pH and (**C**) fold effect of activatory agents for the indicated mutant channels. The effect of high extracellular K^+ (90mM) on (**D**) Y299A and (**E**) Y299L mutant channels.*

Remarkably, the conservative substitution Y299F also resulted in a channel with significant shifts in all the parameters measured (figure 6.10). The Y299F mutation produced a similar increase in basal current and reduction in pH sensitivity as seen with the Y299L mutation. However, unlike the Y299L mutant Y299F showed no activation by BL-1249.

6.3.3 Functional characterisation of alternative mutations to A301 and A302

The results obtained from the I230 and Y299 mutagenesis studies suggest that interactions between the interface of TM3 and TM4 are important for channel gating. One turn of the α-helix below Y299 are residues A301 and A302 (figure 6.11), which were both identified as GoF mutations in the genetic complementation screen (A301E and A302C). In order to further examine the properties of this region of TM4 additional substitutions at the A301 and A302 residues were made and examined.

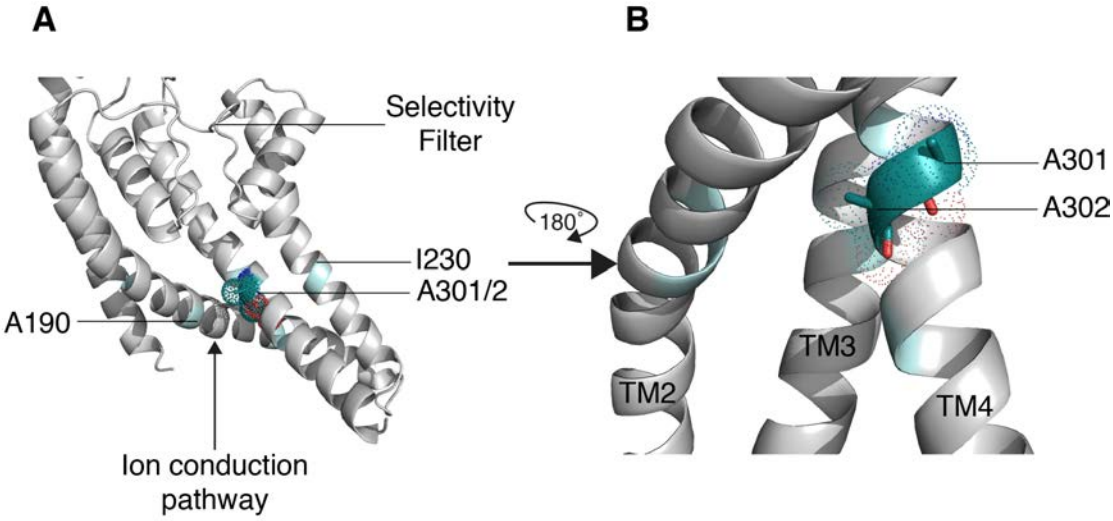


Figure 6.11: *The position of the twin alanine motif (teal dots) in TM4, based on a TRAAK-based TREK-1 homology model. (**A**) A301 and A302 are shown from inside the ion conduction pathway, from a side on view. (**B**) The same residues are shown relative to their position within the interhelical fenestration, following a 180˚ turn of the protein model shown in figure A, along the horizontal axis.*

As several A302 mutations were identified using the genetic complementation assay (aspartate, cysteine and valine substitutions were all able to rescue growth) functional assays were conducted primarily on A301 substitutions. However, it is interesting to note that A302C, A302D and A302V mutations all increased basal current and decreased sensitivity to modulation by external pH, BL-1249 and DEPC (figure 6.12).

Following characterisation of the A301E GoF mutant in chapters four and five, aspartate, arginine, valine and glycine substitutions were all created in position 301. All of these mutations resulted in significant activation of the channel (figure 6.12) and none of the A301 mutant channels were able to

respond to activators DEPC or BL-1249 to the same extent as wild type channels, and were all largely unresponsive to extracellular pH modulation.

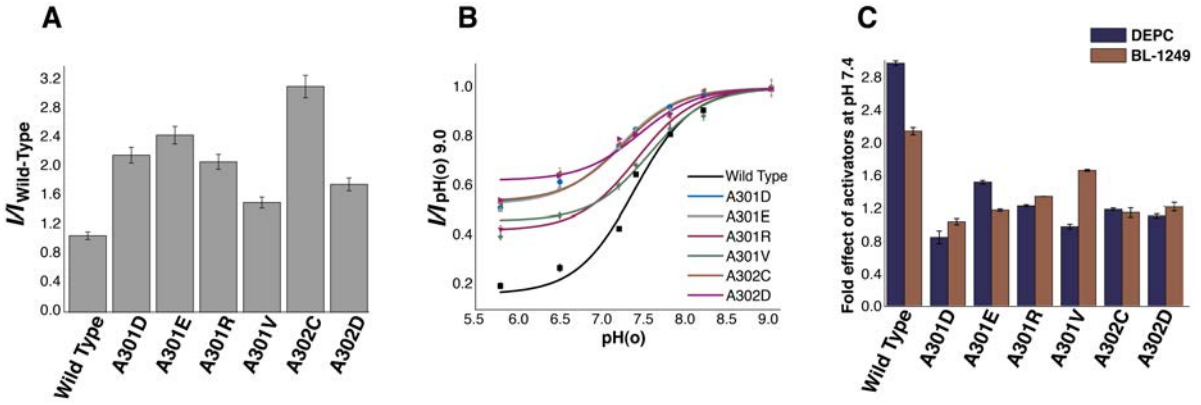


Figure 6.12: *Examination of the impact of amino-acid substitutions at residue A301 and A302. (**A**) Normalised whole cell current amplitude, as observed when channels are expressed in Xenopus oocytes at 0mV at pH 7.4. (**B**) Normalised external pH and (**C**) fold effect of activatory agents for the indicated mutant channels.*

6.4 The unique properties of S164 mutations

S164P was identified as a GoF mutation using the genetic complementation assay. This mutation, found in the extracellular vestibule of TREK-1, was the only activatory mutation that did not have significant effects on the basal activity of the channel (figure 6.13). Furthermore, the S164P mutation was also unique among GoF mutations because S164P mutant channels were completely insensitive to external pH (figure 6.13). Indeed, while a loss of pH sensitivity was observed for other GoF mutations, this was generally connected to an increase in basal activity. For example, while the I230N mutation significantly reduced pH sensitivity, this mutant also exhibited very large basal currents (figure 6.8).

Alternative mutations in place of S164 were made and tested using the genetic complementation assay, described in section 4.5.1. While none of the mutations to position 164, apart from S164P, were able to complement growth, it was clear, from the effects of mutations S164P and S164Y that this residue was still of great interest and should be examined further. We therefore tested the effects of other substitutions at position 164.

6.4.1 Alternative mutations to residue S164

It was interesting that S164P and S164Y mutations had dramatic effects in reducing and increasing external pH sensitivity, respectively (figure 6.13). To understand why these mutations had these effects on channel function, alternative mutations of residue S164 were examined. For example, if the effects of S164Y were the result of an increase of sidechain volume, S164F mutants should conserve the functional characteristics of S164Y mutant channels. Alternatively, if the hydroxyl group of the tyrosine side chain is involved in increasing external pH sensitivity, then S164F and S164Y would exhibit distinctly altered functional properties.

Interestingly, S164F mutants displayed increased proton sensitivity above pH 7, though had little effect on basal activity (figure 6.13). Moreover, while S164F mutants responded to activators DEPC and BL-1249 with wild type-like efficacy, S164Y mutant channels showed increased sensitivity to both activators. However, the increased sensitivity of S164Y to the activatory agents is likely to be due to the reduced basal activity of these mutant channels.

The S164E mutation produced channels with significantly decreased basal current (<20% of wild type current), though was able to reduce TREK-1 channel sensitivity to external pH. As is consistent with the majority of mutations exhibiting low levels of basal activity, sensitivity to external reagents DEPC and, more robustly, BL-1249 was enhanced. Curiously, S164K mutants produced wild type-like responses to external drug application, and maintained normal whole cell current amplitude (figure 6.13)

The other tested mutations were largely unremarkable in changing channel responses to the tested parameters (figure 6.13). However, it appears that this region of the channel, near the selectivity filter, is involved in channel gating and therefore merited further examination.

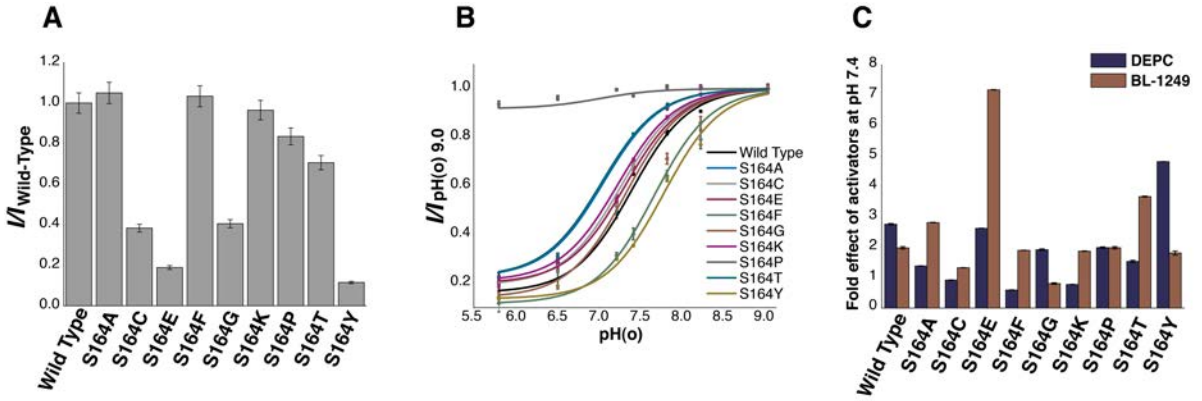


Figure 6.13: *Examination of the impact of amino-acid substitutions to S164. (**A**) Normalised whole cell current amplitude, as observed when channels are expressed in Xenopus oocytes at 0mV at pH 7.4. (**B**) Normalised external pH and (**C**) fold effect of activatory agents for the indicated mutant channels.*

6.4.2 The structural consequences of S164 mutation

In order to determine why different amino acid substitutions at S164 affect a diverse range of channel properties, *in silico* mutagenesis was conducted using the TREK-1 homology model (figure 6.14). When larger amino acids, as in the case of S164E, S164K, S164F or S164Y mutations, novel interactions were identified involving the helical cap above the residue. Shown in figure 6.15, mutation of S164 would alter interaction of this residue with N126, leading to a change in conformation near the selectivity filter. The possible interaction with N126 could explain the different effects of the S164Y and S164F mutations.

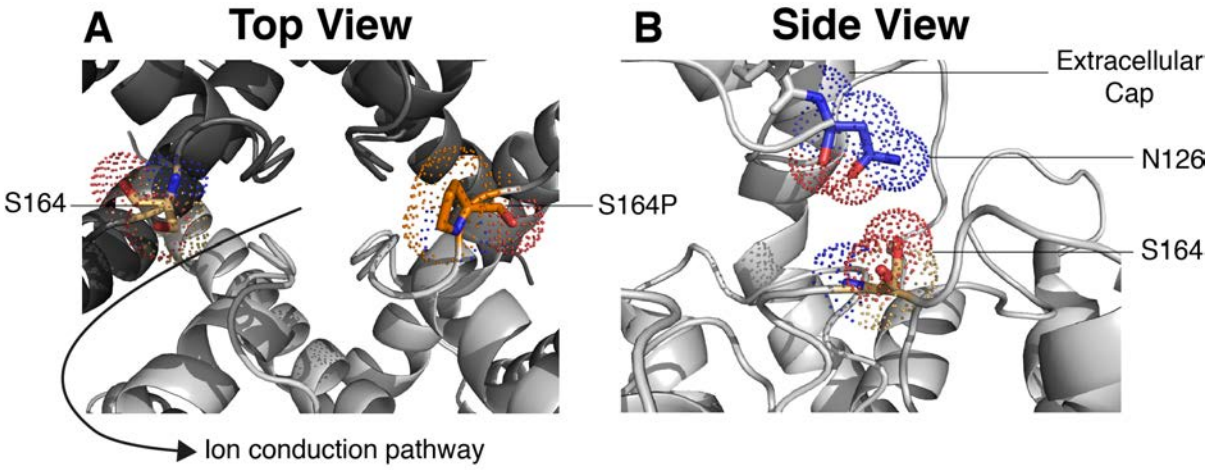


Figure 6.14: *The position of the S164 residues mapped onto a TRAAK-based TREK-1 homology model. (**A**) S164 residues (light orange) and S164P residues (orange) mutated in silico. The channel subunits are shown in different shades of grey. (**B**) S164 (light orange) and the nearest residue, N126 (blue) is too distant for interaction*

6.4.3 The effect of I163 and P165 mutations on TREK-1 function

Given the identification of GoF mutations in position I163 (Bagriantsev *et al.* 2011) and S164 (chapter three), as well as the marked reduction of pH sensitivity by proline introduction at position 164, we examined the effect of mutating the proline residue (P165) that is highly conserved in K2Ps. We also examined the characteristics of I163T mutations using several parameters, including DEPC and BL-1249 modulation (figure 6.15).

The P165S substitution had little effect on external pH sensitivity, though did increase sensitivity to BL-1249 (figure 6.15). However, this is likely to be because of the dramatic reduction (approximately 50%) of basal current. I163 mutant channels slightly reduced pH sensitivity, as well as reduced fold activation by DEPC and BL-1249. The significance of these results is not immediately clear, and so these residues were not examined further.

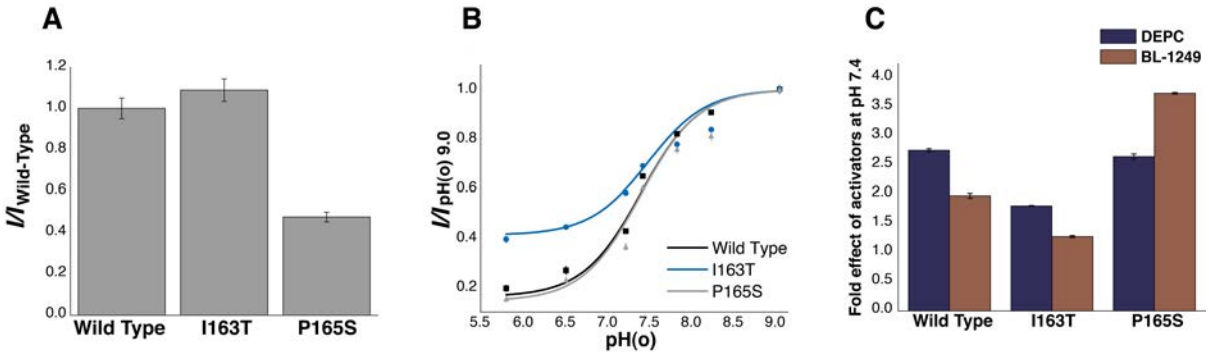


Figure 6.15: *Examination of the impact of amino-acid substitutions to residues adjacent to S164, I163, P165. (**A**) Normalised whole cell current amplitude, as observed when channels are expressed in Xenopus oocytes at 0mV at pH 7.4. (**B**) Normalised external pH and (**C**) fold effect of activatory agents for the indicated mutant channels.*

6.4.4 The role of S164 and the external vestibule in extracellular pH sensitivity

It was previously proposed by Cohen *et al.* that alteration of S164 or the adjacent residues either by mutation or small movements in the selectivity filter would disrupt interactions between R166 and H141 (figure 6.16, Cohen *et al.* 2008). When these residues were mapped onto a KcsA-based TREK-

1 homology model, it appeared that residues H87 and H141 could interact via E84 (Cohen *et al.* 2008).

However, this network of interactions is not visible when analysing the new K2P-based TREK-1 homology model, particularly because the position of the primary proton sensor H141, relative to other residues of interest, is quite different in the new model (figure 6.16). Therefore an alternative mechanism of action would be required to explain how S164 mutations can influence TREK-1 channel pH sensitivity, as well as how histidine residues H141 and H87 communicate to produce a synchronised response to protonation. Our results from mutating the upper TM4 / PH1 region (see section 6.1) suggested that PH1 is highly involved in TREK-1 channel gating and it is possible that H141, which is located near the top of PH1, exerts its effects partly through the movement of the pore helix.

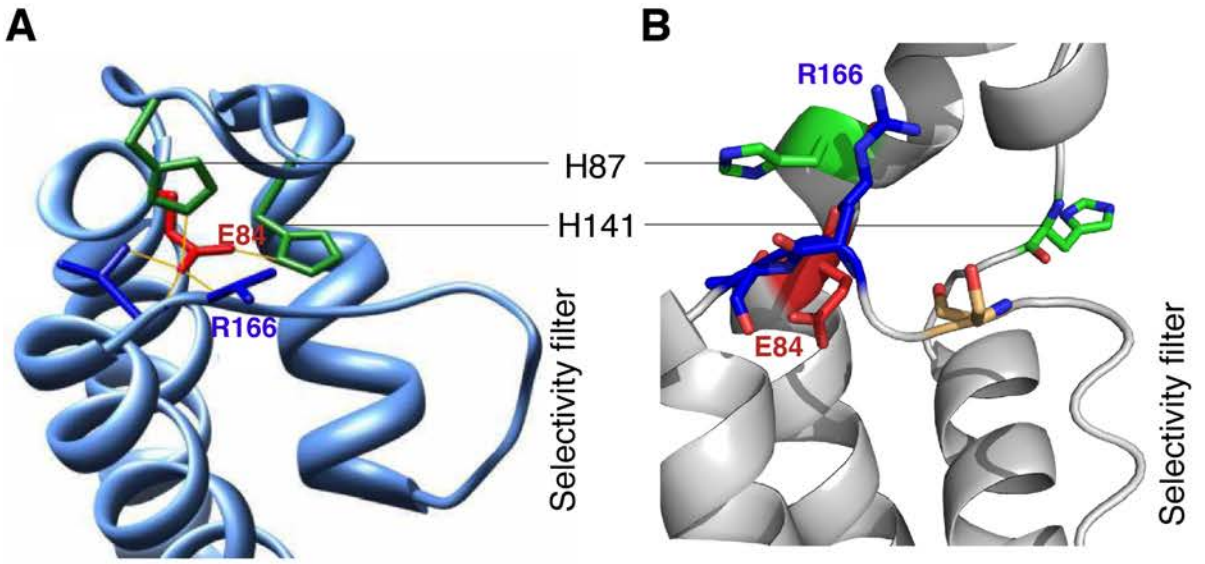


Figure 6.16: *The structure of the extracellular vestibule of TREK-1 channels, shown by a KcsA-based homology model. (**A**) Ribbon representation of the KcsA-based TREK-1 homology model. Predicted hydrogen bonds are shown in yellow. Adapted from Cohen et al. 2008 (**B**) Cartoon representation of TRAAK-based TREK-1 structural model shows a dramatic alteration of the predicted pore structure; note the significant change in position and orientation of the two histidine proton sensor, H87 and H141 (green). Residues R166 and T167 (blue), as well as E84 (red) are shown.*

However, it is interesting to speculate that the S164 residue is involved in a complex network of interactions, responsible for its role in pH-modulated gating at the selectivity filter. As is shown in figure 6.17, it appears that H141 interacts with D143, which forms part of the charged pocket around this histidine residue, following protonation. This interaction could influence the position of a nearby residue in TM1 (K81) which also shares backbone interaction with E84; interestingly, E84A mutants were found to be highly insensitive to extracellular acidosis (figure 4.13). Reorientation of E84 could cause subtle movements of R166, via H87, which is likely to affect the conformation of the nearby selectivity filter. Promisingly, there appears to be a direct interaction between the R166 backbone and the hydroxyl group of S164. It follows, then, that changing the flexibility of the external vestibule close to R166 and the selectivity filter (such as S164P mutation) would therefore noticeably affect channel gating.

Continued overleaf.

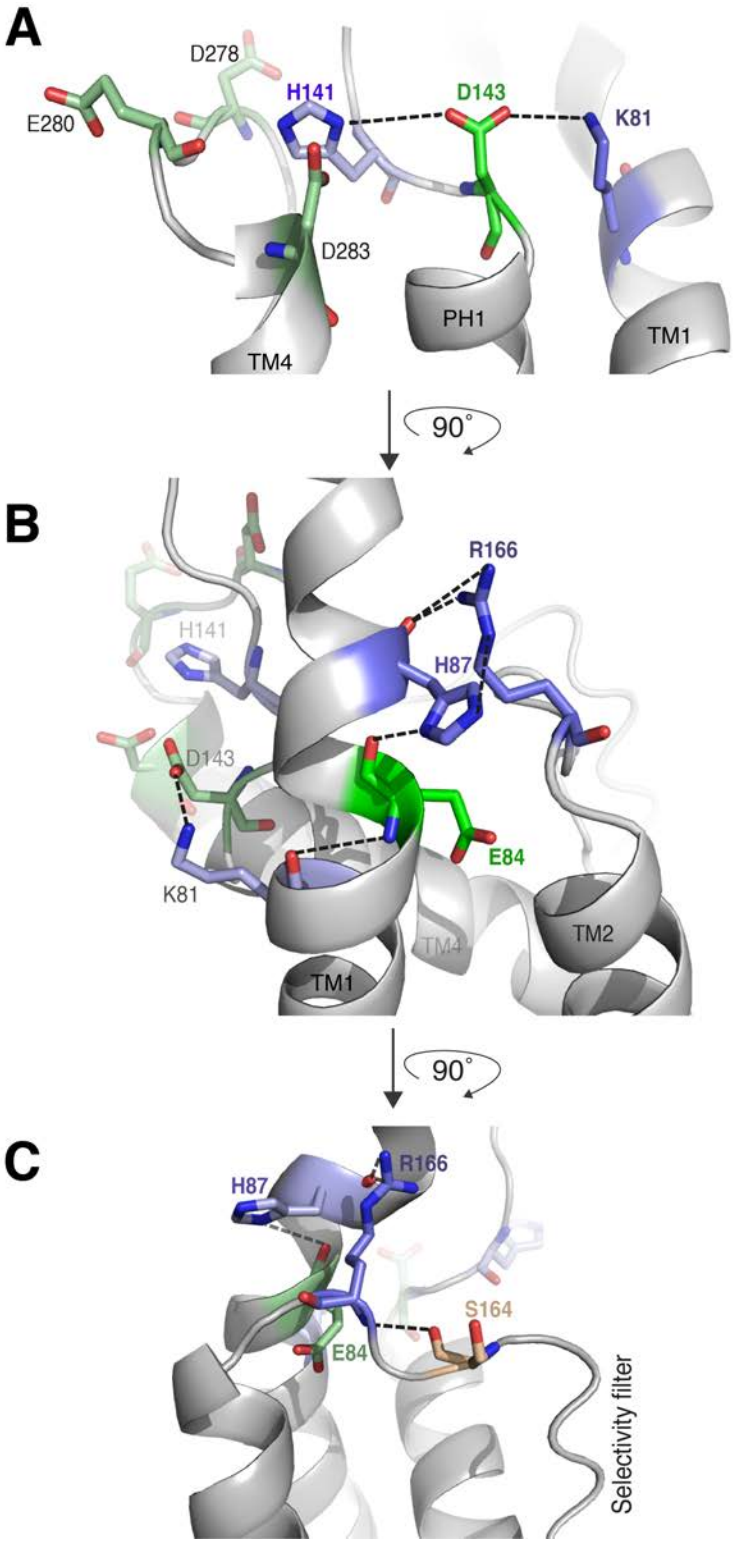


Figure 6.17: *A complex network of interactions responsible for processing signals from proton sensors H141 and H87 to the gating apparatus in the selectivity filter. (**A**) Following protonation of H141, the interaction between this residue and D143 is increased. The resulting movement of D143 disrupts highly charged interaction between K81, in the extracellular portion of TM1, and D143 of PH1. (**B**) The backbone interaction of K81 with E84 causes a subtle effect to the position of the amine-rich ring in H87. Several points of possible interaction have been identified between H87 and R166 residues. (**C**) The proximity of R166 to residues that appear to be involved in gating TREK-1 channels at the selectivity filter, including S164.*

6.5 Reintroduction of DEPC sensitivity to H141C mutant channels

DEPC has proven to be a useful tool in characterising TREK-1 mutations. As our results suggested that a single residue (H141) above PH1 is responsible for the activation of TREK-1 channels by DEPC (figure 5.3), it was hoped that by removing DEPC sensitivity from H141 it could be replaced by introducing a histidine residue in other parts of the channel which are sensitivity to gating. In particular, it was hoped that if S164 is conformationally sensitive, then introduction of a DEPC-responsive histidine residue at this position, the mutant channels (H141C-S164H) would create channels able to respond to DEPC.

Before testing this theory, it was important to determine the effect of the S164H mutation on TREK-1 channel function. This mutant produced wild type-like responses to all of the tested measures of activity (figure 6.18). In particular, it was important that S164H did not alter DEPC sensitivity. Interestingly, the response of S164H mutant channels to extracellular pH inhibition was identical to wild type; both S164H and the double mutant H141C-S164H channels responded to pH similarly to wild type and H141C channels, respectively.

The effects of DEPC application to the S164H mutant channels were remarkable. By itself, the S164H mutation did not alter DEPC sensitivity, and responded to other modulation like wild type channels (figure 6.18). Conversely, H141C did not respond to DEPC and causes an alteration to external pH sensitivity of TREK-1. However, when a histidine was introduced at position S164, DEPC activation was restored to H141C-S164H mutant channels. These results indicate that by causing a dynamic structural change close to the selectivity filter (e.g. by carbethoxylation of S164H by DEPC), TREK-1 channels could be gated. Indeed, the reintroduction of DEPC sensitivity by the H141C-S164H double mutation provides particularly strong evidence that TREK-1 channels are gated close to the selectivity filter.

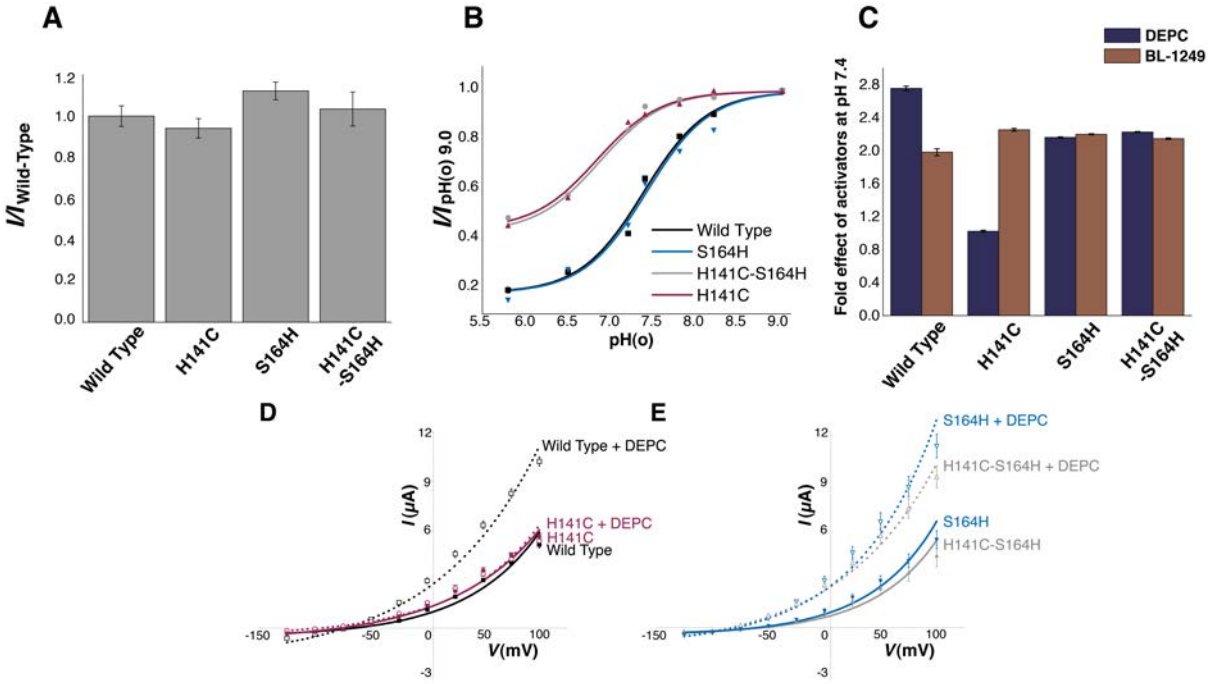


Figure 6.18: *Reintroducing DEPC sensitive to H141C mutants. Normalised (**A**) whole-cell basal current, (**B**) external proton and (**C**) BL-1249 induced responses for the indicated channels. (**D**) and (**E**) Normalised DEPC response for the indicated channels.*

6.6 Is gating of TREK-1 asymmetric?

Alignment of the two PHs revealed an interesting conservation of the FFF-motif aromatic residues in the equivalent positions in both PH1 and PH2 (Appendix IV). Mutations to residues F149 and F150 in PH1 resulted in the dramatic alterations to channel function and, interestingly, aromatic residues were conserved in the equivalent positions in PH2 as Y258 and F259. Figure 6.19 shows a cluster of aromatic residues in PH2 and the adjacent TM helix, TM3. However, these aromatic residues are not in such close proximity to PH2 as seen at the PH1 / TM4 interface (figure 6.2) and the aggregation of aromatic residues near the membrane interface is common (Yau *et al* 1998, Kelkar & Chattopadhyay 2006), suggesting that this clustering of aromatic residues may be coincidental. Nonetheless, following the success of the phenylalanine to leucine substitutions in characterising the upper region of TM4 and PH1, the equivalent mutation was made in PH2 (F259L).

F259L mutant channels had a marked effect in decreasing basal activity, as well as reducing the external pH sensitivity of TREK-1 (figure 6.19). However, unlike the equivalent mutation in PH1,

F259L substitution resulted in mutant channels that were not activated by extracellular agents DEPC and BL-1249. The loss of sensitivity to modulation by F259L mutant channels is difficult to explain, particularly as the target for DEPC modification has been conclusively shown to be in the extracellular loop preceding PH1 (figure 5.3).

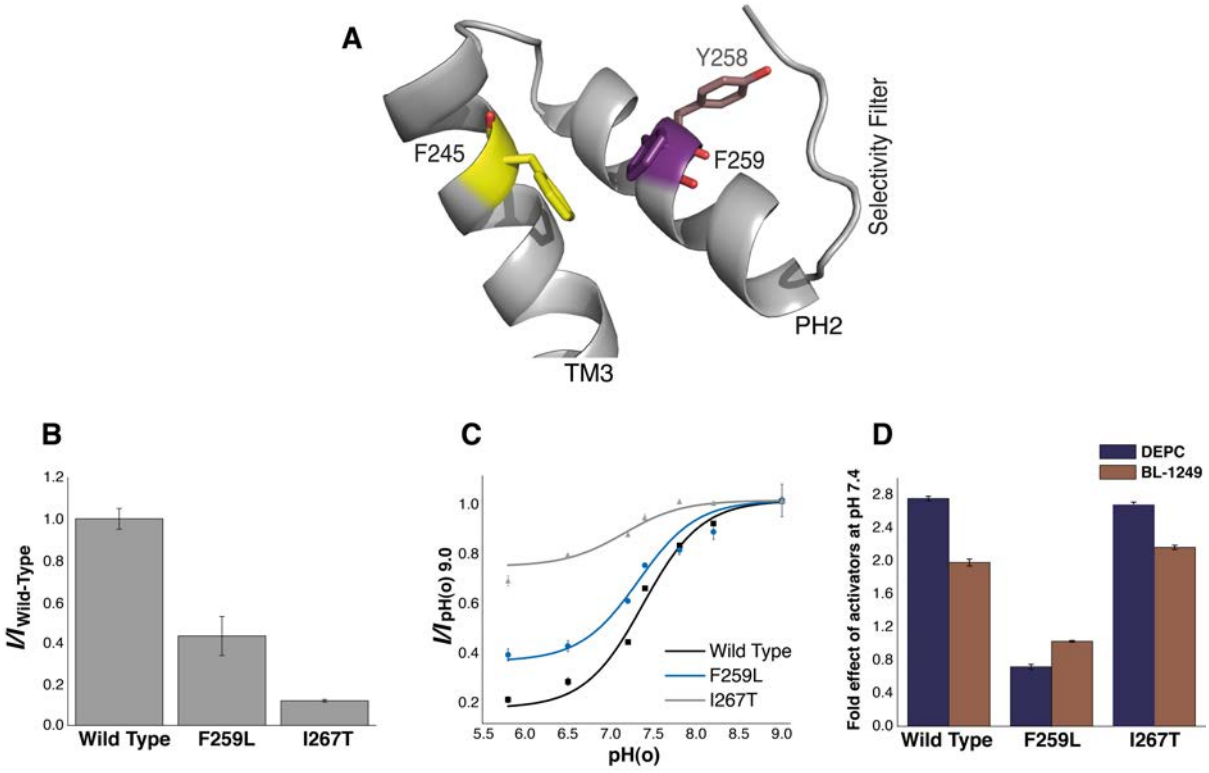


Figure 6.19: (***A***) *F259 (purple) mapped on a structural model of TREK-1 based on K2P channels TRAAK and TWIK-1. Adjacent residues Y258 (brown) and a proposed site for interaction with F259, F245 (yellow), are also shown. (**B**) Normalised whole cell current amplitude, as observed when channels are expressed in Xenopus oocytes at 0mV at pH 7.4. (**B**) Normalised external pH and (**C**) fold effect of activatory agents for the indicated mutant channels.*

However, while the TREK-1 channel appears asymmetric, the selectivity filter possesses pseudo-four-fold symmetry. Therefore, it is unsurprising that changes in and around either of the PHs, would have an effect on channel function; pore mutations have previously been shown to deactivate TREK-1 channels by directly influencing the conformation of the selectivity filter (Brenner & O'Shaughnessy 2008). Nonetheless, it was interesting to identify an aromatic residue in PH2 (F259L) which is involved in regulating TREK-1 channel activity as this shows both PHs can influence gating.

An additional mutation in the selectivity filter connected to PH2, I267T, was identified in an unpublished study. The I267T mutant channel exhibits dramatically reduced basal activity and external pH sensitivity, though responds to application of activators DEPC and BL-1249 with wild type-like efficacy (figure 6.19). This residue is the isoleucline found in the TREK-1 selectivity filter (T-*I*-G-F-G) and so it is not surprising that this mutation can directly influence channel gating, by altering the conformation of the selectivity filter.

The following chapter will summarise that data reported in this thesis, concluding with the presentation of our TREK-1 gating model.

Chapter 7

Conclusions and suggested future studies

7.1 Summary

This study began with the creation of a library of random TREK-1 mutant, by utilising PCR with an unbiased, low-fidelity and error-prone polymerase. Subsequent screening of the random mutant library using a K^+-auxotrophic *S. cerevisiae* strain, SGY1528, identified a number of GoF mutations. While the genetic complementation assay was successful in identifying residues and regions of TREK-1 channels involved in gating, there were inevitably limitations to using this method for characterising mutant channels. Therefore we tested all of the GoF mutations using several parameters; including basal activity, response to external pH and activatory agents, as well as the effect of increased $[K^+]$ on inward currents through these channels. When conducting these experiments, the aim was to be able to map out regions of the channel involved in gating, in order to develop a new gating model. In the following passage, we present our new TREK-1 gating model, with a brief summary of how we came to our conclusions. In addition, we attempt to put our new

model into context within the field of K2P channel gating and to suggest further experiments to confirm our hypotheses regarding TREK-1 gating.

7.2 Our TREK-1 gating model

Following our identification of a group of fifteen mutations that were able to complement K^+-auxotrophic yeast growth, it was important to characterise these channel mutations for their effects on channel function (chapter 4). Our initial investigations indicated that, in general, the GoF mutations markedly increased basal current amplitude. In addition, many mutant channels were able to affect TREK-1 channel response to external protonation. However, there was no demonstrable correlation between a change in extracellular pH sensitivity and basal activity of the mutant channels. Nonetheless it was notable that mutations clustered close together had similar effects on basal current increase, suggesting that the areas in which they were clustered (for example the lower TM helices) are involved in channel activation. Therefore we decided to study the effects of external activators DEPC and BL-1249 on the GoF mutations, in comparison to wild type TREK-1 channels (chapter 5).

DEPC was particularly useful for characterising many of the mutations, as we were successfully able to isolate the binding site as a histidine residue in the extracellular linker domain between TM1 and TM2 (H141), which has also been shown to be central to extracellular pH gating of the channel at the selectivity filter (Cohen *et al.* 2008, Sandoz *et al.* 2009). During the course of this project, it was also suggested by Bagraintsev and Piechotta *et al.*, that TREK-1 channels may be gated predominately at the selectivity filter (Bagraintsev *et al.* 2011, Piechotta *et al.* 2011); a proposition that was supported further by our experiments involving the filter-adjacent GoF mutant S164P. S164P mutant channels were unique in exhibiting a complete loss of sensitivity to external protons while maintaining wild type-like characteristics to other measured parameters. We believe that this effect is due to an indirect interaction with the histidine proton sensors in the extracellular cavity and residue S164. We suggest, in section 6.5, that while movement of the primary proton sensor, H141, may be partly transduced through PH1, affecting the selectivity filter from below, an additional mechanism may be involved in

the external pH-induced inhibition of TREK-1 channels. In brief, following detailed functional and structural examination of S164 and the surrounding residues, it appears that the histidine proton sensors (H87 and H141) may communicate through a series of complex interactions in the extracellular vestibule (figure 6.17).

Another interesting observation we made following the identification of an extracellular target for DEPC-modulation of TREK-1 is that the cluster of hyperactive mutations in the lower helices (e.g. A301D) or C-terminus (e.g. G323R) were insensitive to DEPC-activation. Given the distance across the channel between the lower helices and the external vestibule, these mutations were unlikely to be changing the affinity of DEPC binding at but its efficacy once bound. This is because, even though subtle changes in one part of a protein can affect other regions, the structure of the DEPC 'binding pocket' around H141 was unlikely to be significantly altered by movement of distal regions of the channel, particularly as far down stream as the C-terminal regulatory domain. Moreover, the whole-cell currents of oocytes expressing wild-type TREK-1 channels following DEPC application, was similar to the basal activity of oocytes expressing, for example, E321V mutant channels. This suggests that these mutations were close to fully activated, and therefore were not modulated by DEPC binding, even though the reagent still binds to its target in the extracellular vestibule.

It was clear that the cluster of mutations at the TM-helix interface dramatically influenced the activity, most likely the open probability, of the channel. However, the direct effect of these mutations on channel gating was unclear. The concept of a HBC-like gate, as suggested in chapter 1, is inconsistent with the findings of Piechotta *et al.*, who showed conclusively that TREK-1 channels are likely to be in the 'splayed open' state, originally shown for KcsA channels (Zhang *et al.* 2003), even when the channel is inactive or closed at the filter gate (Piechotta *et al.* 2011). Furthermore, the crystal structure of the closely related TRAAK channel was shows the lower region of TM4 to bend significantly, as to run almost parallel to the inner membrane, which would make closure of the channel by a constriction in the lower helices energetically unfavourable (Brohwan *et al.* 2012).

Nonetheless, the identification of the highly activatory mutations in the lower helices was demonstrative of the role of these helices in channel gating; which is further emphasised by the widely-acknowledged regulatory domain in the C-terminus of TREK-1, signals from which are likely to be transduced via the TM helices (particularly TM4) to the gating apparatus. One solution which is consistent with our data and the conclusions drawn elsewhere (e.g. Rapedius *et al.* 2012) is that the TM-helices move to dynamically communicate with the selectivity filter, without necessarily being opened and closed like a conventional HBC-like gate. It is likely that highly activatory mutations of the residues at the lower TM-helix interface (Y299A, A301E, A302C and I230N) may cause the channel to open by restricting or altering the nature of the movement of TM4, and thereby affect channel function. This movement may well be responsible for the transduction of gating stimuli from the intracellular regulatory domain to the predominant gate, in the selectivity filter, which is consistent with our investigation of the interactions between PH1 and TM4.

This complex relationship between these two helices appears to be central to interactions between the highly conserved residues F149 (PH1) and W290 (TM4). Mutation of these aromatic residues resulted in severe disruption of the PH1-TM4 interface, which appears to result in changes of basal activity, as well as an alteration of channel modulation by protons and external activators (figure 6.4). We propose that this is because the interaction of these two residues allows for the transduction of TM4 movements to the selectivity filter, via PH1. This suggestion is supported by the identification of G152 (in PH1) in a parallel study as a residue vital in controlling the filter gating mechanism (Bagriantsev *et al.* 2012).

From our results and external corroboration it is clear that TREK-1 channels are gated primarily through PH1 and the adjacent TM helix, TM4. Overleaf, in figure 7.1, we present our gating model, which indicates that movement of the TM4 helix is transduced through PH1 to the selectivity filter gate. Residues within at TM helix interface between TM2, TM3 and TM4, are proposed to affect the movement of TM4. As a result, mutation of other residues (particularly I230 and F200) would result in an indirect effect on channel gating at the selectivity filter.

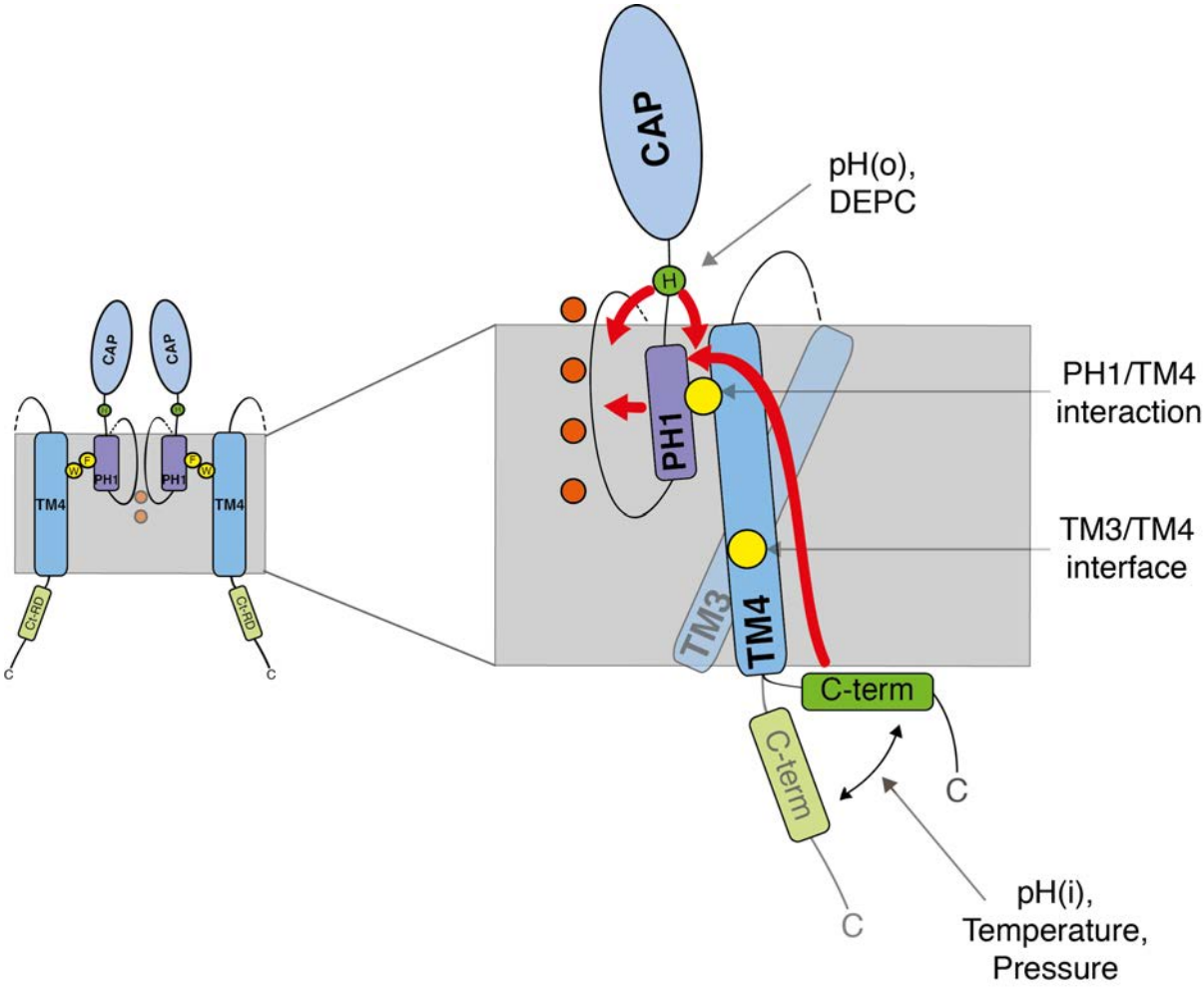


Figure 7.1: *A new TREK-1 gating model, in which movement of the TM helices act primarily through PH1 to affect channel gating. Red arrows indicate the transduction of gating signals.*

The model presented is a simple representation of the work conducted personally, by external collaborators and by research laboratories studying K2P channels. Nonetheless, we believe that this model accurately depicts the chain of events that trigger activation of TREK-1 by external and internal regulation.

Addendum:

Following the completion of our study, a TRAAK structure of greater resolution was published, by the same group who had previously resolved the first TRAAK channel crystal structure (Brohawn *et al.* 2012, Brohawn *et al.* 2013). The most notable difference between this new TRAAK structure (PDB code 4I9W) and the previously reported structure (3U7M) is the domain-swapped chain connectivity,

which enables the helical cap to exchange two outer helices from either subunit, 180˚ around the channels. While this significant change no doubt has a bearing on our understanding of TREK-1 protein folding, the areas outlined in our gating model are well conserved from the previous structure and therefore do not interfere with our conclusions about channel activation.

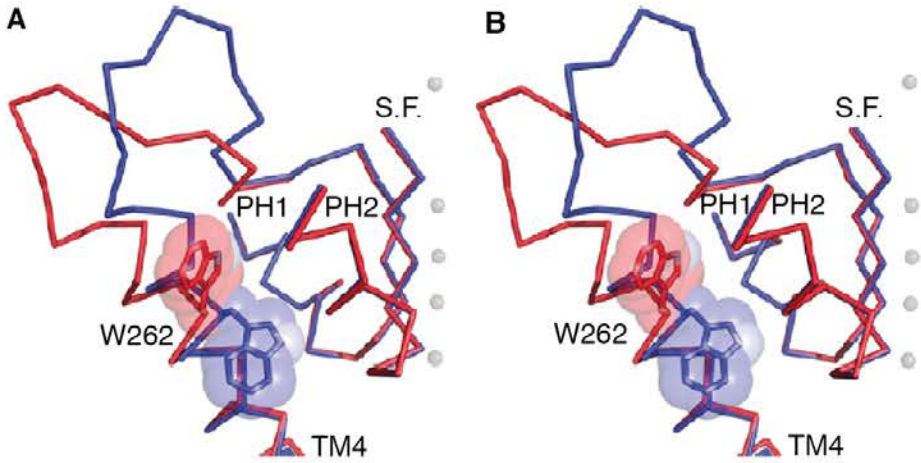


Figure 7.2: *Zoomed-in stereoview of a superposition of the extracellular side of TM4 from the two subunits. One channel subunit is coloured red and the second is blue. PH1, PH2, and TM4 are shown as wires, and W262 (W290 in TREK-1) is shown as sticks with transparent surface. In the blue subunit (which has an open membrane side opening), the extracellular end of TM4 including W262 packs against PH1. In the red subunit (which has a closed membrane side opening), collapse and extension of the selectivity filter to TM4 connection, displacement of TM4 away from PH1, and a rotamer change of W262 results in a loss of the tightly packed interaction observed in the blue subunit around the selectivity filter, leading to opening or closing of the selectivity filter gate. Figure and text adapted from Brohawn et al. 2013.*

However, there is a difference in the angle of the TM4-helix in the two subunits; there appears to be a previously unseen slight bend in the helix of one subunit when superimposed on top of TM4 from the other subunit (not shown). Importantly, the bend in the helix occurs around residue Y299, which is suggests that this region of the channel can move to dynamically regulate the channel. In addition, the equivalent position of W290 (W262 in TRAAK) is different in the two subunits, possibly advocating the movement of this residue in different conformational states of the channel (figure 7.2). Therefore, we were satisfied that the new crystal structures did not conflict with our data, but instead further validated our conclusions.

7.3 Suggested further investigation of K2P gating

While we present our findings with the highest degree of confidence, in the following section, we approach possible further studies that we believe would be beneficial for developing a better understanding of K2P channels.

The identification of F259 and I267 within PH2 and the selectivity filter, suggests that the second pore domain is able to directly affect gating of TREK-1. As such, one of the aims following on from this study should be to continue the study of the PH2, and its apparent role in channel gating.

Further characterisation of the GoF mutations should be carried out using alternative functional examination; because it has been established that C-type gating of TREK-1 is accompanied by an increase of the relative permeability of Na^+ over K^+ (Yuill *et al.* 2007, Bagriantsev *et al.* 2011), it would be interesting to examine the effects of lower-TM4 mutations on the relative K^+ selectivity over other cations. While high external [K^+] was used to characterise the GoF mutants, detailed changes in TREK-1 selectivity were not examined. Moreover, the work of Thomas *et al.* showed that rat TREK-1 channel selectivity for K^+ over Na^+ is regulated by alternative translation initiation (Thomas *et al.* 2008). They showed that a shortened TREK-1 isoform, lacking 56 N-terminal amino acids, was more permeable to sodium than full-length TREK-1 channels, under physiological conditions. This suggests a highly interesting mechanism for channel selectivity, which should be examined further.

It was hoped that our initial investigation into the function of the GoF mutations would include characterisation of the any changes to intracellular pH sensitivity. These experiments are yet to be completed, though it would prove highly valuable to characterise the effects of GoF mutations on intracellular modulation of TREK-1 channels. This is particularly true for the GoF mutations within TM4, as it has been proposed that this helix plays a large part in transduction of the intracellular signals to PH1 and, therefore, the selectivity filter.

Alternatively, the transduction of signals through TM4 could also be explored using other intracellular modulators, such as temperature, membrane stretch or phosphorylation. For example, one such study would involve mimicking phosphorylation of TREK-1 channels by mutation of S348, which would normally inhibit channel activity. Introducing a second mutation, which is known to be highly activatory (e.g. A301E), to the S348 mutant and then examining the functional characteristics of the double mutant may reveal further information about how intracellular stimuli are transduced from the C-terminus to the upper-gating apparatus.

The movement of the TM and pore helices is still unclear from a mechanistic viewpoint. Indeed, a recently study published suggests the possibility that glutamate may permeate through TREK-1 following Gβγ binding, a wholly unexpected finding that highlights the lack of understanding of pore dilation in response to intracellular stimuli (Woo *et al.* 2012). This finding emphasises the need for further research into these channels.

In order to gain a better understanding of the physical changes of conformation required to gate these K2P channels, computational studies must be employed, alongside conventional biochemical and electrophysiological methods, as an additional avenue for research into how these fascinating channels operate.

Appendix I

Qiagen protocols

n.b. all centrifugation steps were carried out at 13,000 rpm in a conventional table-top microcentrifuge (Eppendorf), unless otherwise stated.

DNA purification

1. Add 250μl buffer PB to the 50μl of the DNA solution.
2. Transfer the sample to a QIAquick column (purple) to bind DNA and centrifuge for one minute.
3. Discard the flow-through and place the QIAquick column back in the same collection tube.
4. To wash, add 0.75ml of Buffer PE to the QIAquick column and centrifuge for 30 seconds.
5. Discard the flow-through and centrifuge the QIAquick column for an additional minute to remove excess PE buffer.
6. Place the QIAquick column into a clean 1.5ml microcentrifuge tube.
7. Elute DNA by adding 30μl H_2O to the centre of the QIAquick membrane and centrifuge the column for one minute.

Rapid isolation of plasmid DNA from *E. coli*

1. Resuspend the cell pellet in 250μl buffer P1 (with RNAase) and transfer to a 1.5ml microcentrifuge tube.
2. Add 250μl Buffer P2 and invert gently four-six times to mix. Incubate at room temperature for no more than five minutes.
3. Add 350μl Buffer N3 to each tube and invert immediately, but gently, four-six times to mix.

4. Centrifuge the solution for ten minutes and very gently transfer the clear lysate to a QIAprep spin column.
5. Centrifuge the clear lysate for one minute, to bind the DNA to the Qiaprep spin column membrane. Discard the flow-through.
6. Wash the QIAprep spin column by adding 0.5 ml Buffer PB and centrifuging for one minute. Discard the flow-through.
7. Wash the QIAprep spin column by adding 0.75 ml Buffer PE and centrifuging for one minute. Discard the flow-through.
8. Discard the flow-through, and centrifuge for an additional 1 minute to remove residual wash buffer.
9. Place the QIAprep column in a clean 1.5ml microcentrifuge tube. To elute DNA, add 50-100μl molecular biology grade H_2O to the centre of the QIAprep spin column, centrifuge for one minute.

Rapid isolation of plasmid DNA from *S. cerevisae*

This protocol is a user developed method recommended for plasmid isolation from yeast by Qiagen. The products and reagents used are the same as those used in rapid isolation of plasmid DNA from *E. coli*. This protocol was optimised further by the addition of a second ten minute centrifugation step, which was found to increase the quality of the plasmid DNA yield and, therefore, reliability of subsequent DNA transformation into the subcloning efficiency DH5α *E.coli* cells.

1. Resuspend cell pellet in 250μl buffer P1 (with RNAase) and transfer to a 1.5ml microcentrifuge tube.
2. Add 50-100μl acid washed glass beads (Sigma) to each micro-centrifuge tube and vortex for six minutes.
3. Stand the solution for one minute to allow beads to settle and transfer supernatant to fresh micro-centrifuge tube.
4. Add 250μl Buffer P2 and invert gently four-six times to mix. Incubate at room temperature for five minutes.

5. Add 350μl Buffer N3 to each tube and invert immediately, but gently, four-six times to mix.
6. Centrifuge for ten minutes and very gently transfer the semi-clear lysate into a fresh micro-centrifuge tube. It is important to avoid remixing the pellet at this stage.
7. Repeat the previous step, but instead transfer the clear lysate to a QIAprep spin column.
8. Centrifuge for six minutes. Discard the flow-through.
9. Wash the QIAprep spin column by adding 0.5 ml Buffer PB and centrifuging for one minute. Discard the flow-through.
10. Wash the QIAprep spin column by adding 0.75 ml Buffer PE and centrifuging for one minute. Discard the flow-through.
11. Centrifuge for an additional minute to remove residual wash buffer.
12. Place the QIAprep column in a clean 1.5 ml microcentrifuge tube. To elute DNA, add 25μl molecular biology grade H_2O to the centre of the QIAprep spin column, centrifuge for one minute.

Appendix II

Solutions for Yeast transformations

1000x Mineral Solution

50mg H_3BO_3 (*boric acid*)

4mg $CuSO_4.5H_2O$ (*cupric sulfate pentahydrate*)

10mg KI (*potassium iodide*)

50mg $FeSO_4.7H_2O$ (*ferrous sulfate heptahydrate*)

45mg $MnSO_4.H_2O$ (*manganese sulfate monohydrate*)

90mg NH_4molybdate.4H2O (*molybdic acid ammonium salt tetrahydrate*)

70µl $ZnSO_4.7H_2O$ (*zinc sulfate heptahydrate*)

make up to 100ml with H_2O and filter sterilise

1000x vitamin solution

2mg Biotin (*d-biotin vitamin H*)

400mg D-panthothenic acid (*hemiacalcium salt*)

400mg Nicotinic acid (*niacin*)

400mg Pyridoxine HCl (*vitamin B6*)

400mg Thiamine (*aneurine vitamin B1*)

2g Inositol (*myo-inositol*)

make up to 100ml H_2O and filter sterilse

Lithium Acetate 1M Solution

10.2g LiAc powder (FW = 102)

100ml H_2O

PEG 50% Solution

50g PEG powder (FW=3-4000)

50ml H_2O

TE (Tris/EDTA) Buffer

10ml Tris-HCl 1M

80ml H_2O

2ml EDTA 0.5M (pH8)

Denatured Carrier DNA Solution:

(for each 1μg plasmid DNA transformed)

2μl Salmon testes single stranded DNA (Sigma)

6μl Sterile molecular biology grade H_2O

incubate for ten minutes at ≥100˚C.

Appendix III

Electrophysiology solutions

Solution compositions are presented here. Formula weight for individual components as well as the weight of said component required for one litre of solution are included. In practice, 10x stock solutions were often made for commonly used solutions and diluted accordingly. All solutions were filter sterilised, stored at 4˚C and discarded within 3 months of sterilisation.

OR-2 solution

Calcuim free solution used for Collagenase digestion of *X. laevis* ovary connective tissue.

	Formula weight (g/mol)	**Desired concentration (mM)**	**Amount required for 1l (g)**
NaCl *(Sodium chloride)*	58.443	83	4.82
KCl *(Potassium chloride)*	74.515	2	0.1491
$MgCl_2.2H_2O$ *(Magnesium chloride dihydrate)*	147	1	0.02033
HEPES *(4-(2-hydroxyethyl)-1-piperazineethanesulfonic acid)*	238.3059	5	1.19

Barth's solution

Barth's solution was used for storing oocytes. The media was always supplemented with antibiotic, the nature of which varies for reasons explained in the main body of text.

	Formula weight (g/mol)	**Desired concentration (mM)**	**Amount required for 1l (g)**
NaCl *(Sodium chloride)*	58.443	88	5.414
KCl *(Potassium chloride)*	74.515	1	0.074
$MgSO_4$ *(Magnesium sulfate)*	120.3683	1.68	0.404
HEPES *(4-(2-hydroxyethyl)-1-piperazineethanesulfonic acid)*	238.3059	10	2.383
$Ca(NO_3)_2$ *(Calcium nitrate)*	164.0884	0.47	0.078
$NaHCO_3$ *(Sodium bicarbonate)*	84.0068	2.4	0.202
$CaCl_2$ *(Calcuim chloride)*	110.9848	0.41	0.06

Modified / MES-buffered Barth's solution

Transport solution used by EXRC. This solution was never made personally.

	Formula weight (g/mol)	**Desired concentration (mM)**	**Amount required for 1l (g)**
NaCl *(Sodium chloride)*	58.443	88	5.414
KCl *(Potassium chloride)*	74.515	1	0.074
$MgSO_4$ *(Magnesium sulfate)*	120.3683	1.68	0.404
MES *(2-(N-morpholino)ethanesulfonic acid)*	195.2	5	0.976
$Ca(NO_3)_2$ *(Calcium nitrate)*	164.0884	0.47	0.078
$NaHCO_3$ *(Sodium bicarbonate)*	84.0068	2.4	0.202
$CaCl_2$ *(Calcuim chloride)*	110.9848	0.41	0.06

ND96 solution

ND96 was the base solution of all TEVC recordings. The solution below would be buffered to pH 7.2, 7.4, 7.8. Where pH is not stated, ND96 pH 7.4 was used.

	Formula weight (g/mol)	**Desired concentration (mM)**	**Amount required for 1l (g)**
NaCl *(Sodium chloride)*	58.443	96	5.78
KCl *(Potassium chloride)*	74.515	2	0.14
$CaCl_2.2H_2O$ *(Magnesium sulfate)*	120.3683	1.8	0.26
$MgCl_2$ *(Magnesium chloride)*	95.2115	2	0.19
HEPES *(4-(2-hydroxyethyl)-1-piperazineethanesulfonic acid)*	238.3059	5	1.19

Modified ND96 solution (High $[K^+]$)

	Formula weight (g/mol)	**Desired concentration (mM)**	**Amount required for 1l (g)**
NaCl *(Sodium chloride)*	58.443	8	0.47
KCl *(Potassium chloride)*	74.515	90	6.71
$CaCl_2.2H_2O$ *(Magnesium sulfate)*	120.3683	1.8	0.26
$MgCl_2$ *(Magnesium chloride)*	95.2115	2	0.19
HEPES *(4-(2-hydroxyethyl)-1-piperazineethanesulfonic acid)*	238.3059	5	1.19

Modified ND96 solution (Acidic pH)

Employed in external pH sensitivity studies. This MES buffered modified ND96 solution was more stable below pH 6.8 than the HEPES buffered original[1].

	Formula weight (g/mol)	**Desired concentration (mM)**	**Amount required for 1l (g)**
NaCl *(Sodium chloride)*	58.443	8	0.47
KCl *(Potassium chloride)*	74.515	90	6.71
$CaCl_2.2H_2O$ *(Magnesium sulfate)*	120.3683	1.8	0.26
$MgCl_2$ *(Magnesium chloride)*	95.2115	2	0.19
MES *(2-(N-morpholino)ethanesulfonic acid)*	195.2	5	0.976

[1] http://www.sigmaaldrich.com/life-science/core-bioreagents/biological-buffers/learning-center/buffer-reference-center.html#pH

Modified ND96 solution (Alkaline pH)

Employed in external pH sensitivity studies. This MES buffered modified ND96 solution was more stable above pH 8 than the HEPES buffered original[2].

	Formula weight (g/mol)	**Desired concentration (mM)**	**Amount required for 1l (g)**
NaCl *(Sodium chloride)*	58.443	8	0.47
KCl *(Potassium chloride)*	74.515	90	6.71
$CaCl_2.2H_2O$ *(Magnesium sulfate)*	120.3683	1.8	0.26
$MgCl_2$ *(Magnesium chloride)*	95.2115	2	0.19
Trizma-HCl *(trisaminomethane hydrochloride)*	157.60	10	1.576

[2] http://www.sigmaaldrich.com/life-science/core-bioreagents/biological-buffers/learning-center/buffer-reference-center.html#pH

Appendix IV

Protein Alignments

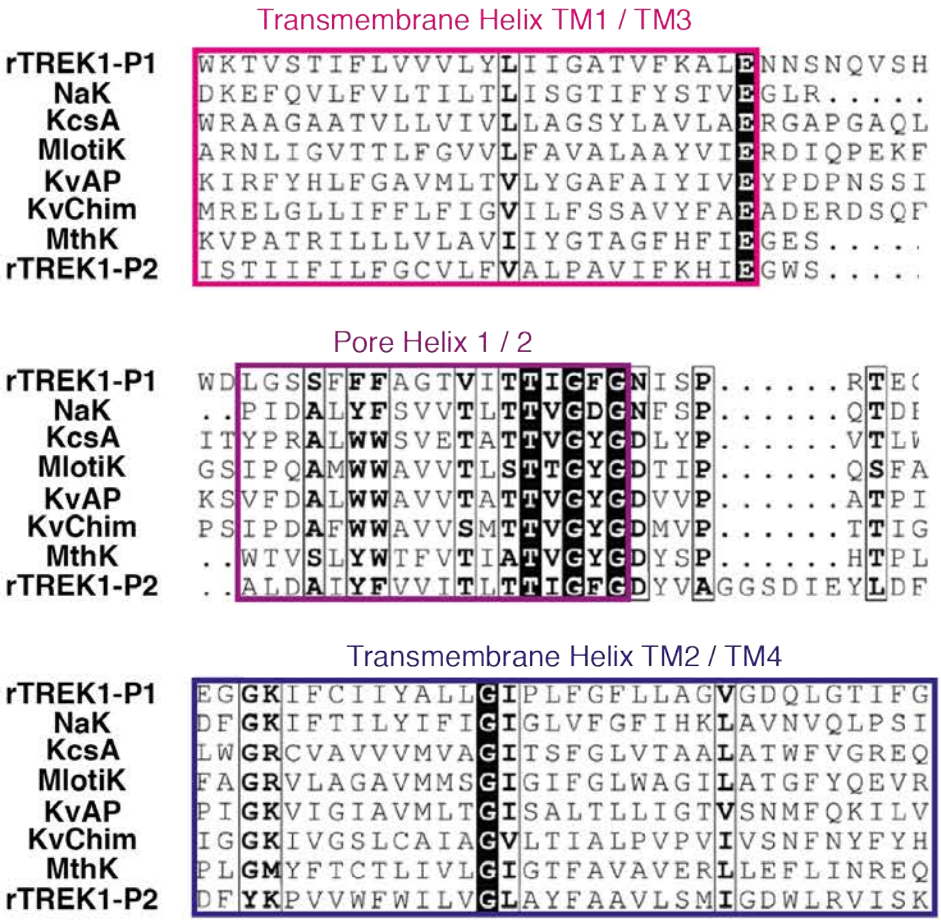
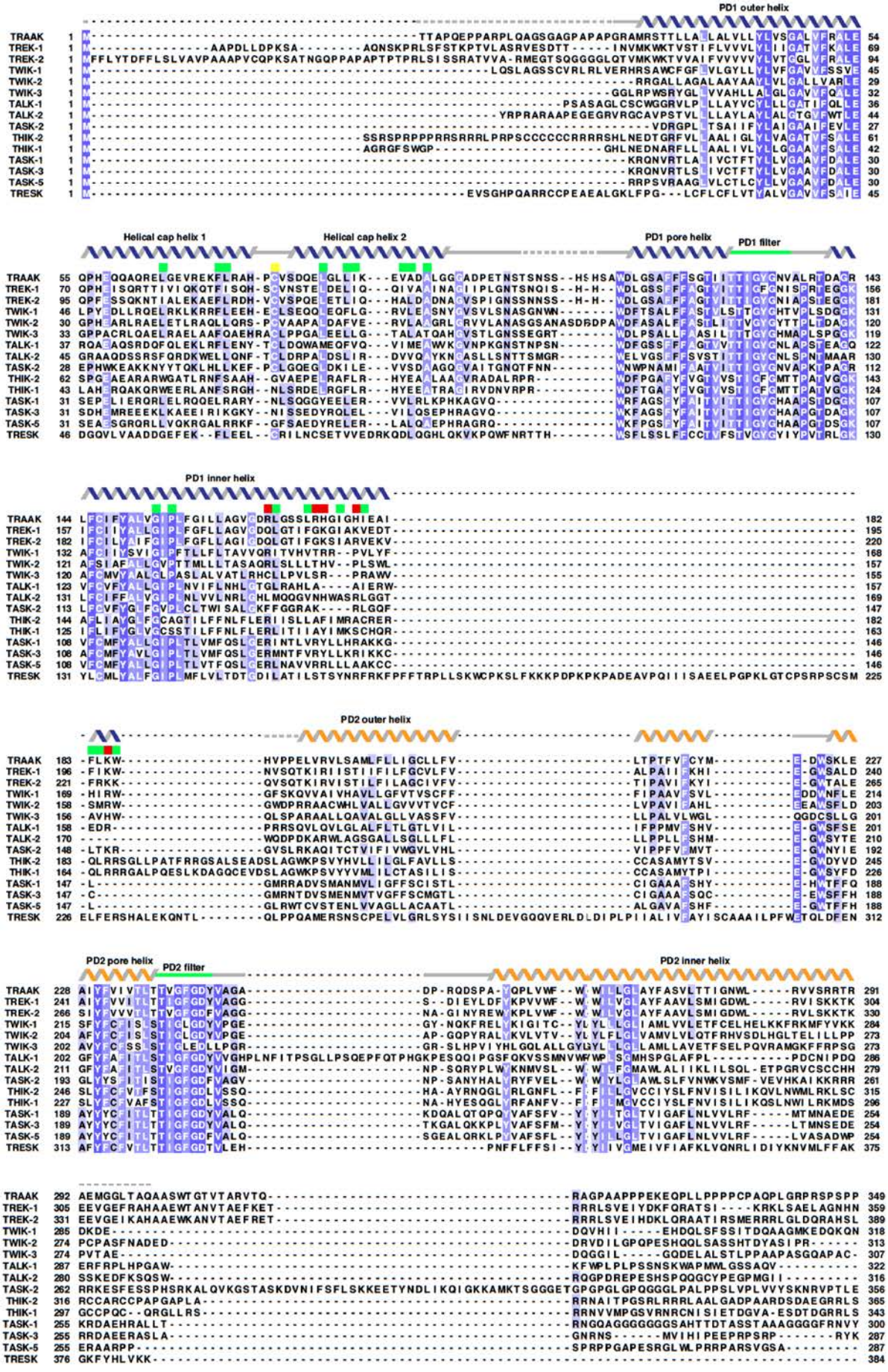


Figure IV a: *An alignment of various single-pore K^+ channels and rat TREK-1. These channels were used as to produce a series of homology models by collaborators in the structure bioinformatics and computational biochemistry sub-department. Conserved residues across the K^+ channel superfamily are shown in black. Adapted from Piechotta et al. 2011, supplementary information.*


PD1 outer helix
Helical cap helix 1
Helical cap helix 2
PD1 pore helix
PD1 filter
PD1 inner helix
PD2 outer helix
PD2 pore helix
PD2 filter
PD2 inner helix
TRAAK
TREK-1
TREK-2
TWIK-1
TWIK-2
TWIK-3
TALK-1
TALK-2
TASK-2
THIK-2
THIK-1
TASK-1
TASK-3
TASK-5
TRESK

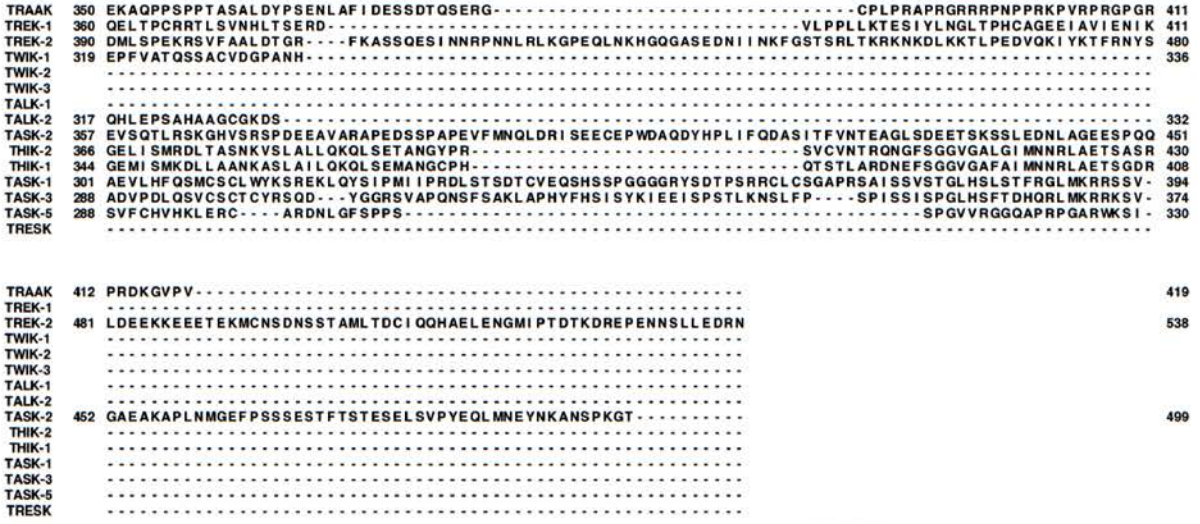


Figure IV b: *Multiple sequence alignment of human K2P channels. Alignment of the 15 human K2P channels is coloured by conservation in a ramp from white (not conserved) to dark blue (highly conserved). Secondary structure of TRAAK is indicated above the sequences and labeled with PD1 and PD2 signifying pore domain 1 and 2, respectively. Large gaps in the alignment are shown as dashed black lines, residues not observed in the crystal structure as dashed gray lines, loops and non-helical secondary structure as solid gray lines, K^+ selectivity filters as green lines, and helices as cartoons. Helices in pore domain 1 are coloured blue and helices in pore domain 2 are coloured orange. In the helical cap, hydrophobic core-forming residues are marked with green boxes and the disulfide bonded C78 (C108 in TREK-1) is marked with a yellow box above the sequence. The hinge glycine (G153 in TRAAK, G181 in TREK-1) and kink proline (P155 in TRAAK, P183 in TREK-1) in the pore domain 1 inner helix are also marked with a green box above the sequence. Figure and text adapted from Brohawn et al. 2012*

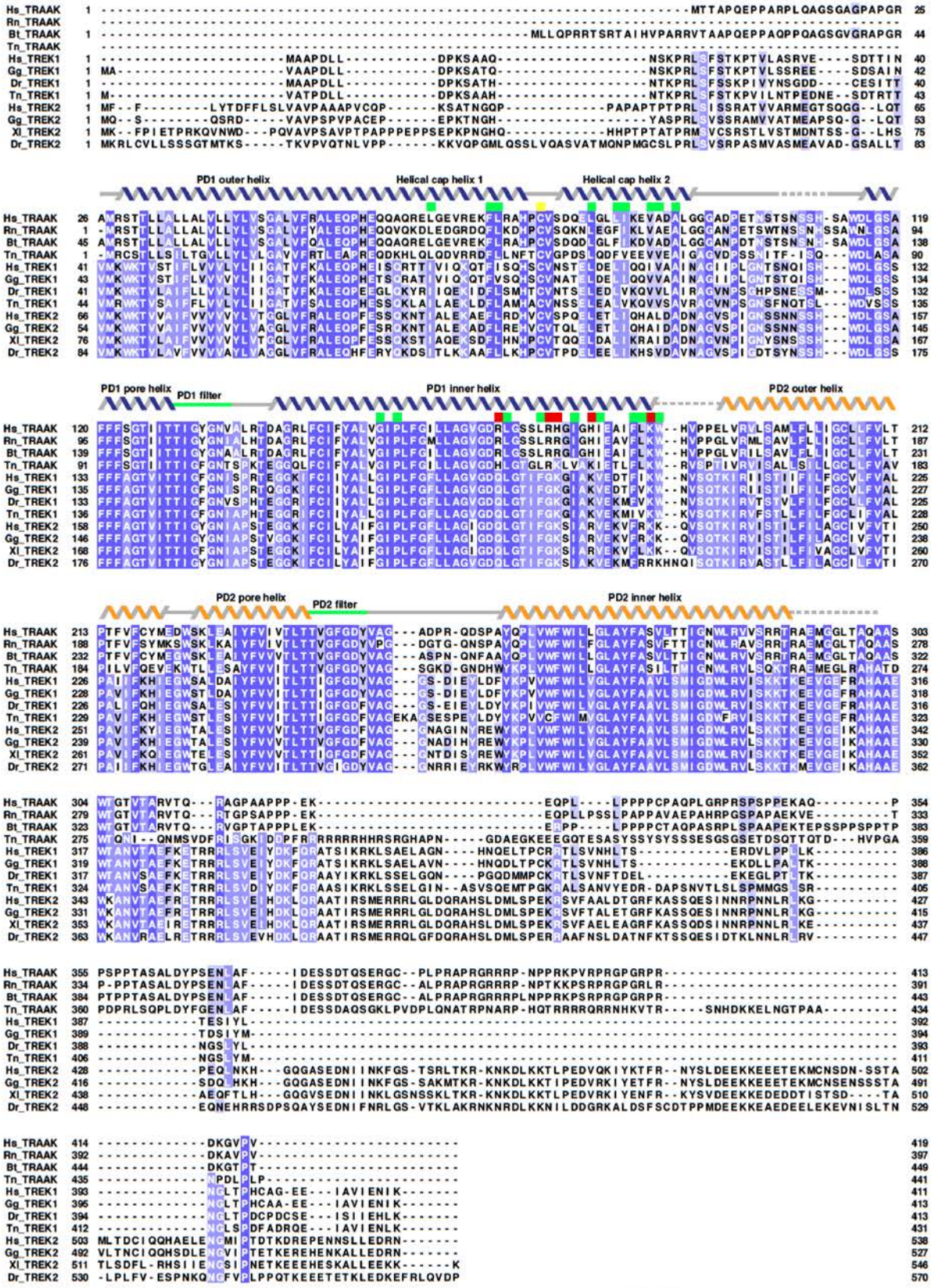


Figure IV c: *Multiple sequence alignment of TRAAK/TREK K2P channels. Alignment of four TRAAK, four TREK-1, and four TREK-2 channels is coloured by conservation in a ramp from white (not conserved) to dark blue (highly conserved). Annotations conserved from figure IV b. Abbreviations used are: Hs, Homo sapiens, Rn, Rattus norvegicus, Bt, Bos taurus, Tn, Tetraodon nigroviridis, Gg, Gallus gallus, Dr, Danio rerio, Xl, Xenopus laevis. Figure and text adapted from Brohawn et al. 2012.*

Appendix V

Unique mutants identified using the genetic complementation assay

Mutant Name	Mutation 1	Mutation 2	Mutation 3	Mutation 4	Mutation 5	Mutation 6
1	R7Q	R47L	R140L	I175N	I422L (fs)	-
2	W290C	-	-	-	-	-
3	V295I	E321V	F325L	A370E	L407P	A415V
4	V349M	R382G		-	-	-
5	P10H	G11S	A301E	-	-	-
6	A104T	A242S	H413L	-	-	-
7	A302T	-	-	-	-	-
8	I130T	S348C	-	-	-	-
9	R7W	L365F	-	-	-	-
10	S219T	K354N	-	-	-	-
11	R7W	L365F	-	-	-	-
12	G169S	F211L	-	-	-	-
13	I130T	S348C	-	-	-	-
14	K286R	-	-	-	-	-
15	N110I	S136T	F232S	-	-	-
16	V349M	Q375N	C380S	L384P	P412R	-
17	P24L	I244M	-	-		-
18	Q98R	I158K	G181E	V289A		-
19	K286R	D353V	Y406N	-	-	-
20	S63F	F232Y	A302V	K354R	E368K	-
21	A14S	F232S	-	-	-	-
22	A17T	S36L	T78M	L389Q	G371V	S348N
23	G11S	S164T	-	-	-	-
24	K32R	H141N	T333I	L384P	-	-
25	A28T	A25S	A239V	I267V	L399F	-
26	I223N	L282P	K426M	-		-
27	E321A	V386A	-	-		-
28	R344W	-	-	-	-	-
29	K25E	A302V	I314L		-	-
30	L117F	F200Y	M306I	fs F340L	-	-
31	I223N	L282P	K426M	-	-	-
32	T333A	T411P	*427E	adds 6AA		-
33	I75V	E113V	V122E	-	-	-
34	F160Y	-	-	-	-	-
35	I257F	R312W	E324G	-	-	-
36	S26Y	W290L	R344W	-	-	-
37	D20N	S140C	W214R	F232S	E339D	-
38	P14L	E321G	-	-	-	-
39	S147P	D287V	S348N	fs H413P	424*	-
40	T343R	-	-	-	-	-

Mutant Name	Mutation 1	Mutation 2	Mutation 3	Mutation 4	Mutation 5	Mutation 6
41	N110K	L114M	Q375*	-	-	-
42	L117F	F200Y	M306I	fs F340L	I347*	-
43	E432V	-	-	-	-	N/A
44	G169S	F211L	L389V	-	-	-
45	F160Y	-	-	-	-	-
46	G11S	L410P	-	-	-	-
47	S52P	E339K	S348N	-	-	-
48	V295I	E321V	F325L	A370E	L407P	A415V
49	F160Y	-	-	-	-	-
50	S26Y	W290L	R344W	-	-	-
51	L282P	-	-	-	-	-
52	D13V	S164P	L389R fs	-	-	-
53	R7W	S136F	I182V	I227N	-	-
54	A53T	Q138H	-	-	-	-
55	A14V	D283Y	-	-	-	-
56	S26Y	W290L	R344W	-	-	-
57	I223N	L282P	K426M	-	-	-
58	A104T	L365V	-	-	-	-
59	E321A	V386A	-	-	-	-
60	I103T	E423G fs	424 trunc	-	-	-
61	-	-	-	-	-	N/A
62	-	-	-	-	-	N/A
63	F291L	-	-	-	-	-
64	Q100H	E168D	G201E	E394G	-	-
65	L2H	F340L	-	-	-	-
66	L2I	-	-	-	-	-
67	A104S	-	-	-	-	-
68	-	-	-	-	-	-
69	G323R	E339K	-	-	-	-
70	G323R	-	-	-	-	-
71	A3V	R222H	L282P	-	-	-
72	K362N	-	-	-	-	-
73	A3V	R222H	L282P	E350V	-	-
74	V48L	L184I	-	-	-	-
75	T94P	L282P	-	-	-	-
76	A18V	S111C	S147A	A178V	-	-
77	T13I	V336I	-	-	-	-
78	E208K	E339A	-	-	-	-
79	S52L	T219S	A303T	-	-	-
80	S90Y	W290C	-	-	-	-
81	G11S	V48L	R312W	E423D	-	-
82	-	-	-	-	-	N/A
83	I97F	R222H	-	-	-	-
84	Q119H	-	-	-	-	-
85	V322M	R346W	Q356K	L396Q	-	-
86	K246Q	V349M	K426K	-	-	-
87	-	-	-	-	-	-
88	R222C	C380S	-	-	-	-
89	S136F	-	del G193	-	-	N/A
90	K246Q	V349M	-	-	-	-

Mutant Name	Mutation 1	Mutation 2	Mutation 3	Mutation 4	Mutation 5	Mutation 6
91	I176F	G201E	S348C	-	-	-
92	Q356K	-	-	-	-	-
93	-	-	-	-	-	-
94	P379S	-	-	-	-	-
95	N55K	S348R	-	-	-	-
96	G197E	S391I	-	-	-	-
97	I230N	Q376*	-	-	-	-
98	E368K	-	-	-	-	-
99	A3V	L196F	E339K	L365V	R382M	L396Q
100	A330S	V361M	L399F	-	-	-
101	V16L	E324Q	-	-	-	-
102	E136D	P287A	-	-	-	-
103	K32R	H141N	T333I	L384P	-	-
104	A190D	L294L	A367V	G371A	S385*	-
105	V295I	E321V	F325L	A370E	L407P	A415V
106	V295I	E321V	F325L	A370D	L407P	A415V
107	L117F	F200Y	M306I	E350V	Del F340	Del I422
108	V295I	E321V	F325L	A370E	L407P	-
109	I228T	T318A	R344W	L389P	-	-
110	S26T	R222H	R326K	F340L	-	-
111	L117F	F200Y	E350V	Del F340	Del I422	-
112	L117F	F200Y	E350V	Del F340	-	-
113	K25E	A302V	I314L	-	-	-
114	S26Y	W290L	R344W	-	-	-
115	A190D	A367V	-	-	-	-
116	L22P	S26P	C234S	-	-	-
117	A190D	A367V	S385*	-	-	-
118	V295I	E321V	F325L	A370E	L407P	A415V
119	S26Y	W290L	R344W	E394G	-	-

Table V a: *Unique mutant clones identified from the random mutant libraries. Individual mutations that complemented yeast growth are shown in green and mutations which were unable to rescue growth are shown in red. Gray text indicates mutant clones that were unique but were identified as false positives. Abbreviations used: 'trunc' for truncation and 'fs' for frame shift mutations.*

Appendix VI

ARTICLE ADDENDUM

Channels 6:6, 1-6; November/December 2012; © 2012 Landes Bioscience

State-independent intracellular access of quaternary ammonium blockers to the pore of TREK-1

Markus Rapedius,[1,†] Matthias R. Schmidt,[2,3,†] Chetan Sharma,[3] Phillip J. Stansfeld,[2] Mark S.P. Sansom,[2,4] Thomas Baukrowitz[1,*] and Stephen J. Tucker[3,4,*]

[1]Physiological Institute; Christian-Albrechts University; Kiel, Germany; [2]Department of Biochemistry; University of Oxford; Oxford, UK; [3]Clarendon Laboratory; Department of Physics; University of Oxford; Oxford, UK; [4]OXION Ion Channels and Disease Initiative, University of Oxford; Oxford, UK

[†]These authors contributed equally to this work.

This manuscript has been published online, prior to printing. Once the issue is complete and page numbers have been assigned, the citation will change accordingly.

We previously reported that TREK-1 gating by internal pH and pressure occurs close to or within the selectivity filter. These conclusions were based upon kinetic measurements of high-affinity block by quaternary ammonium (QA) ions that appeared to exhibit state-independent accessibility to their binding site within the pore. Intriguingly, recent crystal structures of two related K2P potassium channels were also both found to be open at the helix bundle crossing. However, this did not exclude the possibility of gating at the bundle crossing and it was suggested that side-fenestrations within these structures might allow state-independent access of QA ions to their binding site. In this addendum to our original study we demonstrate that even hydrophobic QA ions do not access the TREK-1 pore via these fenestrations. Furthermore, by using a chemically reactive QA ion immobilised within the pore via covalent cysteine modification we provide additional evidence that the QA binding site remains accessible to the cytoplasm in the closed state. These results support models of K2P channel gating which occur close to or within the selectivity filter and do not involve closure at the helix bundle crossing.

Keywords: Ion channel, K2P channel, potassium channel, TREK-1, TRAAK, TWIK-1, docking, homology modeling

Submitted: 08/13/12

Revised: 09/09/12

Accepted: 09/10/12

http://dx.doi.org/10.4161/chan.22153

*Correspondence to: Thomas Baukrowitz and Stephen J. Tucker; Email: t.baukrowitz@physiologie.uni-kiel.de and stephen.tucker@physics.ox.ac.uk

Addendum to: Piechotta PL, Rapedius M, Stansfeld PJ, Bollepalli MK, Ehrlich G, Andres-Enguix I, et al. The pore structure and gating mechanism of K2P channels. EMBO J 2011; 30:3607-19; http://dx.doi.org/10.1038/emboj.2011.268; PMID:21822218.

Introduction

TREK-1 is the prototypical member of the two-pore (K2P) family of potassium channels which are important regulators of cellular electrical excitability.[1,2] However, their gating mechanism remains poorly understood.[3] In other K^+ channels, two structurally distinct gates have been proposed; a lower gate at the intracellular helix bundle-crossing and an upper gate which comprises the outer pore and selectivity filter. Gating at the lower bundle-crossing is thought to involve constriction of the permeation pathway by the pore-lining helices, while the conformational changes at the upper gate probably involve much smaller movements which alter permeation through the selectivity filter.[4]

The relative importance of these two different gating mechanisms in K2P channels remains unclear.[3,5] However, several recent studies have demonstrated an important role for the selectivity filter in TREK-1 channel gating and suggest that movement of the transmembrane helices is primarily involved in transducing intracellular signals to the filter gate rather than closure of the pore at the bundle crossing.[6-8] In one of these studies we used scanning mutagenesis and structural modeling of the TREK-1 pore to identify a quaternary ammonium (QA) binding site within the inner cavity of the pore, and demonstrated that tetrahexylammonium (THexA) ions exhibit state-independent accessibility to this binding site.[8] This result suggested that the bundle crossing remains open even when the permeation pathway is gated shut by intracellular pH and supported a model of TREK-1 gating which occurs close to or within the selectivity filter. Subsequent to this study,

©2012 Landes Bioscience. Do not distribute.

crystal structures of two members of the K2P family, including the related TRAAK channel, were determined and both found to be open at the helix bundle crossing.[9,10] However, these open-state structures still did not exclude the possibility of gating at the bundle crossing and it was noted that the presence of side-fenestrations within these structures might represent an alternative route for QA ions to access their binding site thereby bypassing the bundle-crossing gate.[10]

In this addendum to our original study, we now demonstrate that a structural model of TREK-1 based upon TRAAK provides the best fit to our experimental data and that even hydrophobic blockers such as tetrahexylammonium do not access their binding site through the side fenestrations of the channel. We also provide further direct evidence that the intracellular cavity of TREK-1 remains accessible to pore-blockers in both the open and closed states.

Results and Discussion

Homology modeling of TREK-1. Using the recent crystal structures of two different K2P channels we have re-evaluated our previous structural model of TREK-1 which was based upon the open-state conformation of KvAP (PDB 1ORQ).[8] Homology models of TREK-1 were built using TRAAK (PDB: 3UM7) and TWIK-1 (PDB: 3UKM) as structural templates, and residues within the inner cavity which contribute to the binding site for tetrapentylammonium (TPenA) were predicted by in silico docking of TPenA.[11,12] In order to more accurately score these results, 100–200 individual TREK-1 models were generated per template, and those residues predicted to interact with TPenA were recorded for each model (**Fig. 1A and B**). For comparison to our previous model of TREK-1, the same analysis was also performed using KvAP (PDB 1ORQ) as a structural template (**Fig. 1C**).[8]

These in silico results confirmed our previous observation that TPenA binds within the inner cavity just below the selectivity filter.[8] Furthermore, when compared with the functional scanning mutagenesis data obtained in our previous study, the TRAAK-based model exhibited the least number of false positive interactions with TPenA (**Fig. 1A**) and is therefore likely to represent the most accurate structural model of TREK-1 currently available. This is perhaps not surprising given the high degree of homology between TREK-1 and TRAAK, especially within the transmembrane-pore region. However, our observation that a TWIK-1-based model provides no better fit to the experimental data than our original KvAP-based model highlights differences between the two pore-lining helices (M2 and M4) of TRAAK and TWIK-1.[13,14]

State-independent access of QA blockers to their binding via the permeation pathway. Our previous study proposed that the helix bundle-crossing gate in TREK-1 remains open even in the closed state. This key finding was based upon kinetic measurements of THexA access to its binding site which suggested that this blocking ion had access to its binding site even when the channel was gated closed by changes in intracellular pH and pressure.[8] However, even though the recent crystal structures demonstrate an open bundle-crossing, there are two possible caveats to our original conclusion. First, even when gated closed at pH 8, the open probability of TREK-1 is unlikely to be zero and therefore THexA could possibly enter the pore via infrequent openings of the helix bundle crossing gate (if this is the gate) and subsequent blocker trapping might have caused the observed binding of THexA to the closed state. Second, the crystal structures of both TRAAK and TWIK-1 revealed side-fenestrations between the asymmetric subunits, and our TRAAK-based model of TREK-1 also exhibits similar fenestrations (**Fig. 1D**). This has led to suggestions that hydrophobic QA ions such as THexA might exhibit significant membrane solubility and access their binding site through these fenestrations instead of via the permeation pathway and helix bundle crossing.[10,14]

To address the latter concern we examined the effect of extracellular THexA on TREK-1 whole-cell currents expressed in Xenopus oocytes. If THexA can access the TREK-1 pore via a side fenestration pathway then it would have to do so via permeation of the membrane (**Fig. 1D**) and block would be independent of whether it was applied via the intracellular or extracellular surface. However, we found that THexA had no effect on TREK-1 currents when applied extracellularly, even at 50 μM for over 3 min (data not shown). By contrast, 1 μM THexA rapidly causes 50% block within 250 ms when applied intracellularly and this block is also rapidly reversible.[8] This result suggests that the rapid access of THexA to its binding site is unlikely to occur via these membrane bound pathways. However, access of local anesthetics to the side fenestrations of the voltage-gated sodium channels is thought to occur via such pathways,[15] but these compounds are significantly more hydrophobic than THexA.

Nevertheless, even if access via a membrane permeant pathway is unlikely, this still does not exclude the possibility discussed above that brief openings of a bundle-crossing gate might allow direct access of THexA to its binding site during the closed state. An alternative approach to probe the status of this bundle-crossing gate is the use of sulfhydryl reactive MTS-reagents to probe the accessibility of cysteine residues within the inner cavity of the pore.[16,17] We therefore decided to utilize a quaternary ammonium ion linked to an MTS-reagent, MTS-TBAO (8-(Tributylammonium)octyl methanethiosulfonate). This compound has several potentially advantageous properties: First, it is considerably more hydrophilic than THexA and thus highly unlikely to access the pore via the fenestration pathway; second, it is large and will therefore only enter the pore if the bundle crossing gate is sufficiently wide open; third, the QA moiety is expected to block ion permeation; and finally, when present within the pore it will have a high effective local concentration and thus preferentially modify any accessible cysteines within the inner cavity. Importantly, our model of wild-type TREK-1 predicts that neither of the endogenous cysteines within the TM-helices (C174 and C234) will be accessible from within the inner pore, and intracellular application of 100 μM MTS-TBAO produced only a weak and reversible block (**Fig. 2A**) indicating the suitability of wild-type TREK-1 for cysteine modification studies.

©2012 Landes Bioscience. Do not distribute.

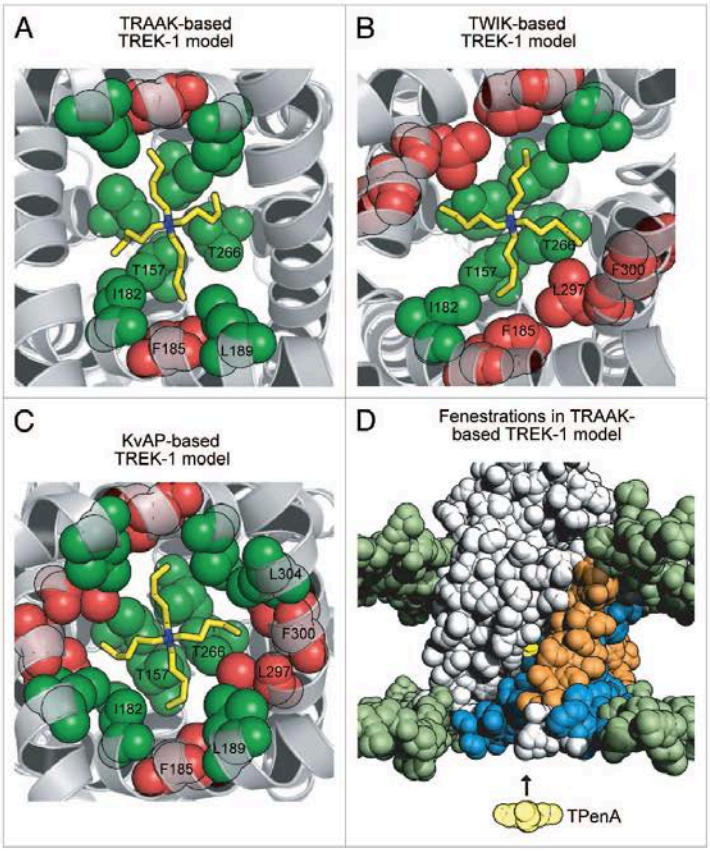


Figure 1. Refined structural models of TREK-1 with TPenA bound. (A) Bottom up view of a structural model of the TREK-1 pore with docked TPenA. The model was based upon the crystal structure of TRAAK (PDB ID: 3UM7). Those residues which interact with TPenA are highlighted as spheres and colored green if they agree with our functional scanning mutagenesis study or red if a false positive. Only residues on one protomer are numbered. (B) Similar model based upon the crystal structure of TWIK-1 (PDB ID: 3UKM). (C) Similar model based upon the crystal structure of KvAP (PDB ID: 1ORQ). (D) Solvent-accessible surface area (SASA) of a TREK-1 model, based on TRAAK, in which the side-fenestrations are still clearly visible. The SASA of the phospholipid head groups is colored green whereas the TREK-1 model is colored gray. For one protomer, the outer (M1 and M3) and inner (M2 and M4) transmembrane helices are highlighted in orange and blue, respectively. The docked TPenA is also visible through the side-fenestration (colored in yellow spheres) and QA ion access to this binding site occurs via the cytoplasmic pore of the channel (indicated by direction of the arrow).

In our previous study, the G186C mutation in TREK-1 exhibited a higher sensitivity to QA ion inhibition compared with wild-type TREK-1 (see also **Figure 2B**).[8] Consistent with this observation, our TREK-1 model suggests that a cysteine at this position would face toward the pore and be in close proximity to the predicted QA binding site. Covalent docking of MTS-TBAO to this site in our new model suggests that the G186C mutant may exhibit increased TPenA affinity via a direct, enhanced interaction with TPenA (**Fig. 2C**).[18] Indeed, application of 20μM MTS-TBAO on G186C TREK-1 channels previously activated by pH 5 resulted in a bi-phasic current decay. The fast phase likely represents reversible block by the TBAO-moiety, while the slower phase follows a monoexponential time course (τ = 18.6 ± 3.9 sec) and most likely represents irreversible covalent attachment of the blocker to this pore cysteine (G186C) because removal of MTS-TBAO did not result in any further current recovery (**Fig. 2D**).

In the closed state (pH 8), application of 20 μM MTS-TBAO to G186C-TREK-1 for only 1 sec resulted in an irreversible reduction in current of > 70%. Using a cumulative reagent application protocol (**Fig. 3A**), the time constant for channel modification was determined to be 0.7 ±

©2012 Landes Bioscience. Do not distribute.

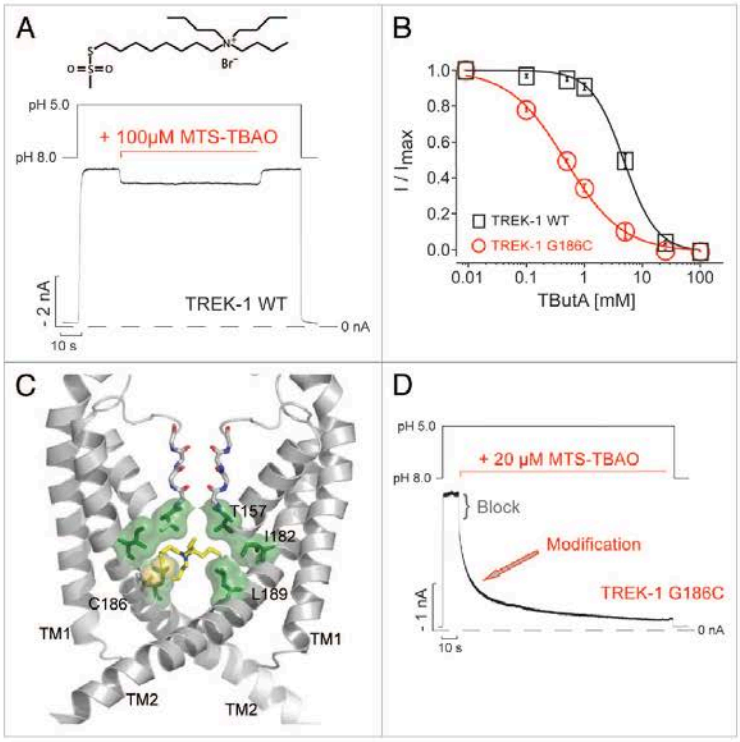


Figure 2. MTS-TBAO block and modification of TREK-1. (A) TREK-1 channel currents expressed in Xenopus oocytes measured at -80 mV in inside-out patches, activated from pH 8 by pH 5 and exposed to MTS-TBAO for 120 sec. A small and reversible block [8.2 ± 0.5% at 100 μM; (n = 4)] by the TBAO-moiety was obtained. (B) Concentration-response curves for tetrabutylammonium (TButA) inhibition of wild-type TREK-1 and G186C channels fitted to a standard Hill function with IC_{50} values and Hill-coefficients of 4.8 ± 0.3 mM and 1.4 ± 0.1 (n = 5) for wt; 0.5 ± 0.1 mM and 1.1 ± 0.1 for G186 (n = 6). Data points represent mean ± SEM (C) Structural model of the P1 subunits in the TREK-1 pore, the M3 and M4 helices from the P2 subunit are removed for clarity. The MTS-TBAO was linked to the introduced cysteines at position 186 with the SH-group in yellow, which is located in close proximity to the predicted QA binding site (green). (D) Application of MTS-TBAO on TREK-1-G186C mutant channels results in an initial fast block [24.2 ± 1% at 20 μM; (n = 5)] followed by a monoexponential time course [τ = 18.6 ± 3.9 sec; (n = 5)] for the modification of this cysteine that irreversibly reduced the current by up to 90%.

0.1 sec (**Fig. 3A and C**). Furthermore, the presence of 1 mM TPenA during MTS-TBAO application to the closed channel (pH 8) profoundly slowed this rate of modification suggesting that both molecules compete for their binding site even when the channel is closed (**Fig. 3B and C**). The fact that channel modification appears faster at pH 8 compared with pH 5 most likely reflects the higher chemical reactivity of cysteines at alkaline pH.[17] Regardless of this, the rapid modification rate observed while the channel is closed makes it unlikely that MTS-TBAO could have entered the pore via infrequent helix bundle-crossing openings. Moreover, the lack of any increase in the modification rate at pH 8 when 10 μM PtdIns(4,5) P_2 application is used to produce a large increase in open probability (**Fig. 3D**) suggests beyond reasonable doubt that access of MTS-TBAO to its binding site within the pore is state-independent.

In summary, these results support our original observations that the helix bundle-crossing in TREK-1 remains open and the inner pore cavity is accessible to QA ions even when the channel is gated closed by intracellular pH.[8] Furthermore, the results are consistent with models of K2P channel gating where the primary gating mechanism is located close to or within the selectivity filter and suggest that any movement of the pore-lining helices is restricted to coupling of the cytoplasmic domains to this gating mechanism rather than closure of the channel at a lower bundle-crossing gate. Consequently, it may be difficult to determine whether the existing crystal structures of TWIK-1 and TRAAK represent fully open or closed state channels, and higher-resolution structures which address the conductive status of the selectivity filter may ultimately be necessary.

©2012 Landes Bioscience. Do not distribute.

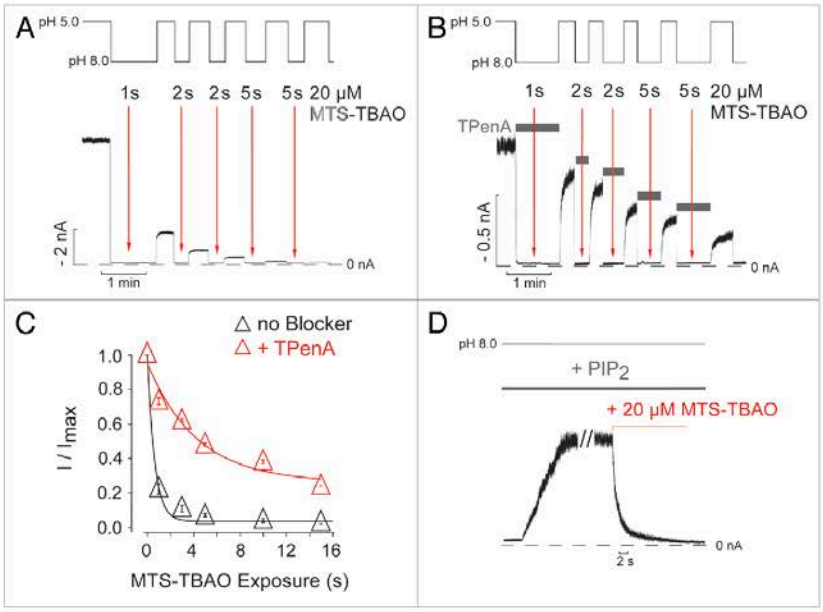


Figure 3. State-independent access of MTS-TBAO to the inner pore of TREK-1. (A) TREK-1 currents activated by pH 5 were exposed to repeated applications of 20 µM MTS-TBAO at pH 8 for the times indicated by the arrows in order to test the accessibility of Cys-186 in the closed state. (B) A similar experiment performed in the presence of 1 mM TPenA, which blocks TREK-1 with an IC_{50} of 13 ± 1 µM.[8] The channels were exposed to the blocker during the time indicated by the horizontal bars that resulted in complete inhibition of the current. Twenty µM MTS-TBAO was then applied to the blocked channel at times indicated by the arrows. (C) Time course of the relative current decline from experiments such as those shown in panels A and B as a function of cumulative reagent exposure (Modification Time x [MTS-TBAO]) resulted in a monoexponential time course of 0.7 ± 0.1 sec (n = 6) in absence and 8.2 ± 0.9 sec (n = 3) in the presence of 1 mM TPenA. Data points represent mean ± SEM (D) Activation of TREK-1-G186C mutant channels by 10 µM PtdIns(4,5)P_2 at pH 8 and subsequent application of MTS-TBAO irreversibly reduced the current by ≈90%. The decay of the current was fitted to a monoexponential function with a Tau (τ) of 1.2 ± 0.1 sec (n = 3).

Materials and Methods

Homology models of human TREK-1 were generated as previously described,[8] but in addition models were also built using the crystal structures of TWIK-1 (PDB: 3UKM, n = 100), and TRAAK (PDB: 3UM7, n = 200) as templates. In the TRAAK-based models of TREK-1, residues Tyr281 – Tyr285, which are in the extracellular loop that connects the selectivity filter and M4, were modeled on TWIK-1. Symmetry restraints were imposed between the two monomers during the modeling procedure. TPenA was docked into the pore of TREK-1 and models were ranked according to their fit to our previous scanning mutagenesis data.[8]

Mutagenesis, cRNA synthesis, oocyte injection and electrophysiology were performed as previously described.[8] MTS-TBAO (Toronto Research Chemicals, Toronto, ON, Canada) was stored as a stock solution in isopropanol at -80°C and diluted every 3h. This was stored on ice and the final dilution was made into the experimental solution immediately prior to each measurement. PtdIns(4,5)P_2 (Avanti Polar Lipids, Alabaster, AL, USA) was stored as a stock solution at -80°C (1 mM in DMSO). It was then diluted to the stated final concentration in the experimental solution, sonicated for 35 min and used within 2–3 h.

Acknowledgments

This work was supported by research grants from the Deutsche Forschungsgemeinschaft, the Wellcome Trust, the Biotechnology and Biological Sciences Research Council and Pfizer Neusentis UK.

References

1. Enyedi P, Czirják G. Molecular background of leak K+ currents: two-pore domain potassium channels. Physiol Rev 2010; 90:559-605; PMID:20393194; http://dx.doi.org/10.1152/physrev.00029.2009.
2. Dedman A, Sharif-Naeini R, Folgering JH, Duprat F, Patel A, Honoré E. The mechano-gated K(2P) channel TREK-1. Eur Biophys J 2009; 38:293-303; PMID:18369610; http://dx.doi.org/10.1007/s00249-008-0318-8.
3. Mathie A, Al-Moubarak E, Veale EL. Gating of two pore domain potassium channels. J Physiol 2010; 588:3149-56; PMID:20566661; http://dx.doi.org/10.1113/jphysiol.2010.192344.
4. Cuello LG, Jogini V, Cortes DM, Pan AC, Gagnon DG, Dalmas O, et al. Structural basis for the coupling between activation and inactivation gates in K(+) channels. Nature 2010; 466:272-5; PMID:20613845; http://dx.doi.org/10.1038/nature09136.
5. Cohen A, Ben-Abu Y, Zilberberg N. Gating the pore of potassium leak channels. Eur Biophys J 2009; 39:61-73; PMID:19404634; http://dx.doi.org/10.1007/s00249-009-0457-6.

©2012 Landes Bioscience. Do not distribute.

6. Bagriantsev SN, Clark KA, Minor DL Jr. Metabolic and thermal stimuli control K(2P)2.1 (TREK-1) through modular sensory and gating domains. EMBO J 2012; 31:3297-308; PMID:22728824; http://dx.doi.org/10.1038/emboj.2012.171.
7. Bagriantsev SN, Peyronnet R, Clark KA, Honoré E, Minor DL Jr. Multiple modalities converge on a common gate to control K2P channel function. EMBO J 2011; 30:3594-606; PMID:21765396; http://dx.doi.org/10.1038/emboj.2011.230.
8. Piechotta PL, Rapedius M, Stansfeld PJ, Bollepalli MK, Ehrlich G, Andres-Enguix I, et al. The pore structure and gating mechanism of K2P channels. EMBO J 2011; 30:3607-19; PMID:21822218; http://dx.doi.org/10.1038/emboj.2011.268.
9. Brohawn SG, del Mármol J, MacKinnon R. Crystal structure of the human K2P TRAAK, a lipid- and mechano-sensitive K+ ion channel. Science 2012; 335:436-41; PMID:22282805; http://dx.doi.org/10.1126/science.1213808.
10. Miller AN, Long SB. Crystal structure of the human two-pore domain potassium channel K2P1. Science 2012; 335:432-6; PMID:22282804; http://dx.doi.org/10.1126/science.1213274.
11. Goodsell DS, Morris GM, Olson AJ. Automated docking of flexible ligands: applications of AutoDock. J Mol Recognit 1996; 9:1-5; PMID:8723313; http://dx.doi.org/10.1002/(SICI)1099-1352(199601)9:1<1::AID-JMR241>3.0.CO;2-6.
12. Sali A, Blundell TL. Comparative protein modelling by satisfaction of spatial restraints. J Mol Biol 1993; 234:779-815; PMID:8254673; http://dx.doi.org/10.1006/jmbi.1993.1626.
13. Braun AP. Two-pore domain potassium channels: Variation on a structural theme. Channels (Austin) 2012; 6:139-40; PMID:22699405; http://dx.doi.org/10.4161/chan.20973.
14. Poulsen H, Nissen P. Structural biology. The inner workings of a dynamic duo. Science 2012; 335:416-7; PMID:22282800; http://dx.doi.org/10.1126/science.1217679.
15. O'Reilly AO, Eberhardt E, Weidner C, Alzheimer C, Wallace BA, Lampert A. Bisphenol a binds to the local anesthetic receptor site to block the human cardiac sodium channel. PLoS One 2012; 7:e41667; PMID:22848561; http://dx.doi.org/10.1371/journal.pone.0041667.
16. Liu Y, Holmgren M, Jurman ME, Yellen G. Gated access to the pore of a voltage-dependent K+ channel. Neuron 1997; 19:175-84; PMID:9247273; http://dx.doi.org/10.1016/S0896-6273(00)80357-8.
17. Karlin A, Akabas MH. Substituted-cysteine accessibility method. Methods Enzymol 1998; 293:123-45; PMID:9711606; http://dx.doi.org/10.1016/S0076-6879(98)93011-7.
18. Morris GM, Huey R, Lindstrom W, Sanner MF, Belew RK, Goodsell DS, et al. AutoDock4 and AutoDockTools4: Automated docking with selective receptor flexibility. J Comput Chem 2009; 30:2785-91; PMID:19399780; http://dx.doi.org/10.1002/jcc.21256.

©2012 Landes Bioscience. Do not distribute.

Bibliography

Adragna, N. & Lauf, P. Role of Nitrite, a Nitric Oxide Derivative, in K-Cl Cotransport during activation of low-potassium sheep red blood cells. *Journal of Membrane Biology* **167**, 157–167 (1998).

Andres-Enguix, I. *et al.* Functional analysis of missense variants in the TRESK (KCNK18) K channel. *Scientific reports* **2**, 237 (2012).

Ashmole, I. *et al.* The response of the tandem pore potassium channel TASK-3 (K2P9.1) to voltage: gating at the cytoplasmic mouth. *The Journal of Physiology* **587**, 4769–4783 (2009).

Ashmole, I., Goodwin, P. & Stanfield, P. TASK-5, a novel member of the tandem pore K^+ channel family. *Pflügers Archiv European Journal …* 828–833 (2001).doi:10.1007/s004240100620

Bagriantsev, S. N., Clark, K. A. & Minor, D. L. Metabolic and thermal stimuli control K(2P)2.1 (TREK-1) through modular sensory and gating domains. *The EMBO journal* **31**, 3297–308 (2012).

Bagriantsev, S. N., Peyronnet, R., Clark, K. A, Honoré, E. & Minor, D. L. Multiple modalities converge on a common gate to control K2P channel function. *The EMBO journal* **30**, 3594–606 (2011).

Ben-Abu, Y., Zhou, Y., Zilberberg, N. & Yifrach, O. Inverse coupling in leak and voltage-activated K^+ channel gates underlies distinct roles in electrical signaling. *Nature structural & molecular biology* **16**, 71–9 (2009).

Bernèche, S. & Roux, B. A gate in the selectivity filter of potassium channels. *Structure (London, England : 1993)* **13**, 591–600 (2005).

Betts, M. J. & Russell, R. B. Amino acid properties and consequences of subsitutions. In *Bioinformatics for Geneticists*. *Wiley* (2003).

Bittner, S., Budde, T., Wiendl, H. & Meuth, S. G. From the background to the spotlight: TASK channels in pathological conditions. *Brain pathology (Zurich, Switzerland)* **20**, 999–1009 (2010).

Bockenhauer, D., Zilberberg, N. & Goldstein, S. A. N. KCNK2: reversible conversion of a hippocampal potassium leak into a voltage-dependent channel. *Nature Neuroscience* **4**, 486–491 (2001).

Brenner, T. & O'Shaughnessy, K. M. Both TASK-3 and TREK-1 two-pore loop K channels are expressed in H295R cells and modulate their membrane potential and aldosterone secretion. *American journal of physiology. Endocrinology and metabolism* **295**, E1480–6 (2008).

Brohawn, S., Mármol, J. del & MacKinnon, R. Crystal structure of the human K2P TRAAK, a lipid- and mechano-sensitive K^+ ion channel. *Science Signalling* 436–441 (2012)

Brohawn, S., Campbell, E. & MacKinnon, R. Domain-swapped chain connectivity and gated membrane access in a Fab-mediated crystal of the human TRAAK K^+ channel. *PNAS* 110(6) 2129-34 (2013)

Buckler, K. & Honore, E. The lipid-activated two-pore domain K^+ channel TREK-1 is resistant to hypoxia: implication for ischaemic neuroprotection. *The Journal of physiology* **1**, 213–222 (2004).

Burch, T. P. & Ticku, M. K. Histidine modification with diethyl pyrocarbonate shows heterogeneity of benzodiazepine receptors. *Proceedings of the National Academy of Sciences of the United States of America* **78**, 3945–9 (1981).

Bushell, T., Clarke, C., Mathie, A. & Robertson, B. Pharmacological characterization of a non-inactivating outward current observed in mouse cerebellar Purkinje neurones. *British journal of pharmacology* **135**, 705–12 (2002).

Chatelain, F. C. *et al.* The pore helix dipole has a minor role in inward rectifier channel function. *Neuron* **47**, 833–43 (2005).

Chemin, J. *et al.* Up- and down-regulation of the mechano-gated K2P channel TREK-1 by PIP2 and other membrane phospholipids. *Pflügers Archiv European Journal of Physiology* **455**, 97–103 (2007).

Clarke, C. E., Benham, C. D., Bridges, a, George, a R. & Meadows, H. J. Mutation of histidine 286 of the human P2X4 purinoceptor removes extracellular pH sensitivity. *The Journal of physiology* **523 Pt 3**, 697–703 (2000).

Cohen, A., Ben-Abu, Y., Hen, S. & Zilberberg, N. A novel mechanism for human K2P2.1 channel gating. Facilitation of C-type gating by protonation of extracellular histidine residues. *The Journal of biological chemistry* **283**, 19448–55 (2008).

Cuello, L. G. *et al.* Structural basis for the coupling between activation and inactivation gates in K^+ channels. *Nature* **466**, 272–275 (2010).

Dascal, N. Voltage Clamp Recordings from *Xenopus* Oocytes. *Current Protocols in Neuroscience* (2001).doi:10.1002/0471142301.ns0612s10

Decher, N. *et al.* Characterization of TASK-4, a novel member of the pH-sensitive, two-pore domain potassium channel family. *FEBS letters* **492**, 84–9 (2001).

Denic, M., Ehrenberg, L., Fedorcsác, I. & Solymosy, F. The effect of diethyl pyrocarbonate on the biological activity of messenger RNA and transfer RNA. *Acta Chem Scand* **24**, 3753–3755 (1970).

Doyle, D. A. *et al.* The structure of the potassium channel: molecular basis of K^+ conduction and selectivity. *Science (New York, N.Y.)* **280**, 69–77 (1998).

Duprat, F., Girard, C., Jarretou, G. & Lazdunski, M. Pancreatic two P domain K^+ channels TALK-1 and TALK-2 are activated by nitric oxide and reactive oxygen species. *The Journal of physiology* **562**, 235–44 (2005).

Duprat, F. *et al.* The neuroprotective agent riluzole activates the two P domain K^+ channels TREK-1 and TRAAK. *Molecular pharmacology* **57**, 906–12 (2000).

Eckert, M., Egenberger, B., Döring, F. & Wischmeyer, E. TREK-1 isoforms generated by alternative translation initiation display different susceptibility to the antidepressant fluoxetine. *Neuropharmacology* **61**, 918–23 (2011).

Enyedi, P. & Czirják, G. Molecular Background of Leak K^+ Currents : Two-Pore Domain Potassium Channels. *Physiological reviews* 559–605 (2010).doi:10.1152/physrev.00029.2009.

Enyedi, P., Braun, G. & Czirják, G. TRESK: the lone ranger of two-pore domain potassium channels. *Molecular and cellular endocrinology* **353**, 75–81 (2012).

Enyedi, P., Braun, G. & Czirják, G. TRESK: the lone ranger of two-pore domain potassium channels. *Molecular and cellular endocrinology* **353**, 75–81 (2012).

Es-Salah-Lamoureux, Z., Steele, D. F. & Fedida, D. Research into the therapeutic roles of two-pore-domain potassium channels. *Trends in pharmacological sciences* **31**, 587–95 (2010).

Feliciangeli, S. *et al.* Potassium channel silencing by constitutive endocytosis and intracellular sequestration. *The Journal of biological chemistry* **285**, 4798–805 (2010).

Fink, M. *et al.* Cloning, functional expression and brain localization of a novel unconventional outward rectifier K^+ channel. *The EMBO journal* **15**, 6854–62 (1996).

Fink, M. *et al.* A neuronal two P domain K^+ channel stimulated by arachidonic acid and polyunsaturated fatty acids. *The EMBO journal* **17**, 3297–308 (1998).

Gabashvili, I. S., Sokolowski, B. H. a, Morton, C. C. & Giersch, A. B. S. Ion channel gene expression in the inner ear. *Journal of the Association for Research in Otolaryngology : JARO* **8**, 305–28 (2007).

Galvani, L. De viribus electricitatis in motu musculari commentarius. *Bon. Sci. Art. Inst. Acad. Comm.* **7**, 363–418 (1791).

Gietz, R. D., Schiestl, R. H., Willems, a R. & Woods, R. a Studies on the transformation of intact yeast cells by the LiAc/SS-DNA/PEG procedure. *Yeast (Chichester, England)* **11**, 355–60 (1995).

Gietz, R. D. & Schiestl, R. H. Frozen competent yeast cells that can be transformed with high efficiency using the LiAc/SS carrier DNA/PEG method. *Nature protocols* **2**, 1–4 (2007).

Goldstein, S. A. N. K2P potassium channels, mysterious and paradoxically exciting. *Science signaling* **4**, pe35 (2011).

Goldstein, S. A. N., Bayliss, D. A., Kim, D., Lesage, F. & Plant, L. D. International Union of Pharmacology . LV . Nomenclature and Molecular Relationships of Two-P Potassium Channels. **57**, 527–540 (2005).

Gruss, M. *et al.* Two-pore-domain K^+ channels are a novel target for the anesthetic gases xenon, nitrous oxide, and cyclopropane. *Molecular pharmacology* **65**, 443–52 (2004).

Gu, W., Schlichthörl, G. & Hirsch, J. Expression pattern and functional characteristics of two novel splice variants of the two-pore-domain potassium channel TREK-2. *The Journal of …* 657–668 (2002).doi:10.1013/jphysiol.2001.013432

Han, J., Truell, J., Gnatenco, C. & Kim, D. Characterization of four types of background potassium channels in rat cerebellar granule neurons. *The Journal of Physiology* **542**, 431–444 (2002).

Heitzmann, D. & Warth, R. Physiology and Pathophysiology of Potassium Channels in Gastrointestinal Epithelia. 1119–1182 (2008).doi:10.1152/physrev.00020.2007.

Herr, W. Diethyl pyrocarbonate: a chemical probe for secondary structure in negatively supercoiled DNA. *Proceedings of the National Academy of Sciences of the United States of America* **82**, 8009–13 (1985).

Heurteaux, C. *et al.* TREK-1, a K^+ channel involved in neuroprotection and general anesthesia. *The EMBO journal* **23**, 2684–95 (2004).

Heurteaux, C. *et al.* Deletion of the background potassium channel TREK-1 results in a depression-resistant phenotype. *Nature neuroscience* **9**, 1134–41 (2006).

Hille, B. Ionic Channels of Excitable Membranes (third edition). *Sinauer* (2001).

Hodgkin, A., Huxley, A. & Katz, B. Measurement of current-voltage relations in the membrane of the giant axon of Loligo. *The Journal of physiology* 424–448 (1952).at <http://www.ncbi.nlm.nih.gov/pmc/articles/PMC1392219/>

Holt, A. G. *et al.* Deafness associated changes in expression of two-pore domain potassium channels in the rat cochlear nucleus. *Hearing research* **216-217**, 146–53 (2006).

Holter, J., Carter, D., Leresche, N., Crunelli, V. & Vincent, P. A TASK3 Channel (KCNK9) Mutation in a Genetic Model of Absence Epilepsy. **25**, (2005).

Honoré, E. The neuronal background K2P channels: focus on TREK1. *Nature reviews. Neuroscience* **8**, 251–61 (2007).

Honoré, E., Maingret, F., Lazdunski, M. & Patel, A. J. An intracellular proton sensor commands lipid- and mechano-gating of the K^+ channel TREK-1. *The EMBO journal* **21**, 2968–76 (2002).

Hoshi, T., Zagotta, W. N. & Aldrich, R. W. Biophysical and molecular mechanisms of Shaker potassium channel inactivation. *Science* **250**, 533–538 (1990).

Irizarry, S. N., Kutluay, E., Drews, G., Hart, S. J. & Heginbotham, L. Opening the KcsA K^+ Channel : Tryptophan Scanning and Complementation Analysis Lead to Mutants with Altered Gating †. 13653–13662 (2002).

Jiang, Y. *et al.* The open pore conformation of potassium channels. *Nature* **417**, 523–6 (2002).

Jiang, Y. *et al.* X-ray structure of a voltage-dependent K^+ channel. *Nature* **423**, 33–41 (2003).

Kahl, B. & Paule, M. The Use of Diethyl Pyrocarbonate and Potassium Permanganate as Probes for Strand Separation and Structural Distortions in DNA. *DNA-Protein Interactions SE - 6* **543**, 73–85 LA – English (2009).

Kandel, E. R., Schwartz, J. H. & Jessell, T. M. Principles of Neural Science (third edition). *Appleton & Lange* (2001).

Kang, D., Choe, C. & Kim, D. Functional expression of TREK-2 in insulin-secreting MIN6 cells. *Biochemical and biophysical research communications* **323**, 323–31 (2004).

Kang, D. & Kim, D. Single-channel properties and pH sensitivity of two-pore domain K^+ channels of the TALK family. *Biochemical and biophysical research communications* **315**, 836–844 (2004).

Kang, D., Mariash, E. & Kim, D. Functional expression of TRESK-2, a new member of the tandem-pore K^+ channel family. *The Journal of biological chemistry* **279**, 28063–70 (2004).

Karmakar, S. & Das, K. P. Identification of histidine residues involved in Zn^{2+} binding to αA- and αB-crystallin by chemical modification and MALDI TOF mass spectrometry. *The protein journal* **31**, 623–40 (2012).

Kelkar, D. a & Chattopadhyay, A. Membrane interfacial localization of aromatic amino acids and membrane protein function. *Journal of biosciences* **31**, 297–302 (2006).

Kennard, L. E. *et al.* Inhibition of the human two-pore domain potassium channel, TREK-1, by fluoxetine and its metabolite norfluoxetine. *British journal of pharmacology* **144**, 821–9 (2005).

Ketchum, K., Joiner, W. & Sellers, A. A new family of outwardly rectifying potassium channel proteins with two pore domains in tandem. *Nature* **376** (1995)

Kim, Y., Bang, H., Gnatenco, C. & Kim, D. Synergistic interaction and the role of C-terminus in the activation of TRAAK K^+ channels by pressure, free fatty acids and alkali. *Pflügers Archiv European Journal of Physiology* **442**, 64–72 (2001).

Kim, Y., Gnatenco, C., Bang, H. & Kim, D. Localization of TREK-2 K^+ channel domains that regulate channel kinetics and sensitivity to pressure, fatty acids and pH i. *Pflügers Archiv European Journal of Physiology* **442**, 952–960 (2001).

Kollewe, A., Lau, A. Y., Sullivan, A., Roux, B. & Goldstein, S. A. N. A structural model for K2P potassium channels based on 23 pairs of interacting sites and continuum electrostatics. *J. Gen. Physiol.* **134**, 53–68 (2009).

La, J.-H., Kang, D., Park, J.-Y., Hong, S.-G. & Han, J. A novel acid-sensitive K^+ channel in rat dorsal root ganglia neurons. *Neuroscience letters* **406**, 244–9 (2006).

Lafrenière, R. G. *et al.* A dominant-negative mutation in the TRESK potassium channel is linked to familial migraine with aura. *Nature medicine* 13–17 (2010).doi:10.1038/nm.2216

Lauritzen, I. *et al.* Polyunsaturated fatty acids are potent neuroprotectors. *The EMBO journal* **19**, 1784–93 (2000).

Lesage, F., Terrenoire, C., Romey, G. & Lazdunski, M. Human TREK2, a 2P domain mechano-sensitive K^+ channel with multiple regulations by polyunsaturated fatty acids, lysophospholipids, and Gs, Gi, and Gq protein-coupled receptors. *The Journal of biological chemistry* **275**, 28398–405 (2000).

Lesage, F., Guillemare, E. & Fink, M. TWIK-1, a ubiquitous human weakly inward rectifying K^+ channel with a novel structure. *The EMBO …* **15**, 1004–1011 (1996).

Liu, C., Au, J. D., Zou, H. L., Cotten, J. F. & Yost, C. S. Potent activation of the human tandem pore domain K channel TRESK with clinical concentrations of volatile anesthetics. *Anesthesia and analgesia* **99**, 1715–22, table of contents (2004).

Liu, H., Enyeart, J. a & Enyeart, J. J. ACTH inhibits bTREK-1 K^+ channels through multiple cAMP-dependent signaling pathways. *The Journal of general physiology* **132**, 279–94 (2008).

Lopes, C. M., Zilberberg, N. & Goldstein, S. A. N. Block of Kcnk3 by protons. Evidence that 2-P-domain potassium channel subunits function as homodimers. *The Journal of biological chemistry* **276**, 24449–52 (2001).

Lopes, C. M. B. *et al.* PIP2 hydrolysis underlies agonist-induced inhibition and regulates voltage gating of two-pore domain K^+ channels. *The Journal of physiology* **564**, 117–29 (2005).

Lopéz-Barneo, J., Hoshi, T., Heinemann, S. H. & Aldrich, R. W. Effects of external cations and mutations in the pore region on C-type inactivation of Shaker potassium channels. *Receptors Channels* **1**, 61–71 (1993).

Madrid, R., Gómez, M. J., Ramos, J. & Rodríguez-Navarro, a Ectopic potassium uptake in *trk1 trk2* mutants of Saccharomyces cerevisiae correlates with a highly hyperpolarized membrane potential. *The Journal of biological chemistry* **273**, 14838–44 (1998).

Maingret, F., Patel, a J., Lesage, F., Lazdunski, M. & Honoré, E. Lysophospholipids open the two-pore domain mechano-gated K^+ channels TREK-1 and TRAAK. *The Journal of biological chemistry* **275**, 10128–33 (2000).

Maingret, F., Patel, a J., Lesage, F., Lazdunski, M. & Honoré, E. Mechano- or acid stimulation, two interactive modes of activation of the TREK-1 potassium channel. *The Journal of biological chemistry* **274**, 26691–6 (1999).

Maingret, F., Honoré, E., Lazdunski, M. & Patel, A. J. Molecular basis of the voltage-dependent gating of TREK-1, a mechano-sensitive K^+ channel. *Biochemical and biophysical research communications* **292**, 339–46 (2002).

Mankelow, T. J. & Henderson, L. M. diethyl pyrocarbonate (DEPC), a histidine-modifying agent : evidence for at least two target sites. **324**, 315–324 (2001).

Mathie, A. Neuronal two-pore-domain potassium channels and their regulation by G protein-coupled receptors. *The Journal of physiology* **578**, 377–85 (2007).

Mazella, J. *et al.* Spadin, a sortilin-derived peptide, targeting rodent TREK-1 channels: a new concept in the antidepressant drug design. *PLoS biology* **8**, e1000355 (2010).

Miller, A. & Long, S. Crystal Structure of the Human Two–Pore potassium channel. *Science Signalling* 432–436 (2012).

Minor, D. L., Masseling, S. J., Jan, Y. N. & Jan, L. Y. Transmembrane structure of an inwardly rectifying potassium channel. *Cell* **96**, 879–91 (1999).

Minor, D. L. An Overview of Ion Channel Structure. *Cell* 201–207 (2009).

Moha ou Maati, H. *et al.* A human TREK-1/HEK cell line: a highly efficient screening tool for drug development in neurological diseases. *PloS one* **6**, e25602 (2011).

Morais-Cabral, J. H., Zhou, Y. & MacKinnon, R. Energetic optimization of ion conduction rate by the K^+ selectivity filter. *Nature* **414**, 37–42 (2001).

Morton, M. J., Abohamed, A., Sivaprasadarao, A. & Hunter, M. pH sensing in the two-pore domain K^+ channel, TASK2. *Proceedings of the National Academy of Sciences of the United States of America* **102**, 16102–6 (2005).

Morton, M. J., Abohamed, A., Sivaprasadarao, A. & Hunter, M. pH sensing in the two-pore domain K^+ channel, TASK2. *Proceedings of the National Academy of Sciences of the United States of America* **102**, 16102–6 (2005).

Niemeyer, M. I. *et al.* Gating of two-pore domain K^+ channels by extracellular pH. *Biochemical Society transactions* **34**, 899–902 (2006).

Niemeyer, M. I., Cid, L. P., Peña-Münzenmayer, G. & Sepúlveda, F. V Separate gating mechanisms mediate the regulation of K2P potassium channel TASK-2 by intra- and extracellular pH. *The Journal of biological chemistry* **285**, 16467–75 (2010).

Noël, J. *et al.* The mechano-activated K^+ channels TRAAK and TREK-1 control both warm and cold perception. *The EMBO journal* **28**, 1308–18 (2009).

O'Connell, D., Mruk, K., Rocheleau, J. M. & Kobertz, W. R. Xenopus laevis oocytes infected with multi-drug-resistant bacteria: implications for electrical recordings. *The Journal of general physiology* **138**, 271–7 (2011).

Ogielska, E. M. & Aldrich, R. W. Functional consequences of a decreased potassium affinity in a potassium channel pore. Ion interactions and C-type inactivation. *The Journal of general physiology* **113**, 347–58 (1999).

Papazian, D. M., Schwarz, T. L., Tempel, B. L., Jan, Y. N. & Jan, L. Y. Cloning of genomic and complementary DNA from Shaker, a putative potassium channel gene from Drosophila. *Science* **237**, 749–53 (1987).

Patel, A. J. *et al.* A mammalian two pore domain mechano-gated S-like K^+ channel. *The EMBO journal* **17**, 4283–90 (1998).

Patel, A. & Honore, E. The TREK two P domain K^+ channels. *The Journal of physiology* **539**, (2002).

Paynter, J. J., Sarkies, P., Andres-Enguix, I. & Tucker, S. J. Genetic selection of activatory mutations in KcsA. *Channels (Austin, Tex.)* **2**, 413–8 (2008).

Paynter, J. J., Shang, L., Bollepalli, M. K., Baukrowitz, T. & Tucker, S. J. Random mutagenesis screening indicates the absence of a separate H^+-sensor in the pH-sensitive Kir channels. *Channels (Austin, Tex.)* **4**, 1–7 (2010).

Pei, L. *et al.* Oncogenic potential of TASK3 (KCNK9) depends on K^+ channel function. *Proceedings of the National Academy of Sciences of the United States of America* **100**, 7803–7 (2003).

Piechotta, P. L. *et al.* TREK Channel Pore Probed by Cysteine Scanning Mutagenesis and Structural Modelling. *Biophysical Journal* **98**, 327a (2010).

Pilarski, J. Q. & Hempleman, S. C. Imidazole binding reagent diethyl pyrocarbonate (DEPC) inhibits avian intrapulmonary chemoreceptor discharge in vivo. *Respiratory physiology & neurobiology* **150**, 144–54 (2006).

Plant, L., Rajan, S. & Goldstein, S. K2P channels and their protein partners. *Current Opinion in Neurobiology* **15**, 326–333 (2005).

Pottosin, I. I., Bonales-Alatorre, E., Valencia-Cruz, G., Mendoza-Magaña, M. L. & Dobrovinskaya, O. R. TRESK-like potassium channels in leukemic T cells. *Pflügers Archiv : European journal of physiology* **456**, 1037–48 (2008).

Raab-Graham, K. F. & Vandenberg, C. a Tetrameric subunit structure of the native brain inwardly rectifying potassium channel Kir 2.2. *The Journal of biological chemistry* **273**, 19699–707 (1998).

Rajan, S. *et al.* THIK-1 and THIK-2, a novel subfamily of tandem pore domain K^+ channels. *The Journal of biological chemistry* **276**, 7302–11 (2001).

Rajan, S., Plant, L. D., Rabin, M. L., Butler, M. H. & Goldstein, S. A. N. Sumoylation Silences the Plasma Membrane Leak K^+ Channel K2P1. *Cell* **141**, 368 (2010).

Rapedius, M. *et al.* H Bonding at the Helix-Bundle Crossing Controls Gating in Kir Potassium Channels. *Neuron* **55**, 602–614 (2007).

Red, L. S., Cells, B., Adragna, N. C. & Lauf, P. K. Membrane Biology Role of Nitrite , a Nitric Oxide Derivative , in K-Cl Cotransport Activation of. **167**, 157–167 (1998).

Rohács, T., Chen, J., Prestwich, G. D. & Logothetis, D. E. Distinct specificities of inwardly rectifying $K(^+)$ channels for phosphoinositides. *The Journal of biological chemistry* **274**, 36065–72 (1999).

Sackin, H., Nanazashvili, M., Palmer, L. G. & Li, H. Role of conserved glycines in pH gating of Kir1.1 (ROMK). *Biophysical journal* **90**, 3582–9 (2006).

Safarian, S. *et al.* The structural and functional studies of His119 and His12 in RNase A via chemical modification. *Journal of protein chemistry* **22**, 643–54 (2003).

Salinas, M. *et al.* Cloning of a new mouse two-P domain channel subunit and a human homologue with a unique pore structure. *The Journal of biological chemistry* **274**, 11751–60 (1999).

Sandoz, G., Douguet, D., Chatelain, F., Lazdunski, M. & Lesage, F. Extracellular acidification exerts opposite actions on TREK1 and TREK2 potassium channels via a single conserved histidine residue. *Proceedings of the National Academy of Sciences of the United States of America* **106**, 14628–33 (2009).

Sano, Y. *et al.* A novel two-pore domain K^+ channel, TRESK, is localized in the spinal cord. *The Journal of biological chemistry* **278**, 27406–12 (2003).

Schulteis, C. T., Nagaya, N. & Papazian, D. M. Intersubunit interaction between amino- and carboxyl-terminal cysteine residues in tetrameric shaker K^+ channels. *Biochemistry* **35**, 12133–40 (1996).

Taglialatela, M., Payne, J. P., Drewe, J. a & Brown, a M. Rescue of lethal subunits into functional K^+ channels. *Biophysical journal* **66**, 179–90 (1994).

Takahira, M., Sakurai, M., Sakurada, N. & Sugiyama, K. Fenamates and diltiazem modulate lipid-sensitive mechano-gated 2P domain K($^+$) channels. *Pflügers Archiv : European journal of physiology* **451**, 474–8 (2005).

Talley, E. M., Solorzano, G., Lei, Q., Kim, D. & Bayliss, D. A. CNS distribution of members of the two-pore-domain (KCNK) potassium channel family. *The Journal of neuroscience : the official journal of the Society for Neuroscience* **21**, 7491–505 (2001).

Talley, E., Lei, Q., Sirois, J. & Bayliss, D. TASK-1, a Two–Pore Domain K^+ Channel, Is Modulated by Multiple Neurotransmitters in Motoneurons. *Neuron* **25**, 399–410 (2000).

Tang, W. *et al.* Functional expression of a vertebrate inwardly rectifying K^+ channel in yeast. . *Molecular Biology of the Cell* **6** , 1231–1240 (1995).

Tertyshnikova, S. *et al.* [(5, 6, 7, 8-tetrahydro-naphthalen-1-yl)-[2(1*H*-tetrazol-5-yl)-phenyl]-amine]: A Putative Potassium Channel Opener with Bladder-Relaxant Properties. *Pharmacology* **313**, 250–259 (2005).

Thomas, D., Plant, L. D., Wilkens, C. M., Mccrossan, Z. A. & N, S. A. potassium channels permeable to sodium. *Neuron* **58**, 859–870 (2008).

Thompson, A. N., Posson, D. J., Parsa, P. V & Nimigean, C. M. Molecular mechanism of pH sensing in KcsA potassium channels. *Proceedings of the National Academy of Sciences of the United States of America* **105**, 6900–5 (2008).

Veale, E. L., Rees, K. a, Mathie, A. & Trapp, S. Dominant negative effects of a non-conducting TREK1 splice variant expressed in brain. *The Journal of biological chemistry* **285**, 29295–304 (2010).

Woo, D. H. *et al.* TREK-1 and Best1 Channels Mediate Fast and Slow Glutamate Release in Astrocytes upon GPCR Activation. *Cell* **151**, 25–40 (2012).

Xiao, J., Zhen, X. & Yang, J. Localization of PIP2 activation gate in inward rectifier K^+ channels. *Nature neuroscience* **6**, 811–8 (2003).

Yau, W. M., Wimley, W. C., Gawrisch, K. & White, S. H. The preference of tryptophan for membrane interfaces. *Biochemistry* **37**, 14713–8 (1998).

Yellen, G. The moving parts of voltage-gated ion channels. *Quarterly reviews of biophysics* **31**, 239–95 (1998).

Yellen, G. channels and their relatives. *Nature* **419**, (2002).

Yuill, K. H., Stansfeld, P. J., Ashmole, I., Sutcliffe, M. J. & Stanfield, P. R. The selectivity, voltage-dependence and acid sensitivity of the tandem pore potassium channel TASK-1: contributions of the pore domains. *Pflügers Archiv : European journal of physiology* **455**, 333–48 (2007).

Zilberberg, N., Ilan, N. & Goldstein, S. A. N. KCNKØ: opening and closing the 2-P-domain potassium leak channel entails “C-type” gating of the outer pore. *Neuron* **32**, 635–48 (2001).

Zylbergold, P., Ramakrishnan, N. & Hebert, T. The role of G proteins in assembly and function of Kir3 inwardly rectifying potassium channels. *Channels (Austin, Tex.)* **4**, 411–21 (2010).